8-2012

Characterization and Quantification of Monomers, Oligomers, and By-Products from Xylan During Biomass Pretreatment

Ching-Shuan Lau
University of Arkansas, Fayetteville

CHARACTERIZATION AND QUANTIFICATION OF MONOMERS, OLIGOMERS, AND BY-PRODUCTS FROM XYLAN DURING BIOMASS PRETREATMENT

CHARACTERIZATION AND QUANTIFICATION OF MONOMERS, OLIGOMERS, AND BY-PRODUCTS FROM XYLAN DURING BIOMASS PRETREATMENT

A dissertation submitted in partial fulfillment
of the requirements for the degree of
Doctor of Philosophy in Biological Engineering

By

Ching-Shuan Lau
University of Technology Malaysia
Bachelor of Chemical Engineering, 2001
University of Arkansas
Master of Science in Chemical Engineering, 2004
University at Buffalo
Master of Business Administration, 2009

August 2012
University of Arkansas

Abstract

Biomass pretreatment generates inhibitory products, which reduce the overall yield of xylose for ethanol production. Understanding of hemicellulose depolymerization into xylose is essential to identify the pretreatment conditions that maximize xylose formation, but minimize the generation of these inhibitory products, such as formic acid and furfural. Thus, the goal of this project is to understand how dilute acid pretreatment parameters affect hemicellulose depolymerization, maximize xylose concentrations, and minimize by-products formation.

To progress towards this goal, rates and mechanisms of hemicellulose release must be determined. Birchwood xylan was used as the starting material to produce xylose oligomers. The hydrolyzed birchwood xylan was then fractionated using centrifugal partition chromatography (CPC) with the solvent system composed of butanol: methanol: water at a 5:1:4 volumetric ratio. The oligomers in the fractionated CPC were identified and quantified using high performance liquid chromatography (HPLC) and high performance anion exchange chromatography with pulsed amperometric detection (HPAEC-PAD), with the calibration curves setup based on the analysis of the commercial grade xylose oligomers reference standards. The identity of fractionated xylose oligomers was also confirmed using mass spectrometry (MS) analysis. The fractionated xylose oligomers were subsequently used in the kinetic study.

The developed kinetic model demonstrated that the formation or degradation of the compounds could be predicted using first order kinetics. At all hydrolysis conditions, DP 1 degraded mostly into formic acid, rather than into furfural. The degradation rates of DP 1 and formic acid were determined to be most influenced by temperature and pH, as reflected by the Arrhenius Equation parameters calculated for the respective compounds. Pretreatment condition

was more favorable for maximizing the yield of xylose monomer at the temperatures between 120 and 160 ˚C, at a pH between 0.43 and 7, because of lower degradation rate of DP 1, and higher degradation rates of xylose oligomers, resulting in a net accumulation of DP 1.

This dissertation is approved for recommendation
to the Graduate Council.

Dissertation Director:

_____
Dr. Danielle J. Carrier

Dissertation Committee:

_____
Dr. Edgar C. Clausen

_____
Dr. Jin-Woo Kim

_____
Dr. Jack O. Lay

_____
Dr. Greg J. Thoma

Dissertation Duplication Release

I hereby authorize the University of Arkansas Libraries to duplicate this dissertation when needed for research and/or scholarship.

Agreed _____
Ching-Shuan Lau

Refused _____
Ching-Shuan Lau

Acknowledgments

I would like to acknowledge the University of Arkansas Department of Biological and Agricultural Engineering, the Ralph E. Martin Department of Chemical Engineering, and the Graduate School for their continued financial assistance and support.

Many thanks to Dr. Danielle Julie Carrier for her continuous guidance, Drs. Ed Clausen, Jin-Woo Kim, Jack Lay, and Greg Thoma for their contributions and support of my graduate education.

I would also like to acknowledge Dr. Jennifer Gidden for her technical assistance in MS analysis, and Dr. Betty Martin, Kris Bunnell, Chris McDaniel, Angele Djioleu, Shiloh Hurd, Kalavathy Rajan, John Murdoch, Julian Abram, and Leland Schrader for their help during various stages of the research.

Finally, I would like to thank the University of Arkansas Graduate School for the Doctoral Academy Fellowship, the National Science Foundation for award #0828875, the U.S. Department of Energy (award #08GO88036) for the purchase of pretreatment equipment, CSREES National Research Initiative (award #2008-01499) for the purchase of HPLC instruments, and Arkansas Plant Powered Production (P3) Center through NSF EPSCoR (award # EPS-1003970) for the acquisition of the CPC instrument.

Table of Contents

List of Tables

List of Figures

of only DP 3.

List of Appendices

Nomenclature

A_o	Pre-exponential factor in min^{-1}.
C	Acid concentration in wt%.
CS	Combined severity.
e	Elementary charge, which has a value of $1.602*10^{-19}$ coulombs.
E	Activation energy in kJ/mol.
E_a	Apparent activation energy in kJ/mol.
E_{kin}	Kinetic energy of the ion in kJ.
k	Reaction rate constant in min^{-1}.
k_1	The overall degradation rate of DP 1in min^{-1}.
k_2	The overall degradation rate of DP 2 in min^{-1}.
k_3	The overall degradation rate of DP 3 in min^{-1}.
k_4	The overall degradation rate of DP 4 in min^{-1}.
k_A	The overall degradation rate of formic acid in $.min^{-1}$
k_F	The overall degradation rate of furfural in $min.^{-1}$
k_{1A}	The formation rates of formic acid from DP 1 in min^{-1}.
k_{1F}	The formation rates of furfural from DP 1 in min^{-1}.
k_{21}	The formation rates of DP 1 from DP 2 in min^{-1}.
k_{31}	The formation rates of DP 1 from DP 3 in min^{-1}.
k_{41}	The formation rates of DP 1 from DP 4 in min^{-1}.
k_{42}	The formation rates of DP 2 from DP 4 in min^{-1}.
k_{AL}	The decomposition rate of formic acid in min^{-1}.

k_{FA}	The formation rates of formic acid from furfural in min^{-1}.
k_{FL}	The decomposition rate of furfural in min^{-1}.
k_0	Pre-exponential factor in Arrhenius Equation in min^{-1}.
L	Distance of field-free region in m.
m	An unitless acid concentration exponent.
m	Ion mass.
pH	Acidity of the aqueous solution in pH.
R	Gas constant, which has a value of 8.314 x 10-3 kJ/mol/K.
R_o	Severity.
T	Hydrolysis temperature in K.
T_b	Reference temperature, which is set to 100˚C.
T_r	Reaction temperature in ˚C.
t	Hydrolysis time of biomass at reaction temperature in min.
t	Flight time of ion in s.
U	Voltage of the charged field in V.
v	Velocity of the ion after acceleration in m/s.
ω	Rit parameter, which is commonly assigned a value of 14.75.
[X]	Concentration of compound X in mmol/L
$[X_1]$	Concentration of DP 1 in mmol/L.
$[X_2]$	Concentration of DP 2 in mmol/L.
$[X_3]$	Concentration of DP 3 in mmol/L.
$[X_4]$	Concentration of DP 4 in mmol/L.

$[X_F]$	Concentration of furfural in mmol/L.
$[X_A]$	Concentration of formic acid in mmol/L.
X_{10}	The initial concentration of DP 1 in mmol/L.
X_{20}	The initial concentration of DP 2 in mmol/L.
X_{30}	The initial concentration of DP 3 in mmol/L.
X_{40}	The initial concentration of DP 4 in mmol/L.
z	Charge number.

1.0 Introduction

Ethanol is a source of renewable biofuel that can replace fossil fuels to power our vehicles. Currently most of the ethanol is produced from corn, which has resulted in a rise in corn prices and created food shortages in certain parts of the country in the latter part of 2008. Because of this sensitive food vs. fuel debate, lignocellulose is thus considered an alternative feedstock for the production of ethanol.

Lignocellulose feedstock basically encompasses wood, grass or any other non-edible plants, including agricultural and forestry residuals. Lignocellulose feedstock is abundant, and is generally low in plantation cost. Some examples of the many plants available for ethanol production are switchgrass, poplar, corn stover, and sweetgum. The three main components of lignocellulose are cellulose, hemicellulose and lignin, of which only cellulose and hemicellulose contain sugars such as glucose and xylose that can be used for ethanol production. However, cellulose and hemicellulose are polymers of which the sugars are not readily available for fermentation. The breakdown of these complex sugars into their monomeric forms, glucose and xylose, is needed before the sugars can be fermented by yeast or other microorganisms into ethanol or other biobased products.

One of the challenges in producing lignocellulosic ethanol is its cost disadvantage as compared to the production of gasoline, or corn-based ethanol. A major portion of the cost for lignocellulosic ethanol production is the pretreatment process, which is critical for the ensuing enzymatic hydrolysis step, which breaks down the complex sugars (DOE, 2006). However, the pretreatment process is also expensive because of the high cost of chemicals used in the process and the high temperatures (up to 250 ˚C), requiring the use of expensive stainless steel

equipment (Lloyd and Wyman, 2004). Moreover, in order to depolymerize hemicellulose into xylose monomer, the pretreatment process results in the production of formic acid and furfural, both of which are inhibitory to the enzymatic hydrolysis and fermentation (Palmqvist et al., 1999, Ximenes et al., 2010). Conversely, a complete depolymerization of hemicellulose into its xylose monomer is necessary for two reasons: (1) xylose monomer is the only xylose form that is fermentable by microorganisms, and thus is essential for a higher ethanol yield from the biomass; (2) partial hydrolysis of hemicellulose will produce xylose oligomers, which decreases enzymatic activities during cellulose depolymerization (Qing and Wyman, 2011).

Thus, the goal of this project is to understand how dilute acid pretreatment parameters affect hemicellulose depolymerization, maximize xylose concentrations, and minimizing by-products formation. The minimization of potentially inhibitory to microbial growth compounds can improve the downstream fermentation process, and ensure all sugar components in the lignocellulosic biomass be converted to ethanol, which thus improves the biomass-to-ethanol production efficiency. To progress towards this goal, rates and mechanisms of hemicellulose release must be determined. The understanding of xylose oligomers depolymerization rate into xylose monomer relative to xylose monomer degradation rate into the by-products can provide the basis in optimizing the hydrolysis conditions to maximize xylose yield.

The study of kinetic rates required large amounts of purified xylose oligomers, the intermediate products for hemicellulose degradation into xylose monomer. Commercially available xylose oligomers are expensive ($200 for 10 mg or $20,000 / g of products). Therefore, in order to facilitate the kinetic study, a less expensive alternative was needed. Birchwood xylan, which costs $200 for 100 g, will be used as the starting material, hydrolyzed into its oligomers mixture, and purified using centrifugal partition chromatography (CPC). Thus, a necessary

intermediate goal of this project is to develop a purification technique of xylose oligomers with the purity comparable to the commercially available source.

2.0 Objectives

The two objectives of this project are:

1. Purification of xylose oligomers using centrifugal partition chromatography.
2. Use these purified xylose oligomers to develop a kinetic model that represents xylose oligomers degradation, which can then be used to maximize xylan-derived monomer concentration, while minimizing the production of by-products, such as furfural and formic acid.

3.0 Literature Review

3.1 Current Developments in Biomass Pretreatment

Plant biomass is composed of cellulose, hemicellulose and lignin. Cellulose is composed entirely of D-glucose linked together by β-1,4,-glucosidic bonds (Jørgensen et al., 2007, Kumar et al., 2009). With a degree of polymerization of 10,000 or higher, cellulose polymers are arranged in a microfibril structure. The intermolecular hydrogen bond in the cellulose structure gives this primary metabolite its tensile strength, makes it insoluble in most solvents, and is partly responsible for its resistance to microbial degradation (Jørgensen et al., 2007). Hemicelluloses are heterogenous polymers made up of different polymers of pentoses, such as xylose and arabinose, hexoses including glucose, mannose and galactose, and uronic acids like 4-o-methylglucuronic acid, D-glucuronic acid, and D-galactouronic acid (Kumar et al., 2009). With a degree of polymerization below 200, hemicellulose can have side chains and some degree of acetylation (Jørgensen et al., 2007). Lignin is a complex, large molecular structure containing cross-linked polymers of phenolic monomers, such as coniferyl alcohol, coumaryl alcohol, and sinapyl alcohol (Kumar et al., 2009). Formed by the polymerization of phenyl propane units, lignin is an amorphous polymer that provides rigidity to the plant cell wall and resistance against microbial attack (Jørgensen et al., 2007). However, lignin is undesirable during biomass pretreatment. The presence of lignin impedes enzymatic hydrolysis by binding to the enzyme rather than allowing the enzymes to act on the cellulose chains (Brodeur et al., 2011, Hodge et al., 2008). Schematics of a plant cell wall are presented in **Figure 1**.

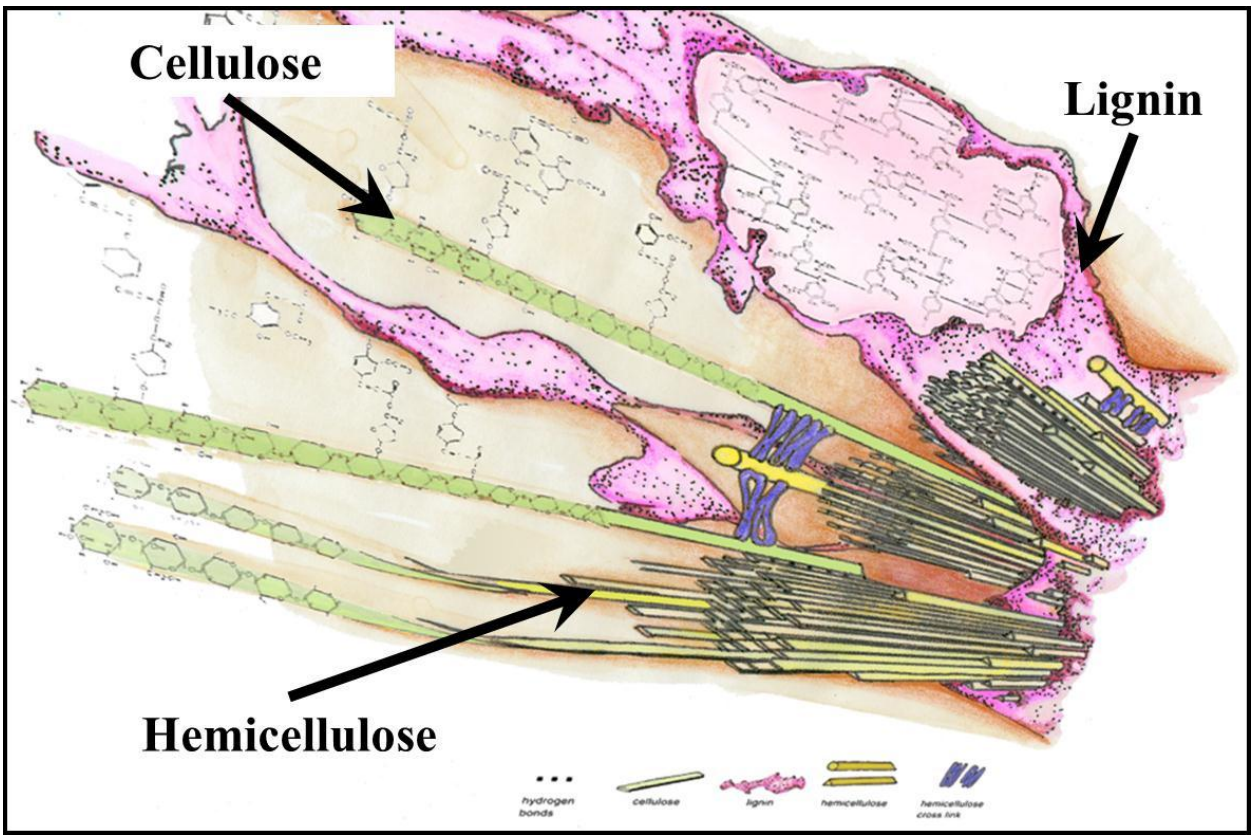

Figure 1: The structure of plant biomass is composed of cellulose, hemicellulose and lignin. (Produced by Zoe Anna Smith).

Cellulose is the largest component in the plant cell wall, accounting for 35-50 wt% of plant dry mass, followed by hemicellulose with 20-35 wt%, and lignin with10-25 wt% (Saha, 2003). The distribution of cellulose, hemicellulose and lignin varies between plant species. Both cellulose and hemicellulose are targeted to be fermentable sugars, but first must be broken down into their monomeric form so that they can be fermented by microorganisms into ethanol, propanol, butanol, or other biobased products (Kumar et al., 2009). The utilization of both sugars is essential to improve the biomass-to-ethanol production efficiency, and thus lower the overall ethanol production cost.

In the overall biomass to fuel process, after the feedstock is harvested and reduced in size, the biomass undergoes pretreatment and enzymatic hydrolysis to produce sugar monomers before being fermented into alcohol (Sharara et al., 2012). The goal of the pretreatment is to disrupt the protection of lignin on the carbohydrates and thus increase the accessibility of the enzymes to cellulose and hemicellulose bonds (Yang and Wyman, 2008). **Figure 2** presents, in a diagram, the effect of pretreatment on the cell wall. There are several leading pretreatment technologies, each with its specific objectives and properties.

Dilute acid pretreatment uses 0.22 - 0.98% aqueous sulfuric acid, at temperatures between 140 and 200˚C for times between 1 min and 2 hours (Sharara et al., 2012). Pretreatment results in the depolymerization of hemicellulose into its monomeric form (soluble in the liquid fraction), while the cellulose remains a constituent of the plant cell wall and is present in the solid fraction, ready to undergo enzymatic hydrolysis. During pretreatment, several degradation products are also formed, which pose problems to the downstream enzymatic hydrolysis and fermentation (Yang and Wyman, 2008).

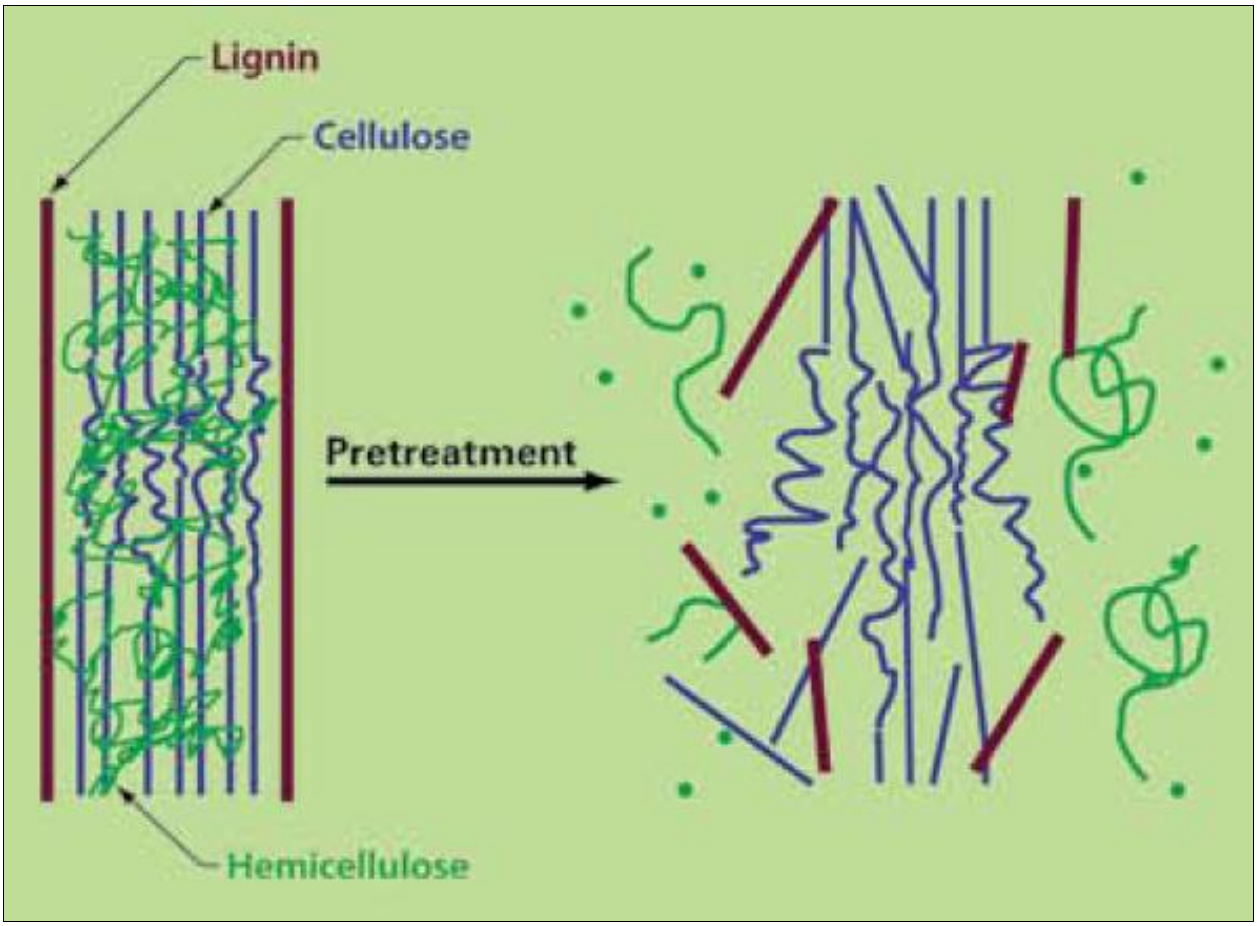

Figure 2: The objective of pretreatment is to disrupt the structure of the cell wall, allowing the polysaccharides of cellulose and hemicellulose to be more susceptible to enzymes that will break down the polysaccharides into sugar monomers. Picture is reproduced from (Mosier et al., 2005).

The ammonia fiber explosion (AFEX) process treats biomass with liquid ammonia at pressures of 1.4 - 4.8 MPa, temperatures from 60 - 200 ˚C and times of 5 - 45 min (Sharara et al., 2012). The ammonia causes depolymerization of lignin and breakdown of lignin-carbohydrate linkages. AFEX-treated hemicellulose remains in the oligomeric form, which requires additional enzymes to break down the oligomers into monomers (Mosier et al., 2005). Also, the high cost of ammonia prompts the need for ammonia recovery, which drives up the pretreatment cost (Brodeur et al., 2011).

Lime pretreatment involves slurrying calcium hydroxide or sodium hydroxide with water, spraying the mixture onto the biomass material, and storing the material for a period of hours to weeks. The temperature of the pretreatment process ranges from 25 - 150 ˚C (Sharara et al., 2012). Lignin and the acetyl and various uronic acid substitutions on hemicellulose are removed from the biomass, which improves the reactivity of the remaining polysaccharides (Mosier et al., 2005). Although the reaction of lime pretreatment is slower than other pretreatment technologies, the relatively low cost of lime, its safe handling, and the reusability of lime in lime kilns are the advantages of this technology (Yang and Wyman, 2008).

Controlled pH pretreatment uses water to react with biomass at 170 - 200 ˚C from 5 - 20 min (Sharara et al., 2012). The pH of the pretreatment is controlled between 4 and 7 to avoid the formation of degradation products such as furfural and hydroxylmethyl furfural, but yet improve the enzyme susceptibility of cellulose (Yang and Wyman, 2008). Potassium hydroxide is used for pH control in this pretreatment (Weil et al., 1998). The hemicellulose produced from the pretreatment remains as oligosaccharides, which required enzyme to breakdown into monosaccharides (Mosier et al., 2005).

Ammonia recycle percolation (ARP) pretreatment passes aqueous ammonia (5 - 15 wt %) through biomass at 80 - 180 ˚C, with the ammonia separated from the biomass and recycled in the effluent (Yang and Wyman, 2008). The ARP-treated solid contains short-chained cellulosic material with high glucan content and low lignin, while the aqueous ammonia contains the majority of the lignin (75-85%) and some hemicellulose (50-60%) (Brodeur et al., 2011). As a result, the remaining solid is more digestible to enzymes, without experiencing the formation of additional inhibitory products. However, high energy costs and liquid loadings are the disadvantages of the ARP process (Yang and Wyman, 2008).

Ionic liquids (IL), which have low vapor pressure, low toxicity, and high stability have also been used in biomass pretreatment. The IL pretreatment of biomass is usually conducted at ambient pressures, temperatures of 90 - 130 ˚C and times of 1 - 24 hrs. The anion of the IL breaks up the cellulose crystalline hydrogen bonded structure, thus making cellulose more accessible to enzyme hydrolysis, while lignin and hemicellulose are not affected by the treatment. However, the high cost of ILs and its potential toxicity to fermenting microorganisms are several of its drawbacks as compared to other pretreatment technologies (Brodeur et al., 2011).

The features and the advantages of the leading pretreatment technologies are summarized in **Table 1**. Dilute acid pretreatment, despite its drawbacks, is commonly used in biomass pretreatment because of the effectiveness of dilute acid in breaking down hemicellulose and the low cost of sulfuric acid (Lloyd and Wyman, 2004). Moreover, the ease of use in dilute acid pretreatment allowed the adoption of this technology on a wide range of biomass feedstocks (Wyman, 1999). A good understanding of dilute acid pretreatment would thus improve the biomass-to-sugar yield and reduce the cost of hemicellulose hydrolysis.

Table 1: Summary of leading pretreatment technologies

Pretreatment method	Advantages	Disadvantages
Dilute acid	• Effective in breaking down hemicellulose • Low acid cost	• Formation of inhibitors
Ammonia fiber explosion (AFEX)	• Effective in removing lignin • Low formation of inhibitors	• High ammonia cost
Lime	• Effective in removing lignin and hemicellulose • Low cost of lime	• Slow reaction
Controlled pH	• Low formation of inhibitors	• Incomplete hydrolysis of hemicellulose
Ammonia recycle percolation (ARP)	• Effective in removing lignin and hemicellulose • Low formation of inhibitors	• High energy requirement • Low solids loading
Ionic liquid (IL)	• Effective in removing cellulose	• High cost of solvent • Toxic to microorganisms

3.2 Hemicellulose Degradation Pathways

The composition and arrangement of cellulose in all plant species is identical. However, that is not the case for hemicellulose as the composition and arrangement vary from plant species to plant species. Hemicelluloses are classified according to the main sugar in the backbone of the polymer, xylan (β-1,4-linked xylose) or mannan (β-1,4-linked mannose). Xylan, with chains of xylose molecules linked by β-1,4-bonds, is the most common hemicellulose. As an example, the percentage of xylose in birchwood xylan, rice bran neutral xylan, arabinoxylan, and corn fiber xylan is 89%, 46%, wheat 66%, and 51% xylose, respectively, with the remaining sugar being arabinose, glucose, mannose, and galactose (Saha, 2003).

Although dilute acid is most likely the pretreatment that will be scaled-up, it poses problems in terms of producing inhibitory degradation products that hinder enzymatic hydrolysis and fermentation. During dilute acid pretreatment, the degradation of xylan will yield xylose oligomers of different lengths, before forming the coveted xylose monomers. Additionally, xylose has been documented to form furfural and formic acid during dilute acid hydrolysis (Nimlos et al., 2006, Palmqvist and Hahn-Hägerdal, 2000). Both compounds inhibit the fermentation of carbohydrate monomers into ethanol, where it was shown to reduce the specific growth rate, the cell-mass yield on ATP and specific ethanol productivities (Palmqvist et al., 1999). Moreover, insufficient hydrolysis of hemicellulose will result in a high concentration of xylose oligomers, which inhibit the enzymatic hydrolysis of cellulose and xylan (Kumar and Wyman, 2009, Qing and Wyman, 2011). Therefore, a high quality sugar stream from xylan requires a practically complete conversion of xylan into xylose monomer without producing excessive amount of inhibitory by-products.

The formation of inhibitory products, such as furfural and formic acid, results during xylose degradation in the presence of acid. In a study conducted using quantum mechanical calculations supported by NMR data, Nimlos et al. (2006) showed that in the presence of mildly hot acidic solutions, xylose can form furfural and three molecules of water when the oxygen at hydroxyl group number two (O2) was protonated, as shown in **Figure 3**. Similarly, the protonation of the oxygen at hydroxyl group number three (O3) results in the formation of formic acid and a 4-hydroxylbut-2-enal, a four carbon molecule. The protonation of oxygen at other hydroxyl groups did not result in any new compound formation and will remain as xylose molecule.

Furfural, which itself is a feedstock for other desired compounds such as furfuryl alcohol, furan, tetrahydrofuran, 5-hydroxylmethylfurfural, and methyl-tetrahydrofuran (MTHF), can further degrade into a carbonaceous species, known as humin (Weingarten et al., 2010, Dias et al., 2005, O'Neill et al., 2009). Using ZSM-5 zeolite in H^+ form at 413 to 493 K, the degradation of xylose and furfural was examined (O'Neill et al., 2009). Furfural formed from xylose degradation was unstable and degraded further into formic acid. The rate of furfural degradation increased at elevated temperature. For example, the furfural concentration was reduced by half from its maximum concentration in 10 min at 493 K. The resulting formic acid, which had lower concentrations when compared to that of furfural at temperature between 413 and 433 K, was unstable at 493 K, and rapidly degraded to solid species. The amount of solid formation was directly correlated to the decline in furfural concentrations, suggesting that furfural degraded directly into solids (O'Neill et al., 2009). Worth nothing, although formic acid is formed by furfural degradation, it can also form furfural via an autocatalytic mechanism (Antal et al., 1991,

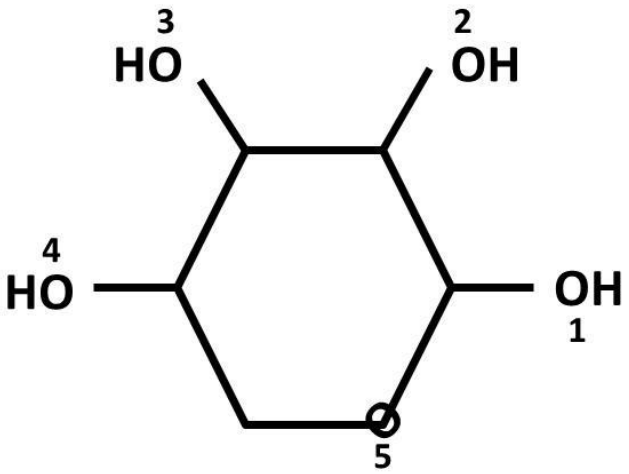

Protonation on	Results
O1	Reform xylose
O2	Furfural Formed
O3	Formic Acid Formed
O4	Unlikely
O5	Unlikely

Figure 3: The protonation of hydroxyl groups on a xylose molecule from a quantum mechanical modeling by (Nimlos et al., 2006).

Dias et al., 2005). Therefore the reaction of furfural to formic acid can be considered reversible, thus complicating the understanding of a degradation study.

Formic acid formed from xylose degradation is not stable, especially at high temperatures, usually above 320 ˚C. At temperatures between 320 and 500 ˚C, in the absence of added oxygen, formic acid can degrade to form carbon dioxide, carbon monoxide, hydrogen and water (Yu and Savage, 1998). Water was determined to have a catalytic effect on the decarboxylation of formic acid into carbon dioxide, hydrogen and water, and the dehydration of formic acid to form carbon monoxide and water (Akiya and Savage, 1998, Yu and Savage, 1998). Thus, dilute acid pretreatment conditions provide an ideal medium in which hemicellulose can degrade into a mixture of inhibitory compounds.

The summary of hemicellulose degradation is shown in **Figure 4**. Birchwood xylan, which is a type of hemicellulose, depolymerizes into xylose oligomers of various lengths, before forming xylose monomer. Further reaction resulted in the degradation of xylose monomer into furfural and formic acid, both of which are undesired for the enzymatic hydrolysis and fermentation. Furfural can degrade further into formic acid and solids, while formic acid can degrade into carbon dioxide, carbon monoxide, water, and hydrogen. Worth noting, the reaction path of furfural degradation into formic acid is a reversible reaction.

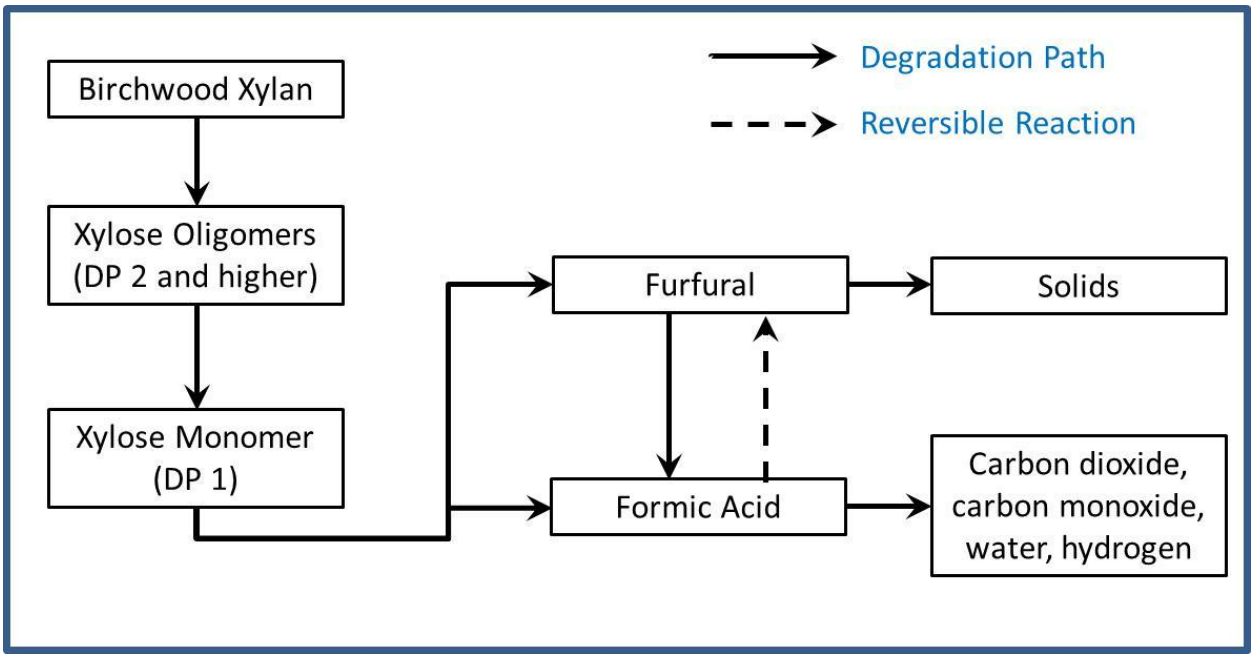

Figure 4: Summary of hemicellulose degradation path.

3.3 Current Study of Hemicellulose Kinetics

Several studies have been conducted to characterize hemicellulose depolymerization kinetics. In a study conducted by Kumar and Wyman (2008), pure xylose oligomers, such as xylobiose (DP 2), xylotriose (DP 3), xylotetraose (DP 4), and xylopentaose (DP 5) were purchased from a commercial source. Most likely these purchased compounds were of high quality, bearing little resemblance to biomass hydrolysates, which contains other sugars. Kumar and Wyman (2008) hydrolyzed xylose and the purchased oligomers at 160 ˚C at four different pH conditions: 1.45, 2.75, 4.75 and 7.00 for 0 to 90 min. The concentrations of xylose and each oligomer were determined at the end of the hydrolysis cycle. From the study, the depolymerization of xylose monomer and oligomers was characterized by first order kinetics. Also, the degradation pathways were found to be non-linear: DP 4 could depolymerize directly into a mixture of DP 1, DP 2, DP 3, and by-products, rather than into solely DP 3. The presence of acid, as indicated by a lower pH during hydrolysis, reduced the decomposition of lower DP oligomers, such as DP 2 and DP 3, into by-products. On the other hand, the pH effect was less noticeable on DP 4 and DP 5, as reflected by the negligible rate of by-product formation.

The work by Kumar and Wyman (2008) led to several major conclusions: (1) the depolymerization of xylose oligomers was non-linear, resulting in the fact that all possible depolymerized compounds should be considered while setting up the kinetic models; (2) the depolymerization of most, if not all of the compounds studied, could be modeled by first-order kinetic relationships, which greatly simplify the reaction model; (3) the concentration of the studied compounds may possibly affect the depolymerization rate constants. In the study by Kumar and Wyman (2008), the kinetic model was determined to be independent of xylose concentrations, barring that they were in the range of 1 to 5 mg/mL.

Although informative, the study conducted by Kumar and Wyman (2008) could be improved. First, the formation of by-products, such as formic acid, and furfural, could be monitored. The study lumped the loss of all the xylose oligomers and monomer into one general degradation products term, without tracking the formation of individual by-products. Secondly, the commercially available xylose oligomers were not representative of the oligomers that are hydrolyzed from processed biomass. Naturally produced xylose oligomers from biomass commonly contain acetyl groups (Palmqvist and Hahn-Hägerdal, 2000), which may not depolymerize according to the model developed by Kumar and Wyman (2008) which was based on oligomers that were devoid of acetyl groups. Lastly, the number of variables used in the Kumar and Wyman (2008) kinetic model can be increased where, in addition to hydrolysis time, pH and temperature can also be included.

In another study, Morinelly et al. (2009) used three types of biomass, including aspen, balsam, and switchgrass as the raw materials for the study of xylose oligomer depolymerization. The hydrolysis of the feedstock was analyzed at three distinct temperatures: 150, 160 and 175 ˚C, using 0.25, 0.50, and 0.75 wt% sulfuric acid, for 0 to 180 min. Total oligomers, xylose monomer, furfural, and xylose degradation by-products were determined at different hydrolysis times. Worth noting, the quantification of xylose oligomers in this study was based on a total sugar analysis, a method developed by National Renewable Energy Laboratory (NREL), which measures the increase in xylose monomer after complete hydrolysis of xylose oligomers into xylose monomer (Sluiter et al., 2006). Therefore, all xylose oligomers were termed as one single compound, rather than measured individually as in the study by Kumar and Wyman (2008). Morinelly et al. (2009) also determined that first order kinetics provided a good approximation of the model in characterizing all of the compounds of interest. The initial composition analysis of

each biomass material showed that the dry weight of xylan, the polysaccharide form of xylose, in aspen, balsam, and switchgrass were 14.60, 6.23, and 19.73%, respectively, with the remaining mass composed of lignin and polysaccharides of other sugars, such as glucose, galactose, arabinose, and mannose. The kinetic models provided a satisfactory curve fit to the concentration of xylose monomer. However, the xylose oligomer and furfural data were not as accurately characterized by the model. The lack-of-fit of xylose oligomer data by the model could be attributed to the technique used in this study to quantify xylose oligomers, which did not measure the concentration of individual xylose oligomers. Each xylose oligomer had a different depolymerization rate, as shown in the work of Kumar and Wyman (2008), and thus contributed differently to the rate of formation of xylose. The lack-of-fit of the furfural data was caused by the presence of other sugars, mainly arabinose, which can also degrade into furfural. However, the study reported by Morinelly et al. (2009) did offer several useful insights: The selection of pure xylose source for the kinetic study is important to avoid the introduction of furfural from other monosaccharides, such as arabinose, which would not be monitored during the study. Also, solids loading should be considered and incorporated into the kinetic study. In the study by Morinelly et al. (2009), a 5% solid loading of biomass during hydrolysis resulted in faster degradation of oligomers and higher concentrations of furfural as compared to that of 10% solid loading, under similar conditions of temperature and acid concentration. According to Morinelly et al. (2009), the effect could possibly be attributed to the lower concentration of neutralizing minerals present in the biomass.

In another study, Chen et al. (2007) used corn stover to determine the formation of 19 hemicellulose-derived degradation products. The biomass was hydrolyzed under 12 different pretreatment conditions, with temperature ranging from 160 to 200 ˚C, hydrolysis times between

2 and 64 min, and at a constant 0.7% acid concentration. The concentration of each degraded compound was measured at different hydrolysis times for each pretreatment condition. Combined severity (CS), which combines temperature (T_r), hydrolysis time (t), and acid concentration (pH) into one variable, was introduced in the model. The relationship between combined severity and its component variables is shown as follows:

$$\text{Severity } (R_o) = t * \exp (T_r - 100/ \omega) \quad \textbf{(1)}$$

$$\text{Combined severity (CS)} = \log (R_o) - \text{pH} \quad \textbf{(2)}$$

where

t = hydrolysis time of biomass at reaction temperature, in min.

T_r = reaction temperature, in ˚C.

ω = fit parameter, which is commonly assigned a value of 14.75.

pH = acidity of the aqueous solution, as pH.

The study by Chen et al. (2007) focused on the ω value of the combined severity, which was commonly thought to be a constant of 14.75. Through trial and error, the combined severity was calculated using different ω values to produce the best curve fit of the concentration of individual compounds as a function of combined severity. Accordingly, the ω value was calculated for each compound. With a known ω value, the rate of formation for the compound could be determined. The study by Chen et al. (2007) did not include xylose oligomers. However Chen et al. (2007) drew several important conclusions. First, the ω value was not constant, as shown in the results, contradicting the commonly held belief that it should be treated as a constant (Chen et al., 2007). Finally, furfural, a product from xylose degradation, did not display

a first-order formation rate, which was opposite to the belief that furfural degradation was considered to be a first order reaction by Rose et al. (2000).

In conclusion, the approach taken by Kumar and Wyman (2008) showed that the depolymerization of oligomers into monomers and lower depolymerization (DP) products occurred simultaneously as the degradation products were produced. Hydrolyzing real life oligomers would have proven to be a better representation of biomass deconstruction. In pioneering work, Li et al. (2003) produced oligomers standards, up to a degree of polymerization of ten, from oat spelt xylan, detecting them by ion-moderated partition chromatography. However, no separation was carried out, indicating that securing sufficient oligomer accumulation proved challenging. Because no method of oligomer fractionation was devised, their accumulation was difficult, and for this reason, Kumar and Wyman (2008) had to conduct the degradation study with purchased oligomers. Moreover, in the Kumar and Wyman (2008) study, degradation products were not identified, but lumped together. Kumar and Wyman (2008) calculated the degradation and depolymerization reaction constants by assuming that the reaction rates remained constant throughout the depolymerization process. In the other approach adopted by Morinelly et al. (2009), the depolymerization of hemicellulose into oligomers, xylose, furfural and formic acid was assumed to occur in a linear fashion. By using aspen, balsam, and switchgrass feedstocks as the starting material, first order reaction constants were calculated, but the developed reaction model for xylose oligomers and furfural did not exactly fit the experimental data because of the difference in the depolymzering rate of various xylose oligomers, and the presence of different sugars such as arabinose and glucose, which could also form furfural. The study by Chen et al. (2007) indicated that the use of combined severity was

not accurate in predicting the hydrolysis conditions because the ω value in the combined severity equation varies for different compounds.

Currently available kinetic models for hemicellulose degradation do not address the relationship between the rate of degradation of xylose oligomers and the solvent system, including temperature. Further understanding xylose oligomers, through the development of a robust kinetic study will provide a better understanding of xylan depolymerization at various hydrolysis conditions, which should lead to increased ability to predict hydrolysis conditions that produce maximum xylose, but minimize the production of by-products.

3.4 Severity Constant

The combined severity parameter is a summation of various effects of different hydrolysis conditions, such as temperature, pH of the solvent, and the duration of hydrolysis. This allows comparison of the pretreatment performance based on sugar and inhibitor yield.

3.4.1 Equation of Combined Severity

The concept of combined severity parameter assumes that the overall reactions display a first-order dependence on key reaction components, such as lignin and carbohydrates, maintaining its rate constant dependent on reaction temperature through the Arrhenius-type relationship. Moreover, the determination of these parameters is based on the average reaction rate over a long but finite reaction time, rather than based on the initial reaction rate (Chum et al., 1990).

The combined severity (CS) used in pretreatment is defined as:

$$CS = \log \{t * e^{[(Tr - Tb) / \omega]}\} - pH \quad \textbf{(3)}$$

where:

t = hydrolysis time of biomass at reaction temperature, in min.

T_r = reaction temperature, in ˚C.

T_b = reference temperature, which was set to 100˚C.

ω = fit parameter, which is commonly assigned to a value of 14.75.

pH = acidity of the aqueous solution, in pH.

As shown in **Equation 3**, combined severity is a function of hydrolysis time (t), reaction temperature (T_r), and the pH of the hydrolysate (pH). The fit parameter (ω), is related to the activation energy via

$$\omega = T_f^2 * R / E_a \quad \textbf{(4)}$$

where:

T_f = temperature chosen to be in the middle of the range of experimental conditions, in ˚C.

R = universal gas constant.

E_a = apparent activation energy.

As shown in **Equation 4**, the fit parameter (ω) is related to the activation energy of the reaction, and thus varies for different feedstock materials, each with different compositions of cellulose and hemicellulose. According to Chen et al. (2007), for the Organosolv removal of xylan and glucan from aspen wood, a value of ω = 11 in the calculation of combined severity parameter gave a good curve fit to experimental results, while the removal of lignin required an ω =10 value for the optimal fit of data. Therefore, ω is an empirically determined value that provides the best data fit for the relationship between combined severity parameter and the key measurement such as the percentage of hemicellulose removal for the Organosolv process, the yield of monosaccharides, or the formation of inhibitors. Determination of the ω value can be conducted in other pretreatment systems, such that the optimum carbohydrate yields can be obtained.

3.4.2 Modification of Combined Severity Constant

The combined severity constant has been widely reported when comparing different pretreatment conditions, such as lime pretreatment hydrolysis, ammonia fiber explosion (AFEX), steam explosion, and dilute acid hydrolysis (Pedersen and Meyer, 2010). The analysis of hydrolysis conditions that generate optimum monosaccharide yields are often linked to the calculated combined severity constant. However, variations in yield were noted within similar combined severity constants (Lloyd and Wyman, 2005). In one study on the effects of dilute acid hydrolysis on corn stover, constant severity values were inadequate to account for all the reactions that were occurring in the hydrolysate matrix (Chen et al., 2007). Chen et al. (2007) reported that the combined severity parameter was poorly correlated to the accumulation of degradation products. When comparing hydrolysis conditions using similar combined severity parameter but different reaction temperatures and times, the treatment conditions with higher temperature were consistently observed to yield higher degradation products concentrations, as compared to those obtained at lower temperature conditions. Based on the collected data, Chen et al. (2007) modified the value of ω used in the combined severity parameter to improve the prediction of the product accumulation. From the resulting modification, the value of ω was determined to be compound dependent. For example, the formation of formic acid had better correlation to the combined severity with an ω value of 9 for furfural, as compared to an ω value of 6. Therefore the use of combined severity is strictly empirical, as shown by the determination of ω value using the best data-fit.

3.5 Arrhenius Equation

The Arrhenius equation is a practical tool to relate the degradation rates, encountered during dilute acid pretreatment, to temperature and sulfuric acid concentration. The Arrhenius equation is presented in **Equation 5** (Esteghlalian et al., 1997, Jensen et al., 2008, Jin et al., 2011, Nabarlatz, et al., 2004, Xiang et al., 2004, Yat et al., 2008).

$$k = A_o C^m \exp(-E/RT) \quad \textbf{(5)}$$

where k is the reaction rate constant (min^{-1}), A_o is the pre-exponential factor (min^{-1}), C is the acid concentration (wt%), m is the acid concentration exponent, E is the activation energy in (kJ/mol), R is the gas constant (8.314×10^{-3} kJ/mol/K), and T is the hydrolysis temperature (K). A typical value for the unitless m ranges between 0.4 and 1.6 (Lloyd and Wyman, 2004).

The sulfuric acid concentration used in the calculations is in the range of 0.25% and 1% acid (Yat et al., 2008). However, the above equation cannot be used for calculations depicting solvent system devoid of acid because the acid concentration term C would be zero, reducing the value of degradation rate, k, to zero. Because the consideration of a water only hydrolysis is essential because of the benefits of eliminating sulfuric acid during the pretreatment, an alternate approach was considered. The kinetic model as proposed by Saeman (1945) and Kim et al. (2012) with the following equation:

$$k = [k_0 \times (H^+)^m] \times \exp(-E/RT) \quad \textbf{(6)}$$

where k_0, (H^+),and m are the pre-exponential factor in min^{-1}, the concentrations of hydrogen ion in mol/L, and the unitless acid concentration exponent, respectively.

3.6 Analytical Methods

Hemicellulose and cellulose are made up of carbohydrates, a group of organic compounds that contain aldehyde or ketone functional groups, with molecular formula of $C_n(H_2O)_n$ (Levy and Fügedi, 2006). The molecular structure of carbohydrates ranges from the simplest form of monosaccharides, such as glucose, mannose, xylose, fructose, and arabinose, to the complex structure of oligosaccharides and polysaccharides, such as starch and cellulose.

3.6.1 HPLC

Liquid chromatography, coupled with an RI detector, has been used extensively in the biofuel industry to detect carbohydrates. Sluiter et al. (2006) published a protocol that is used by the National Renewable Energy Laboratory (NREL) that uses high performance liquid chromatography (HPLC) columns, packed with ionic resin, using size exclusion and ligand exchange mechanisms, to achieve separation of different types of monosaccharides, as well as to determine the different molecular weight of oligosaccharides. The chromatographic response of carbohydrate in RI detector is linear and quantitative (Sluiter et al., 2006). Because the RI detector is not compatible with eluents flowing in the gradient mode, all HPLC protocols that utilize an RI detector need to be conducted with isocratic mobile phases, limiting the selectivity of analytes during the separation of carbohydrates.

3.6.2 CPC-ELSD

Centrifugal partition chromatography (CPC) is a liquid-liquid separation technique that does not contain a solid support (Shibusawa et al., 2003). A CPC column consists of many channels connected in series through ducts, arranged in a circle around the rotor, parallel to the centrifugal field (Foucault et al., 1993). One of the liquid phases becomes the stationary phase of the CPC because of the rotation of the CPC rotor, creating a density difference between the two phases, while the second liquid phase becomes the mobile phase (Marchal et al., 2002).The CPC can be operated in two modes: ascending or descending. In ascending mode, the denser liquid phase is injected first into the CPC column and acts as the stationary phase. The less dense liquid phase is then injected into the rotor and eluted through the CPC column, and acts as the mobile phase. Conversely, in the descending mode, the less dense liquid phase will become the stationary phase, while the denser liquid phase becomes the mobile phase (Marchal et al., 2002). By not using solid phase column supports, CPC columns allow the solutes to access the full volume of the column, as opposed to the volumes filled with packing material in solid phase systems (Berthod et al., 2007). CPC has been documented in the fractionation of various compounds, such as sugars (Shinomiya et al., 1999), flavonoids (Engelberth et al., 2008, Shibusawa et al., 2003), and antibiotics (Wang-Fan et al., 2000).

ELSD detection is more universal than the RI detector by allowing for gradient mobile phase elution. The mobile phase entering the ELSD is nebulized and vaporized, and thus has no effect on the detection of the remaining solute materials. Therefore, nonvolatile compounds, such as carbohydrates, are suitable for ELSD detection (Wei and Ding, 2000). The connection of ELSD to CPC allows the detection of eluted compounds from CPC, even if the phase composition of the eluent changes.

3.6.2 HPAEC-PAD

3.6.2.1 Theory of pulsed amperometric detection (PAD)

Pulsed amperometric detection is a type of electrochemical detector that targets specifically on hydroxyl (OH) groups in carbohydrates (Cataldi et al., 2000), and offers several advantages over other common type of detectors in the detection of carbohydrates. The detection of carbohydrates by pulsed amperometric detection is based on the targeting of hydroxyl (OH) groups in carbohydrates (Cataldi et al., 2000). PAD is superior to ELSD because the quantification of carbohydrates is more reproducible in complex sample matrix (Cataldi et al., 2003). Gold and platinum are commonly used as the electrodes in PAD to sense the target compounds. The oxidation of carbohydrates on the electrode surface creates a current of which its amount is related to the extent of oxidation on the electrode surface. The detection of carbohydrates by pulsed amperometric detector is generally conducted in three stages (Cataldi et al., 2000, Dionex Corporation, 2004, Johnson et al., 1993, Olk, 2008) as shown in **Figure 5**.

1. Amperometric detection: An electrical potential is established at the electrode surface to facilitate the oxidation process of hydroxyl groups in carbohydrates on the electrode surface where the free radicals (·OH) produced from the oxidation process will be absorbed by the electrode surface. The potential on the electrode was selected to promote the oxidation of hydroxyl groups and the adsorption of the free radicals on the electrode surface. As more oxidized compounds are formed on the surface, the surface reactivity of the electrodes attenuate because of the poisoning of the surface of the electrodes. The oxidation process creates a new voltage on the electrode electrodes and thus electrical current is generated by the oxidation process (Dionex Corporation, 2004).

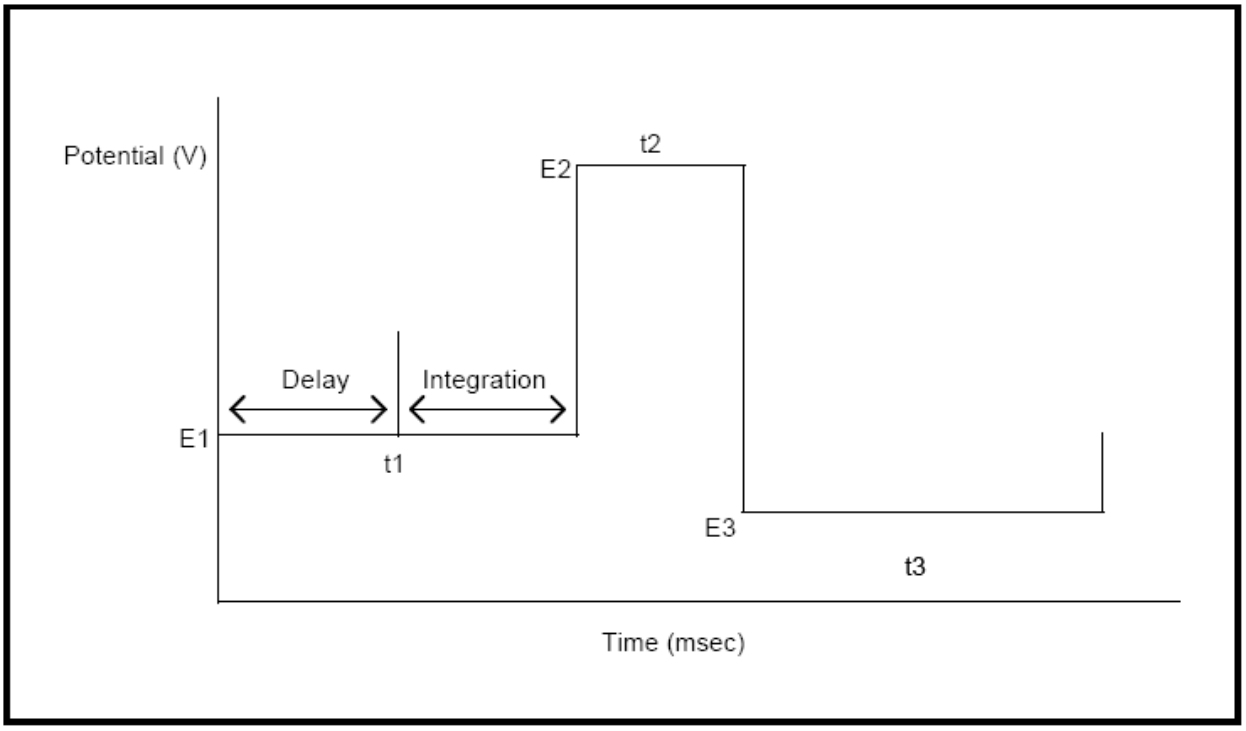

Figure 5: Three stages of pulsed amperometric detection, with E1 as the amperometric detection potential, E2 as the oxidative cleaning potential, and E3 as the reductive reaction potential (Dionex Corporation, 2004).

2. Oxidative cleaning: The accumulated detection products cause extensive fouling on the electrode surface. Therefore to remove the products from the electrode surface, the potential across the electrode is raised to a high positive potential to desorb the compounds from the electrode surface. The electrode surface is completely oxidized at this high electrical potential and the oxidized compounds are completely removed from the surface of the electrode.
3. Reductive reaction of electrode: Following a high positive potential, the electrode surface is applied with a negative potential to reduce the electrode surface back to electrode. The reactivity of the electrode is restored to the level prior to the detection, and thus be ready for the next cycle of compounds detection.

The produced current from the amperometric detection during the oxidation stage of electrode by the hydroxyl group of carbohydrates can be quantified as either an average current during this detection stage, or integrated as the coulomb of electrons transferred, which are proportional to the amount of hydroxyl groups is reacted to the electrode surface (Olk, 2008). The amperometric detection using multiple steps of electro potential control has thus given the name of the detection as pulsed amperometric detection.

3.6.2.2 Application of pulsed amperometric detection

A pulsed amperometric detector can be used for the detection of carbohydrates. The instruments used for separating the analytes prior to the detection include high performance anion exchange chromatography (HPAEC).

A HPAEC-PAD takes advantages of the weak acid nature of carbohydrates, by separating them at high pH (Dionex Corporation, 2004). Carbohydrates have a pKa of about 12, and thus at high pH, will dissociate and be separated by a HPAEC column, which is filled with base-stable anion that is suitable for high pH applications. The common silica-based column is not suitable at high pH applications because it will be dissolved in high pH conditions. Separation of carbohydrates is achieved because of the affinity of ionized groups on the carbohydrates, for the retention time is shortest for monosaccharides, then disaccharides and finally oligosaccharides. The retention time of the sugar analytes is proportional to the degree of polymerization of the carbohydrates. Sodium hydroxide is used widely as the mobile phase to create the high pH condition necessary for the dissociation of carbohydrates. The addition of sodium acetate in sodium hydroxide reduces the retention time of the carbohydrates analytes. However, when using dilute alkaline mobile phase (10-20 mM NaOH), carbonate uptake in the mobile phase will interfere with the chromatographic elution, and thus causing shifting of retention time (Cataldi et al., 2003).

Because of different pKa values, each monosaccharide can be separated from one another through alkaline mobile phase elution. However, a strong alkaline mobile phase creates co-elution of the monosaccharides because of the close proximity of pKa values among the monosaccharides (e.g. fructose has pKa of 12.03, mannose has pKa of 12.08, xylose has pKa of 12.15, glucose has pKa of 12.28, galactose has pKa of 12.39 (Dionex Corporation, 2004). The

use of pure water as mobile phase allows a higher selectivity of the separation. However, two problems are created with the use of water or dilute alkaline mobile phases: 1) lost of ion-exchange capacity of the column; and, 2) the incompatibility with the PAD to detect the separated carbohydrates. The first problem was overcome by the regeneration of the column with concentrated NaOH to restore the ion-exchange capacity of the column after each elution that uses weak alkaline or water. The second problem was addressed by adding a base to the eluents to raise the pH for PAD. The use of water eluents for monosaccharide separations in HPAEC column results in long retention time of the elution, a condition that can be addressed with the addition of sodium acetate in the mobile phase. The resulting separation results in faster elution, without compromising the separation resolution (Cataldi et al., 2003). The use of water or dilute alkaline eluents ([OH-] as low as 2 mM) is necessary for monosaccharides separation because each monosaccharide has a retention time very close to one another. Shorter retention times among eluted compounds, can lead to the misidentification of neighboring peaks. Therefore, careful consideration is needed in balancing the shorter elution time with the need of obtaining satisfactory separation resolution among the peaks.

3.6.1 MALDI-TOF-MS

Carbohydrate molecules, which are polar, are not easily vaporized, a condition necessary for MS detection. Therefore derivatization of carbohydrates (Burke et al., 1987, Camilleri et al., 1998, Crowell and Burnett, 1967, Fox, 1999) and matrix assisted laser absorption ionization mass spectrometry (MALDI-MS) were used in MS analysis of carbohydrates to improve the detection of the molecules.

MALDI is a soft ionization technique that was developed to detect biomolecules, which tends to be more fragile, and susceptible to molecular fragmentation, using conventional ionization methods. The use of a matrix material, which generally consists of small organic molecules, protects the analytes that are embedded in the matrix from the bombardment of photon during the ionization. Moreover, the matrix material can also absorb the laser light, which thus increases the intensity of the analytes, while at the same time, minimizes the fragmentation of analytes. MALDI is therefore commonly used in detecting large molecules such as proteins.

The ability of the analyte to embed into the lattice structure of the matrix is a precondition for MALDI process. During the ionization by laser under high vacuum condition, both the sample and matrix molecules are vaporized, and released into the gas phase. The vaporized molecules are then drawn towards an electrode mounted a few mm away. The electrostatic field generated by the electrode causes the molecules to accelerate from the sample surface towards the analyzer at different velocity based on the m/z ratio of the molecules.

3.6.1.1 Principle of time-of-flight (TOF) mass analyzer

The TOF mass analyzer determines the molecular mass of the ions by measuring the period of time between the acceleration of the molecules and the time they impact on the detector. The ionized molecules accelerated by an electrostatic field will subsequently pass a field-free drift region, which can be 1 to 4 m long. The separation of molecules is achieved through the difference in the *m/z* ratio of the molecules: heavier molecules with higher *m/z* ratio will take longer time to impact the detector than the lighter molecules. Knowing the accelerated voltage and the length of the drift region, the *m/z* ratio of a molecule can be calculated by measuring the flight time of the molecule (Bruker Corporation, 2004).

The kinetic energy of an accelerated ion is defined as:

$$E_{kin} = \frac{1}{2} m v^2 = z * e * U \quad \textbf{(7)}$$

The velocity of ion can be calculated by measuring the ion flight time and the distance of field-free region of the flight tube:

$$v = L / t \quad \textbf{(8)}$$

Replacing **Equation 7** with velocity from **Equation 8**:

$$E_{kin} = \frac{1}{2} m (L/t)^2 = z * e * U \quad \textbf{(9)}$$

$$m/z = 2 * e * U * (t/L)^2 \quad \textbf{(10)}$$

where

E_{kin} = kinetic energy of the ion

m = ion mass

v = velocity of the ion after acceleration

z = charge number

e = elementary charge, $1.602*10^{-19}$ coulombs

U = voltage of the charged field

L = the distance of field-free region

t = flight time of ion

As shown in **Equations 7 - 10**, the m/z ratio of an ionized molecule is proportionally influenced by the square of flight time of ion (t), given the known voltage (U) and the distance of field-free region (L). The measurement of flight time can thus provide the related mass information of the molecules. Calibration of TOF is accomplished with well-known reference masses.

3.6.1.2 Applications of MALDI-TOF-MS

The MALDI-TOF-MS was created mainly to detect fragile compounds, such as biomaterial, which can easily be fragmented using conventional ionization method. The use of matrix material to protect the analytes allows a higher intensity of analytes when applied with high laser intensity and less fragmentation of analyte during ionization for easier identification of compounds with large molecular mass. Moreover, the mass range of TOF mass analyzer is theoretically without limitation, although the resolution and sensitivity will be reduced when analyzing sample with a wide mass range (Bruker Corporation, 2004).

3.7 Plan of Work

In summarizing the current literature on xylose oligomer and by-production detection and kinetics, there were several areas that required further study. First, the model of xylose oligomers depolymerization developed by Kumar and Wyman (2008) was based on the commercial grade xylose oligomers that were not representative of the biomass hydrolysates, which contain other sugars and impurities, such as lignin and acetate. Our study utilized in-house purified xylose oligomers made from commercial grade birchwood xylan. Although it does not represent all biomass substrates, birchwood xylan does contain minor impurities, namely other sugars. The results from the proposed study will provide an insight into dilute acid biomass pretreatment.

Second, the mass of the degraded xylose monomer and oligomers into by-products was not accounted for in the Kumar and Wyman (2008). Understanding the by-products formation is important in order to develop pretreatment strategies that minimize their formation. The work by Morinelly et al. (2009) provided an understanding of furfural formation, but did not include formic acid formation. Moreover, the model developed by Morinelly et al. (2009) was not adequately representative of the furfural data because other sugars, which were not monitored but were present in the study, can also degrade into furfural. Our approach of using high-purity xylan would help to minimize the number of products formed because of its simplified hemicellulose structure.

Third, the model developed by Kumar and Wyman (2008) did not take into consideration different hydrolysis temperatures. Moreover, although different pH was considered in their model, varying pH conditions were not presented as a variable. The study by Morinelly et al. (2009) utilized a model that could not be fitted for the solvent systems devoid of acid. Therefore,

our study designed to include both temperature and pH, to examine the effect of hydrolysis through the use of a modified Arrhenius Equation on hemicellulose depolymerization will allow us to present the degradation rates of xylose oligomers in water, as well as in solvents with different acid concentrations.

Lastly, the kinetic model developed by Kumar and Wyman (2008) was based on mass concentrations, which deviates from the common practice of using molar concentrations. The degradation of xylose oligomers resulted in an overall increase in the molar concentration during the hydrolysis, and thus the total number of moles was not constant during the hydrolysis. Therefore, our study will use molar concentration as the basis in developing the kinetic model, which will be a more common practice.

Our study will focus on the degradation kinetics of xylan-derived oligomers during dilute acid pretreatment, with the end goal of developing a kinetic model for the breakdown of xylose monomer and oligomers under various water and dilute acid pretreatment conditions. Three variables will be used for various pretreatment conditions: pH of solvent ranging from water (pH 7) to 1 v/v% sulfuric acid (pH 0.43), hydrolysis temperature (120 – 200 °C), and hydrolysis time (0 – 60 min). The pH range of 0.43 - 7 was chosen because it encompasses most of the common dilute acid hydrolysis conditions. Similarly, the temperature range of 120 - 200 °C is common in dilute acid pretreatment. The selection of 160 °C as an experimental condition would also provide a basis for comparison of the degradation rates to the rates obtained by Kumar and Wyman (2008) and Morinelly et al. (2009). The initial concentrations of all compounds used in this study were 1 mg/mL, which is similar to the starting condition used in the study by Kumar and Wyman (2008). Although the concentration used in this study was a lot lower than the concentration used in industry, which can be up to 130 mg/mL, the study

minimized the influence of mass transfer limitations, which is a significant factor at above 20% w/w solids concentration (Hodge et al., 2008).

4.0 Materials and Methods

4.1 Materials

Birchwood xylan, xylose (DP 1), furfural and dimethyl sulfoxide (DMSO) were purchased from Sigma-Aldrich (St. Louis, MO). Xylobiose (DP 2), xylotriose (DP 3), xylotetraose (DP 4), xylopentaose (DP 5), and xylohexaose (DP 6) were purchased from Megazyme (Wicklow, Ireland). Glucose and heptane were obtained from Alfa-Aesar (Ward Hill, MA). Tetrahydrofuran (THF) was purchased from J.T. Baker (Phillipsburg, NJ). Ethanol was purchased from Koptec (King of Prussia, PA). Butanol was purchased from Avantor Performance Materials, Inc (Center Valley, PA). Acetonitrile, ethyl acetate, hexane, methanol, and sulfuric acid were purchased from EMD Chemicals (Gibbstown, NJ). Chloroform, isopropanol, and formic acid were obtained from EM Science (Gibbstown, NJ). Calcium carbonate was obtained from Fisher Scientific (Fair Lawn, NJ). Sodium hydroxide was purchased from Mallinckrodt Chemicals (Phillipsburg, NJ). Sodium acetate was acquired from Thermo Scientific (Sunnyvale, California). Acetic acid was purchased from VWR Scientific Products (West Chester, PA). Water was obtained from a Direct-Q system (Millipore, Billerica, MA). All solvents were of HPLC grade.

4.2 Methods

4.2.1 High Performance Liquid Chromatography (HPLC) Identification and Quantification

Analysis and quantification of monomers were performed using a Waters Alliance High Performance Liquid Chromatography (HPLC) system (model 2695, Waters Corporation, Milford, MA) fitted with an SP-G precolumn and an SP0810 column (Shodex, Kawasaki, Japan). The samples were analyzed as described by (Martin et al., 2010). Xylose, and glucose were quantified based on peak area using calibration curves generated with purchased standards.

Analysis and quantification of xylose oligomers were performed using a Waters Alliance HPLC system (model 2695, Waters Corporation, Milford, MA) employing a Micro-Guard De-Ashing pre-column and Aminex HPX-42A column (Bio-Rad, Hercules, CA), with the column temperature set at 85˚C. Samples were processed at an eluent flow rate of 0.2 mL/min. Xylose oligomers in each sample were quantified based on peak height using calibration curves generated with purchased DP 2, DP 3, DP 4, DP 5, and DP 6 standards. Xylose monomer and oligomers were detected using a refractive index (RI) detector (model 2414, Waters Corporation, Milford, MA).

Analysis and quantification of furfural, formic acid, and acetic acid were performed using a Waters 2695 HPLC system (Waters Corporation, Milford, MA) equipped with an Micro-Guard cation H (Bio-rad, Hercules, CA) refill cartridges guard column and Aminex HPX-87H column (Bio-Rad, Hercules, CA) heated to 55°C. The eluent was 0.005 M aqueous sulfuric acid at a flow rate of 0.6 mL/min. Detection was obtained with a Waters 2996 Photodiode Array Detector (Milford, MA) set at 280 nm for furfural and 210 nm for formic acid and acetic acid. Samples were quantified based on peak area using calibration curves generated using purchased standards.

4.2.2 High-Performance Anion-Exchange Chromatography with Pulsed Amperometric Detector (HPAEC-PAD) Identification and Quantification

Analysis and quantification of xylose monomer and oligomers were performed using High-Performance Anion-Exchange Chromatography with Pulsed Amperometric Detection (HPAEC-PAD). The HPAEC-PAD system was a Dionex ICS-5000 Ion Chromatography System equipped with an ICS3/5 electrochemical detector (ED), pH-Ag/AgCl reference electrode, 3x250 mm-CarboPac PA200 analytical column, and 3x50-mm CarboPac PA200 guard column (Dionex Corporation, Sunnyvale, CA). The HPAEC-PAD system was controlled using Chromeleon® software (Dionex Corp). The analytical method was modified from the Dionex product manual for CarboPac PA200 columns and Dionex Technical Notes 110 (Dionex Corporation, 2011). Samples were manually injected into a 25-µL sample loop before separation on the analytical column.

A gradient solution was used to separate compounds. Mobile phases consisted of 100 mM NaOH (Solvent A) and 100 mM NaOH with 320 mM sodium acetate (solvent B). Both solvents were padded with regular helium gas. The gradient began condition began with 100% solvent A and was maintained for 15 min. The gradient was then linearly changed to 50% Solvent A, 50% solvent B over 40 min. The gradient was then changed to 100% solvent B over 1 min. This condition was held for 4 min before it was changed to 100% solvent A over 1 min. The column was allowed to re-equilibrate at this condition for 9 min. The gradient method was summarized in **Table 2**. The flow rate was 0.5 mL/min for the 70-min analysis. The analytical column, guard column, and the ED were maintained at 35 ˚C. The concentration of xylose monomer and oligomers were calculated based on the peak area of their corresponding peaks.

Table 2: Gradient method employed in HPAEC-PAD analysis with CarboPac PA200 analytical column and CarboPac PA200 guard column, a 25-µL sample injection, and 0.5 mL/min flow rate.

Time	Flow (mL/min)	%A	%B
0	0.5	100	0
15	0.5	100	0
55	0.5	50	50
56	0.5	0	100
60	0.5	0	100
61	0.5	100	0
70	0.5	100	0

4.2.3 Production of xylose oligomers

The hydrolysis of xylan was carried out using two different hydrolysis conditions: dilute acid hydrolysis and hot water hydrolysis. The dilute acid hydrolysis was conducted in the early stages of the project to determine the conditions that favor xylose oligomers production. Hot water hydrolysis was later adopted to improve the yield of xylose oligomers, and minimize the introduction of sulfuric acid to the detection systems. The presence of sulfuric acid in the hydrolysate required neutralization with calcium carbonate, which could lead to inconsistent retention times during HPAEC-PAD analysis. Alternatively, the use of sodium hydroxide to neutralize sulfuric acid hydrolysate would irreversibly degrade the HPLC column because of the higher solubility of sodium sulfate in the hydrolysate, which would react with the lead or silver counter ions in the HPLC column. Therefore the use of water as the hydrolysate, neutralized with sodium hydroxide would minimize the negative impacts to both detectors.

4.2.3.1 Dilute acid hydrolysis of xylan

Xylan hydrolysis was carried out using 500 mg of birchwood xylan in 20 mL of 0.98 v/v% aqueous sulfuric acid in a thick-walled stainless-steel reactor (interior diameter of 14.22 mm, wall thickness of 5.59 mm, length of 200 mm, for a total chamber volume of 32 mL). The loaded reactor was submerged in an industrial fluidized sand bath (Techne Ltd, Burlington, NJ) at 130˚C for 20 min.

These hydrolysis conditions were selected as optimum from experiments using 0.98% sulfuric acid at 130 ˚C for reaction times of 20–60 min. The fluidized sand bath was preheated 2 h prior to the experiment, and the hydrolysis began once the reactor was submerged in the fluidized sand bath. After hydrolysis, the reactor was quenched in cool water for 1 min. The reactors were then stored in a 4˚C cold room for 30 min. After cooling, the hydrolysate was

recovered, and the volume and pH of the hydrolysate were recorded. The hydrolysate was then neutralized to pH 6-8 using $CaCO_3$ while being continuously stirred for 12–24 h. A small quantity of the sample was filtered using a 0.45-µm PTFE syringe filter (VWR International, West Chester, PA), followed by filtration through a 0.2-µm nylon syringe filter (National Scientific, Rockwood, TN) before being analyzed by HPLC. The remaining aliquot was filtered through a 1-µm PTFE syringe filter (Whatman, Florham Park, NJ) and then lyophilized using a Labconco (Kansas City, MO) freeze-drier system.

4.2.3.2 Hot water hydrolysis of xylan

Xylan hydrolysis was carried out using 800 mg of birchwood xylan in 20 mL of water in a 32-mL stainless-steel reactor. The loaded reactor was submerged in an industrial fluidized sand bath at 200˚C for 60 min. After hydrolysis, the reactor was quenched in cool water for 1 min and stored in a 4˚C cold room for 30 min. After cooling, the hydrolysate was neutralized to pH 6-8 using 100 mM NaOH while being continuously stirred for 30 s. A small quantity of the sample was filtered through a 0.45-µm PTFE syringe filter (VWR International, West Chester, PA), followed by filtration through a 0.2-µm nylon syringe filter (National Scientific, Rockwood, TN) before being analyzed using HPLC and HPAEC-PAD. The remaining aliquot was filtered through a 1-µm PTFE syringe filter (Whatman, Florham Park, NJ), placed in clean glass tubes, and dried using an Automatic Environmental Speed Vac System (SpeedVac) (Savant Model AES 1010, Ramsey, MN) on the lowest heat setting.

4.2.4 Fractionation of Xylose Oligomers

4.2.4.1 Solvent System and Sample Preparation

For the CPC runs, the solvent system of THF: DMSO: water in a 6:1:3 volumetric ratio was prepared in a 2-L separatory funnel, allowing for full mixing and equilibration. The upper phase, mostly THF, and the lower phase, mostly water and DMSO, were allowed to settle for at least 2 h before being collected in separate containers. The CPC was operated in the ascending mode, where the DMSO- and water-rich lower phase was used as the stationary phase, and the THF-rich upper phase was used as the mobile phase. An additional solvent system of butanol: methanol: water in a 5:1:4 volumetric ratio was also prepared in the same fashion as the THF: DMSO: water solvent system. For the butanol: methanol: water solvent system, the CPC was also operated in the ascending mode, where the butanol-rich upper phase was used as the mobile phase and the methanol- and water-rich lower phase was used as the stationary phase.

With respect to sample preparation, 0.5–1.0 g of crude extract was reconstituted in 10 mL of the selected solvent system. The sample was then filtered through a 0.45-μm PTFE syringe filter before being injected into the CPC system.

4.2.4.2 Setup for Kromaton CPC (For THF: DMSO: water Solvent System)

The CPC separation was performed using a bench scale CPC from Kromaton Technologies (Angers, France), fitted with an evaporative light scattering detector (ELSD) (SofTA Corporation, Westminster, CO). The DMSO- and water-rich lower phase was pumped into the 200-mL column using a Waters 510 pump (Waters, Milford, MA) at 8.5 mL/min while the rotor was spinning at 200 rpm. Once the column was filled with the lower phase, which took about 30 min, the pump was stopped. The rotor speed was increased to 1000 rpm, before the THF-rich upper phase was introduced into the CPC rotor at 8.5 mL/min. The stationary phase

volume was determined once the upper phase exited from the CPC rotor. A 10-mL sample was injected into the 10-mL sample loop, and then introduced into the CPC rotor; this was the start of the CPC run. The flow rate was maintained at 8.5 mL/min, and fractions were collected immediately after the start of the CPC run using a Waters Fraction Collector III (Milford, MA). Each fraction was collected over a 1-min period, equivalent to 8.5 mL, for a total duration of 120 min. The ELSD was set up with a 50 psig air pressure with ultra-pure nitrogen, a 25 ˚C spray chamber temperature, and a 55 ˚C drift tube temperature. The mobile and stationary phases had volumes of 131 and 69 mL, respectively, as determined from the CPC run. The operating pressure of the 120-min CPC run was approximately 250 psig.

4.2.4.3 Setup for Kromaton CPC (For Butanol: Methanol: Water Solvent System)

The CPC run for the butanol: methanol: water solvent system was similar to that of the THF: DMSO: water solvent system, with a few exceptions. Firstly, the flow rate was reduced to 4.89 mL/min during the introduction of the butanol-rich mobile phase, while the loading of the methanol- and water-rich stationary phase was maintained at 8.5 mL/min. Secondly, the fraction collection began 40 min after the start of the CPC run, each with a 2-min collection time, equivalent to 9.78 mL, for a total collection time of 240 min. Thirdly, the total run time of the CPC run was increased to 280 min, as compared to 120 min of the CPC run using the THF: DMSO: water solvent system. The volumes of the mobile and stationary phases were 109 and 91 mL, respectively, with the operating pressure at approximately 440 psig.

4.2.4.4 Setup for Armen CPC (For Butanol: Methanol: Water Solvent System)

The CPC separation was performed using a CherryOne DS bench scale Counter Current Chromatography (CCC) control system from Cherry Instruments (Chicago, IL), which utilized a CPC rotor from Armen Instruments (Saint-Avé, France). Detection was achieved using an ELSD

(Softa Corp) with the same setup as for the Kromaton system. The 250-mL rotor was first filled with lower phase at 10 mL/min with the rotor spinning at 500 rpm. Once the rotor was completely filled with the stationary phase, which took approximately 30 min, the CPC rotor speed was increased to 2,300 rpm. At that point, the upper phase was introduced into the CPC rotor at a flow rate of 8 mL/min. The mobile phase volume was determined once the upper phase exited the CPC rotor. A 30-mL sample was injected into the 30-mL sample loop and then introduced into the CPC rotor; this was the start of the CPC run. The flow rate was set at 8 mL/min, and the phases were reversed at 165 min to begin the extrusion process. Fractions were collected using a Foxy R1 Fraction Collector (Teledyne Isco, Lincoln, NE). Fraction collection began 75 min after sample injection and lasted for a duration of 125 min, with each fraction being collected over 1 min. From the 200-min CPC run, the mobile and stationary phases were 132 and 118 mL, respectively, with the operating pressure at approximately 650 psig.

4.2.4.5 Analysis of CPC Fractions

Fractions collected from CPC runs were dried using a SpeedVac, reconstituted in water, and analyzed for monomer and oligomer concentrations using the HPLC and HPAE-PAD methods described previously. The yield was calculated as the mass of compounds detected in CPC fractions as determined by HPLC divided by the mass of birchwood xylan used in producing the sample that was injected into the CPC.

4.2.5 Mass Spectrometry Analysis of Xylose Oligomers

4.2.5.1 Matrix Assisted Laser Desorption Ionization (MALDI) analysis

Matrix assisted laser desorption ionization (MALDI) was used to verify the molecular weight and purity of the DP 3, DP 5, and DP 6 standards. The analysis was conducted using a Bruker Ultraflex II (Bruker Daltonics Inc., Billerica, MA) tandem time of flight (TOF/TOF) equipped with a SmartBeam® laser (Bruker Daltonics Inc., Billerica, MA), operated in a positive-ion, reflection mode. The matrix used was 1 M of 2,5-dihydroxybenzoic acid in 90% methanol. Samples were mixed with the matrix in a 1:1 (v/v) ratio, spotted onto a stainless steel MALDI target plate, and allowed to dry.

4.2.5.2 Electrospray Ionization Mass Spectrometry (ESI-MS) Analysis

Electrospray ionization mass spectrometry (ESI-MS) was performed on a quadrupole-time of flight mass spectrometer. Samples were mixed with methanol (with 0.1% formic acid) and directly infused into the ESI source via a syringe pump. Mass spectra were obtained in the positive ion mode.

4.2.6 Kinetic Study

4.2.6.1 Experimental Design

The experimental objective was to determine the depolymerization rate of xylose oligomers, as well as to provide a mass closure of the compounds during the depolymerization process. The experimental approach included the analysis of the degradation of DP 1, DP 2, DP 3, DP 4, furfural, and formic acid, each at three different temperatures and three different acid concentrations with two replicates for each condition, resulting in a total of 108 runs. Each run consisted of four to six samples, with each sample representing a different hydrolysis time. The overall experimental matrix is summarized in **Table 3**. DP 1, furfural, and formic acid used in the experiment were acquired from commercial sources, while DP 2, DP 3, and DP 4 were produced from the hydrolysis of birchwood xylan followed by CPC fractionation. All compounds in the experiments started with 1 mg/mL concentration.

An additional 24 preliminary runs were also conducted to determine the effect of concentration on xylose degradation rate. The experimental approach involved the use of purchased DP 1 at three different concentrations, two different temperatures, and two different sulfuric acid concentrations with two replicates for each condition. Each run consisted of six sample points. The example matrix can be seen in **Table 4**.

Table 3: Experimental matrix for main kinetic study

Compounds	Concentration (mg/mL)	Temperature (˚C)	Acid Concentration (v/v%)	Replicates
DP 1	1	120	0	2
DP 2		160	0.1	
DP 3		200	1	
DP 4				
Formic Acid				
Furfural				

Table 4: Experimental matrix for preliminary kinetic study

Compounds	Concentration (mg/mL)	Temperature (˚C)	Acid Concentration (v/v%)	Replicates
DP 1	1	120	0	2
	2	200	1	
	5			

4.2.6.2 Experimental Setup

The kinetics experiment was performed using six thick-walled stainless-steel reactors. Each reactor had an interior diameter of 14.22 mm, wall thickness of 5.59 mm, and length of 100 mm, for a total chamber volume of 16 mL. A 5-mL sample volume was added to each reactor tube. The 5-mL sample volume was selected to conserve samples, without affecting the reaction of samples, as determined experimentally. Once loaded, the reactor end-caps were tightened with a wrench. The hydrolysis time began 75 s after the reactors were submerged in the industrial fluidized sand bath as described earlier in the hydrolysis of birchwood xylan. The sand bath was preheated for at least an hour before each experiment, and the temperature of the sand bath was verified to reach the set temperature using a hand-held heat gun. Because of the inherent variation of the fluidization, the bath temperature fluctuated within ± 5˚C of the target temperature. Each replicate of the reactor was placed at the opposite corner of the initial reactor to account for the uneven heat distribution. Each reactor, representing a different hydrolysis time, was submerged into the sand bath for a set time, but at the end of each run, all the reactors were removed from the sand bath at the same time. Once the reactors were removed from the sand bath, they were quenched within 20 s in tap water to halt the reaction and reduce pressure. Each reactor tube was then opened, and the liquid was transferred to clear glass tubes, neutralized with calcium carbonate, filtered through a 0.2-μm filter, and analyzed using HPLC.

4.2.7 Data analysis

All reactors within each run were conducted under isothermal conditions, and their initial compositions were identical. Therefore, each individual reactor tube representing different hydrolysis times of the particular compound at a specific temperature and acid concentration can be interpreted as the degradation rate of the compound under isothermal conditions.

4.2.7.1 Reaction Model

Based on the literature studies on hemicellulose degradation, and **Figure 4** summarizing the hemicellulose degradation path, the reaction model of xylose oligomers is presented in **Figure 6**. The constants k_1, k_2, k_3, k_4, k_F, k_A are the overall degradation rates of DP 1, DP 2, DP 3, DP 4, furfural, and formic acid, respectively, in min^{-1}; and k_{41}, k_{42}, k_{31}, k_{21}, k_{1F}, k_{1A}, k_{FA} are the formation rate constants of DP 1 from DP 4, DP 2 from DP 4, DP 1 from DP 3, DP 1 from DP 2, furfural from DP 1, formic acid from DP 1, and formic acid from furfural, respectively, in min^{-1}, k_{FL} and k_{AL} are the decomposition rate constants of furfural and formic acid, respectively.

There are several underlying assumptions in developing the reaction model: 1) all degradation reactions are of first order kinetic; 2) the reaction is irreversible. Although experimental and literature review showed that formic acid can produce furfural, the reaction rate is negligible in comparison to the forward reaction of furfural degrading into formic acid, and thus can be deemed negligible; and 3) xylose monomer is responsible for the formation of furfural. Xylose oligomers (DP 2, DP 3, DP 4) have to depolymerize to DP 1, before further degradation into furfural.

4.2.7.2 First Order Kinetics

According to first order kinetics, the reaction rate is:

$$d[X] / dt = - k * [X] \quad \textbf{(11)}$$

where [X] is the concentration of compound X in mmol/L, t is the hydrolysis time in min, k is the rate of compound degradation, which has units of min^{-1}. Therefore d[X]/dt is the rate of change for compound X with respect to time.

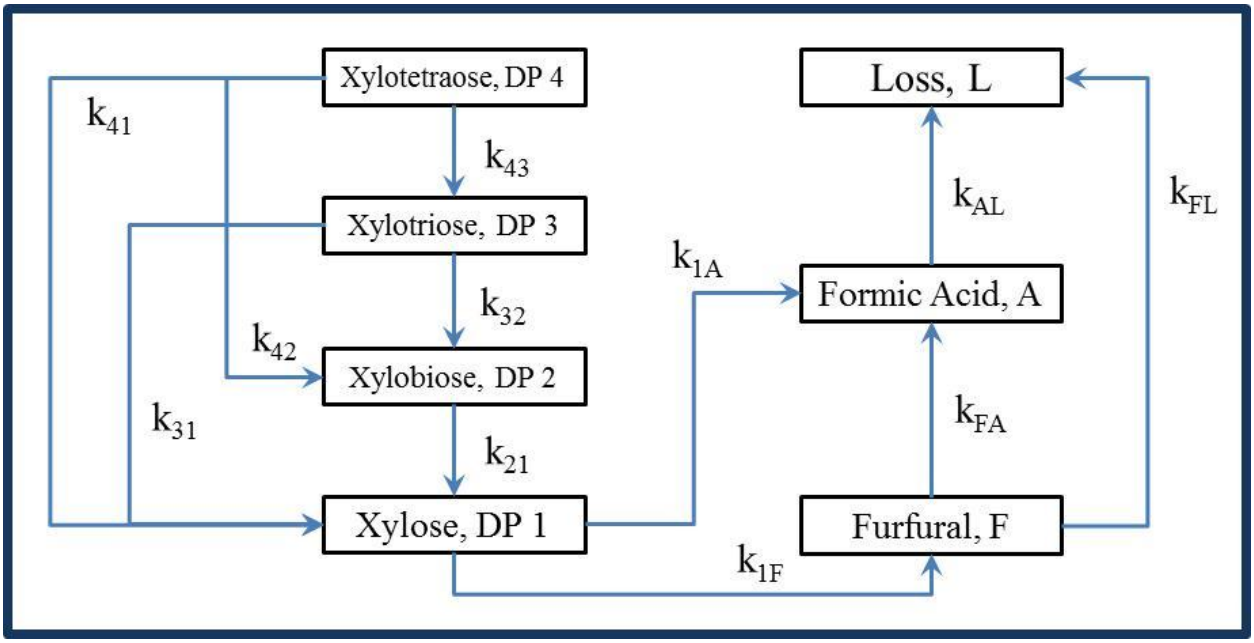

Figure 6: The degradation model of xylose oligomers. k_1, k_2, k_3, k_4, k_F, k_A are the overall degradation rate constants for DP 1, DP 2, DP 3, DP 4, furfural, and formic acid, respectively, in min^{-1}; and k_{41}, k_{42}, k_{31}, k_{21}, k_{1F}, k_{1A}, k_{FA} are the formation rate constants of DP 1 from DP 4, DP 2 from DP 4, DP 1 from DP 3, DP 1 from DP 2, furfural from DP 1, formic acid from DP 1, and formic acid from furfural, respectively, in min^{-1}. The rate constants k_{FL} and k_{AL} are the decomposition rate of furfural and formic acid, respectively.

Using **Equation 11** and the summary of **Figure 6**, the mass balance for DP 1, DP 2, DP 3, DP 4, furfural, and formic acid are:

$$d[X_1] / dt = - k_1 * [X_1] + k_{41} * [X_4] + k_{31} * [X_3] + 2 * k_{21} * [X_2] \quad \textbf{(12)}$$

$$d[X_2] / dt = - k_2 * [X_2] + 2* k_{42} * [X_4] + k_{31} * [X_3] \quad \textbf{(13)}$$

$$d[X_3] / dt = - k_3 * [X_3] + k_{41} * [X_4] \quad \textbf{(14)}$$

$$d[X_4] / dt = - k_4 * [X_4] \quad \textbf{(15)}$$

$$d[X_F] / dt = - k_F * [X_F] + k_{1F} * [X_1] \quad \textbf{(16)}$$

$$d[X_A] / dt = - k_A * [X_A] + k_{1A} * [X_1] + k_{FA} * [X_F] \quad \textbf{(17)}$$

where $[X_1]$, $[X_2]$, $[X_3]$, $[X_4]$, $[X_F]$, $[X_A]$ are the concentrations of DP 1, DP 2, DP 3, DP 4, furfural, and formic acid, respectively, in mmol/L; k_1, k_2, k_3, k_4, k_F, k_A are the overall degradation rate constants of DP 1, DP 2, DP 3, DP 4, furfural, and formic acid, respectively, in min^{-1}; and k_{41}, k_{42}, k_{31}, k_{21}, k_{1F}, k_{1A}, k_{FA} are the formation rate constants of DP 1 from DP 4, DP 2 from DP 4, DP 1 from DP 3, DP 1 from DP 2, furfural from DP 1, formic acid from DP 1, and formic acid from furfural, respectively, in min^{-1}.

The relationship between the overall degradation and the formation rates of individual compounds can be summarized in the following equations:

$$k_1 = k_{1F} + k_{1A} \quad \textbf{(18)}$$

$$k_2 = k_{21} \quad \textbf{(19)}$$

$$k_3 = k_{31} \quad \textbf{(20)}$$

$$k_4 = k_{41} + k_{42} \quad \textbf{(21)}$$

$$k_F = k_{FA} + k_{FL} \quad \textbf{(22)}$$

$$k_A = k_{AL} \quad \textbf{(23)}$$

where k_{FL} and k_{AL} are the decomposition rate constants of furfural and formic acid, respectively.

The expression of individual compound concentrations $[X_1]$, $[X_2]$, $[X_3]$, $[X_4]$, $[X_F]$, and $[X_A]$ with respect to time were performed using normal integrations. The integration relationships are presented in **Appendix 1**. The integration routine was also performed using Matlab software for verification purposes, and the result is shown in **Appendix 2**.

The overall degradation rate constants, k_1, k_2, k_3, k_4, k_F, and k_A, and the individual formation rate constants for k_{41}, k_{42}, k_{31}, k_{21}, k_{1F}, k_{1A}, and k_{FA} for each compound were estimated by minimizing the differences between experimental and predicted data using the Excel Solver Routine.

4.2.7.3 Arrhenius Equation

With the estimated values at nine different hydrolysis conditions studied for each compound, a second data fitting was performed on each set of degradation rate constants to obtain the Arrhenius constant for each compound, according to the following equation, derived from **Equation 6**:

$$k = [k_0 \times (H^+)^m] \times \exp(-E/RT) \quad \textbf{(24)}$$

where k, k_0, (H^+), m, E, R, and T are the first-order rate constant in min^{-1}, pre-exponential rate constant in min^{-1}, hydrogen ion concentration in mol/L, unitless acid concentration exponent, activation energy in kJ/mol, gas constant in kJ/mol/K, and the hydrolysis temperature in K, respectively.

5.0 Results and Discussions

5.1 Compound Identification and Quantification

5.1.1 HPLC Analysis

Three HPLC columns and two detectors were used to analyze the compounds during the HPLC analysis. Sample chromatograms of xylose and glucose monosaccharides are shown in **Figure 7**, and had retention times at 48 and 51 min, respectively. The retention times of xylose-oligomer standards, DP 2, DP 3, DP 4, DP 5, and DP 6, are shown in **Figure 8**, and were determined to be 49, 45, 41, 38, and 36 min, respectively. The retention times of formic acid, acetic acid and furfural are shown in **Figure 9**, and were determined to be 14, 15 and 45 min, respectively.

Quantification of each compound was done by establishing respective calibration curves that compared the peak area at different concentrations. **Figure 10** shows the calibration curves for glucose and xylose using peak area as a function of the concentration of the monosaccharides. The regressions were linear with high R^2 values over a concentration of 0 – 20 mg/mL.

When using the HPLC set-up for xylose oligomer analysis, the resolution between adjacent peaks was poor, jeopardizing the estimation of corresponding areas. Li et al. (2003) used an identical HPLC column, but used the peak height to determine the concentration of corresponding xylose oligomers, yielding better accuracy. Therefore, the concentrations of xylose oligomers were calibrated using the peak height instead of peak area, as shown in **Figure 11**.

The calibration curves for formic acid, acetic acid, and furfural are shown in **Figure 12**. As with glucose and xylose, peak area was plotted as a function of concentrations for the formic acid, acetic acid, and furfural. The regressions lines were linear with high R^2 values over a concentration of 0 – 40 mg/mL for formic acid and acetic acid, and 0 – 0.45 mg/mL for furfural.

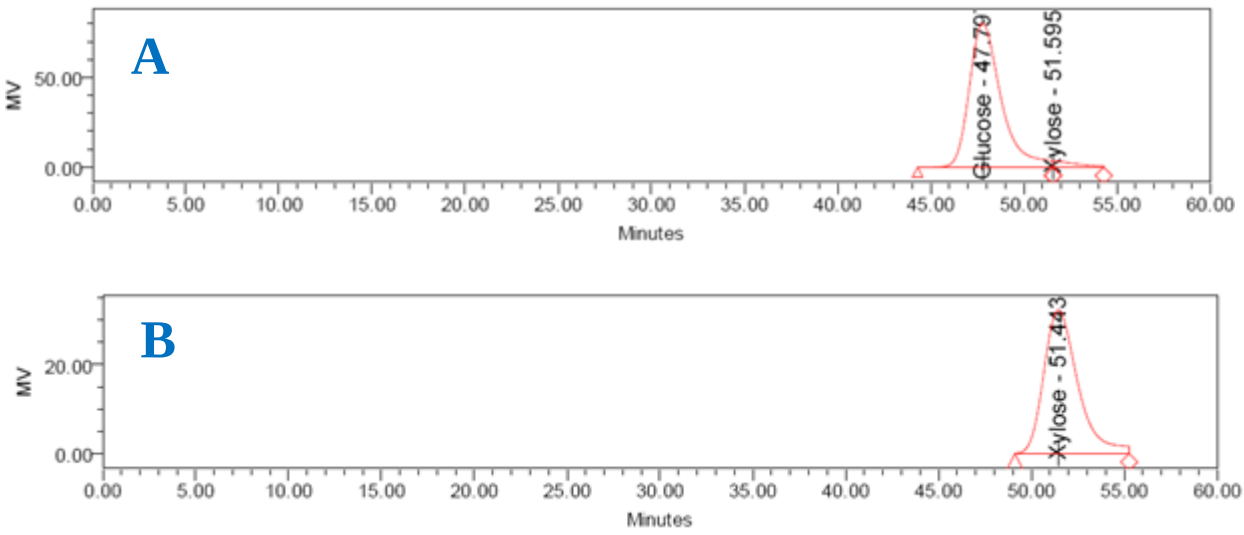

Figure 7: HPLC chromatogram of **(A)** glucose standard at 2 mg/mL, and **(B)** xylose standard at 1 mg/mL, analyzed using a Shodex SP0810 column heated to 85 ˚C. The samples were processed with water as the mobile phase at a flow rate of 0.2 ml/min. The compounds were detected using a refractive index (RI) detector.

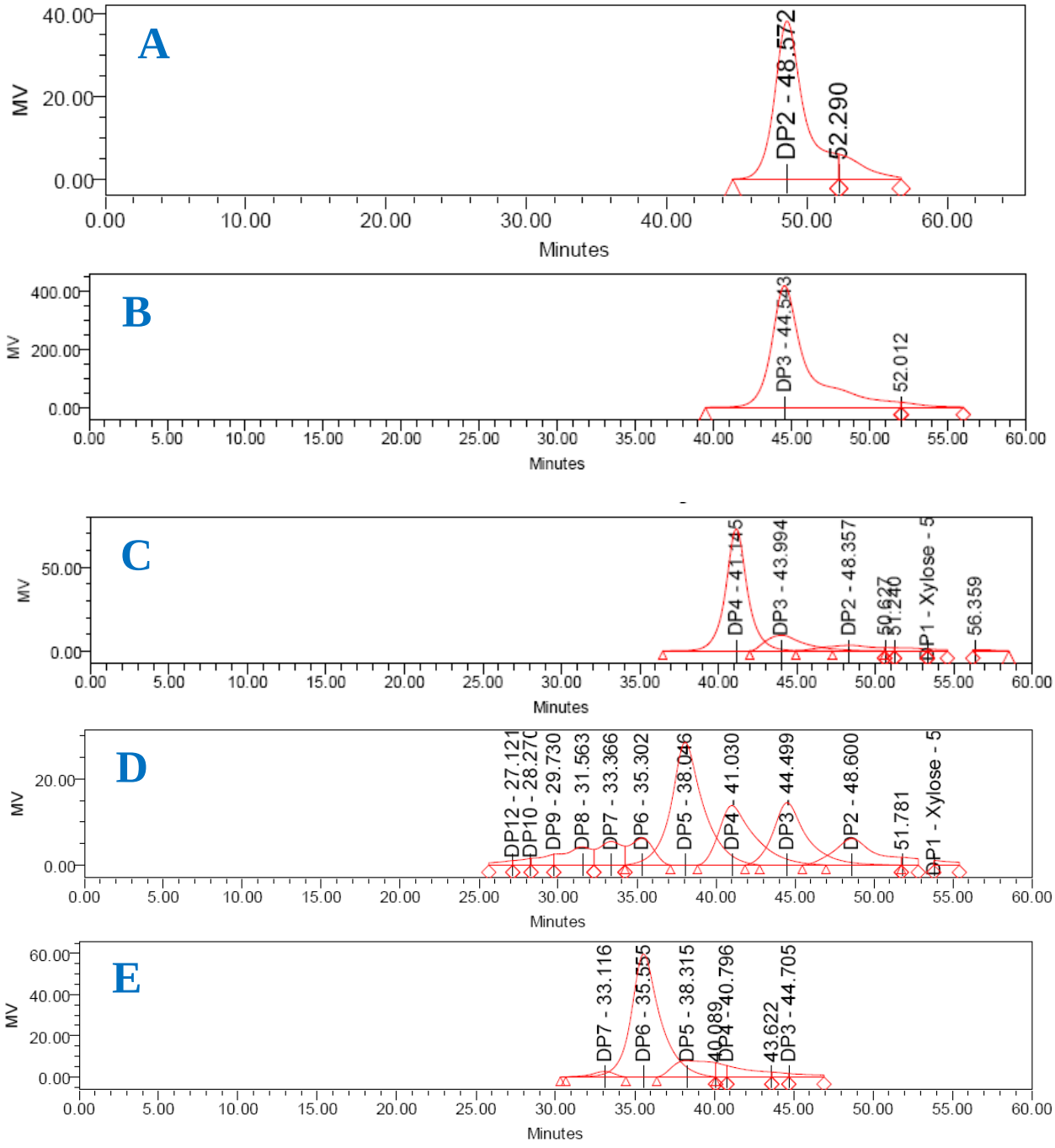

Figure 8: HPLC chromatogram of **(A)** DP 2 standard, **(B)** DP 3 standard, **(C)** DP 4 standard, **(D)** DP 5 standard, and **(E)** DP 6 standard, analyzed using Biorad Aminex HPX-42A column heated to 85 ˚C. The samples were processed with water as the mobile phase at a flow rate of 0.2 ml/min. The compounds were detected using refractive index (RI) detector.

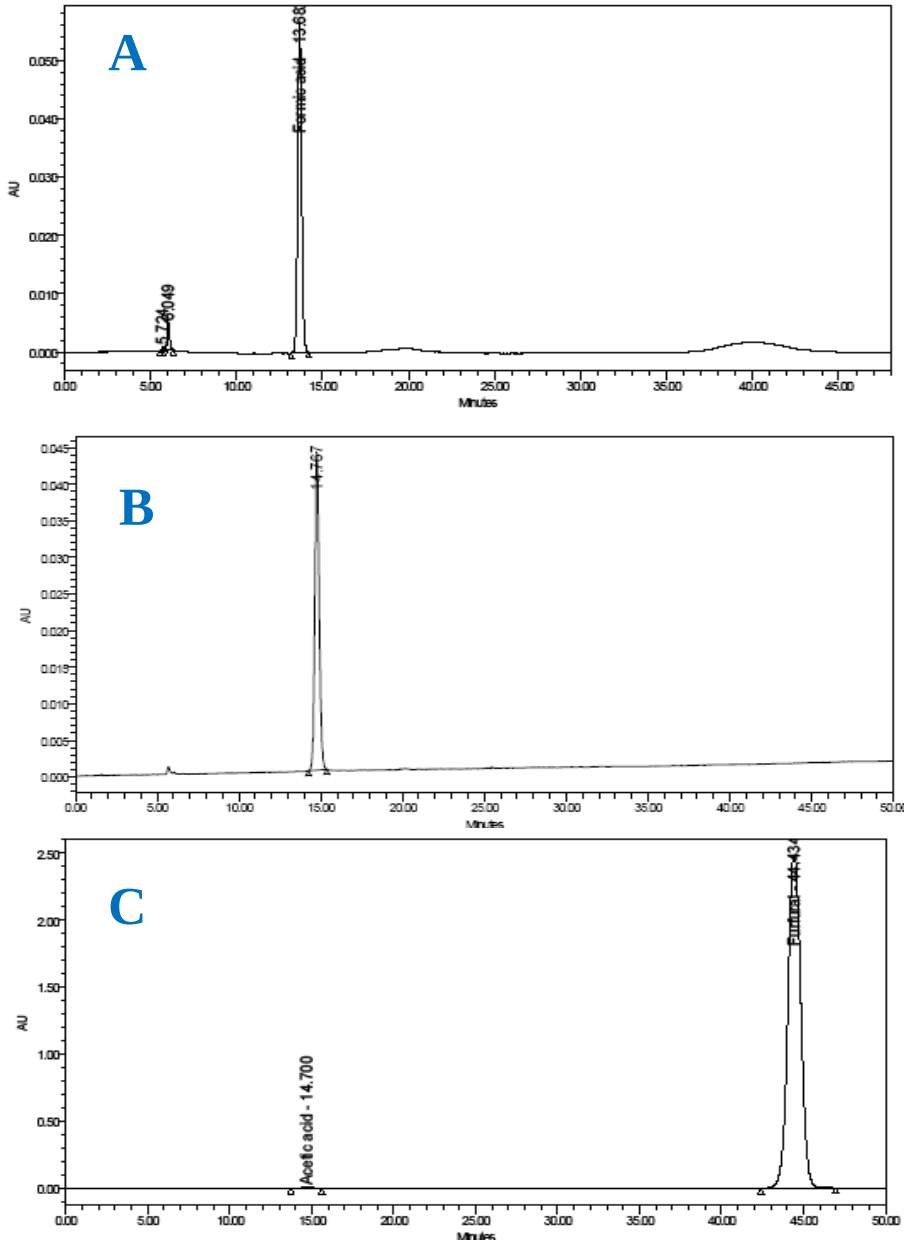

Figure 9: HPLC chromatogram of **(A)** formic acid standard, **(B)** acetic acid standard, **(C)** furfural standard, analyzed using a Biorad Aminex HPX-87H column heated to 55 ˚C. The sample was processed with 0.005 M aqueous sulfuric acid as the mobile phase at a flow rate of 0.6 ml/min. All compounds were detected using an UV detector set at a 210 nm wavelength for formic and acetic acid, and a 280 nm wavelength for furfural.

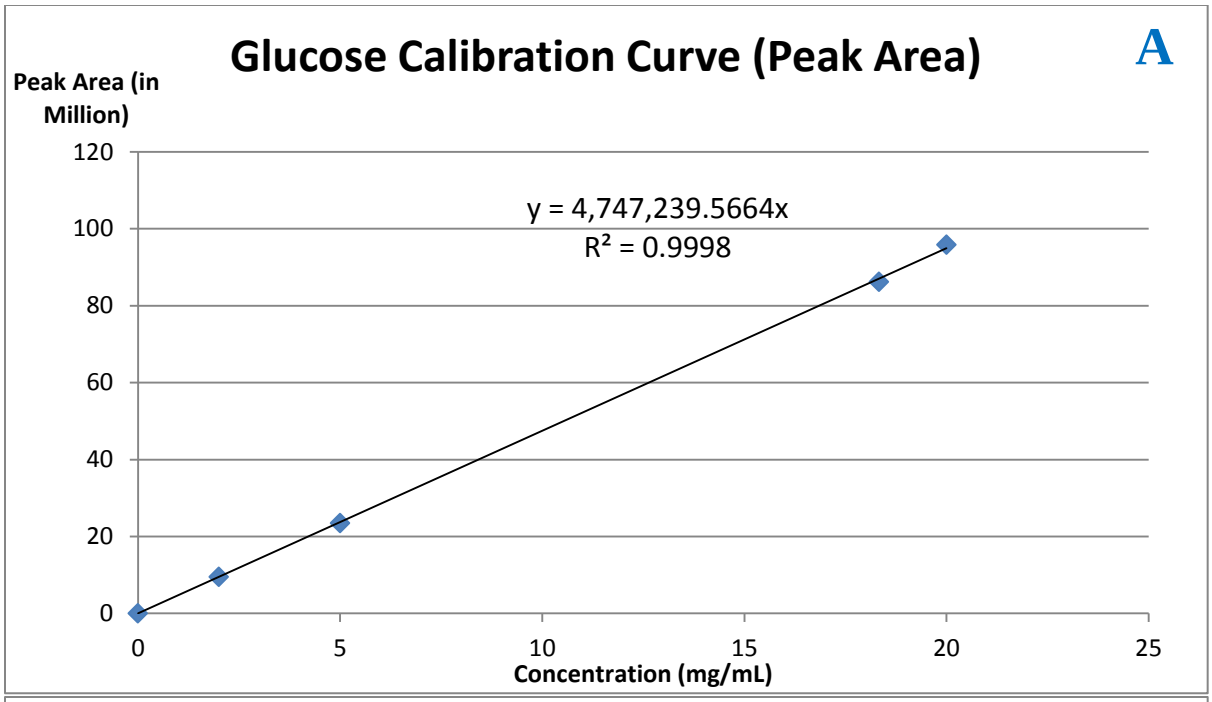

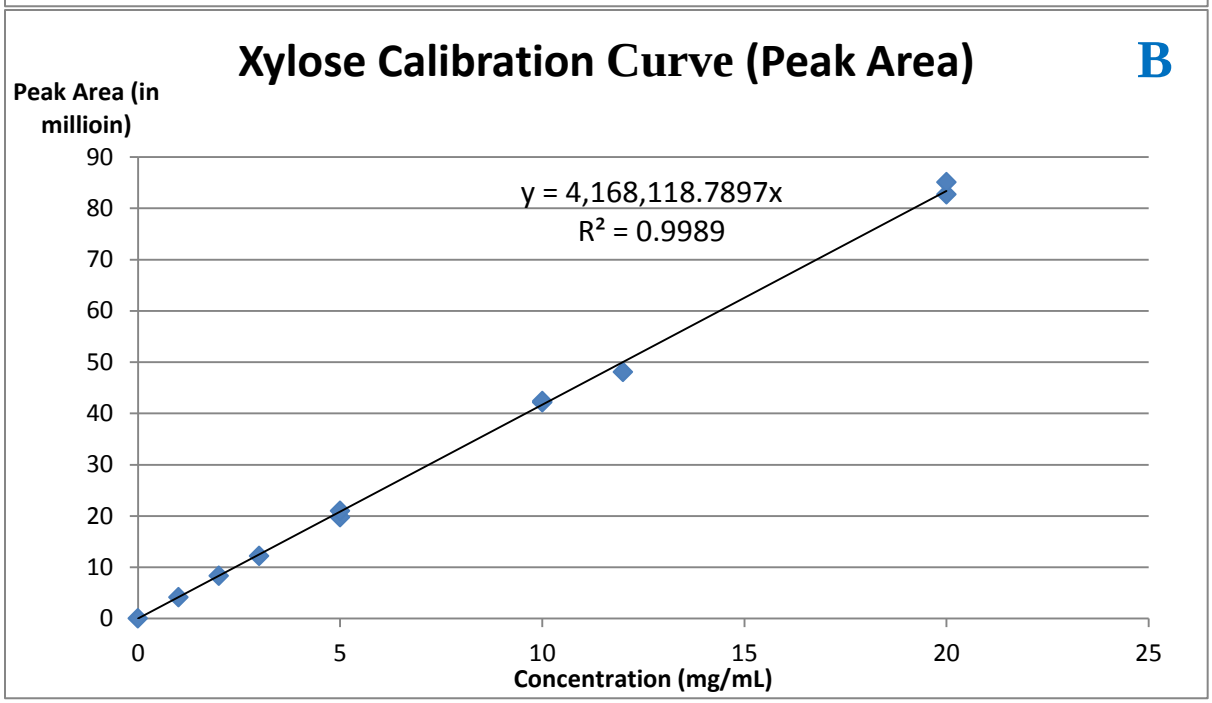

Figure 10: Calibration curve of **(A)** glucose standard, and **(B)** xylose standard, using Shodex SP-810 column. The calibration curves are based on the peak area of the respective compounds.

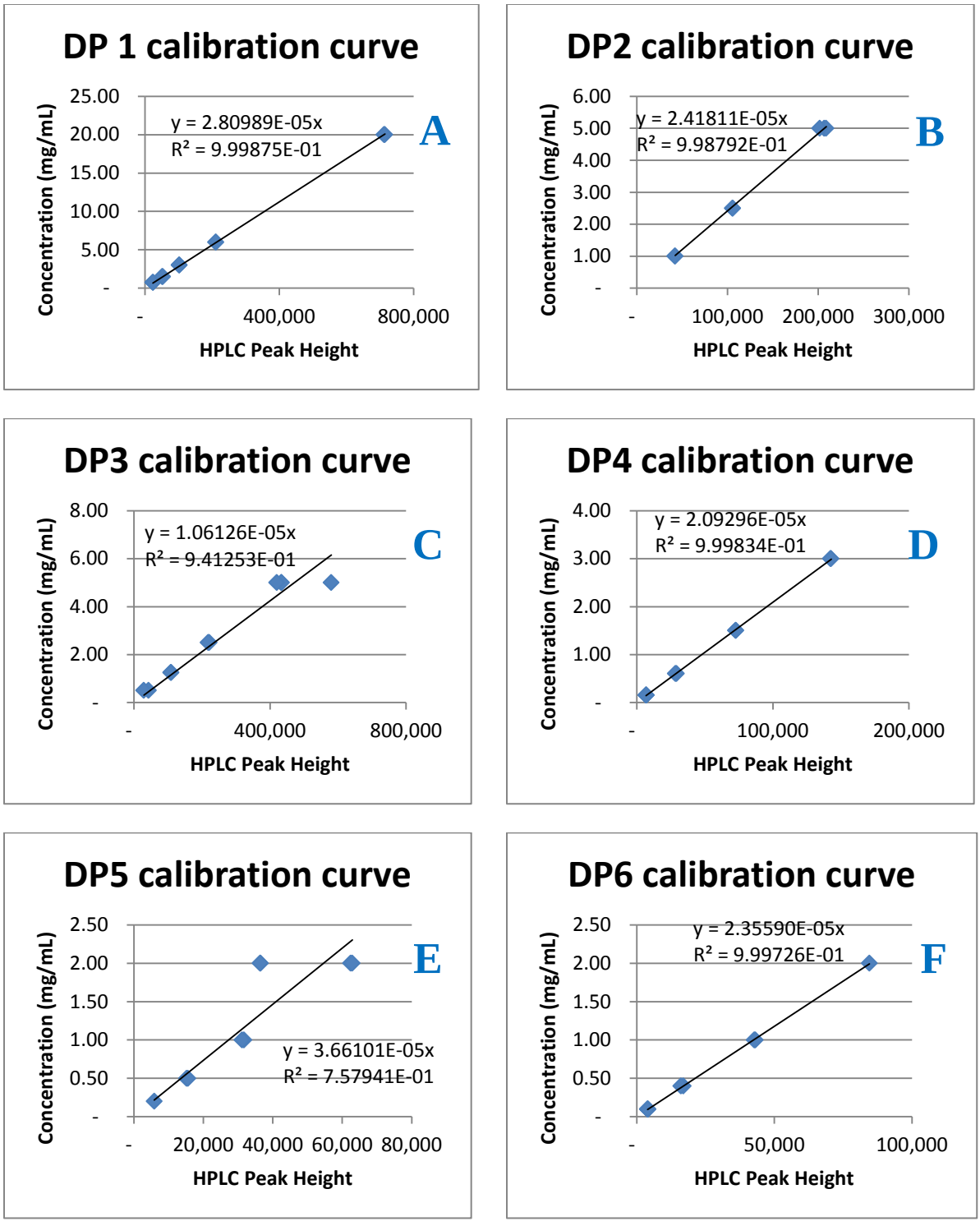

Figure 11: Calibration curve of **(A)** DP 1, **(B)** DP 2, **(C)** DP 3, **(D)** DP 4, **(E)** DP 5, and **(F)** DP 6 standards using Biorad Aminex HPX-42A column. The calibration curves are based on the peak heights from the respective standards.

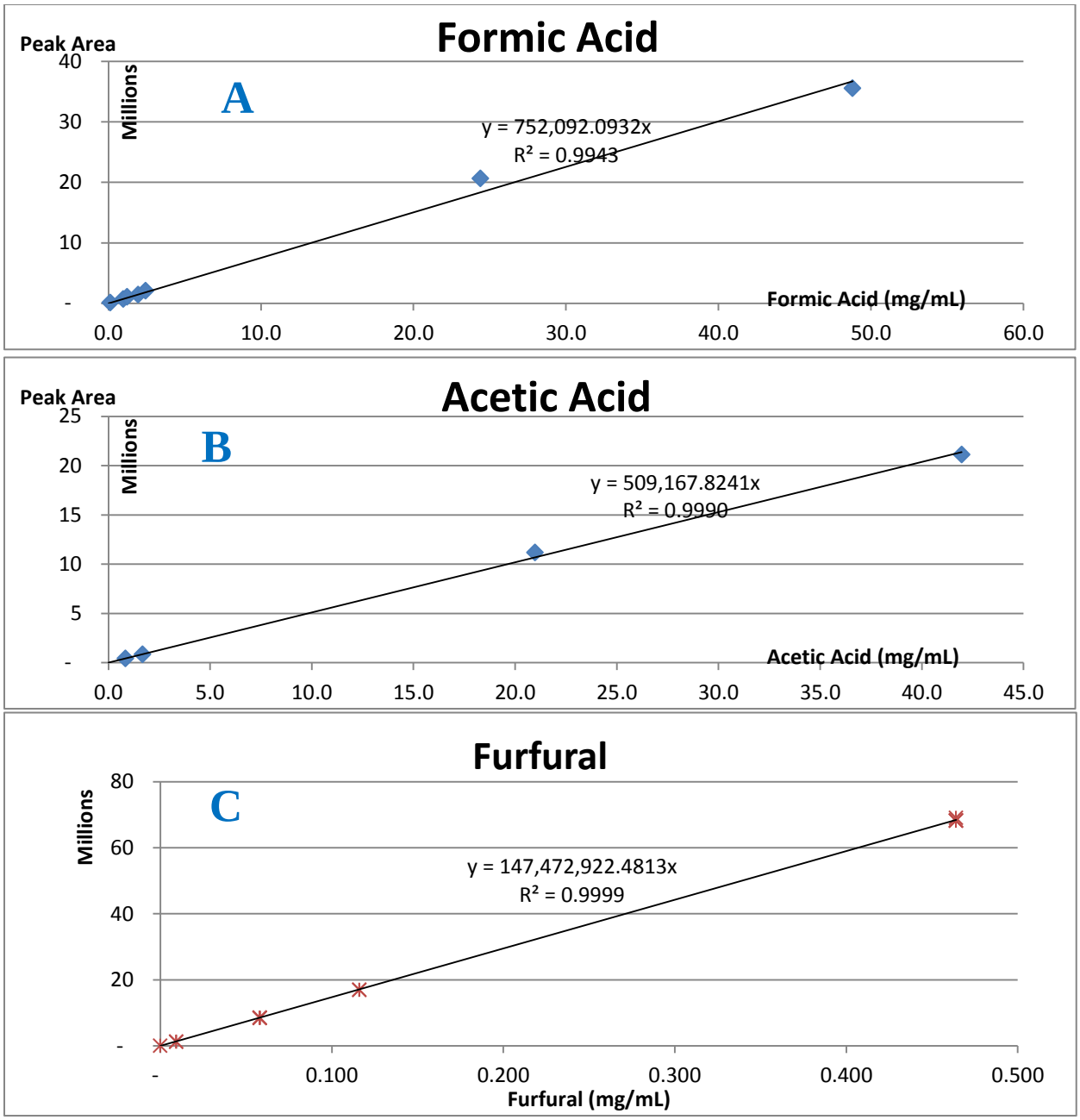

Figure 12: Calibration curve of **(A)** formic acid, **(B)** acetic acid, and **(C)** furfural, using Biorad Aminex HPX-87H column and a UV detector at a 210 nm (formic acid and acetic acid) and a 280 nm (furfural) wavelengths. The calibration curves are based on the peak area of the compounds.

5.1.2 High Performance Anion Exchange Chromatography with Pulsed Amperometric Detector (HPAEC-PAD) Analysis for Carbohydrates

Xylose monomer oligomers were analyzed in HPAEC-PAD analysis. The retention times of DP 1, DP 2, DP 3, DP 4, DP 5, and DP 6 were 2.7, 3.4, 4.5, 6.4, 9.8, and 15.8 min, respectively, as shown in **Figure 13**.

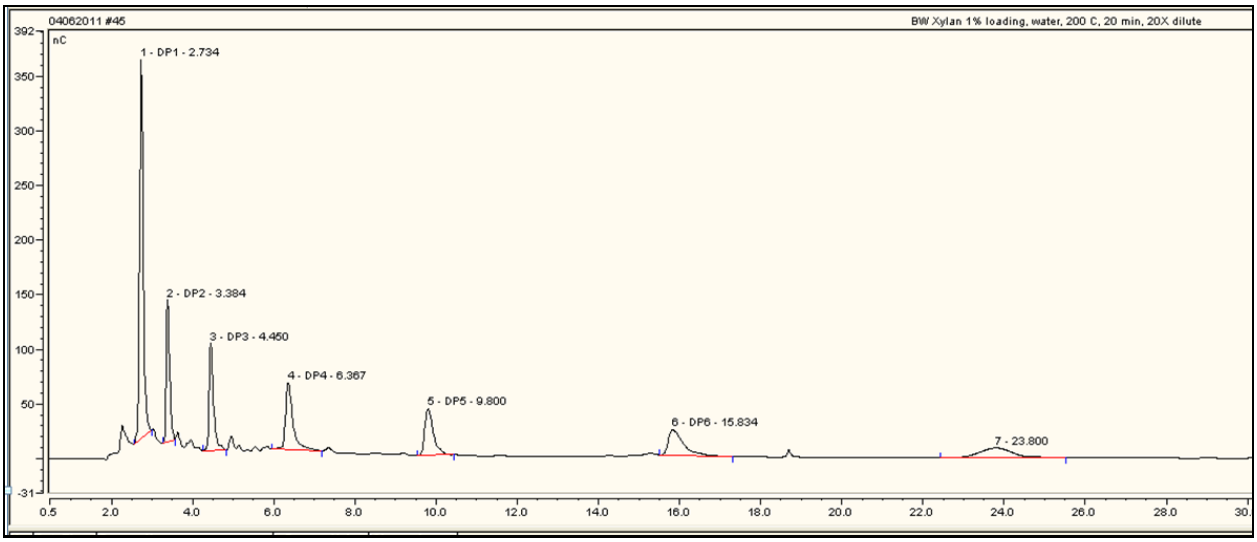

Figure 13: HPAEC-PAD chromatogram of the hydrolyzed birchwood xylan consisting of DP 1, DP 2, DP 3, DP 4, DP 5, and DP 6. The retention times of DP 1, DP 2, DP 3, DP 4, DP 5, and DP 6 were 2.7, 3.4, 4.5, 6.4, 9.8, and 15.8 min, respectively.

5.2 Xylose Oligomers Production

Birchwood xylan was used as the starting material in the production of xylose oligomers. The monosaccharide composition analysis was performed by adding 0.5 gram of birchwood xylan into 20 mL (2.5 % solid loading) of 0.98% v/v aqueous sulfuric acid, before the mixture was loaded to a stainless steel reactor, and hydrolyzed at 130 ˚C for 50 min. The monosaccharide composition of birchwood xylan was determined to contain 93% xylose, with the remaining monosaccharides accounted as glucose, mannose and arabinose, which was determined from the peak area (**Figure 14**). Because of its high monosaccharide purity, birchwood xylan was used to produce in-house xylose oligomers. On the other hand, the results presented in **Figure 14** indicated that no xylose oligomers were obtained, hindering the subsequent experimental plan.

In order to prevent xylose oligomers from being depolymerized completely into xylose monomers, the hydrolysis conditions for birchwood xylan were decreased in severity by reducing the hydrolysis time from 50 min to 20 min. The resulting hydrolysate contained xylose oligomers, ranging in length from DP 2 to DP 11. As shown in **Figure 15**, DP 2, DP 3, and DP 4 were detected at retention times of 49, 45, and 41 min, respectively. From the results presented in **Figure 15**, it was inferred that the mass production of xylose oligomers should concentrate on DP 2, DP 3, and DP 4. To further increase the concentration of DP 2, DP 3, and DP 4, the hydrolysis conditions were refined. The hydrolysis parameters were set within the following ranges: 120 to 240 ˚C, for 10 to 240 min, with solid loading rate from 2.5% to 10.0%.

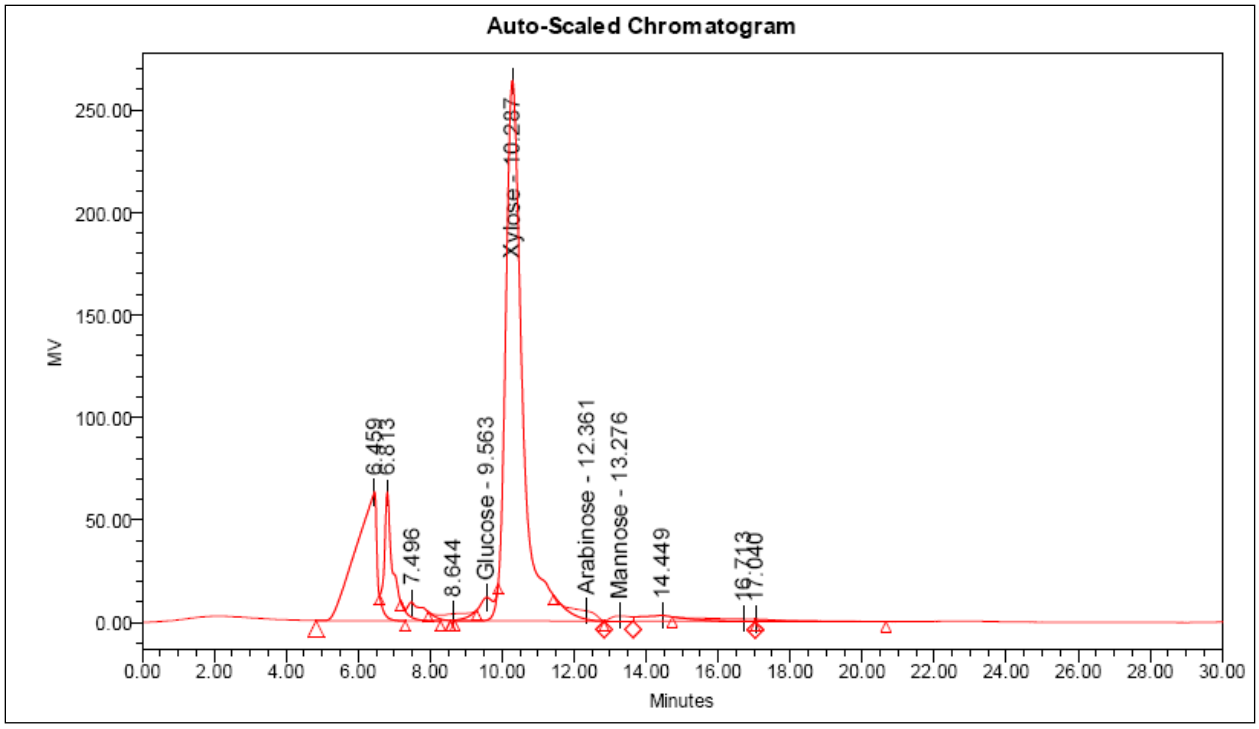

Figure 14: HPLC chromatogram of birchwood xylan hydrolyzed hydrolyzed at 130 ˚C for 50 min using 0.98 v/v% sulfuric acid using Shodex SP-810 column heated to 85 ˚C. The sample was processed with water as the mobile phase at a flow rate of 0.2 ml/min. The compound was detected using a refractive index (RI) detector.

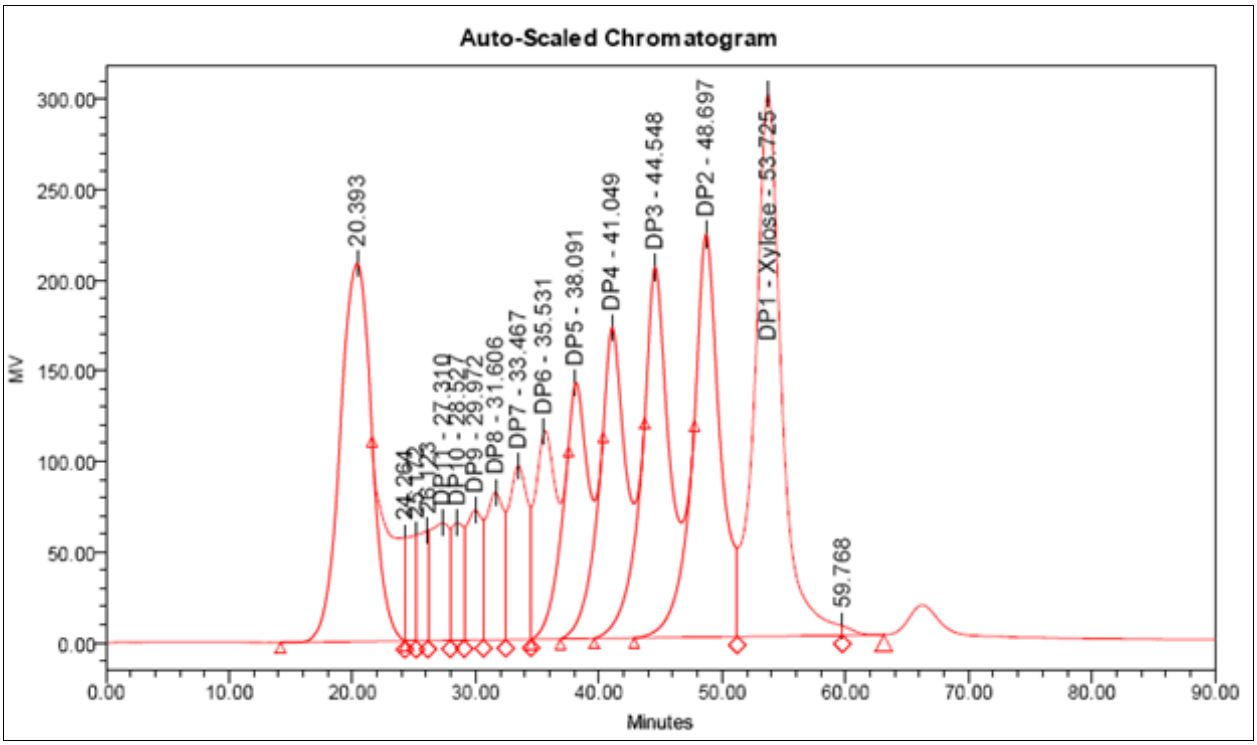

Figure 15: HPLC chromatogram of hydrolyzed birchwood xylan containing xylose monomer (DP 1) and oligomers (DP 2 and higher) analyzed using Biorad Aminex HPX-42A column heated to 85 ˚C. The sample was processed with water as the mobile phase at a flow rate of 0.2 ml/min. The compound was detected using refractive index (RI) detector. DP 1, DP 2, DP 3, and DP 4 were detected at retention times of 54, 49, 45, and 41 min, respectively.

From a series of experiments, the optimum hydrolysis condition for birchwood xylan, which produced the highest yield of DP 2, DP 3, and DP 4, was determined to be 200 ˚C water for 60 min of hydrolysis time and a solid loading rate of 4% (0.8 g in 20-mL solvent). At this optimum hydrolysis condition, the yield of DP 1, DP 2, DP 3, DP 4, and DP 5 based on 1000 mg of birchwood xylan was 94, 60, 25, 36, and 43 mg /g birchwood xylan, respectively.

5.3 Fractionation of Xylose Oligomers

With the production of xylose oligomers from birchwood xylan capabilities in place, the next stage of the process was to fractionate the xylose oligomers using centrifugal partition chromatography (CPC) technology. Without any known solvent systems documented in the literature on xylose oligomers fractionation, a new CPC solvent needed to be developed. As the first step, the best solvent to dissolve xylose oligomers would be determined from a list of eleven solvents that were readily available in the laboratory. Aliquots of hydrolyzed birchwood xylan, which had been neutralized, filtered and completely dried, were added to each tested solvent. The mixtures were thoroughly mixed, filtered, and analyzed for the presence of xylose oligomers by HPLC. From the resulting analysis, water and DMSO were shown to be the best solvent for xylose oligomers separation (**Table 5**). Foucault and Chevolot, (1998) also noted that DMSO was a good solvent for xylose oligomers separation, and specifically the solvent system composed of THF: DMSO: water. With a potential solvent system in hand, THF: DMSO: water, the next step was to determine the volumetric ratio of each solvent in the makeup of the THF: DMSO: water solvent system. Using a phase diagram for THF: DMSO: water, as shown in **Figure 16**, (Foucault et al., 1993), eight different solvent combinations, ranging from 20 - 70% THF, 10 - 60% DMSO and 10 - 40% water, were tested. Solvent makeup needed to be within two phase regions of the solvent system, a condition required for the operation of CPC. The selection criteria were: (1) the ability of the solvent to form two phases; and, (2) good partition coefficient values for xylose oligomers. The determination of partition coefficient values was according to the method previously used by Engelberth et al. (2008).

Table 5: Solvent affinity study for xylose oligomers.

Solvent	Suitability for CPC Solvent	Detectable Compounds
Water	Excellent	Detectable from xylose (DP 1) to xylose 12-mer (DP12)
Acetonitrile	Poor	Detectable of DP 1 only
Butanol	OK	Detectable from DP 1 to xylotriose (DP 3) only
Chloroform	Poor	Detectable of DP 1 only
DMSO	Excellent	Detectable from DP 1 to DP 12
Ethanol	OK	Detectable from DP 1 to DP 3 only
Ethyl Acetate	No	None
Heptane	No	None
Methanol	Good	Detectable from DP 1 to xylohexaose (DP 6) only
Hexane	No	None
Isopropanol	No	None

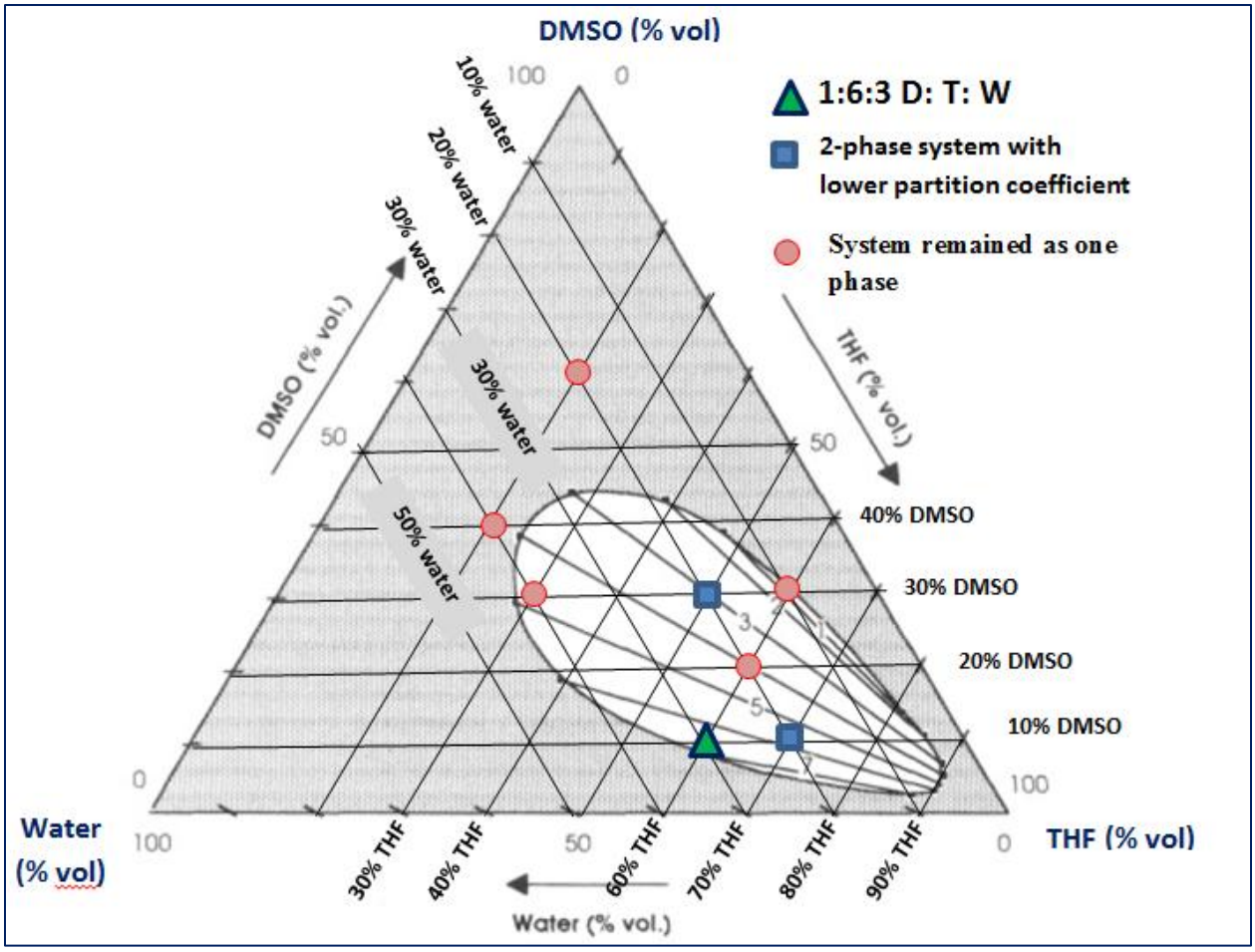

Figure 16: The solubility diagram of THF: DMSO: water system at 20˚C. The white ellipsoid region corresponds to the biphasic zone. The triangle point indicated the optimum solvent system of THF: DMSO: water at 6:1:3 volumetric ratio. This solvent combination was used for xylose oligomers separation (Adapted from Foucalt et al., 1993).

The THF: DMSO: water system at 6:1:3 ratio was selected because of the best partition coefficient values among the solvent system tested, as shown in **Table 6**. The partition coefficients of DP 1, DP 2, DP 3, and DP 4 were 0.25, 0.15, 0.09, and 0.01, respectively. Although the partition coefficients were not within the ideal range of $0.50 < K < 2.00$ (Marston and Hostettmann, 2006), THF: DMSO: water solvent system prepared in the 6:1:3 ratio was used for the purification of xylose oligomers.

With the solvent system in hand, oligomer purification could be initiated on the CPC. Xylose oligomers were prepared according to the steps previously reported for birchwood xylan hydrolysis, and injected onto the CPC for fractionation. Each injection contained 0.5 – 1.0 g of equivalent crude birchwood xylan, which had been hydrolyzed, neutralized, and dried. A typical CPC run, operating at 1000 rpm in the ascending mode, with an 8.8 ml/min mobile phase flow rate, resulted in the xylose oligomers eluting between 35 and 78 min. The ELSD chromatogram of the CPC run is presented in **Figure 17**. The collected fractions were dried and reconstituted in water for HPLC analysis. The identity and quantity of the distinct oligomers present in the corresponding fractions were determined by HPLC analysis. The identity of each oligomer was confirmed by co-chromatography with the available oligomer standards. As shown in **Table 7**, the amount and purity of compounds collected from the CPC separations, based on one g of birchwood xylan, were 25.26 mg of DP 1 at 91.9% purity, 10.71 mg of DP 2 at 85.1% purity, 4.15 mg of DP 3 at 54.7% purity, 5.03 mg of DP 4 at 38.3% purity, and 3.31 mg of DP 5 at 30.4% purity. The purity of xylose oligomers was calculated as the peak area of the compound divided by the sum of peak area of DP 1 to DP 12. This methodology resulted in a publication: Lau et al. (2011).

Table 6: Properties of various dimethyl sulfoxide, tetrahydrofuran and water solvent combinations.

T:D:W[a] ratio	Settling time (s)	Top Phase (% volume)	Number of replicates	Partition coefficient				
				Xylose (DP 1)	Xylobiose (DP 2)	Xylotriose (DP 3)	Xylotetraose (DP 4)	Xylopentaose (DP 5)
6:1:3	60	42.90%	3	0.25 ± 0.01	0.15 ± 0.02	0.09 ± 0.01	0.01 ± 0.02	0
7:1:2	70	67.10%	3	0.11 ± 0.00	0.04 ± 0.00	0	0	0
6:2:2	>180	NA	NA	NA	NA	NA	NA	NA
3:3:4	∞	NA	NA	NA	NA	NA	NA	NA
5:3:2	40	42.90%	3	0.13 ± 0.01	0.04 ± 0.01	0.01 ± 0.01	0	0
6:3:1	∞	NA	NA	NA	NA	NA	NA	NA
2:4:4	∞	NA	NA	NA	NA	NA	NA	NA
2:6:2	∞	NA	NA	NA	NA	NA	NA	NA

[a] T, Tetrahydrofuran; D, Dimethyl sulfoxide; W, Water

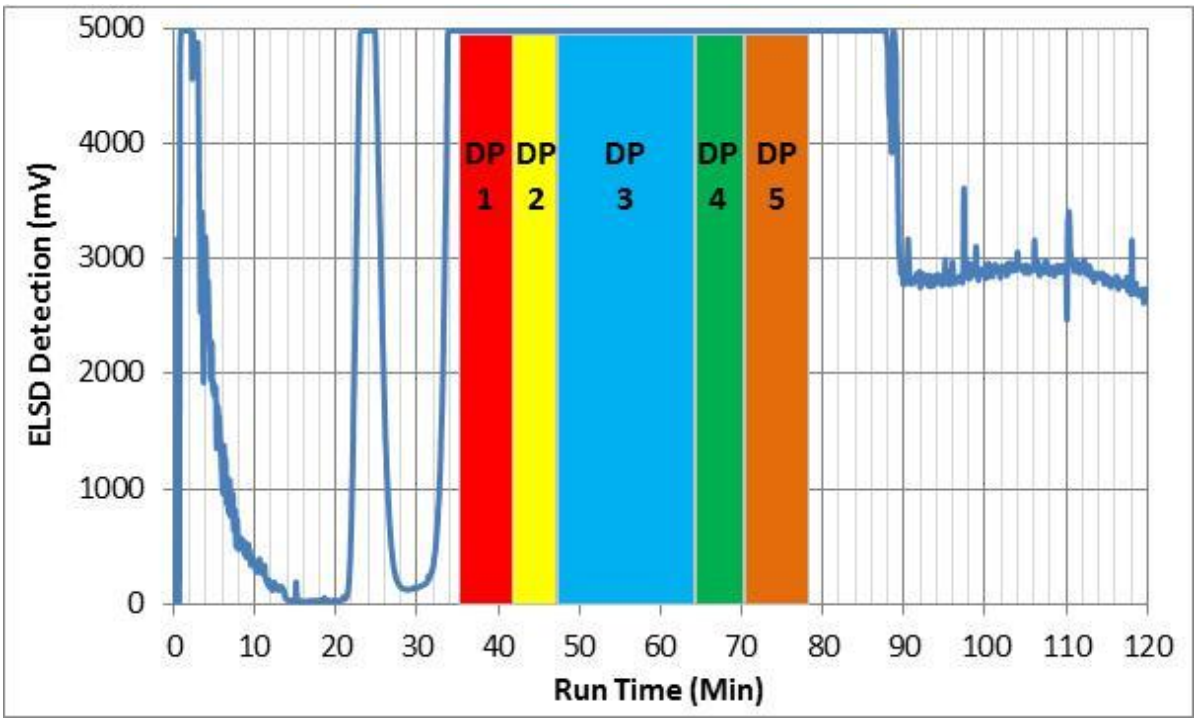

Figure 17: Centrifugal partition chromatography (CPC) chromatogram for hydrolyzed birchwood xylan using the THF: DMSO: water solvent system prepared in the 6:1:3 volumetric ratio. The Kromaton CPC instrument operated at 8.5 ml/min flow rate, rotating at 1,000 rpm, in the ascending mode. The evaporative light scattering detector (ELSD) was set at 25˚C spray chamber temperature, a 55˚C drift tube temperature, and a 50 psig air pressure using ultra-pure nitrogen. Each CPC run used 0.5 – 1.0 g of birchwood xylan. The purity and yield of the xylose oligomers from the CPC fractionation are shown in **Table 7**.

Table 7: Yield of the CPC fractionated xylose monomer and oligomers.

Fractionated Compounds	Yield of each compound (mg/g xylan)	Purity[a] (%)
DP 1 – Xylose	25.26 ± 3.35	90.08 ± 2.52
DP 2 – Xylobiose	10.71 ± 1.91	83.01 ± 2.92
DP 3 – Xylotriose	4.15 ± 0.59	50.76 ± 5.59
DP 4 – Xylotetrose	5.03 ± 0.71	35.77 ± 3.63
DP 5- Xylopentaose	3.31 ± 2.08	31.19 ± 1.07
Total Yield:	48.46 ± 1.95	

[a] Purity is calculated as the peak area of the compound divided by the sum of peak area of DP 1 – DP 12 (xylose 12-mer).

Unfortunately, the CPC fractions that were purified with the THF: DMSO: water solvent system had two disadvantages: (1) the compounds were not of sufficient purity such that they could be used in subsequent kinetic studies; and, (2) the DMSO was very difficult to dry down. The presence of the DMSO residue in the fraction was problematic because it promoted the dehydration of xylose, thereby falsely increasing the yield of furfural (Dias et al., 1995, O'Neill et al., 2009), thwarting the subsequent kinetic study.

Therefore, a new CPC solvent system, other than the THF: DMSO: water system, was sought. According to the previous solvent affinity study, as shown in **Table 5**, water and alcohols, such as methanol, ethanol and butanol, showed promised for xylose oligomers fractionation. Specifically, based on the solvent selection reported by Foucault and Chevolot (1998), solvent systems that included heptane, ethyl acetate, and chloroform showed the most promise for carbohydrate fractionation.

Accordingly, the partition coefficients of xylose oligomers were determined in the following seven solvent systems: (1) butanol: ethanol: water at 4:1:4; (2) chloroform: methanol: water at 7:13:8; (3) butanol: acetic acid: water at a 4:1:5; (4) butanol: formic acid: water at 3:6:14; (5) heptane: ethyl acetate: ethanol: water at 4: 5: 3: 3; (6) heptane: ethyl acetate: methanol: water at 6: 1: 6: 1 and at (7) 2:1: 2: 1 ratio. The calculated partition coefficients with the seven solvent systems are shown in **Table 8**.

Table 8: Partition coefficients for xylose monomer and oligomers in various solvent systems that contained alcohol components as compared to the existing DMSO: THF: water system that was reported by Lau et al. (2011).

Solvent System	Volumetric Ratio	DP4	DP3	DP2	DP1
DMSO: THF: Water	1:6:3	0.00 ± 0.01	0.02 ± 0.00	0.05 ± 0.00	0.12 ± 0.00
Butanol: Ethanol: Water	4:1:4	0.01 ± 0.01	0.03 ± 0.00	0.07 ± 0.00	0.15 ± 0.00
Chloroform: Methanol: Water	7:13:8	37.90	29.52 ± 13.85	11.37 ± 3.93	4.77 ± 1.37
Butanol: Acetic Acid: Water	4:1:5	0.02	0.04	0.07	0.15
Butanol: Formic Acid: Water	3:6:14			0.02	0.07
Heptane: Ethyl Acetate: Ethanol: Water	4:5:3:3	0	0	0	0.01 ± 0.00
Heptane: Ethyl Acetate: Methanol: Water	6:1:6:1	0	0	0	0.01 ± 0.01
Heptane: Ethyl Acetate: Methanol: Water	2:1:2:1	0	0	0	0.01 ± 0.01

The THF: DMSO: water solvent system of 6:1:3 volumetric ratio was used as a control. Of the seven tested solvent systems, butanol: ethanol: water at 4:1:4, chloroform: methanol: water at 7:13:8, and butanol: acetic acid: water at a 4:1:5 yielded similar partition coefficients than that of the THF: DMSO: water solvent system at 6:1:3. The chloroform: methanol: water at 7:13:8 ratio was discarded because of the chloroform toxicity which may cause handling problems. The butanol: acetic acid: water at 4:1:5 ratio solvent system was discarded because of the need to neutralize the fractions with calcium carbonate prior to HPLC analysis, presenting procedural difficulties. The solvent system of butanol: ethanol: water at 4:1:4 was selected for further xylose oligomers fractionation, because of its comparable partition coefficient of xylose oligomers to that of the THF: DMSO: water solvent system.

Having established that the butanol: ethanol: water mixture was a good solvent system for the xylose oligomers purification, experiments had to be conducted to refine the volumetric solvent ratio. A list of twelve mixtures, containing either butanol: ethanol: water or butanol: methanol: water, and its effect on partition coefficients and corresponding settling times is shown in **Table 9**. Among the twelve combinations, butanol: methanol: water at 4:1:4 and 5:1:4 volumetric ratio yielded the optimal partition coefficient values for xylose oligomers separation. For the solvent system consisting of butanol: methanol: water at 4:1:4, the partition coefficient values for DP 1, DP 2, DP 3, DP 4, and DP 5 were 0.166, 0.087, 0.041, 0.018, and 0.010, respectively. Using the solvent system of butanol: methanol: water at 5:1:4, the partition coefficient values for DP 1, DP 2, DP 3, DP 4, and DP 5 were 0.158, 0.081, 0.038, 0.016, and 0.008, respectively. Partition coefficients calculated with the butanol: ethanol: water solvent systems were comparable to those of the THF: DMSO: water solvent system.

Table 9: Partition coefficients for xylose monomer and oligomers in various butanol, methanol/ethanol and water solvent combinations.

Solvent System	Solvent Ratio	Settling time (s)	DP5	DP4	DP3	DP2	DP1
BuOH : EtOH : Water	4:1:4	45	-	0.009 ± 0.001	0.022 ± 0.002	0.058 ± 0.003	0.127 ± 0.006
BuOH : EtOH : Water	5:1:4	36	-	0.006 ± 0.000	0.015 ± 0.001	0.044 ± 0.003	0.104 ± 0.009
BuOH : EtOH : Water	4:1:5	41	-	0.008 ± 0.000	0.021 ± 0.001	0.056 ± 0.000	0.124 ± 0.003
BuOH : EtOH : Water	6:1:3	70	-	0.007	0.019	0.049	0.113
BuOH : EtOH : Water	3:1:6	51	-	0.008 ± 0.002	0.023 ± 0.003	0.059 ± 0.002	0.129 ± 0.001
BuOH : EtOH : Water	4:2:4	NA*					
BuOH : MeOH : Water	4:1:4	59	0.010 ± 0.000	0.018 ± 0.000	0.041 ± 0.001	0.087 ± 0.003	0.166 ± 0.001
BuOH : MeOH : Water	5:1:4	48	0.008 ± 0.001	0.016 ± 0.001	0.038 ± 0.002	0.081 ± 0.004	0.158 ± 0.004
BuOH : MeOH : Water	4:1:5	56	0.006 ± 0.001	0.012 ± 0.002	0.028 ± 0.001	0.068 ± 0.002	0.138 ± 0.004
BuOH : MeOH : Water	6:1:3	NA*					
BuOH : MeOH : Water	3:1:6	61	0.003 ± 0.004	0.011 ± 0.000	0.027 ± 0.002	0.063 ± 0.003	0.135 ± 0.002
BuOH : MeOH : Water	4:2:4	NA*					

*NA: the solvent mixture did not form two distinct phases, but remained as one homogenous phase.

The solvent system butanol: methanol: water at 5:1:4 was selected for further CPC purification because of the high partition coefficient values that were calculated for xylose oligomers.

CPC fractionation was carried out under similar operating condition as the THF: DMSO: water solvent system. The process included injection of 0.5 – 1.0 g of equivalent crude birchwood xylan, with the CPC rotor operating at 1000 rpm in the ascending mode. The flow rate was 4.89 ml/min; fraction collection started 40 min after the sample injection, and the collection time was set at 2 min per fraction, such that each fraction contained 9.78 mL of eluent. The fractions containing xylose oligomers eluted between 80 and 280 min after the time of the sample injection. A typical ELSD chromatogram of a CPC run is presented in **Figure 18**. The collected fractions were dried and reconstituted in water for HPLC analysis, where the identity and quantity of the separated oligomers present in the corresponding fractions were determined. The HPLC analyses of the separated oligomers are presented in **Figure 19**.

As shown in **Table 10**, the amount and purity of the oligomers collected from the Kromaton CPC runs from 1 g birchwood xylan hydrolysate were 37.11 mg of DP 1 at 89.7% purity, 23.05 mg of DP 2 at 99.7% purity, 9.34 mg of DP 3 at 98.9% purity, 16.41 mg of DP 4 at 94.2% purity, and 14.54 mg of DP 5 at 68.1% purity.

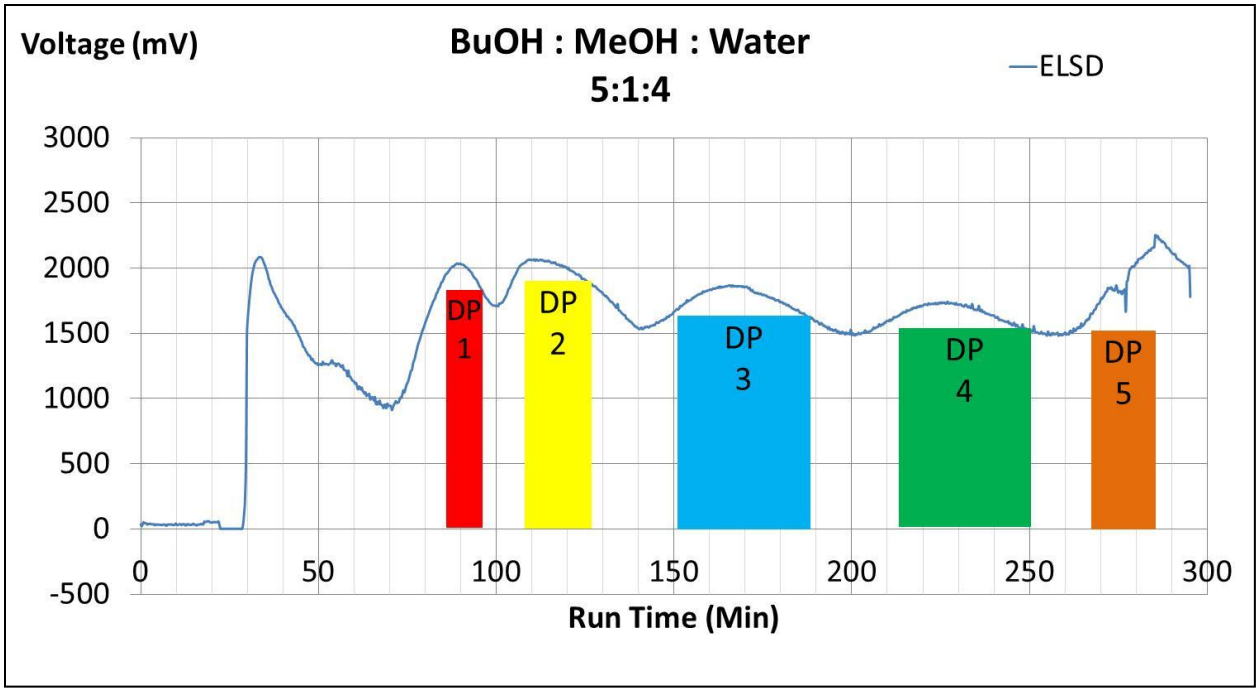

Figure 18: Centrifugal partition chromatography (CPC) chromatogram for hydrolyzed birchwood xylan using the butanol: methanol: water solvent system at 5:1:4 volumetric ratio. The Kromaton CPC operated at 4.89 ml/min flow rate, rotating at 1000 rpm, in the ascending mode. The evaporative light scattering detector (ELSD) was set at 25˚C spray chamber temperature, a 55˚C drift tube temperature and a 50 psig air pressure using ultra-pure nitrogen. The HPLC chromatograms of the individual fractions of xylose monomer and oligomers are shown in **Figure 19**.

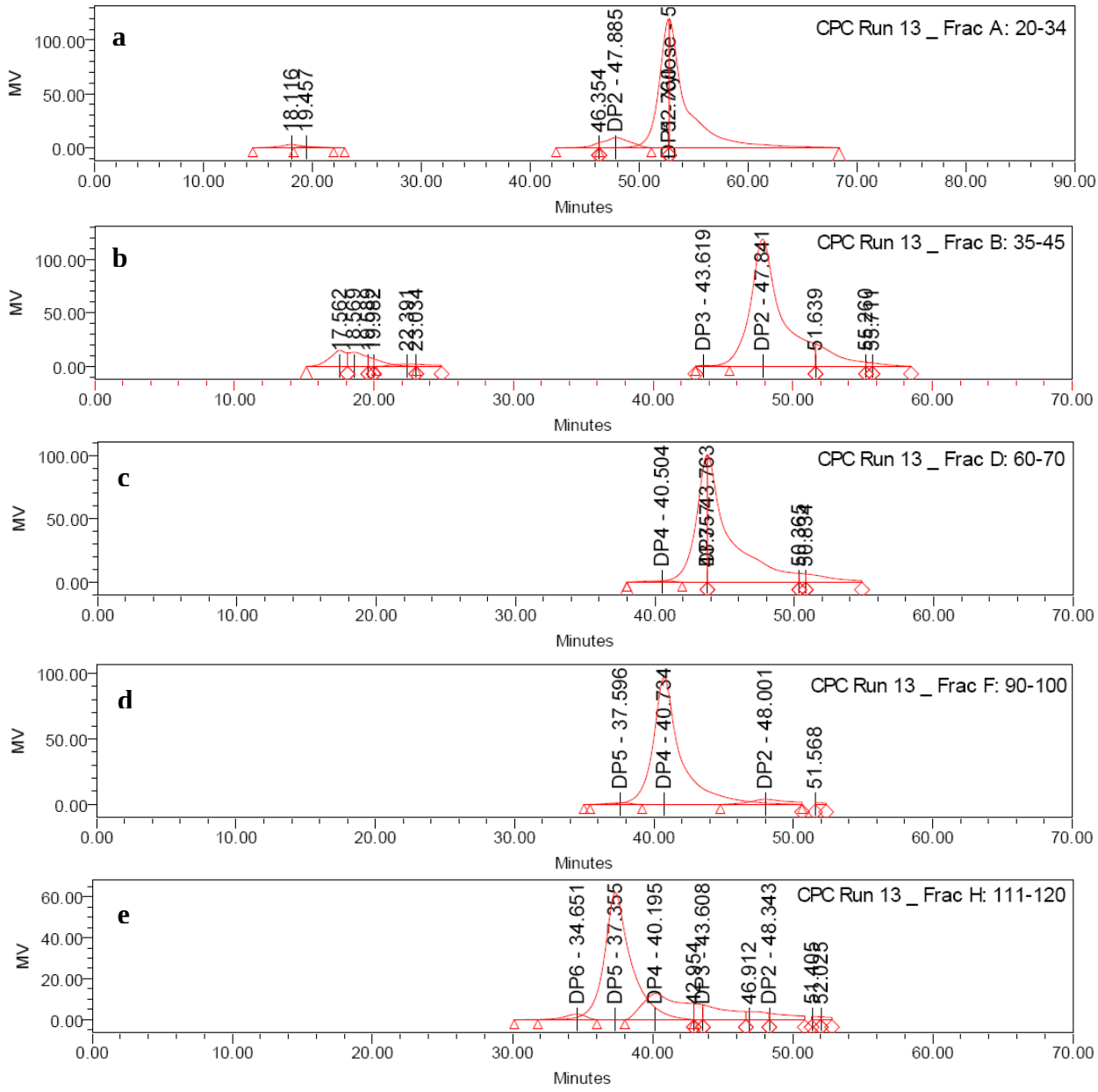

Figure 19: HPLC chromatograms of the fractions collected from the CPC exercise presented in **Figure 18. (a)** chromatogram of xylose-rich fraction collected between 80 and 108 min; **(b)** chromatogram of xylobiose (DP2)-rich fraction collected between 110 and 130 min (DP2); **(c)** chromatogram of xylotriose (DP3)-rich fraction collected between 160 and 180 min; **(d)** chromatogram of xylotetraose (DP4)-rich fraction collected between 220 and 240 min; **(e)** chromatogram of xylopentaose (DP5)-rich fraction collected between 262 and 280 min.

Table 10: Yield of the CPC fractionated xylose monomer and DP 2 - DP 5.

Fractionated Compounds	Yield of each compound (mg/g xylan)	Purity[a] (%)
DP1 – Xylose	37.11	89.68
DP2 – Xylobiose	23.05	99.66
DP3 – Xylotriose	9.34	98.87
DP4 – Xylotetrose	16.41	94.19
DP5- Xylopentaose	14.54	68.06
Total Yield:	63.34	

[a] Purity is calculated as the peak area of the compound divided by the sum of peak area of DP 1 – DP 12 (xylose 12-mer).

In the middle of 2011, the Kromaton CPC instrument was replaced by an Armen CPC instrument because of a leaking rotor in the Kromaton CPC. Therefore the solvent system of butanol: methanol: water at 5:1:4 was later used in the Armen CPC instrument. Because of differences between the rotor size and setup, the Armen CPC equipment was operated at a different flow rate and a rotational speed. The operating conditions of the Armen CPC run were set at 2300 rpm, and a flow rate of 8 ml/min. Also, in order to reduce the overall CPC run time, the butanol-rich mobile phase was swapped for the water-rich phase, in a process known as the extrusion mode. Swapping solvents at the end of a run ensured that the harder-to-be-eluted compounds get flushed from the column. In the optimized operating condition, the extrusion mode began 165 min after the time of the initial sample injection. The ELSD chromatogram of a typical run using the new Armen CPC equipment, performing the extrusion mode, is shown in **Figure 20**.

Using the butanol: methanol: water at 5:1:4 solvent system, xylose oligomers, which were necessary for the subsequent kinetic study, were produced in large quantities. After ten repeated CPC runs, the quantity and sugar purity of DP 2, DP 3, and DP 4 collected were 350 mg at 91% purity, 150 mg at 71% purity, and 100 mg at 49% purity, respectively. The composition of each xylose oligomers is shown in **Table 11**. The purity of the fractionated xylose oligomers were considered satisfactory because most of the sugar impurities were of DP 1 and lower DP oligomers, which would not affect the degradation rates of the higher DP oligomers.

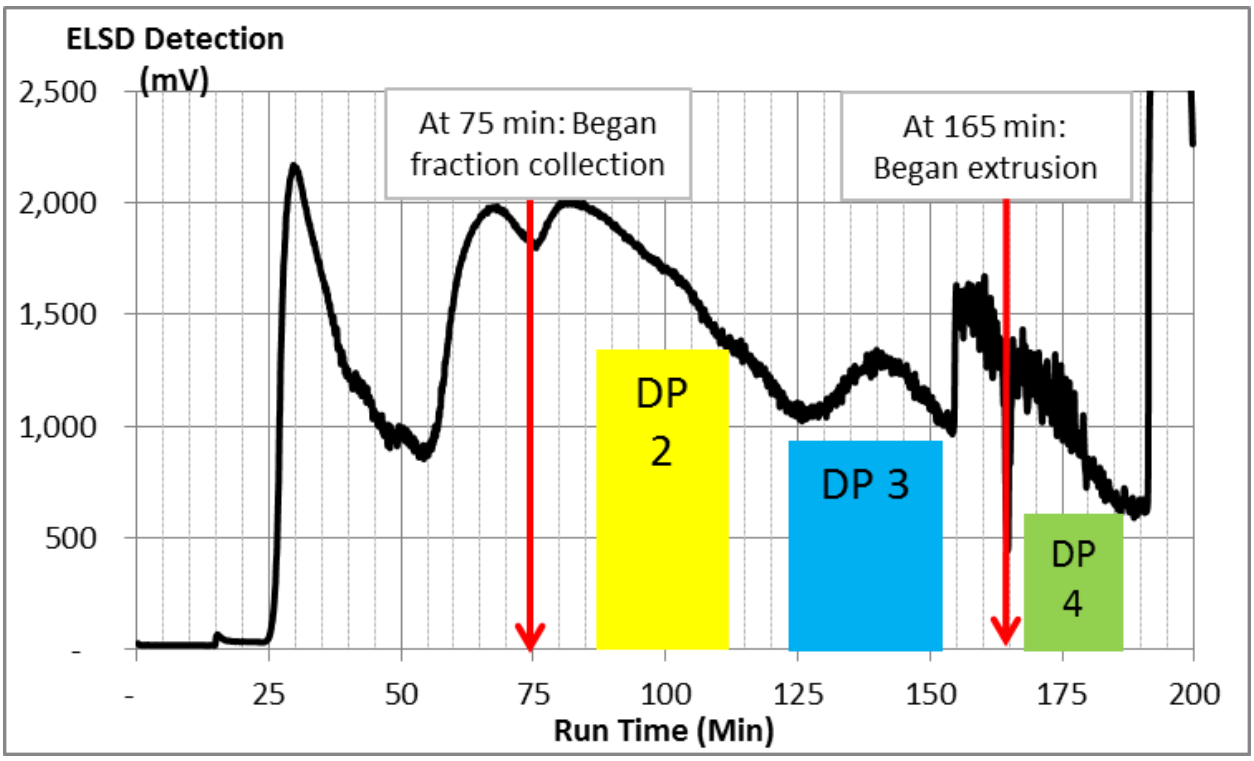

Figure 20: Centrifugal partition chromatography (CPC) chromatogram for hydrolyzed birchwood xylan using the solvent system of butanol: methanol: water at 5:1:4 volumetric ratio. The Armen CPC instrument operated at 8.0 ml/min flow rate, rotating at 2300 rpm, in the ascending mode. The evaporative light scattering detector (ELSD) was set at 25˚C spray chamber temperature, a 55˚C drift tube temperature and a 50 psig air pressure using ultra-pure nitrogen.. Xylobiose (DP2)-rich fraction collected between 87 and 111 min DP 2; DP 3-rich fraction collected between 123 and 153 min; chromatogram of xylotetraose DP 4-rich fraction collected between 168 and 186 min.

Table 11: Purity of CPC-fractionated oligomers used in kinetic study.

	DP 2	**DP 3**	**DP 4**
Total Amount (mg)	350	150	100
Sugar Purity*	91%	71%	49%
DP 1 (mg/mL)	0.13	0.12	0.07
DP 2 (mg/mL)	**1.11**	0.55	0.22
DP 3 (mg/mL)	0.03	**0.88**	0.37
DP 4 (mg/mL)	-	0.05	**1.01**
DP 5 and 6 (mg/mL)	-	-	0.11
Formic Acid (mg/mL)	0.42	-	0.71
Furfural (mg/mL)	-	-	-

* Sugar purity was determined based on the peak area detected in HPLC analysis

5.4 Mass Spectrometry (MS)

The identity of the fractionated xylose oligomers were initially confirmed by HPLC, based on the peak retention times of authentic xylose oligomers standard. Additionally, the CPC-fractionated xylose oligomers and the xylose oligomers standards were submitted to the Arkansas Statewide Mass Spectrometry Facility for the MS analysis to verify the identity of the xylose oligomers.

The molecular mass of each xylose oligomer standard was confirmed using MALDI-MS analysis as presented in **Figure. 21**. Using the MALDI-MS conditions described in the materials and methods, using these samples, all xylose oligomers were observed as gas-phase sodium adduct ions. Therefore, DP 3, DP 5 and DP 6 had significant ions at *m/z* of 437, 701 and 833, respectively, corresponding to the molecular weight of the individual xylose oligomers with sodium ion. Similarly, the ionized standards were observed as the M+23 rather than the M+1 ions, which is rather common for natural products which contain excess sodium.

Using a similar MALDI analytical method on the partially hydrolyzed birchwood xylan shown to contain an assortment of xylose oligomers (**Figure 22**). The MS spectrum confirmed the presence of a sodium molecule attached to each of the xylose oligomers.

Because of the limitation of MALDI analysis in analyzing compounds with low molecular weight, such as DP 1 and DP 2, ESI-MS was also used to verify the molecular weight of the compounds (**Figure 23**). Similar to the results obtained from the MALDI analysis, the ESI-MS spectrum showed the presence of a sodium molecule attached to the xylose oligomer standards. The xylose oligomers collected from the CPC fractionation were also analyzed by ESI-MS and showed the presence of a sodium molecule attached to the xylose oligomers. The presence of xylose oligomers was confirmed by ESI-MS to match the results from the HPLC analysis.

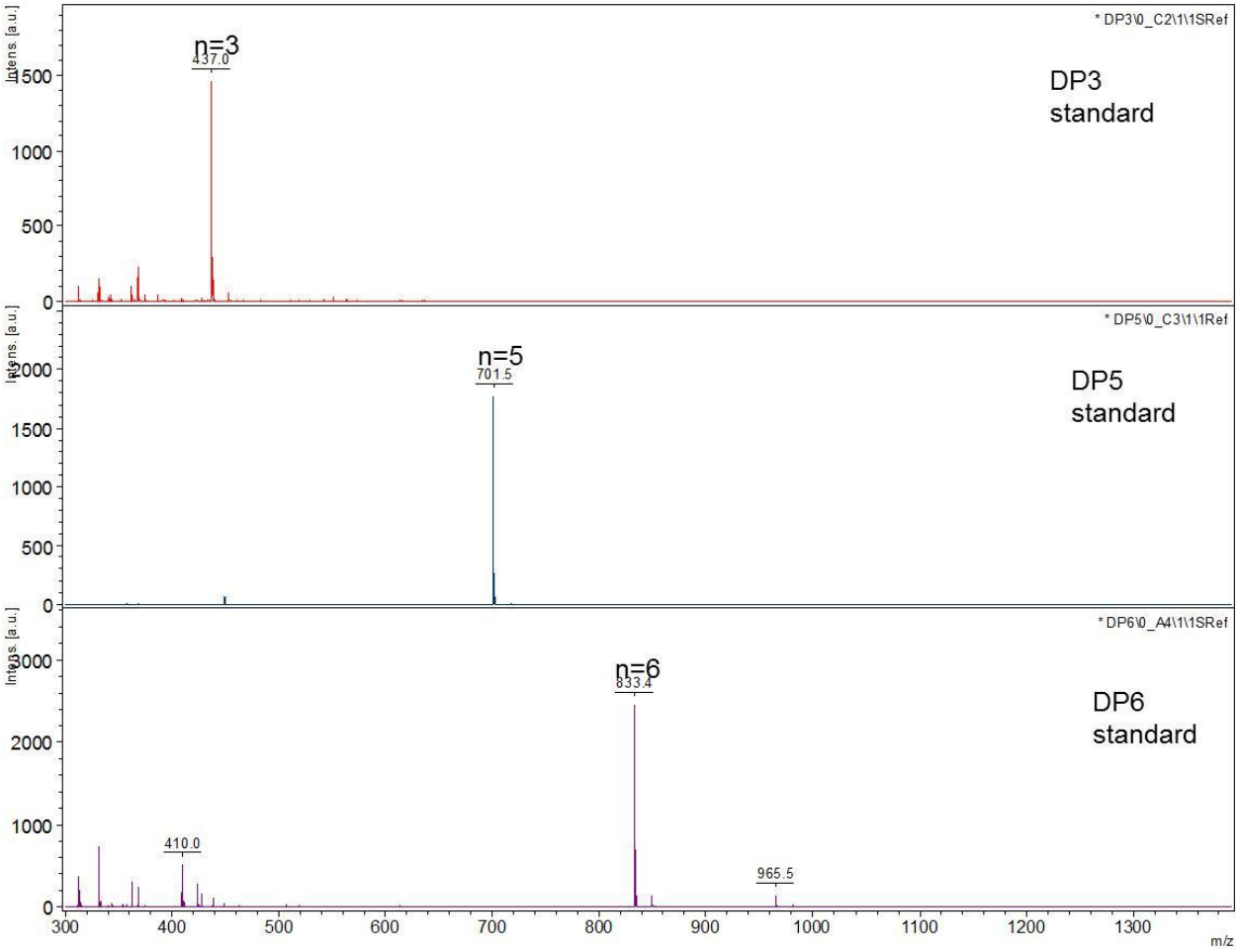

Figure 21: MALDI-MS spectra of DP 3, DP 5, and DP 6 standards.

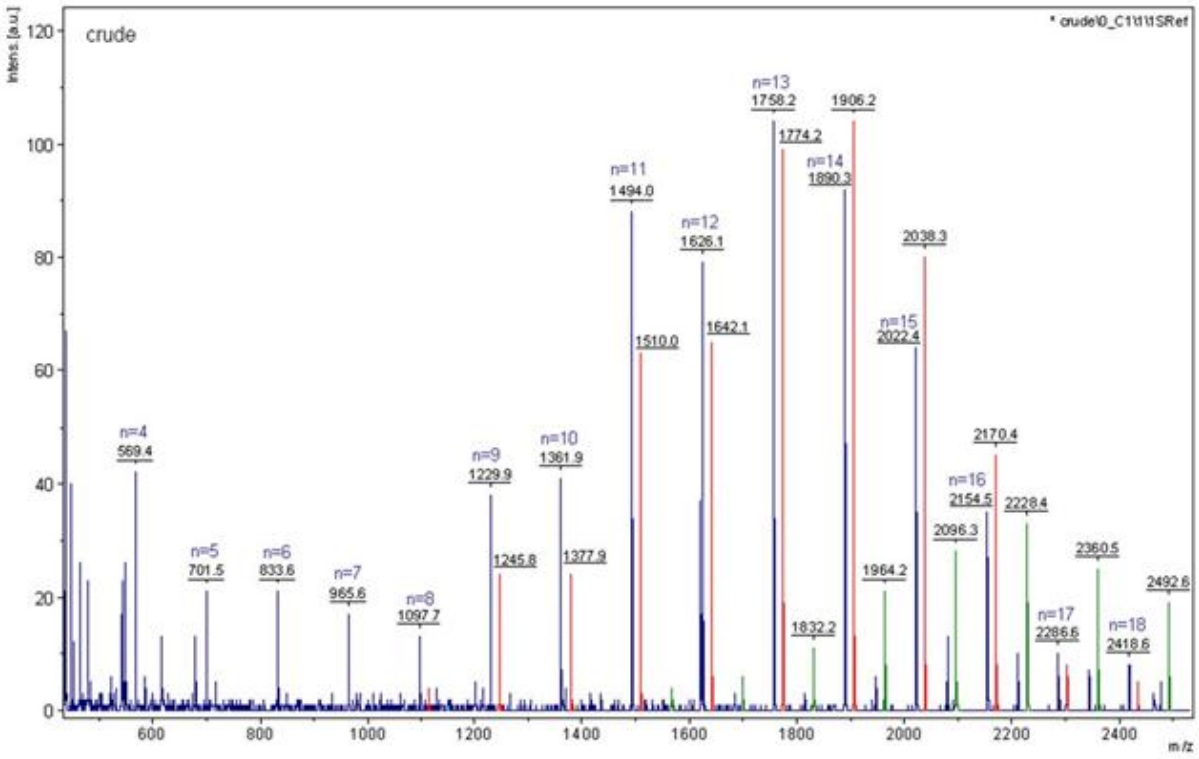

Figure 22: MALDI-MS spectra of hydrolyzed birchwood xylan consisting of xylose monomer and oligomers.

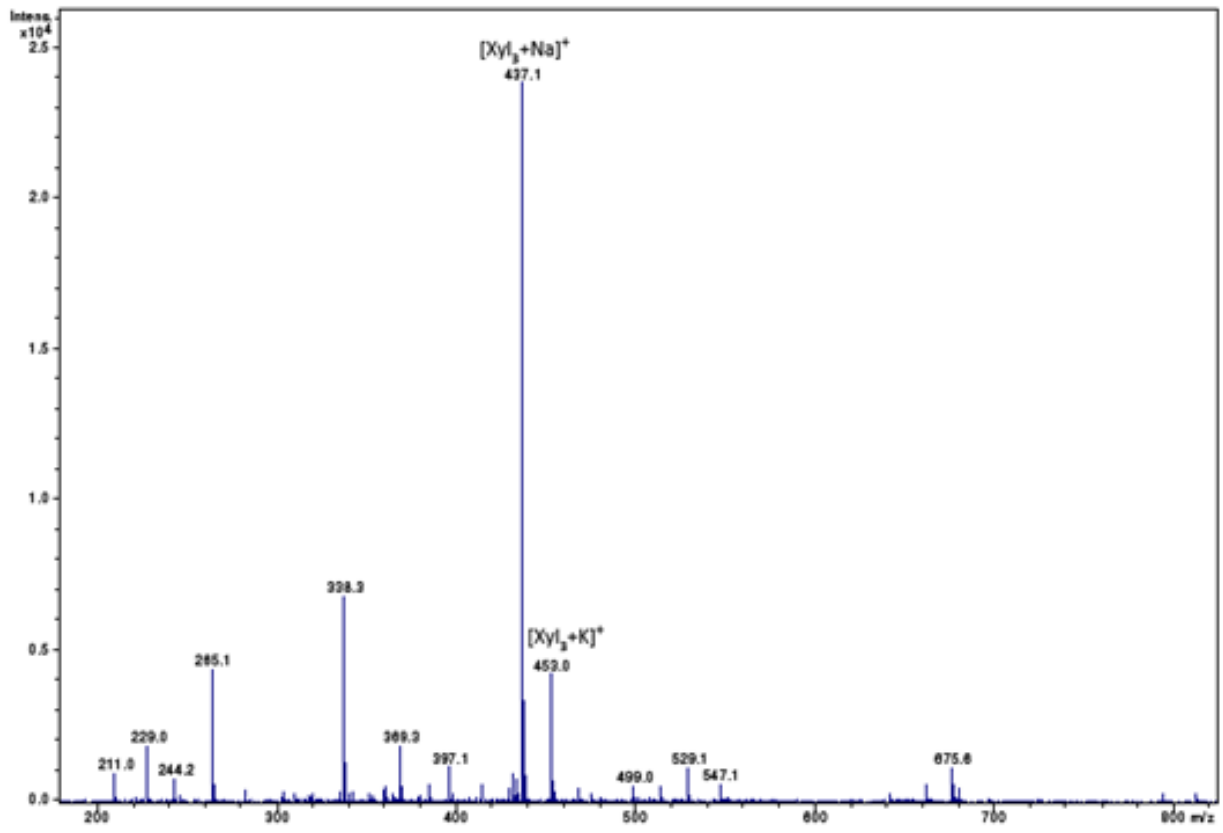

Figure 23: ESI-MS spectra of hydrolyzed birchwood xylan consisting of DP 3 standard.

Results presented in **Figure 24, 25** and **26**, confirmed that the CPC fractionated compounds were indeed DP 3, DP 4, and DP 5. With the xylose oligomers in hand, it was now possible to proceed to the kinetic analysis section.

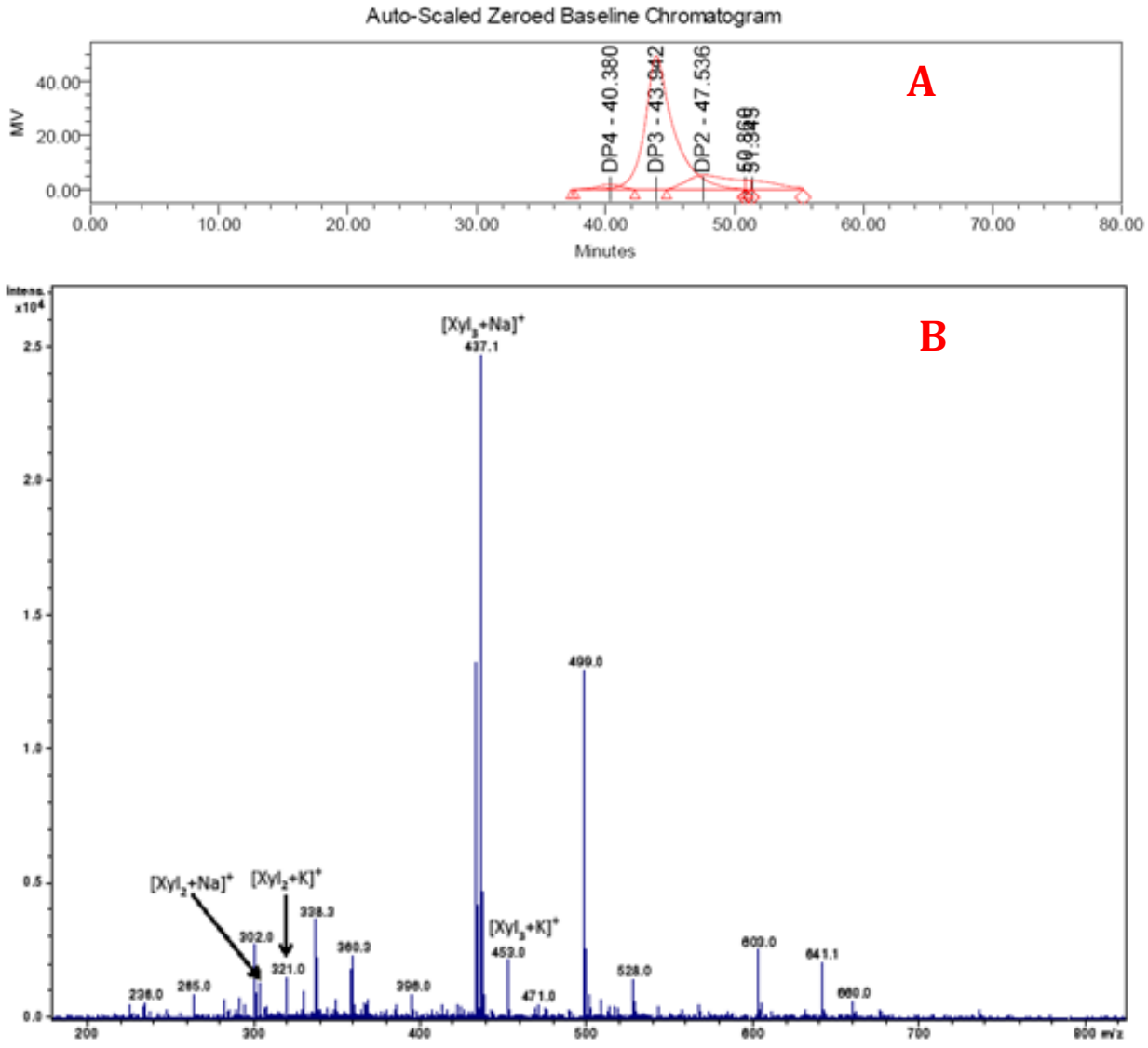

Figure 24: (A) HPLC chromatogram, and **(B)** ESI-MS spectra of CPC-fractionated DP 3. The ESI-MS spectra verify the presence of DP 3 as indicated in the HPLC analysis.

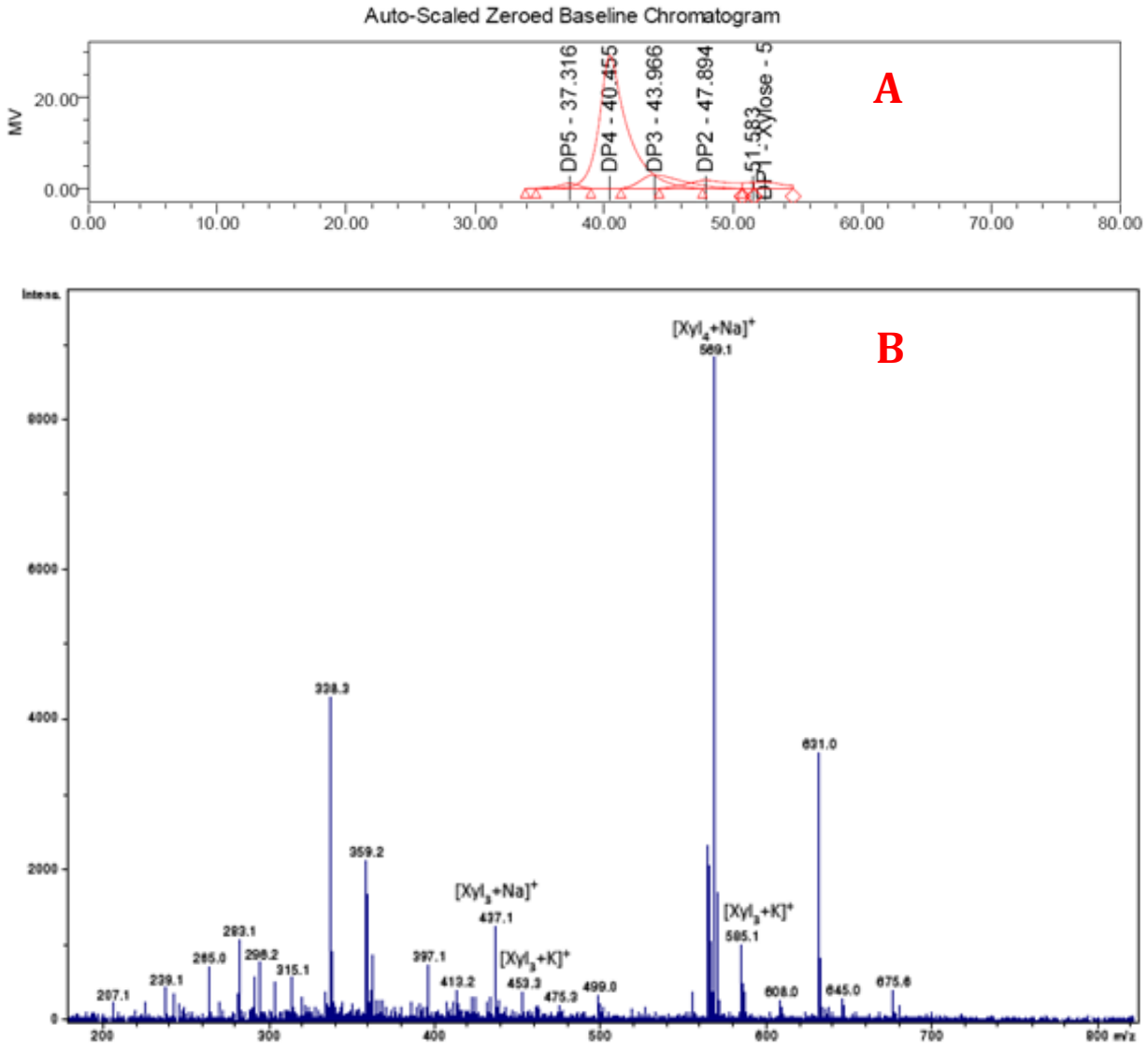

Figure 25: (A) HPLC chromatogram, and **(B)** ESI-MS spectra of CPC-fractionated DP 4. The ESI-MS spectra verify the presence of DP 4 as indicated in the HPLC analysis.

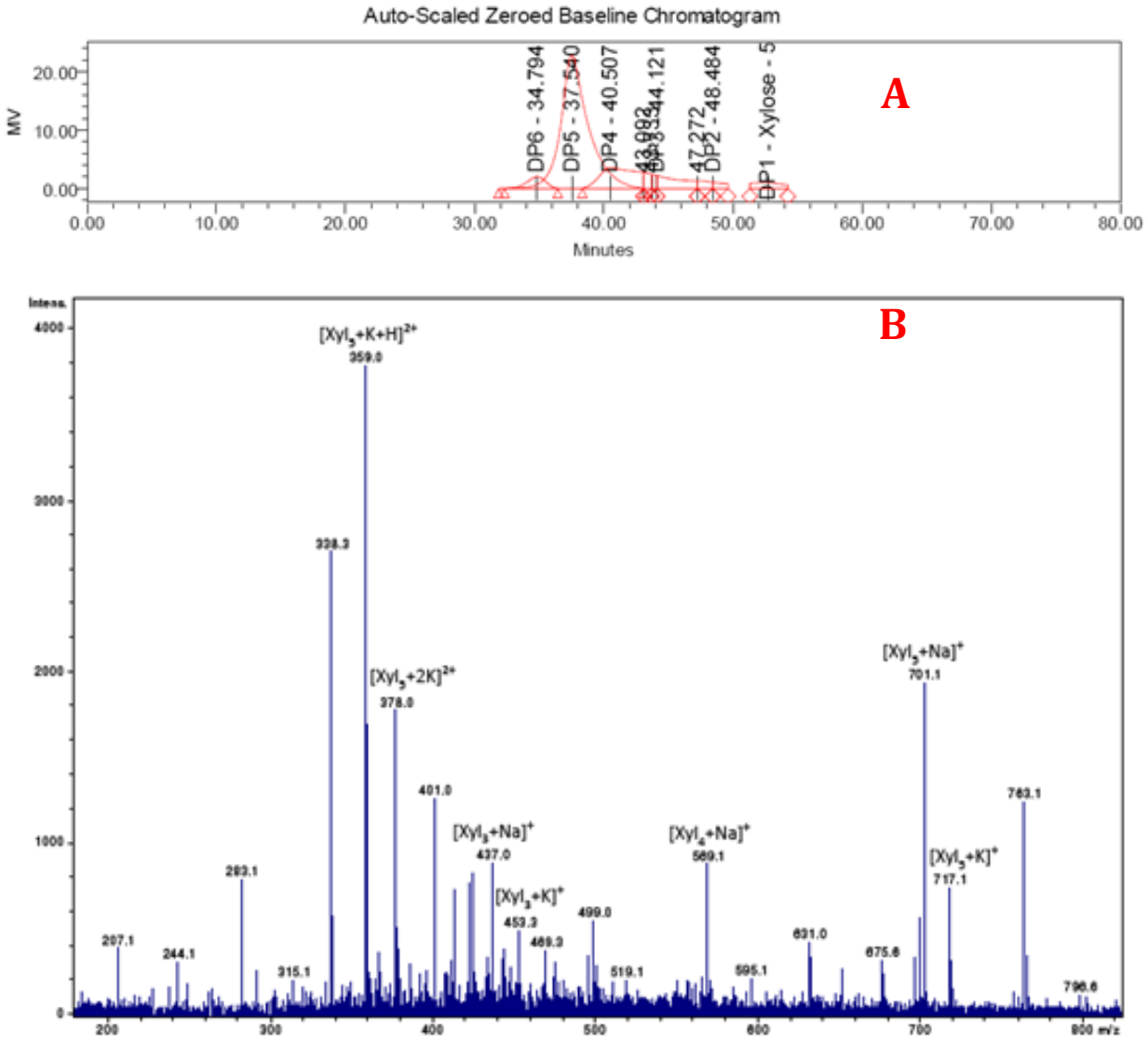

Figure 26: (A) HPLC chromatogram, and **(B)** ESI-MS spectra of CPC-fractionated DP 5. The ESI-MS spectra verify the presence of DP 5 as indicated in the HPLC analysis.

5.5 Kinetic Study

5.5.1 Preliminary Experiment

A total of 24 preliminary experiments at 1, 2, 5 g/L of xylose were conducted to determine the potential effect of initial DP 1 concentration on the degradation rate of DP 1. These experiments were conducted to determine if, indeed, the degradation of xylose was following a first order kinetic reaction. The natural logarithm of C/C_0 as a function of time was plotted for experiments with water at 120 ˚C, 1 v/v% acid at 120 ˚C, water at 200 ˚C, and 1 v/v% acid at 200 ˚C. Results are shown in **Figure 27**, where C and C_0 are the concentrations of xylose at time t and time zero, respectively. Following the first order reaction, ln (C/C_0) decreased linearly with time for each of the tested DP 1 concentrations of 1, 2, and 5 g/L.

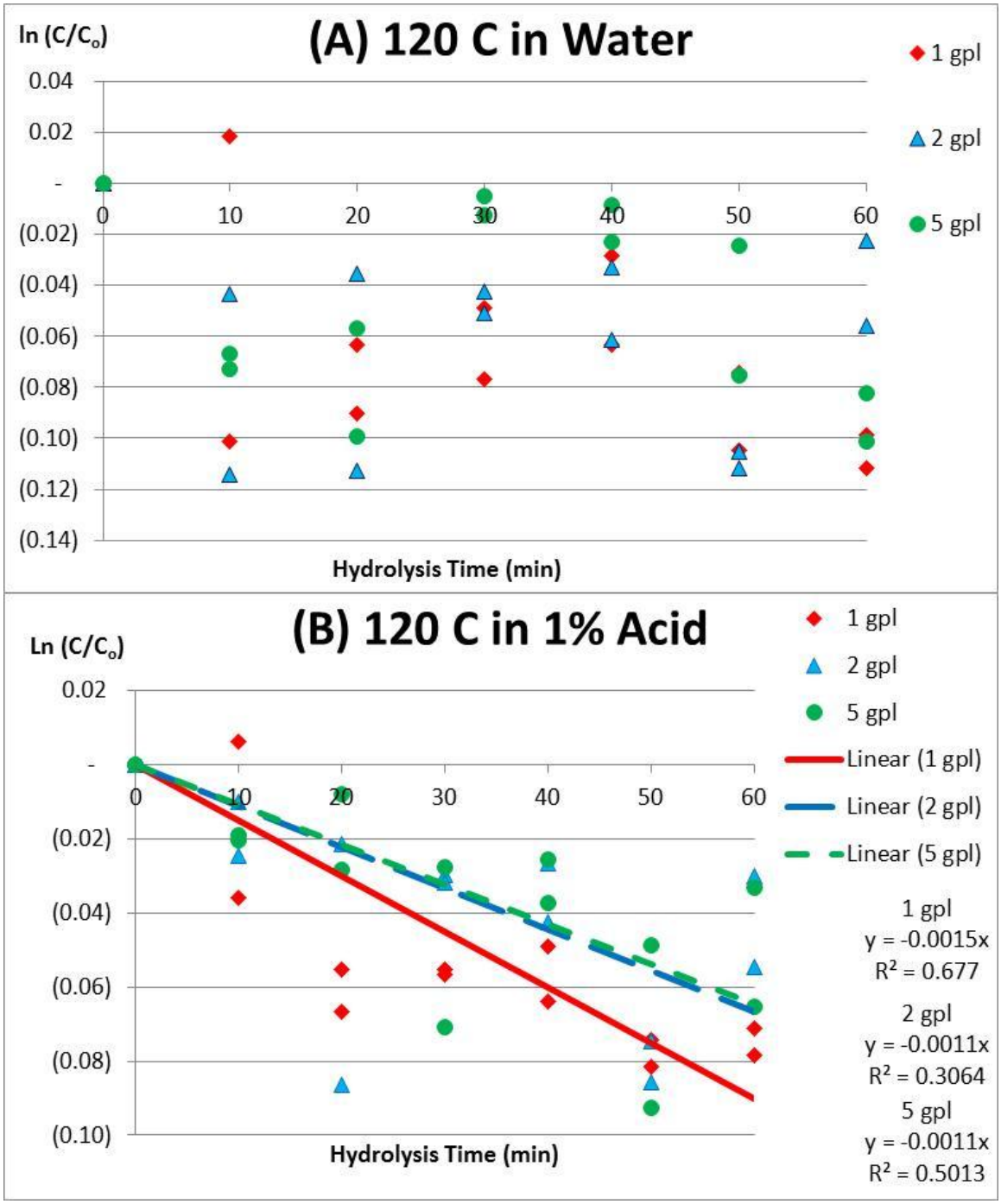

Figure 27: Degradation profile of DP 1 at 1, 2, and 5 g/L (gpl) initial concentration in **(A)** 120 ˚C water and **(B)** 120 ˚C, 1 v/v% sulfuric acid.

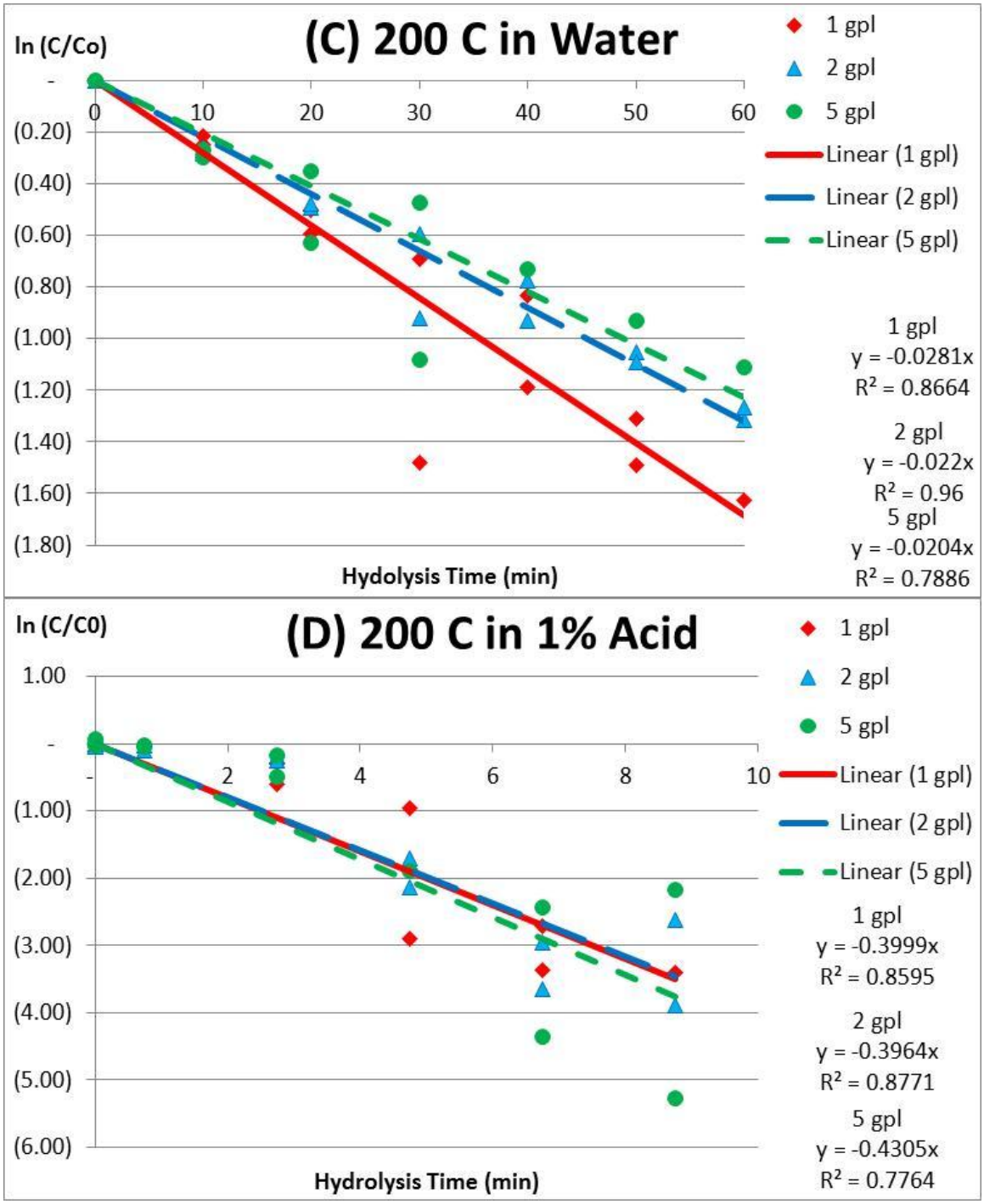

Figure 27: Degradation profile of DP 1 at 1, 2, and 5 g/L (gpl) initial concentration in **(C)** 200 ˚C water and **(D)** 200 ˚C, 1 v/v% sulfuric acid.

The inherent experimental variation caused by the imperfect mixing of DP 1 solution, as well as the uneven heat distribution within the sand bath reactor resulted in an imperfect linear regression of DP 1 concentration with time, as shown by the R^2 values that were as low as 0.31. As shown in **Figure 27**, it was observed that there was practically no degradation with water at 120 ˚C; therefore no regression lines were plotted for these data sets. When there was a reaction, such as the hydrolysis at 120 ˚C with 1 v/v% acid, the R^2 values ranged from 0.31 to 0.68, as shown in **Table 12**. Worth noting, the lines had to be plotted through the origin because in a first order reaction, the changes of DP 1 concentration from its initial concentration, in natural logarithm scale, at time zero should be zero. In other words, the concentration of DP 1 at time zero should be equal to its initial concentration.

As the hydrolysis conditions became more severe, as with water or 1 v/v% acid at 200 ˚C, the effect of experimental variation on the regression lines became less significant as compared to the time effect at the more severe hydrolysis conditions. As a result, the R^2 values improved from 0.78 to 0.96, further confirming that the concentration of DP 1 degrades according to the first order reaction model.

Table 12: The R^2 values of the changes in DP 1 concentration from its initial concentration, in natural logarithm scale, as a function of time, as shown in **Figures 27.**

Initial DP 1 concentration	**1 g/L**	**2 g/L**	**5 g/L**
120 ˚C using 1 v/v% acid	0.68	0.31	0.50
200 ˚C using water	0.87	0.96	0.79
200 ˚C using 1 v/v% acid	0.86	0.88	0.78

The objective of the preliminary study was to determine the effect of the initial DP 1 concentration on the DP 1 degradation rate. In a first order reaction, the reaction rate should be independent of initial concentration. In order to verify the reaction order, a statistical analysis using F test was conducted on the slopes of each initial DP 1 concentration at all four hydrolysis conditions, as shown in **Table 13**. The P-value provides the statistical information of the F test to determine if the degradation rates, as determined by the slopes of the data in **Figures 27**, were statistically different among the three initial DP 1 concentrations. A P value smaller than 5% would indicate that the degradation rates between the pair of initial DP 1 concentrations were different, which would suggest that the initial DP 1 concentration would affect the degradation rates. From the F-test analysis in **Appendix 3**, and summarized in **Table 13**, the P values of the hydrolysis conditions at the three initial DP 1 concentrations were all less than 5%, indicating that the degradation rates at any of the three initial DP 1 concentration were not statistically different from one another. Worth noting, although no regression lines were plotted for the hydrolysis with water at 120 ˚C, a regression analysis was performed on the data at this hydrolysis condition to determine the effect of different initial DP 1 concentration. The statistical analysis showed that the degradation rate of DP 1 was independent of the initial DP 1 concentration, and that the results obtained from the subsequent oligomers and by-products study using a 1 g/L initial concentration can be extrapolated to include the hydrolysis conditions with 2 and 5 g/L initial concentrations. More importantly, the determination that the degradation rate of DP 1 is independent of the initial concentration matches the criteria of a first order reaction.

Table 13: P values of F test in comparing the degradation rates of 1, 2, and 5 g/L (gpl) of initial xylose concentrations at three different hydrolysis conditions.

P values of F-Test	1 gpl vs. 2 gpl	1 gpl vs. 5 gpl	2 gpl vs. 5 gpl
120 ˚C using water	7%	11%	38%
120 ˚C using 1 v/v% acid	11%	55%	84%
200 ˚C using water	96%	85%	29%
200 ˚C using 1 v/v% acid	24%	26%	26%

5.5.2 Main Experiment

In the experimental design, a total of 108 experiments were planned to determine the effect of temperature and pH on the degradation rates of xylose monomer, oligomers, and by-products. However, because DP 3 and DP 4 proved more difficult to obtain in high purity than originally anticipated, the number of experiments was reduced due to limited quantity of DP 3 and DP 4 obtained from the CPC fractionation. Out of the six tested compounds, DP 1, DP 2, formic acid, and furfural were fully explored at all nine hydrolysis conditions. DP 4 was tested in only four out of the nine conditions: water at 160 ˚C, 0.1 v/v% acid at 160 ˚C, 1 v/v% acid at 160 ˚C, and water at 200 ˚C. DP 3 was tested in the above four hydrolysis conditions, and also at 0.1 v/v% acid at 200 ˚C. All data points for DP 1, DP 2, DP 3, formic acid, and furfural had two replicates. Because of the limited amount of DP 4, only a limited number of data points were repeated for the experiments. Worth noting, 0.1 v/v% and 1 v/v% sulfuric acid are equivalent to 0.18 wt% and 1.8 wt% sulfuric acid, respectively. The calculated pH for the 0.1 v/v% acid was 1.43, while the 1 v/v% acid was pH 0.43. In addition, through the experiment, a time of 1.25 min (75 s) was needed for the sample in the stainless steel tubes to reach the temperature of the sand bath, the hydrolysis time began 1.25 min (75 s) after submerging the stainless steel tubes into the sand bath reactor. The equations that were used to describe xylose oligomers depolymerization and by-products formation are presented in the Materials and Methods section.

The experimental data are shown in **Figure 28 - 33**. For the hydrolysis of DP 4, as shown in **Figure 28**, less than 15% of initial DP 4 remained after 40 min of hydrolysis with water at 160 ˚C, 0.1 v/v% sulfuric acid at 160 ˚C, 1 v/v% sulfuric acid at 160 ˚C, and water at 200 ˚C. Among the four tested hydrolysis conditions, 160 ˚C water was the least severe condition, and resulted in 13% of DP 4 remaining after 40 min.

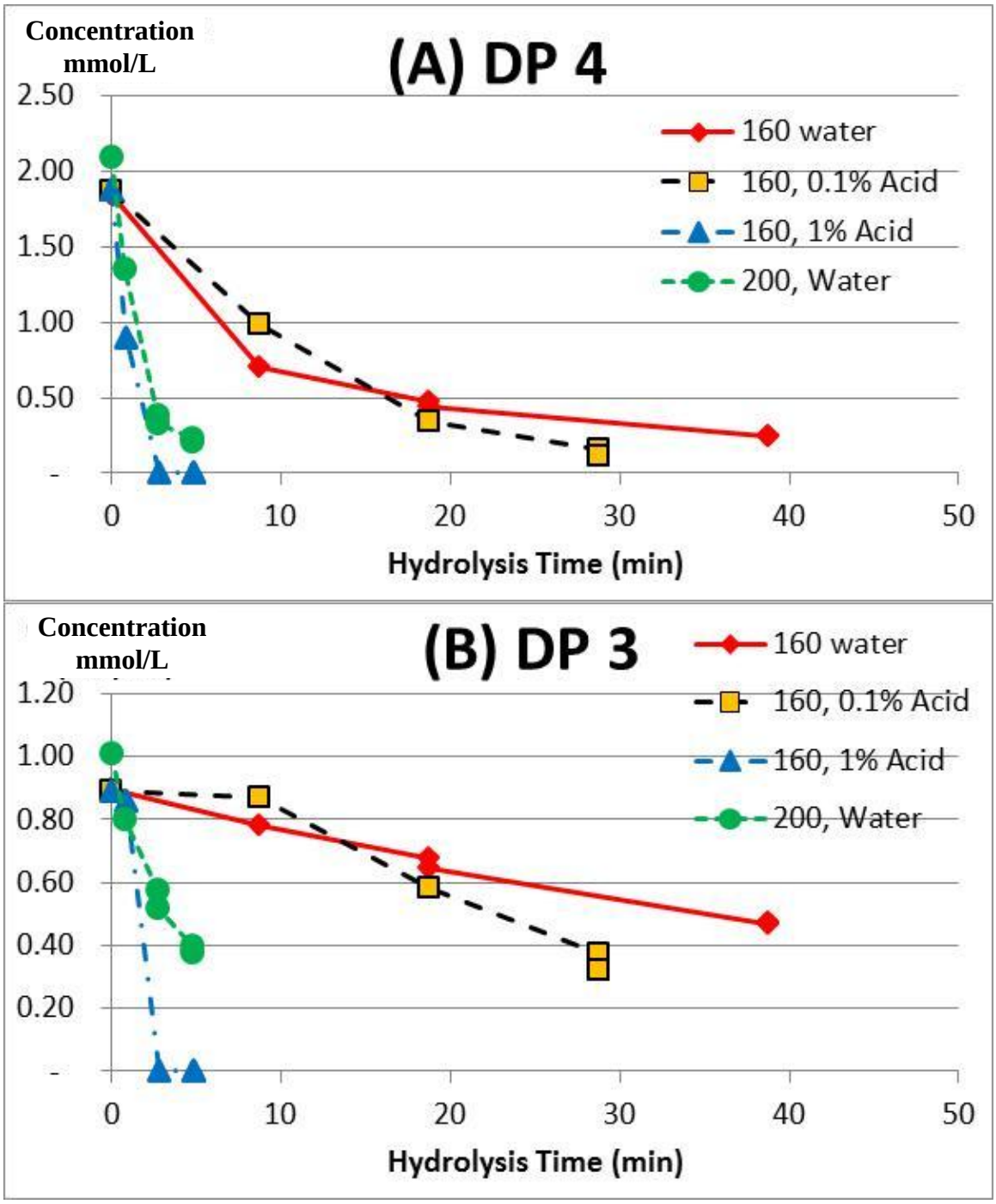

Figure 28: The experimental data showing the molar concentration of **(A)** DP 4 and **(B)** DP 3 as a function of hydrolysis time during the hydrolysis of DP 4 in 160 ˚C water, 160 ˚C of 0.1v/v% sulfuric acid, 160 ˚C of 1 v/v% sulfuric acid, and 200 ˚C water.

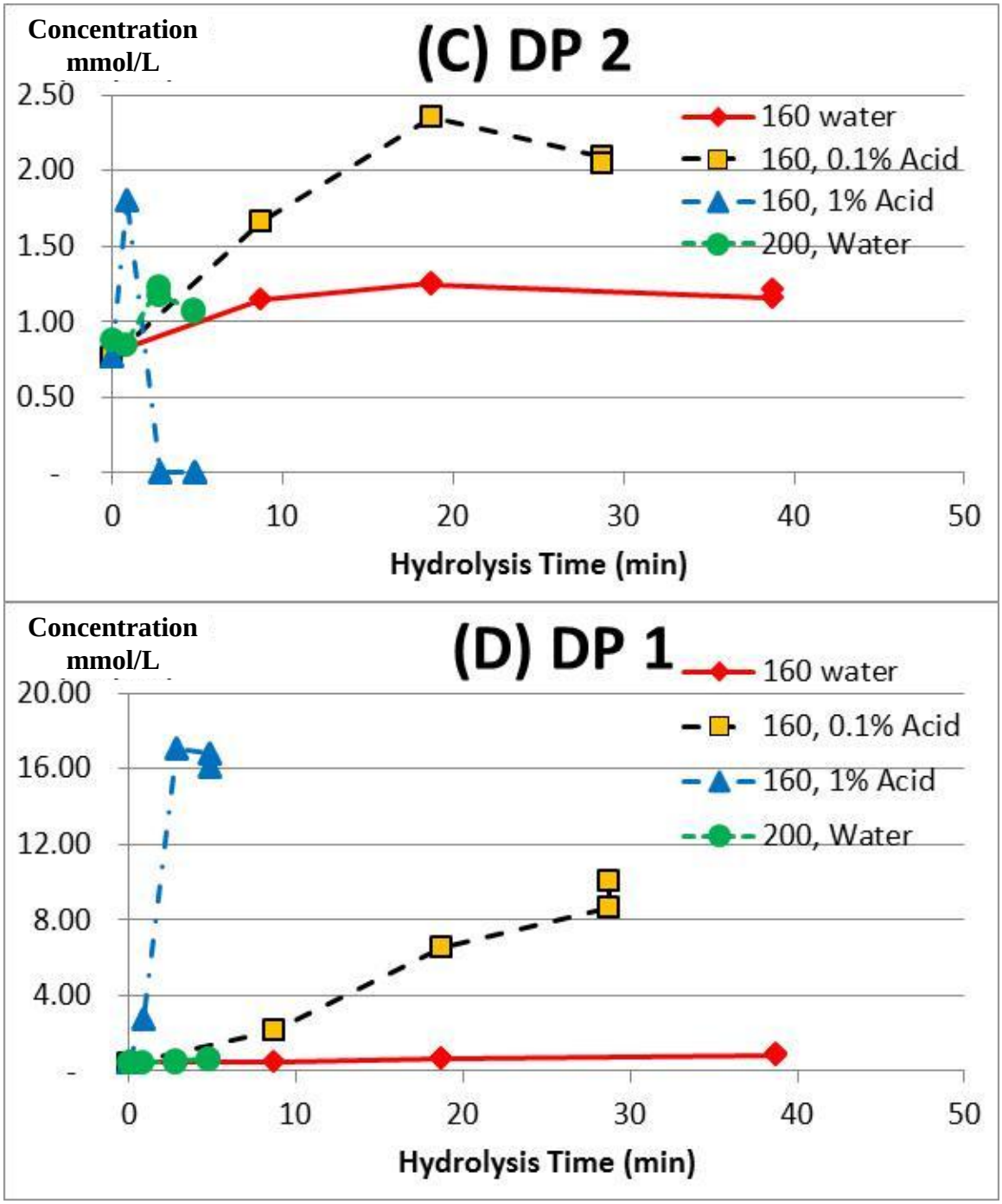

Figure 28: The experimental data showing the molar concentration of **(C)** DP 2 and **(D)** DP 1 as a function of hydrolysis time during the hydrolysis of DP 4 in 160 ˚C water, 160 ˚C of 0.1v/v% sulfuric acid, 160 ˚C of 1 v/v% sulfuric acid, and 200 ˚C water.

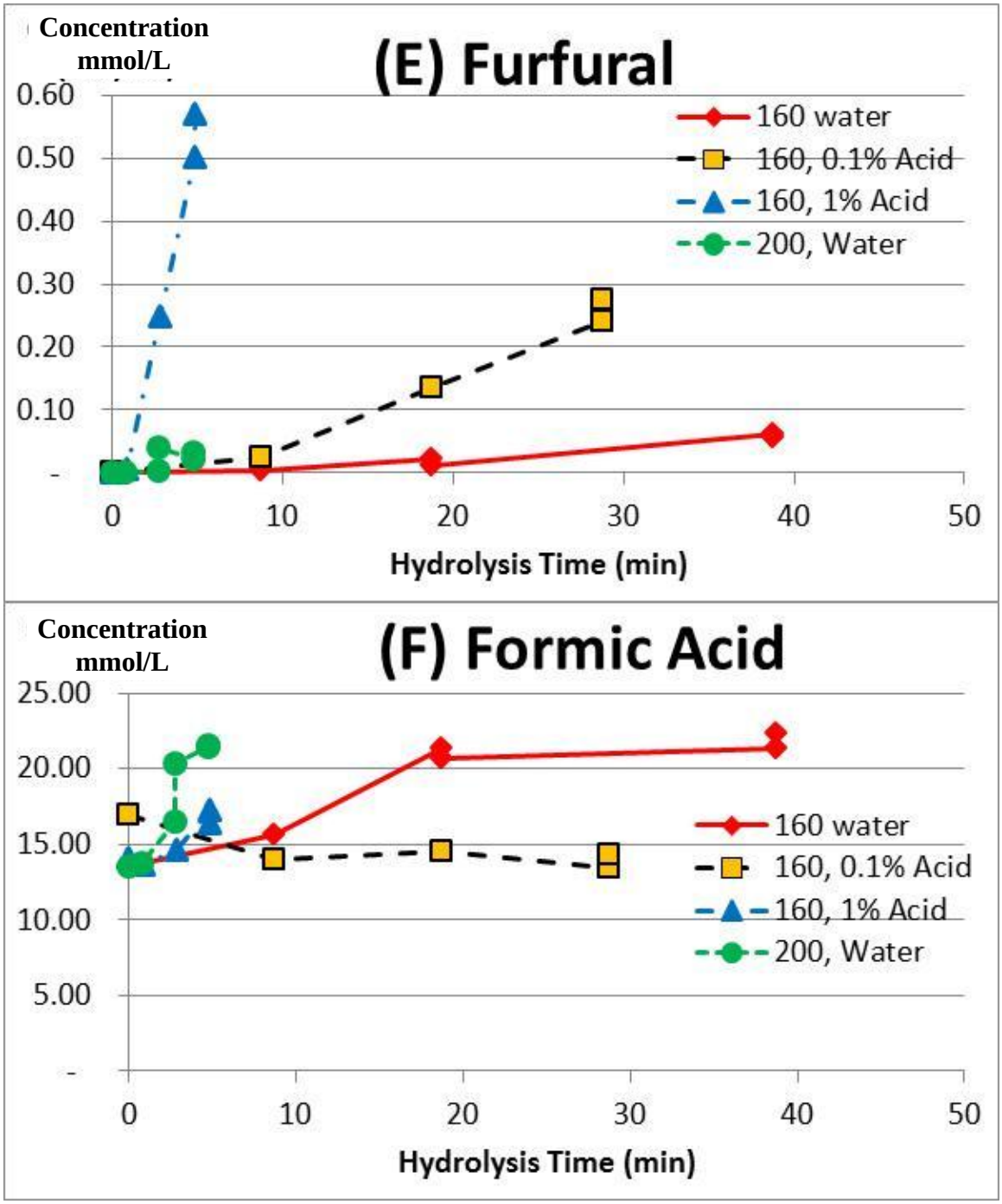

Figure 28: The experimental data showing the molar concentration of **(E)** furfural and **(F)** formic acid as a function of hydrolysis time during the hydrolysis of DP 4 in 160 ˚C water, 160 ˚C of 0.1v/v% sulfuric acid, 160 ˚C of 1 v/v% sulfuric acid, and 200 ˚C water.

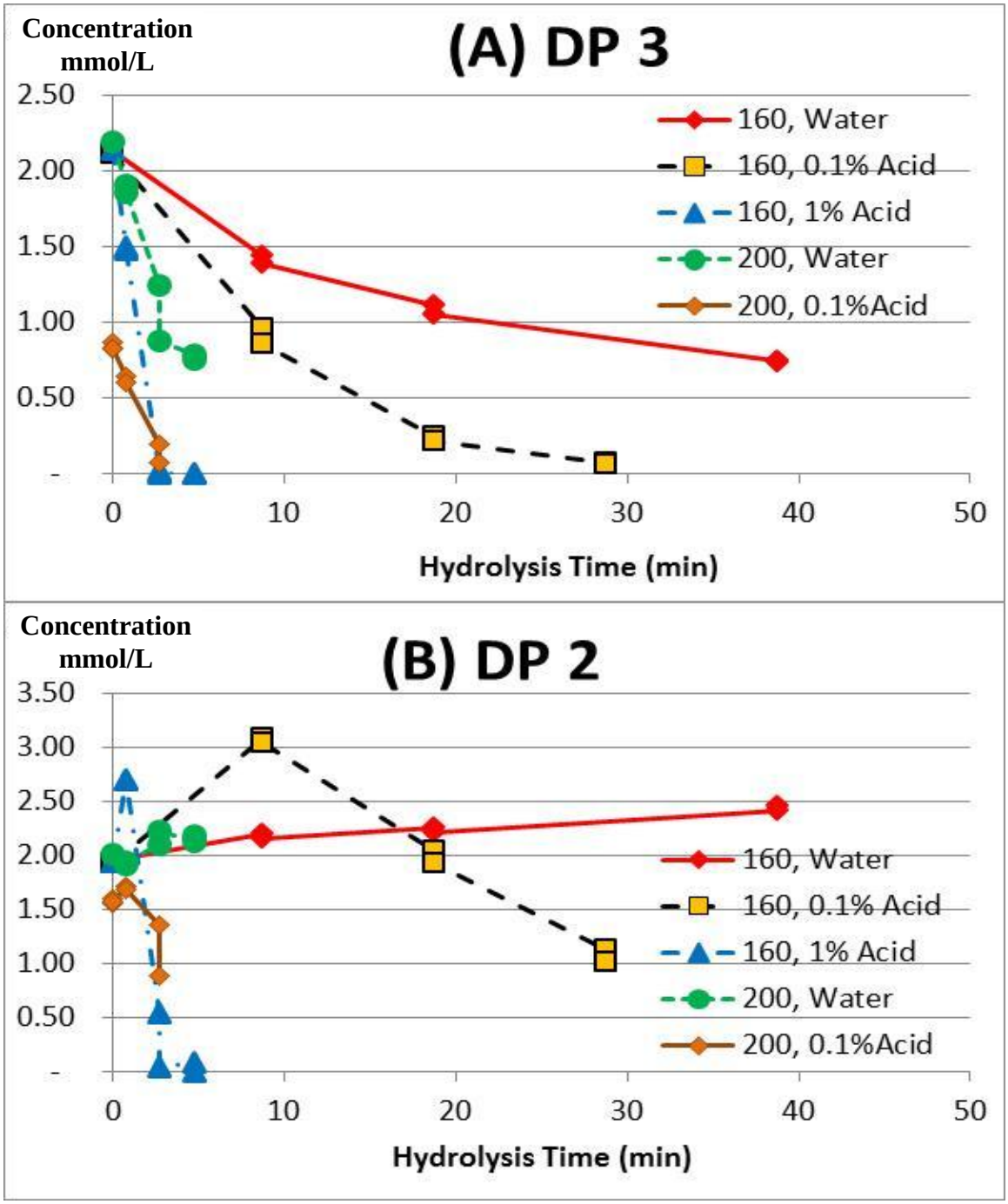

Figure 29: The experimental data showing the molar concentration of **(A)** DP 3 and **(B)** DP 2 as a function of hydrolysis time during the hydrolysis of DP 3 in 160 ˚C water, 160 ˚C of 0.1v/v% sulfuric acid, 160 ˚C of 1 v/v% sulfuric acid, 200 ˚C water, and 200 ˚C of 0.1v/v% sulfuric acid.

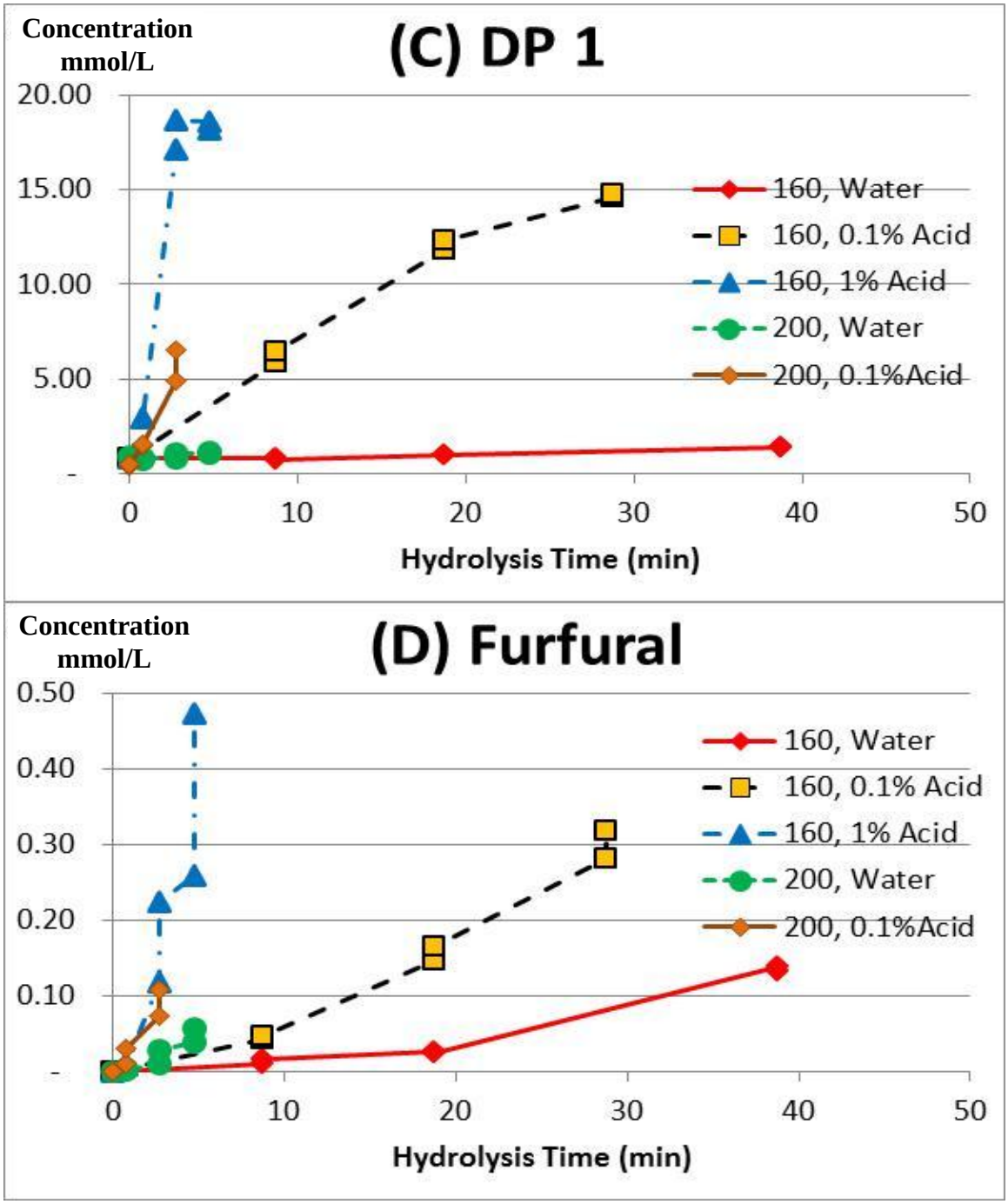

Figure 29: The experimental data showing the molar concentration of **(C)** DP 1 and **(D)** furfural as a function of hydrolysis time during the hydrolysis of DP 3 in 160 ˚C water, 160 ˚C of 0.1v/v% sulfuric acid, 160 ˚C of 1 v/v% sulfuric acid, 200 ˚C water, and 200 ˚C of 0.1v/v% sulfuric acid.

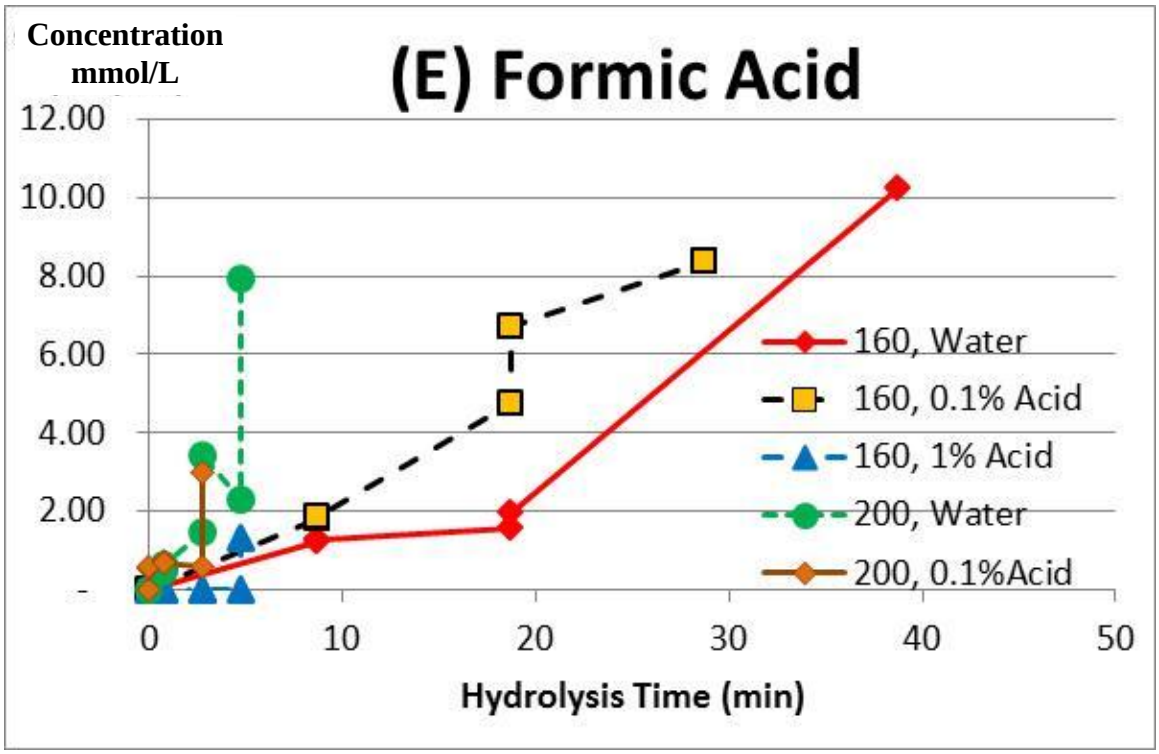

Figure 29: The experimental data showing the molar concentration of **(E)** formic acid as a function of hydrolysis time during the hydrolysis of DP 3 in 160 ˚C water, 160 ˚C of 0.1v/v% sulfuric acid, 160 ˚C of 1 v/v% sulfuric acid, 200 ˚C water, and 200 ˚C of 0.1v/v% sulfuric acid.

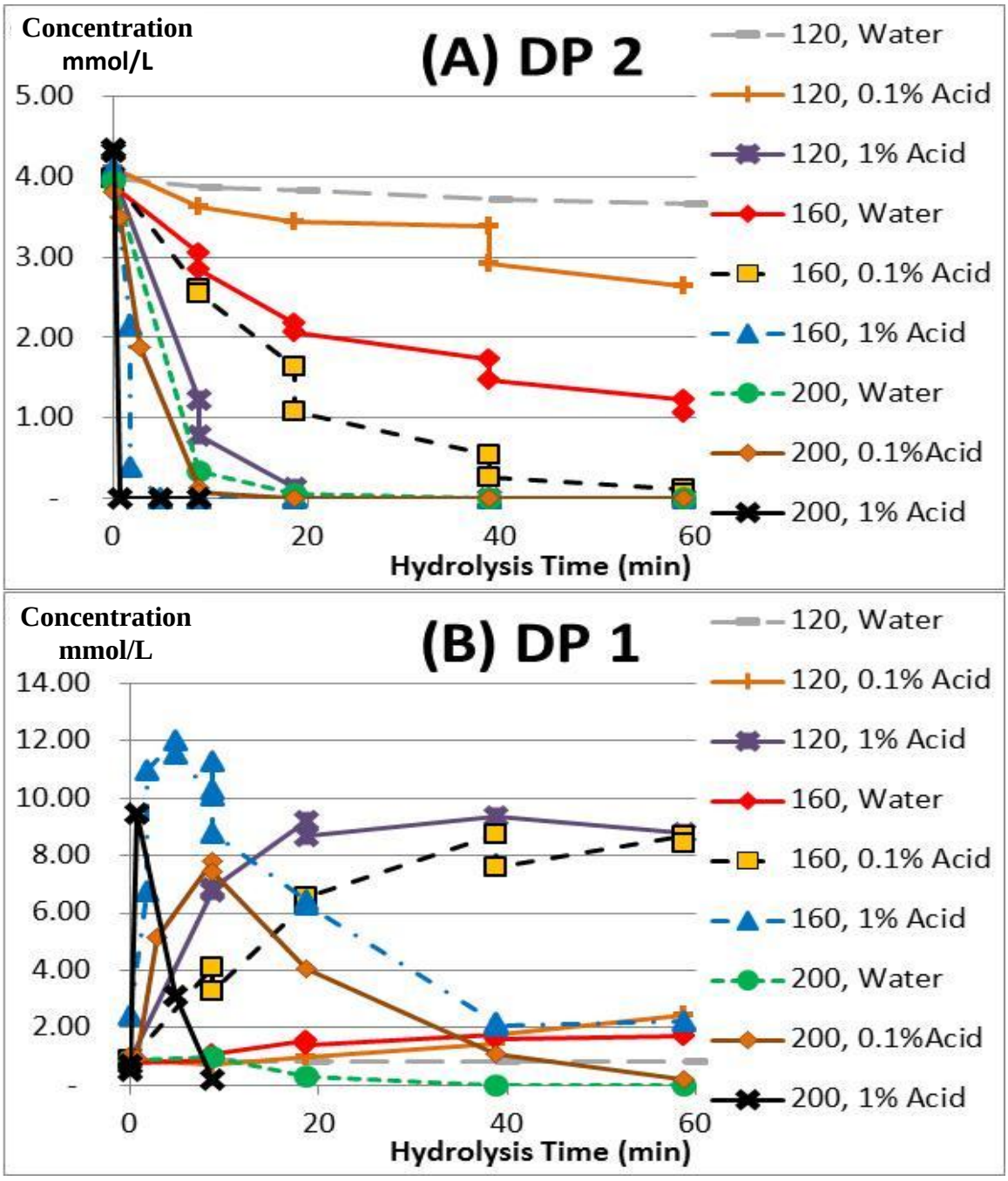

Figure 30: The experimental data showing the molar concentration of **(A)** DP 2 and **(B)** DP 1 as a function of hydrolysis time during the hydrolysis of DP 2 in 120 ˚C water, 120 ˚C of 0.1v/v% sulfuric acid, 120 ˚C of 1 v/v% sulfuric acid, 160 ˚C water, 160 ˚C of 0.1v/v% sulfuric acid, 160 ˚C of 1 v/v% sulfuric acid, 200 ˚C water, 200 ˚C of 0.1v/v% sulfuric acid, and 200 ˚C of 1v/v% sulfuric acid.

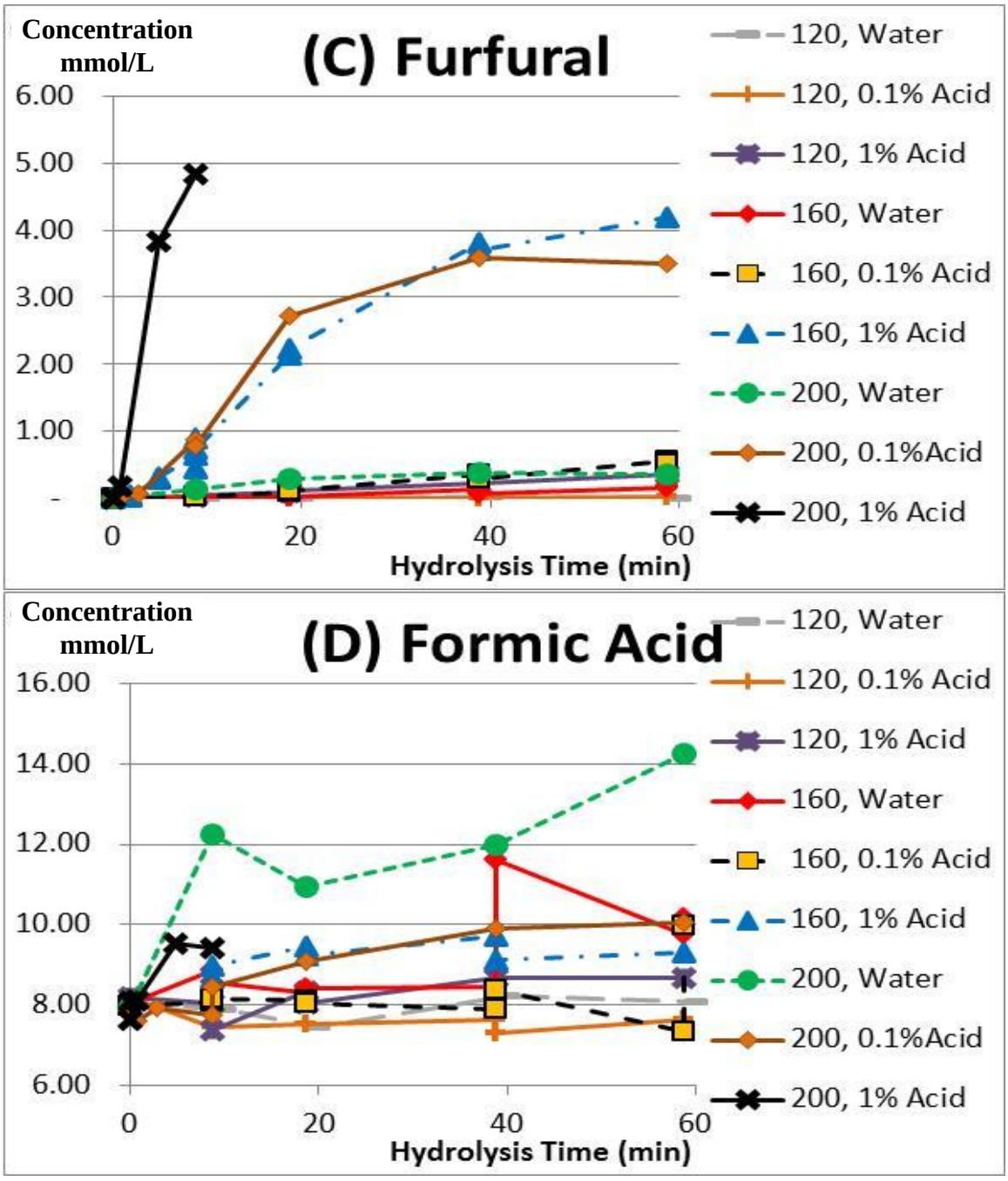

Figure 30: The experimental data showing the molar concentration of **(C)** furfural and **(D)** formic acid as a function of hydrolysis time during the hydrolysis of DP 2 in 120 ˚C water, 120 ˚C of 0.1v/v% sulfuric acid, 120 ˚C of 1 v/v% sulfuric acid, 160 ˚C water, 160 ˚C of 0.1v/v% sulfuric acid, 160 ˚C of 1 v/v% sulfuric acid, 200 ˚C water, 200 ˚C of 0.1v/v% sulfuric acid, and 200 ˚C of 1v/v% sulfuric acid.

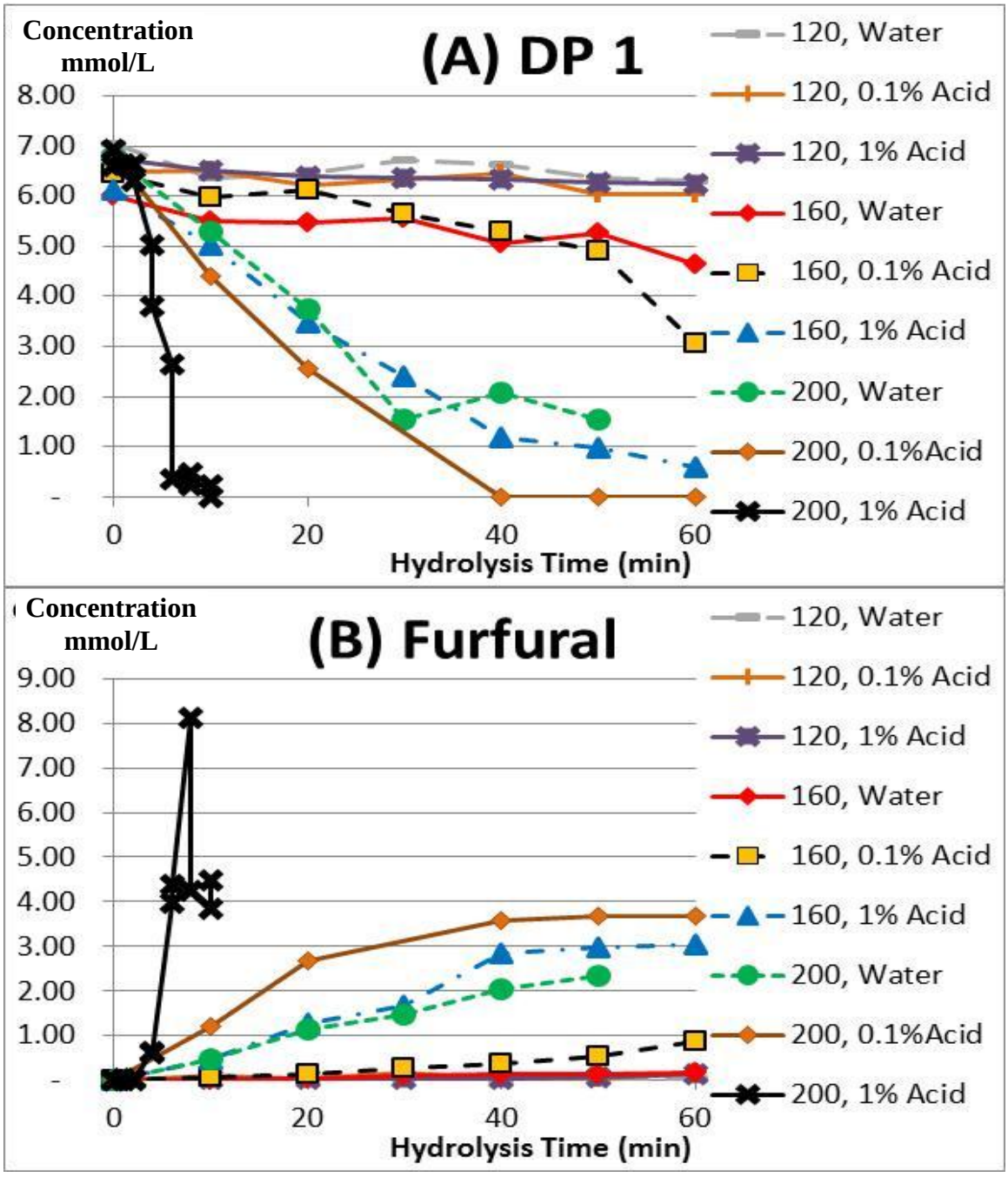

Figure 31: The experimental data showing the molar concentration of **(A)** DP 1 and **(B)** furfural as a function of hydrolysis time during the hydrolysis of DP 1 in 120 ˚C water, 120 ˚C of 0.1v/v% sulfuric acid, 120 ˚C of 1 v/v% sulfuric acid, 160 ˚C water, 160 ˚C of 0.1v/v% sulfuric acid, 160 ˚C of 1 v/v% sulfuric acid, 200 ˚C water, 200 ˚C of 0.1v/v% sulfuric acid, and 200 ˚C of 1v/v% sulfuric acid.

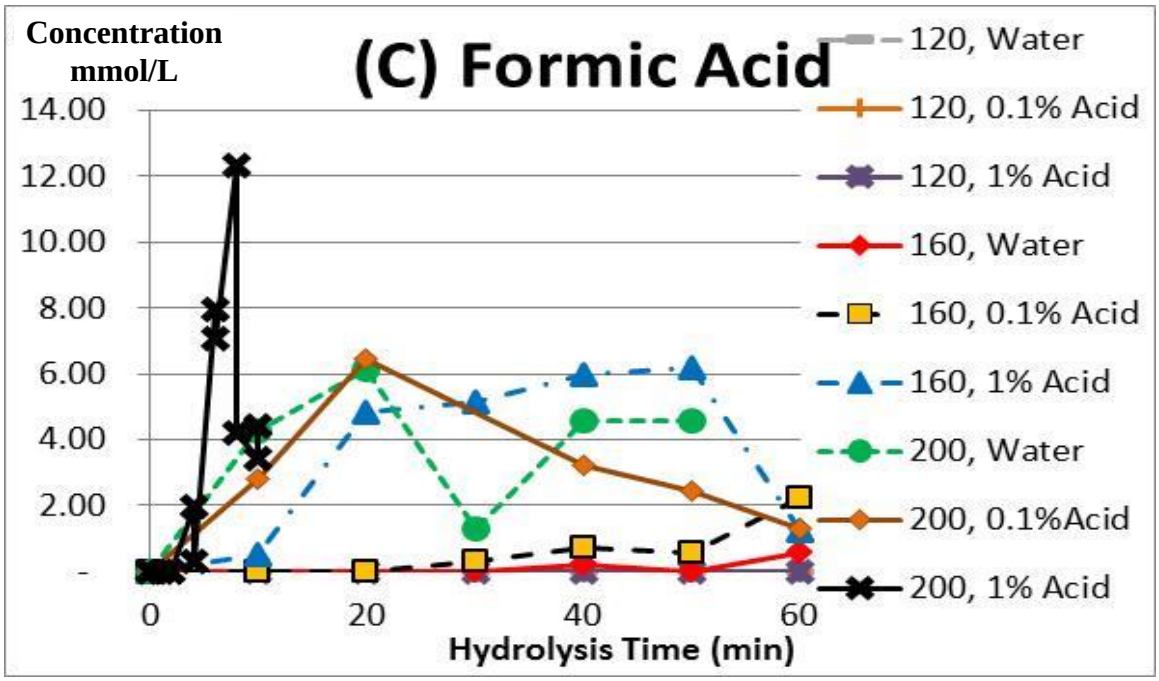

Figure 31: The experimental data showing the molar concentration of **(C)** formic acid as a function of hydrolysis time during the hydrolysis of DP 1 in 120 ˚C water, 120 ˚C of 0.1v/v% sulfuric acid, 120 ˚C of 1 v/v% sulfuric acid, 160 ˚C water, 160 ˚C of 0.1v/v% sulfuric acid, 160 ˚C of 1 v/v% sulfuric acid, 200 ˚C water, 200 ˚C of 0.1v/v% sulfuric acid, and 200 ˚C of 1v/v% sulfuric acid.

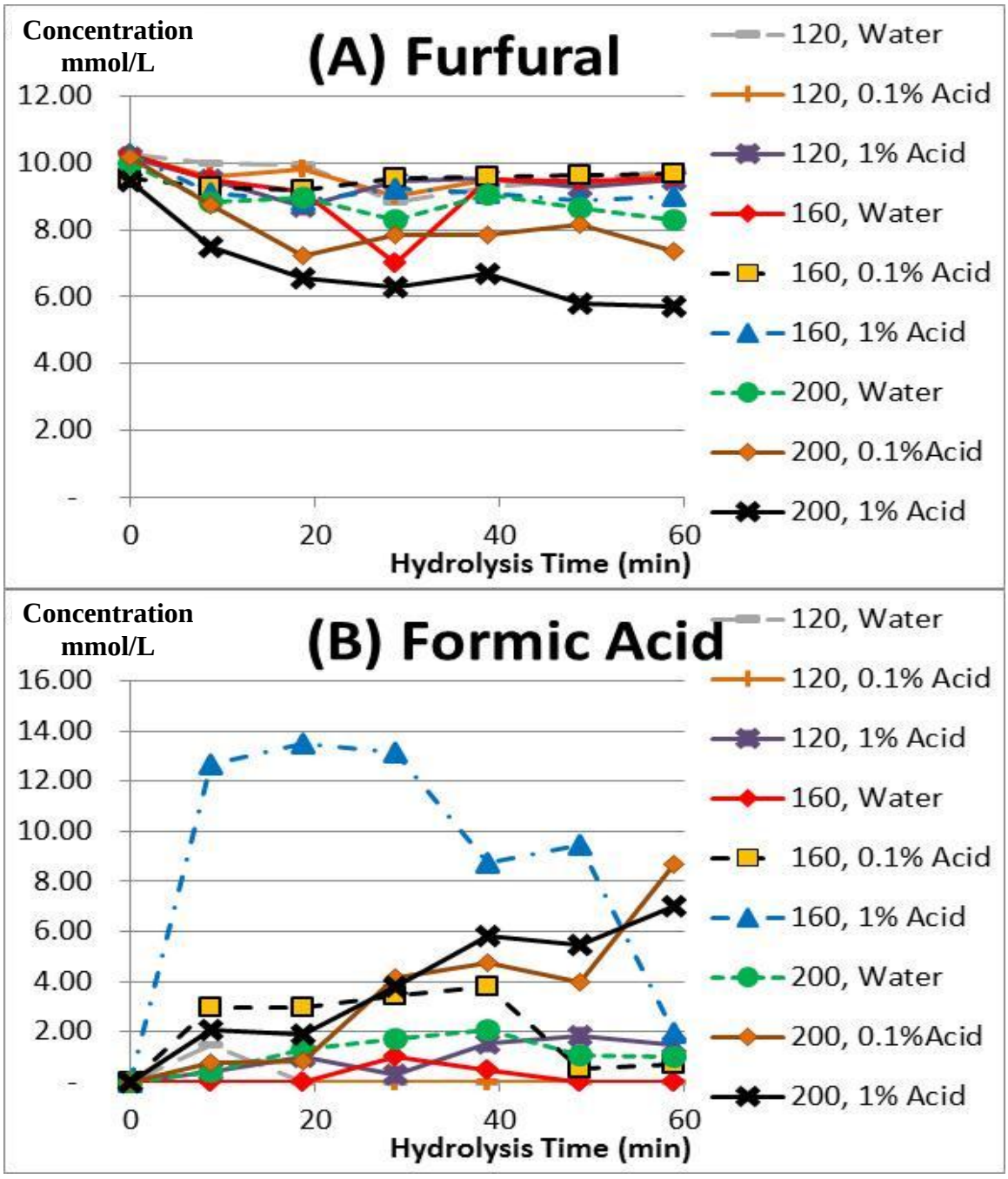

Figure 32: The experimental data showing the molar concentration of **(A)** furfural and **(B)** formic acid as a function of hydrolysis time during the hydrolysis of furfural in 120 ˚C water, 120 ˚C of 0.1v/v% sulfuric acid, 120 ˚C of 1 v/v% sulfuric acid, 160 ˚C water, 160 ˚C of 0.1v/v% sulfuric acid, 160 ˚C of 1 v/v% sulfuric acid, 200 ˚C water, 200 ˚C of 0.1v/v% sulfuric acid, and 200 ˚C of 1v/v% sulfuric acid.

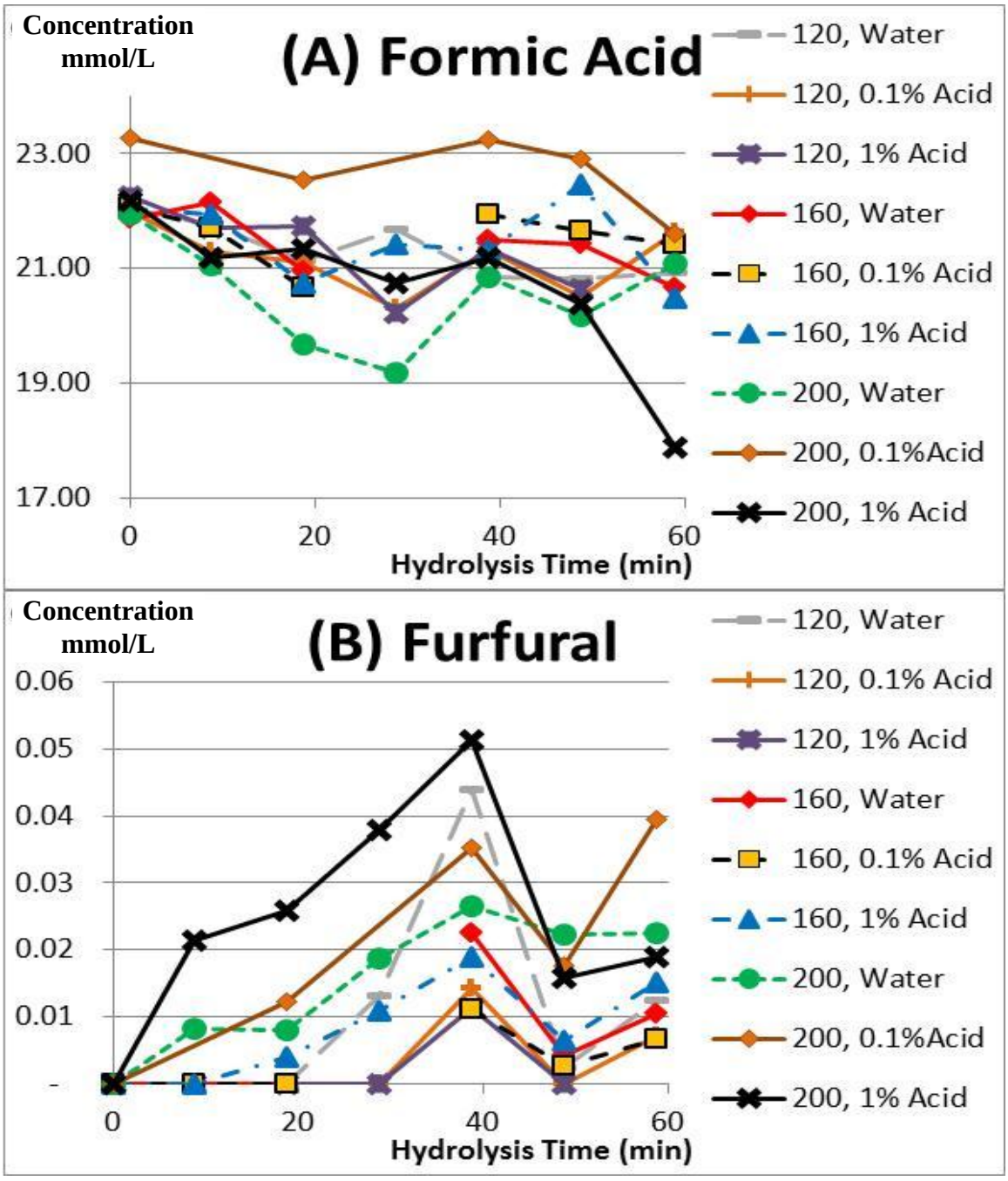

Figure 33: The experimental data showing the molar concentration of **(A)** formic acid and **(B)** furfural as a function of hydrolysis time during the hydrolysis of formic acid in 120 ˚C water, 120 ˚C of 0.1v/v% sulfuric acid, 120 ˚C of 1 v/v% sulfuric acid, 160 ˚C water, 160 ˚C of 0.1v/v% sulfuric acid, 160 ˚C of 1 v/v% sulfuric acid, 200 ˚C water, 200 ˚C of 0.1v/v% sulfuric acid. and 200 ˚C of 1v/v% sulfuric acid.

At the most severe hydrolysis condition, 1 v/v% acid at 160 ˚C, all of the DP 4 was fully depolymerized within 5 min, into a mixture of DP 3, DP 2, DP 1, furfural, and formic acid, as shown in **Figure 28**. At 160 ˚C with 0.1 v/v% acid, which was more severe than water hydrolysis at 200 ˚C, 10% of DP 4 remained after 5 min of hydrolysis; DP 2 and DP 3 were completely depolymerized into DP 1 and by-products within 5 min of the hydrolysis. Because of the rapid depolymerization rate, the highest observed concentrations of furfural were with 0.1 and 1 v/v% sulfuric acid at 160 ˚C. Conversely, during slower depolymerization, such as with 160 ˚C water, 0.1 v/v% sulfuric acid at 160 ˚C, and 200 ˚C water, most of the initial DP 4 remained as xylose oligomers, namely DP 2, DP 3, and DP 4. Specifically 40, 51, and 31% of xylose oligomers remained, respectively, in xylose equivalent moles, in water at 160 ˚C after 40 min, 0.1v/v% sulfuric acid at 160 ˚C after 30 min, and water at 200 ˚C after 5 min, respectively.

The hydrolysis of DP 3 was conducted in water at 160 ˚C, 0.1 v/v% sulfuric acid at 160 ˚C, 1 v/v% sulfuric acid at 160 ˚C, water at 200 ˚C, and 0.1 v/v% sulfuric acid at 200 ˚C. Among the five hydrolysis conditions, 1 v/v% sulfuric acid at 160 ˚C, and 0.1 v/v% sulfuric acid at 200 ˚C resulted in a complete depolymerization of DP 3 within 5 min of the hydrolysis, mainly into DP 1 and furfural, as shown in **Figure 29**. On the other hand, during the least severe hydrolysis condition, the hydrolysis with water at 160 ˚C, 34% of DP 3 remained after 40 min of the hydrolysis. Worth noting, a high accumulation rate of formic acid was observed in all five DP 3 hydrolysis conditions, except at the hydrolysis condition with 1 v/v% sulfuric acid at 160 ˚C, suggesting that the accumulation rate of formic acid from the degradation of furfural and DP 1 was higher than the decomposition of formic acid in the studied hydrolysis conditions. However, with 1 v/v% sulfuric acid at 160 ˚C, the degradation of formic acid was as fast as its

accumulation, resulted in an insignificant concentration of formic acid throughout the hydrolysis process.

The hydrolysis of DP 2 was conducted in all nine hydrolysis conditions, namely 120 ˚C water, 0.1 v/v% sulfuric acid at 120 ˚C, 1 v/v% sulfuric acid at 120 ˚C, 160 ˚C water, 0.1 v/v% sulfuric acid at 160 ˚C, 1 v/v% sulfuric acid at 160 ˚C, 200 ˚C water, 0.1 v/v% sulfuric acid at 200 ˚C, and 1 v/v% sulfuric acid at 200 ˚C. The data are presented in **Figure 30**. As expected, during the less severe hydrolysis conditions, such as the hydrolysis in 120 ˚C water, 0.1 v/v% sulfuric acid at 120 ˚C, 160 ˚C water, and 0.1 v/v% sulfuric acid at 160 ˚C, the DP 2 remaining after 60 min of hydrolysis were 92%, 64%, 27%, and 1%, respectively. During the other five more severe hydrolysis conditions, namely 1 v/v% sulfuric acid at 120 ˚C, 1 v/v% sulfuric acid at 160 ˚C, 200 ˚C water, 0.1 v/v% sulfuric acid at 200 ˚C, and 1 v/v% sulfuric acid at 200 ˚C, complete depolymerization of DP 2 was observed within 60 min of the hydrolysis. However, the time for complete depolymerization of DP 2 into DP 1 was less than 20 min for 1 v/v% sulfuric acid at 120 ˚C, 1 v/v% sulfuric acid at 160 ˚C, 200 ˚C water, 0.1 v/v% sulfuric acid at 200 ˚C, and 1 v/v% sulfuric acid at 200 ˚C hydrolysis conditions. Although a high concentration of DP 1 was initially observed during the more severe hydrolyses, such as the hydrolyses of 1 v/v% sulfuric acid at 160 ˚C, 0.1 v/v% sulfuric acid at 200 ˚C, and 1 v/v% sulfuric acid at 200 ˚C, DP 1 was degraded within 20 min into furfural concentrations of 4.1, 3.5 and 4.9 mmol/L, respectively. Interestingly, the hydrolysis conditions of 1 v/v% sulfuric acid at 160 ˚C, 0.1 v/v% sulfuric acid at 200 ˚C, and 1 v/v% sulfuric acid at 200 ˚C resulted in a formic acid concentration of 9 mmol/L, while the less severe hydrolysis in 200 ˚C water yielded 14 mmol/L, the highest concentration of formic acid. In all the hydrolysis conditions for DP 2 depolymerization, the accumulation rate of formic acid was less noticeable, as compared to that of DP 3

depolymerization, possibly caused by the high initial concentration of formic acid in the DP 2 sample, as a result of the difficulty in the CPC fractionation, in separating DP 2 from formic acid.

Similar to DP 2, DP 1 was also hydrolyzed at all nine hydrolysis conditions, as shown in **Figure 31**. After 60 min of hydrolysis, all three experiments conducted at 120 ˚C resulted in high survival rate of DP 1, as shown by 89%, 93%, and 93% of DP 1 remaining in 120 ˚C water, 0.1 v/v% sulfuric acid at 120 ˚C, and 1 v/v% sulfuric acid at 120 ˚C, respectively. On the other hand, during the most severe hydrolysis conditions of 0.1 v/v% sulfuric acid at 200 ˚C, and 1 v/v% sulfuric acid at 200 ˚C, there was no DP 1 remaining after 40 min of the hydrolysis. Interestingly, in the hydrolysis condition with 1 v/v% sulfuric acid at 200 ˚C, the resulting furfural and formic acid were quickly degraded within 10 min of the experiment, indicating that even furfural and formic acid cannot survive in the severe hydrolysis condition.

The hydrolysis of furfural was conducted at all nine hydrolysis conditions. The survival rate of furfural after 60 min of hydrolysis ranged from 60 – 100%, with the lowest concentration of furfural remaining in the hydrolysis condition with 1 v/v% sulfuric acid at 200 ˚C, as shown in **Figure 32**. At most of the hydrolysis conditions, noticeable buildup of formic acid concentration was observed, especially in the hydrolysis condition with 1 v/v% sulfuric acid at 160 ˚C, confirming that the degradation of furfural resulted in the formation of formic acid. These results point to the fact that furfural degradation leads to formic acid accumulation. The hydrolysis condition with 1 v/v% sulfuric acid at 160 ˚C was the most favorable condition for the accumulation of formic acid. This is an important observation because formic acid inhibits enzymatic hydrolysis (Kumar and Wyman, 2009). Worth noting, in the hydrolysis condition with 1 v/v% sulfuric acid at 200 ˚C, 60% of furfural remained after 60 min of hydrolysis, in contrast to the furfural formed from DP 1 hydrolysis, where the furfural concentration was 55% off the

maximum furfural concentration within 2 min, under the same hydrolysis condition. The rate of furfural degradation was faster in the presence of xylose and formic acid, possibly affected by the buildup of formic acid in the hydrolysate, resulted in a harsher hydrolysis condition.

The hydrolysis of formic acid was similarly conducted at all nine hydrolysis conditions. Formic acid, albeit at a slower rate, was degraded as temperature and acid concentration increased, as shown in **Figure 33**. At the most severe hydrolysis condition with 1 v/v% sulfuric acid at 200 ˚C, 81% of formic acid remained after 60 min of the hydrolysis, as compared to the other eight hydrolysis conditions, where 93 - 98% of formic acid remained after 60 min of the hydrolysis. The resultant furfural formed from the degradation of formic acid was also not strongly influenced by the temperature or the pH, as the formation rate of furfural was almost indistinguishable among all nine hydrolysis conditions. However, the detection of furfural from the degradation of formic acid provided the confirmation that the reaction of furfural into formic acid was indeed a reversible reaction, although the forward reaction is dominant, as shown by the higher concentration of formic acid from furfural, as compared to the formation of furfural from formic acid.

The experimental data collected in **Figures 28 – 33** were subsequently fitted to the model, as shown by **Equations 12 - 23**. Three different methods were used in estimating the parameters in the kinetic model. The first method, which was shown in **Equation 25**, was conducted by minimizing the sum of squares between the predicted data and the experimental data, as was conducted by Kumar and Wyman (2008) and Kim et al. (2012). However, because most of the formic acid concentration was higher than the concentrations of other compounds, the predicted parameter was biased towards the sum of squares from the formic acid concentrations.

Therefore, a normalized sum of squares method was adopted, as shown in **Equation 26**. By normalizing the sum of the squares for the error with respect to the individual data, all data were given equal consideration prevent the bias of optimization towards larger values in the experimental data. Worth noting, both methods were conducted by minimizing the sum of squares values to determine the optimum parameters in the kinetic model.

Non-normalized sum of the squares method, $S1 = \sum (\text{Predicted data} - \text{Experimental data})^2$ **(25)**

Normalized sum of the squares method, $S2 = \sum [(\text{Predicted data} - \text{Experimental data})^2 / (\text{Experimental data})^2]$ **(26)**

R^2 method, $S3 = \sum \{1 - [(\text{Predicted data} - \text{Experimental data})^2 / (\text{Experimental data} - \text{Average of experimental data})^2]\}$ **(27)**

However, neither of the methods was adequate in predicting the experimental data. The non-normalized sum of the squares method were ineffective in predicting the concentration of several compounds, such as DP 1, DP 2, DP 3 and formic acid concentrations in 160 ˚C water, furfural concentration in 0.1 v/v% sulfuric acid at 160 ˚C, and DP 1, DP 2, and formic acid concentrations in 200 ˚C water. Moreover, the k values for DP 4 at 160 ˚C water, DP 3 in 0.1 v/v% sulfuric acid at 160 ˚C, and DP 1 at 200 ˚C water, which were 2.0, 10.0, and 2.3 min^{-1}, respectively, were suspiciously higher than the k values for the corresponding compounds at more severe hydrolysis conditions.

Alternatively, the method using normalized sum of the squares were ineffective in predicting furfural concentration in 120 ˚C water, furfural concentration in 0.1 v/v% sulfuric acid

at 120 ˚C, DP 1 in 160 ˚C water, furfural and formic acid concentrations in 1 v/v% sulfuric acid at 160 ˚C, DP 1 in 200 ˚C water, and DP 1 in 1 v/v% sulfuric acid at 200 ˚C. In addition to that, the k values for DP 1 and formic acid in 1 v/v% sulfuric acid at 200 ˚C, which were 8.1 and 8.9 min^{-1}, respectively, were at least one magnitude higher than the k values at other less severe conditions. The over estimation of the k values for both DP 1 and formic acid in 1 v/v% sulfuric acid at 200 ˚C were noticeable in the model, as the model predicted the depletion of both DP 1 and formic acid concentrations faster than the actual degradation of either compounds. The figures for both the non-normalized and normalized sum of the squares methods are presented in **Appendices 4** and **5**, respectively.

Therefore, a third alternative of using R^2 method was adopted to improve the curve fitting of the model. The kinetic parameters were estimated by maximizing the sum of the R^2 values of all compounds, as shown in **Equation 27**. Using the R^2 method, the experimental data were fitted more accurately by the model, as indicated both graphically of the model, and the higher R^2 values for all the compounds. The comparison of the sum of the squares for the error and R^2 values for the three methods were summarized in **Table 14**. As shown in **Table 14**, method 1, method 2, and method 3 are the estimation of parameters based on minimizing non-normalized sum of the squares of the error, minimizing normalized sum of the squares of the error, and maximizing the R^2 values of all the compounds, respectively. Not surprisingly, method 1 and method 2 yielded the lowest values of non-normalized sum of the squares of the error (SSE) and normalized SSE, respectively, while method 3 yielded the highest average R^2 values among the three methods.

Table 14: Comparison of three different methods in estimating parameters in kinetic model. Method 1, 2, and 3 are the estimation of parameters based on minimizing non-normalized sum of the squares of the error, minimizing normalized sum of the squares of the error, and maximizing the R^2 values of all the compounds, respectively. The non-normalized sum of the squares of the error (SSE), the normalized SSE, and the R^2 values were calculated according to the equations as shown in **Equations 25**, **26**, and **27**, respectively.

	Non-normalized SSE			Normalized SSE			Average R^2		
	Method 1	Method 2	Method 3	Method 1	Method 2	Method 3	Method 1	Method 2	Method 3
120 ˚C, Water	7.8	550.0	12.8	190.8	26.4	160.7	-0.12	-17.03	0.08
120 ˚C, 0.1% Acid	12.1	41.1	12.3	2,665.6	14.6	481.4	-0.79	-13.25	0.21
120 ˚C, 1% Acid	42.5	51.0	49.7	18.0	11.5	24.2	0.26	0.43	0.58
160 ˚C, Water	405.8	530.6	518.6	1,618.7	70.5	317.8	-19.82	-5.28	-0.27
160 ˚C, 0.1% Acid	368.0	423.5	506.5	84.4	33.4	73.6	-0.81	0.03	0.19
160 ˚C, 1% Acid	1,599.7	3,428.1	1,981.6	503.2	67.8	406.3	-36.80	-18.34	0.21
200 ˚C, Water	287.3	10,617.4	438.2	81,333.7	142.7	3,052.8	-203.50	-12.58	-0.36
200 ˚C, 0.1% Acid	272.5	2,393.4	335.7	7,100.5	61.4	7,465.3	-0.55	-4.37	0.16
200 ˚C, 1% Acid	467.1	16,228.9	474.5	9,870.3	116.5	11,093.2	0.58	-23.92	0.58

The fit of model to the experimental data was determined by the R^2 values of the regression, which was calculated using the following equation:

$$R^2 = 1 - SSE / SST \quad \textbf{(28)}$$

where SSE is the sum of the squares for the error, and SST is the sum of the squares total. SSE is the sum of the squares between the predicted data and the experimental data, while SST is the sum of the squares between the experimental data and the average values of the data. All calculations were based on the molar concentrations of the compound. The negative values in some R^2 calculation were contributed by the poor model fit to the experimental data, suggesting that the experimental data were better represented by assuming that the concentrations of the compounds are independent of the hydrolysis time, which would result in the sum of the squares for the error equaled to the sum of the squares total, and thus yielded the R^2 values of zero. The option of setting the concentration independent of hydrolysis time was not considered because it is counterintuitive to the first order reaction kinetics, where the concentration of compounds changes over time.

5.5.2.1 Hydrolysis Condition at 120 ˚C Using Water

The degradation rate constants for DP 1 (k_1), DP 2 (k_2), furfural (k_F), and formic acid (k_A), were calculated as 0.0044, 0.0003, 0.0014, and 0.0013 min^{-1}, respectively. The individual formation rate constants k_{21}, k_{1F}, k_{1A}, and k_{FA} were determined to be 0.0003, 0.0001, 0.0043, and 0.0014 min^{-1}, respectively, while the decomposition rate of furfural and formic acid, k_{FL} and k_{AL} ,were determined to be 0.0000 and 0.0013 min^{-1}, respectively. The data and the best-fit model predictions for each compound are presented in **Figures 34 - 37**. The R^2 values of the model fits are presented in **Table 15**.

The model provided a good fit to the experimental data for the concentrations of DP 1 and DP 2, as reflected by the R^2 values of 0.61 – 0.97. Similarly, the concentration of formic acid was well predicted by the model as shown by the R^2 values of 0.74 – 0.95. However, the R^2 values were not calculated for the formic acid concentration during the hydrolysis of DP 1 and furfural, because there was no formic acid concentration detected in the experiment, resulting in zero value for the sum of the squares total (SST) in the R^2 calculation. The model did not predict furfural concentrations accurately, as reflected by the low R^2 values of -2.71, -1.03, and 0.26 for the hydrolysis of DP 1 and DP 2, furfural, respectively. The low R^2 values for furfural were due to the optimization of the model, where the concentrations of DP 1, DP 2, and formic acid were better represented by the model at the expense of furfural concentration.

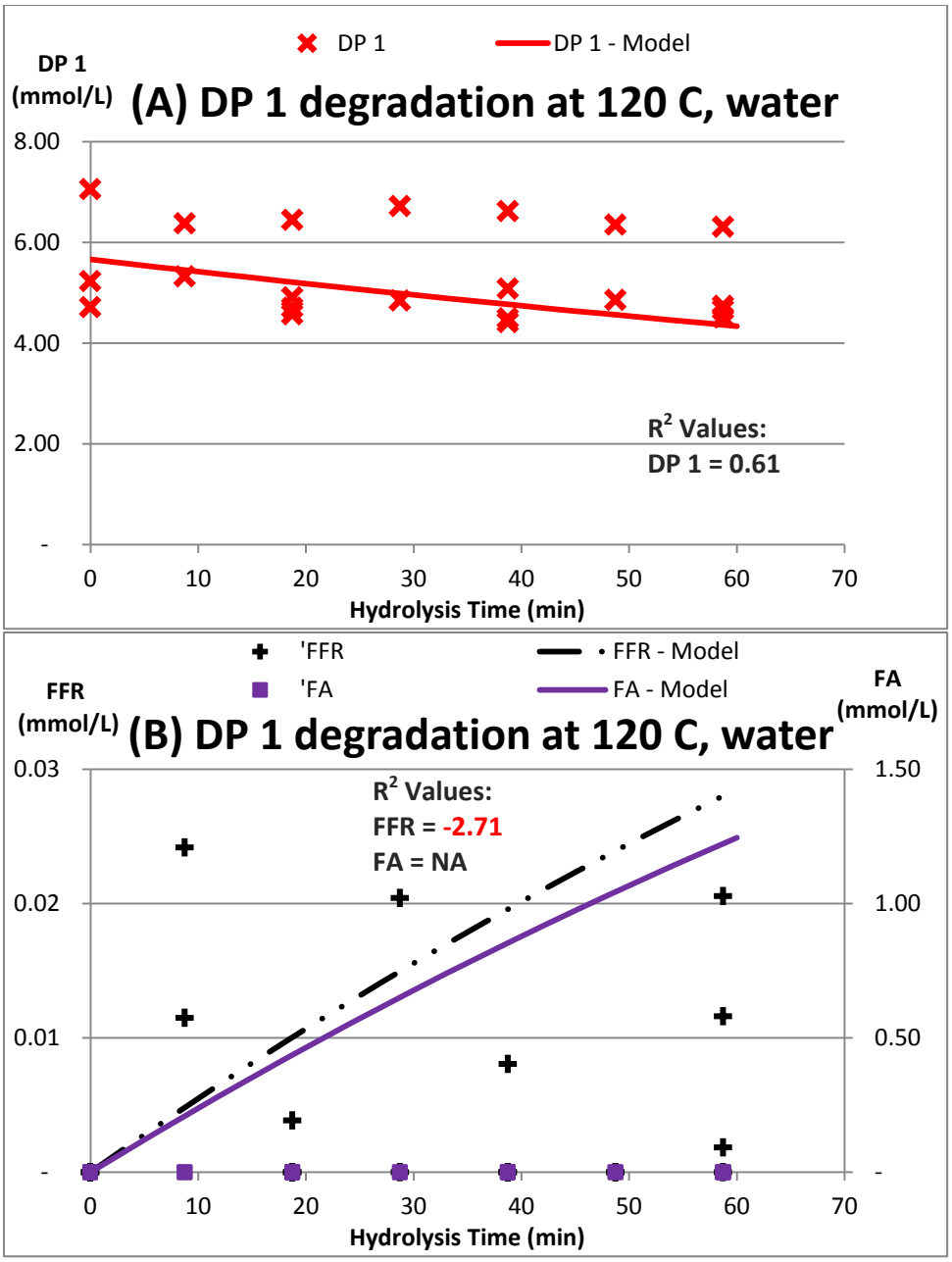

Figure 34: The best-fit model prediction and data of **(A)** DP 1, **(B)** furfural (FFR) and formic acid (FA) for the hydrolysis of DP 1 at 120 ˚C using water.

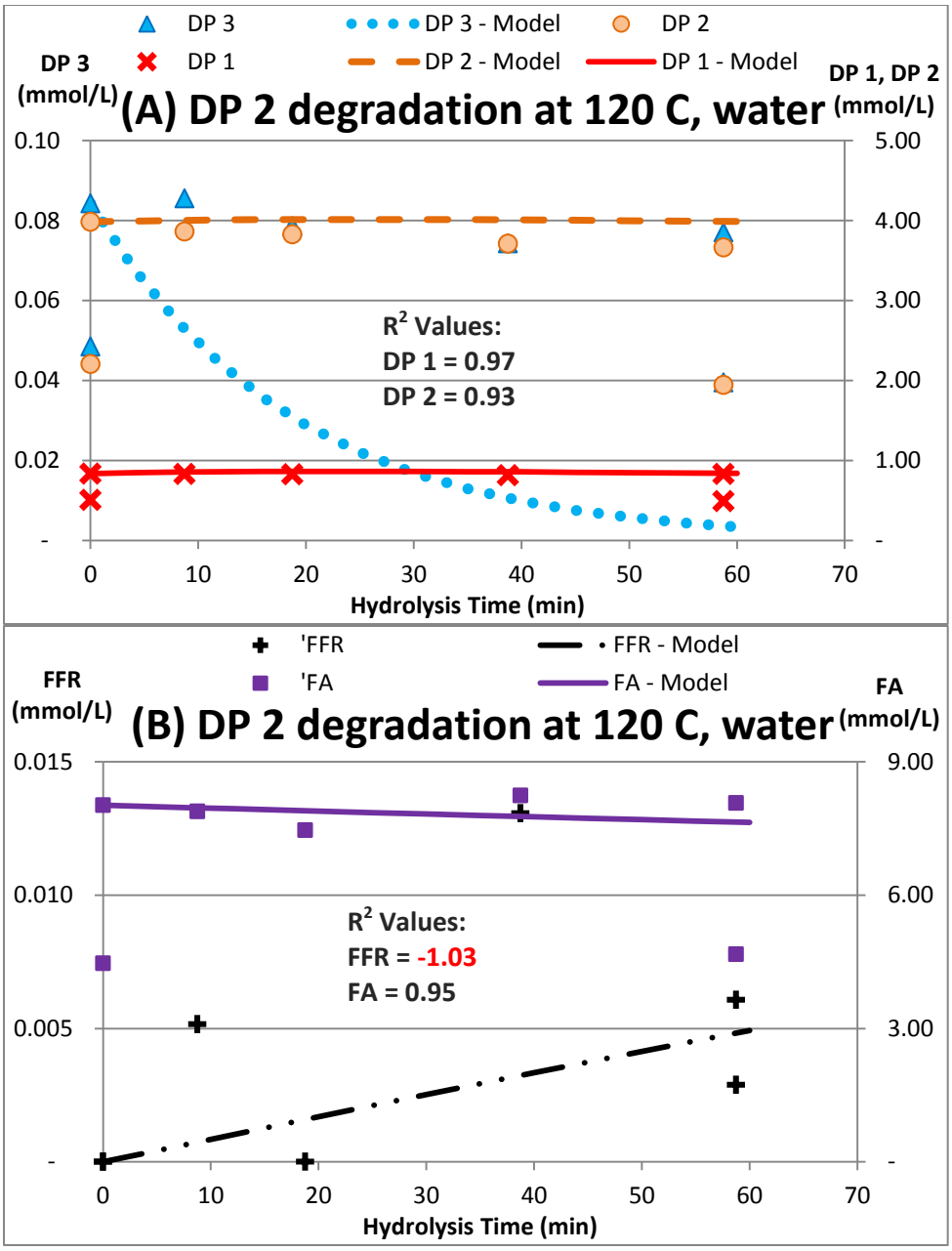

Figure 35: The best-fit model prediction and data of **(A)** DP 2 containing some DP 3 impurities and DP 1, **(B)** furfural (FFR) and formic acid (FA) for the hydrolysis of DP 2 at 120 ˚C using water.

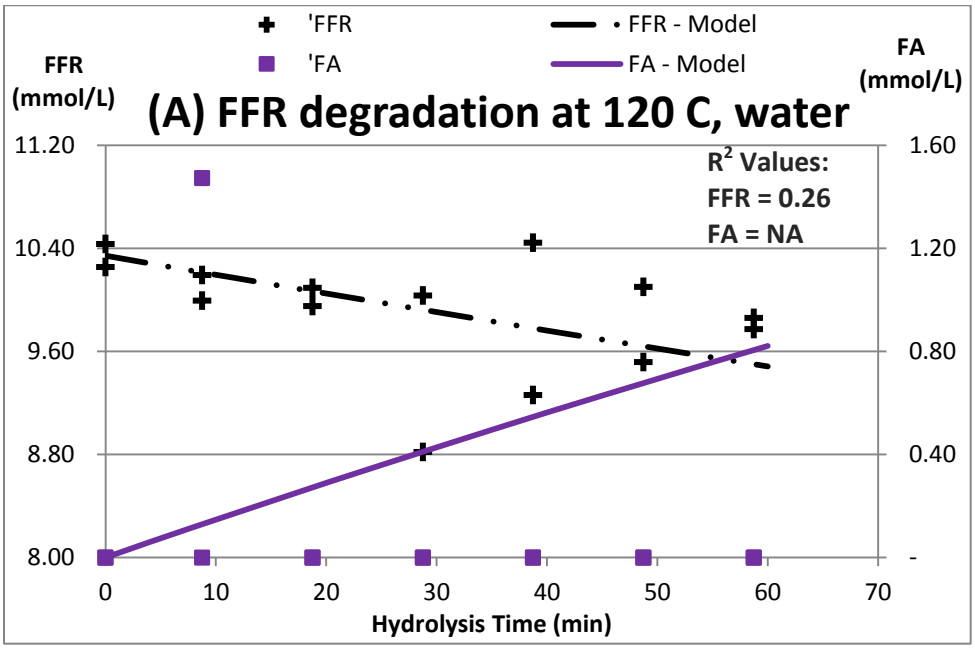

Figure 36: The best-fit model prediction and data of **(A)** furfural (FFR) and formic acid (FA) for the hydrolysis of furfural at 120 ˚C using water.

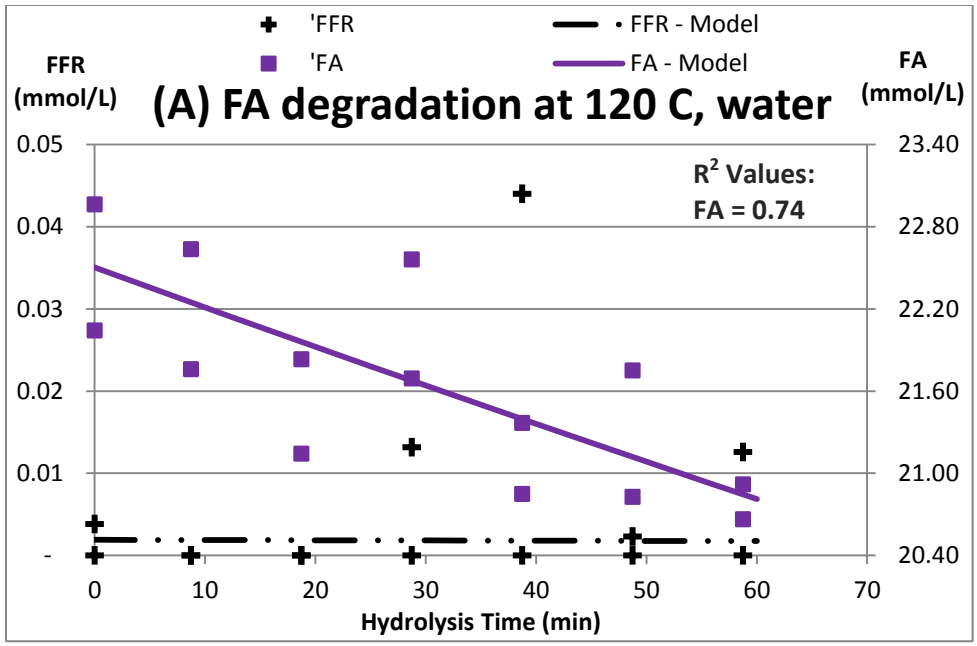

Figure 37: The best-fit model prediction and data of **(A)** formic acid (FA) and furfural (FFR) for the hydrolysis of formic acid at 120 ˚C using water.

Table 15: The R^2 values of the changes of DP 1, DP 2, formic acid (FA), and furfural (FFR), in mmol/L, as a function of hydrolysis time in 120 ˚C water, as shown **Figures 34- 37**.

	Hydrolysis of DP 1	Hydrolysis of DP 2	Hydrolysis of FA	Hydrolysis of FFR
DP 1	0.61	0.97		
DP 2		0.93		
FA	NA[#]	0.95	0.74	NA[#]
FFR	(2.71)	(1.03)		0.26

The R^2 values were not calculated because the experimental value was zero, i.e. the concentration of the compound was below the detection limit.

5.5.2.2 Hydrolysis Condition at 120 ˚C Using 0.1 v/v% Sulfuric Acid

The degradation rate constants for DP 1 (k_1), DP 2 (k_2), furfural (k_F), and formic acid (k_A), were calculated as 0.0013, 0.0038, 0.0015, and 0.0015 min^{-1}, respectively. The individual formation rate constants k_{21}, k_{1F}, k_{1A}, and k_{FA} were determined to be 0.0038, 0.0001, 0.0012, and 0.0003 min^{-1}, respectively, while the decomposition rate of furfural and formic acid, k_{FL} and k_{AL} were determined to be 0.0012 and 0.0015 min^{-1}, respectively. The data and the best-fit model predictions for each compound are presented in **Figures 38 - 41**. The R^2 values of the model fits are presented in **Table 16**.

The model provided a good fit to the experimental data for the concentrations of DP 1 and DP 2, as reflected by the R^2 values of 0.64 – 0.71. However, the model did not predict the concentrations of formic acid accurately, as reflected by the low R^2 values of -0.81, 0.28, and -0.32 for the hydrolysis of DP 2, formic acid and furfural, respectively. The R^2 value was not calculated for the formic acid concentration during the hydrolysis of DP 1 because there was no formic acid concentration detected in the experiment, resulting in zero value for the sum of the squares total (SST) in the R^2 calculation. Similarly, the model provided a poor prediction of furfural concentrations during the hydrolysis of DP 1 and furfural, as shown by the R^2 values of -0.18 and 0.00, although the model did provide a better estimation of furfural concentration during the hydrolysis of DP 2, as shown by the R^2 value of 0.87. The low R^2 values for furfural and formic acid were due to the optimization of the model, where the concentrations of DP 1 and DP 2 were better represented by the model at the expense of furfural and formic acid concentrations.

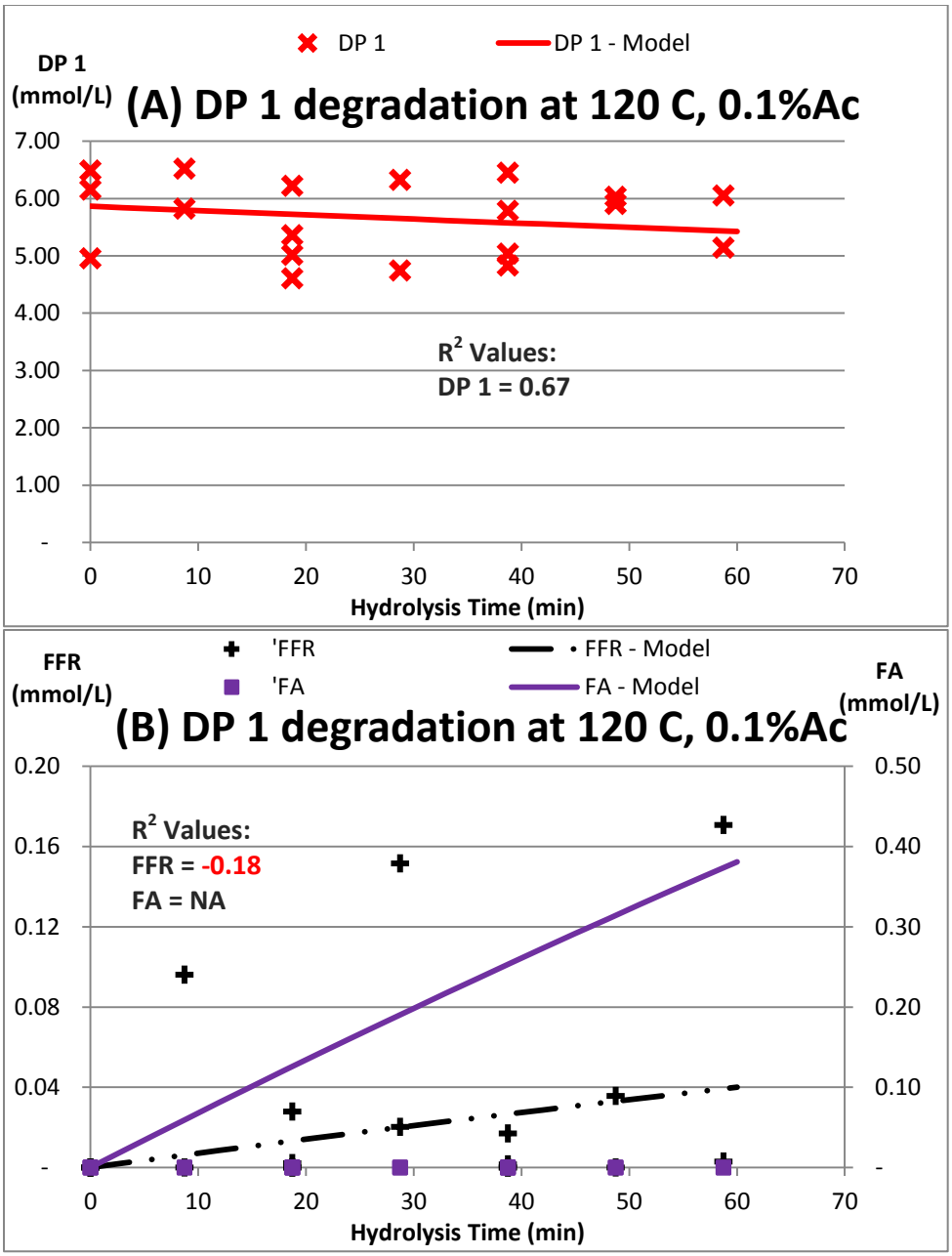

Figure 38: The best-fit model prediction and data of **(A)** DP 1, **(B)** furfural (FFR) and formic acid (FA) for the hydrolysis of DP 1 at 120 ˚C using 0.1 v/v% sulfuric acid.

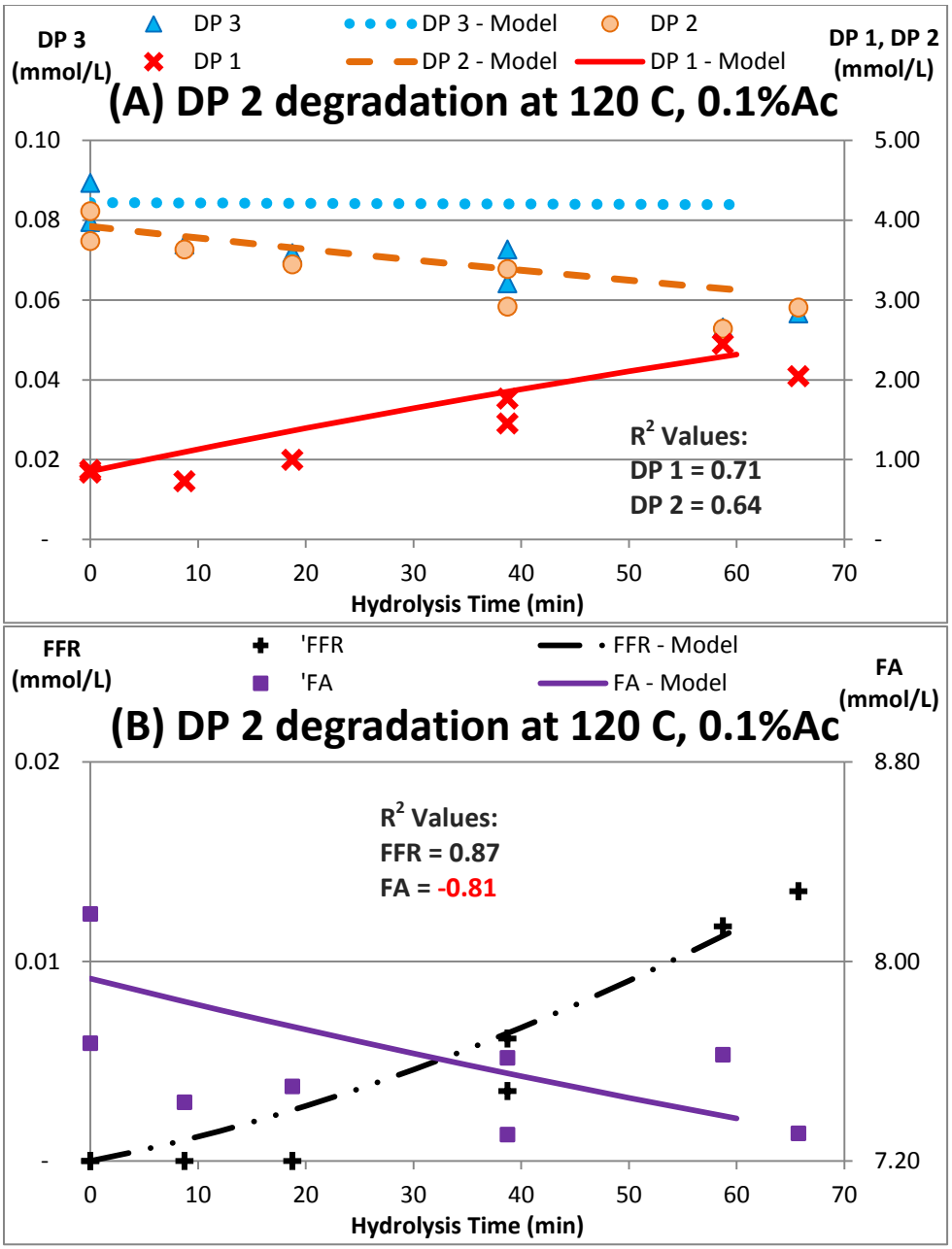

Figure 39: The best-fit model prediction and data of **(A)** DP 2 containing some DP 3 impurities and DP 1, **(B)** furfural (FFR) and formic acid (FA) for the hydrolysis of DP 2 at 120 ˚C using 0.1 v/v% sulfuric acid.

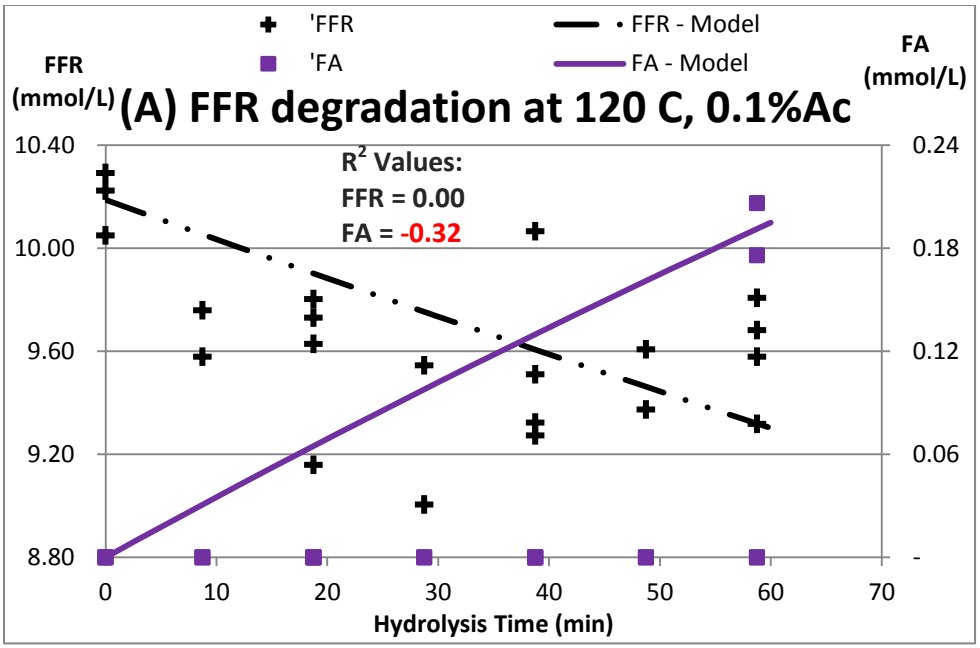

Figure 40: The best-fit model prediction and data of **(A)** furfural (FFR) and formic acid (FA) for the hydrolysis of furfural at 120 ˚C using 0.1 v/v% sulfuric acid.

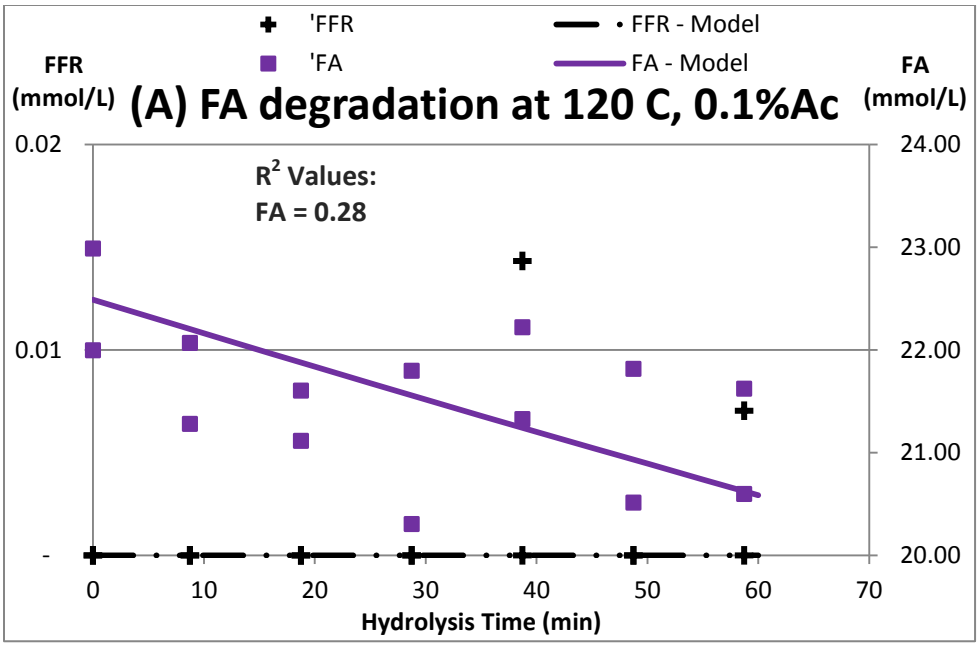

Figure 41: The best-fit model prediction and data of **(A)** formic acid (FA) and furfural (FFR) for the hydrolysis of formic acid at 120 ˚C using 0.1 v/v% sulfuric acid.

Table 16: The R^2 values of the changes of DP 1, DP 2, formic acid (FA), and furfural (FFR), in mmol/L, as a function of hydrolysis time in 120 ˚C using 0.1 v/v% sulfuric acid, as shown **Figures 38 - 41**.

	Hydrolysis of DP 1	Hydrolysis of DP 2	Hydrolysis of FA	Hydrolysis of FFR
DP 1	0.67	0.71		
DP 2		0.64		
FA	NA[#]	(0.81)	0.28	(0.32)
FFR	(0.18)	0.87		0.00

The R^2 value was not calculated because the experimental value was zero, i.e. the concentration of the compound was below the detection limit.

5.5.2.3 Hydrolysis Condition at 120 ˚C Using 1 v/v% Sulfuric Acid

The degradation rate constants for DP 1 (k_1), DP 2 (k_2), furfural (k_F), and formic acid (k_A), were calculated as 0.0019, 0.2513, 0.0026, and 0.0012 min^{-1}, respectively. The individual formation rate constants k_{21}, k_{1F}, k_{1A}, and k_{FA} were determined to be 0.2513, 0.0005, 0.0014, and 0.0025 min^{-1}, respectively, while the decomposition rate of furfural and formic acid, k_{FL} and k_{AL} were determined to be 0.0000 and 0.0012 min^{-1}, respectively. The data and the best-fit model predictions for each compound are presented in **Figures 42 - 45**. The R^2 values of the model fits are presented in **Table 17**.

The model provided a good fit to most of the experimental data for the concentrations of DP 1, DP 2, furfural, and formic acid, except for the hydrolysis of furfural, as reflected by the R^2 values of 0.49 – 0.98. The concentrations of DP 1 and DP 2, in particular, are well represented by the model, as shown by the R^2 values of 0.75 – 0.98. The concentrations of furfural and formic acid were not well represented by the model, as shown by the R^2 values of 0.26, and 0.00, respectively. Similar to the other hydrolysis conditions at120 ˚C, the R^2 value was not calculated for the formic acid concentration during the hydrolysis of DP 1 at 120 ˚C using 1 v/v% sulfuric acid, because there was no formic acid concentration detected in the experiment.

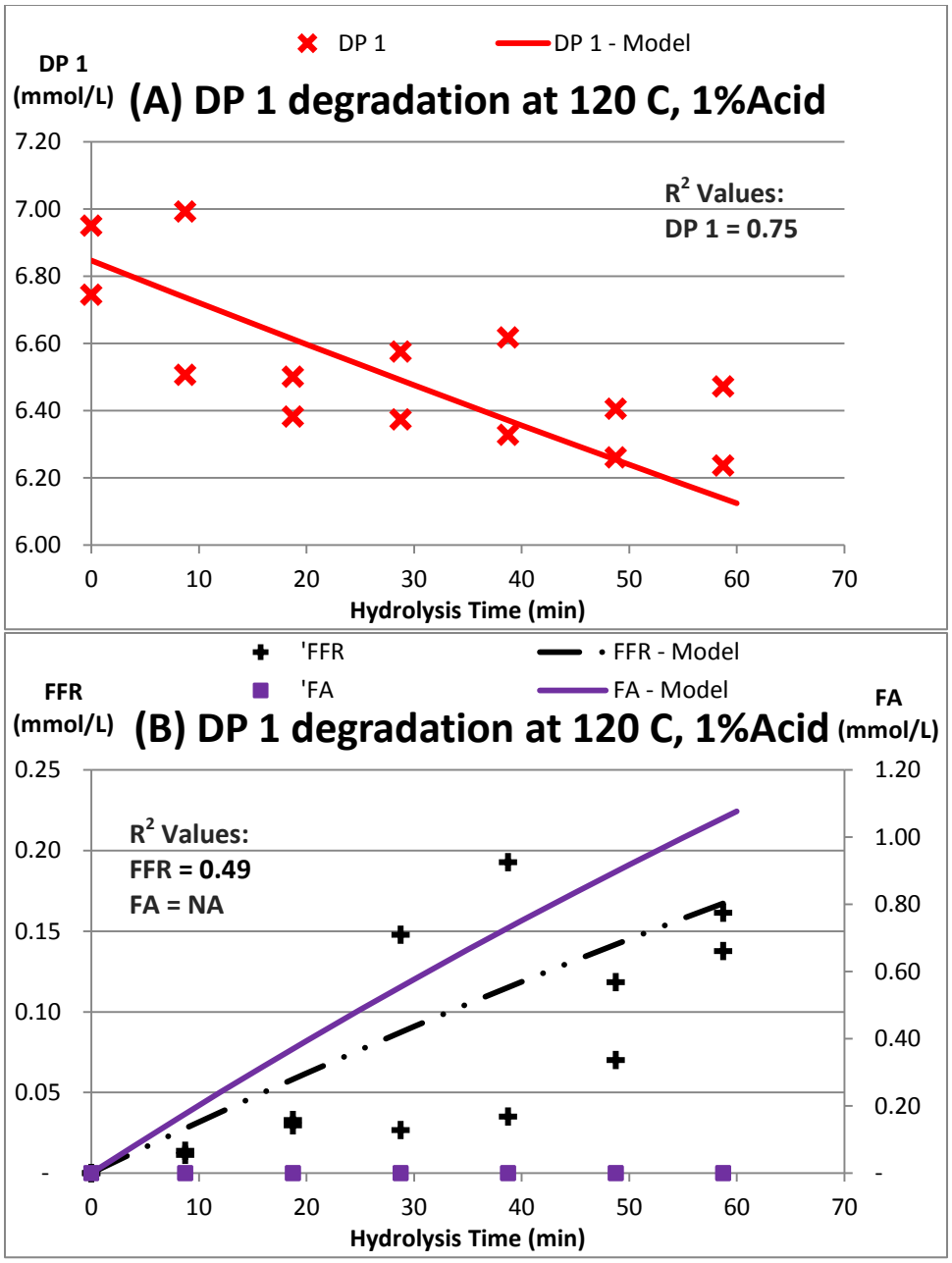

Figure 42: The best-fit model prediction and data of **(A)** DP 1, **(B)** furfural (FFR) and formic acid (FA) for the hydrolysis of DP 1 at 120 ˚C using 1 v/v% sulfuric acid.

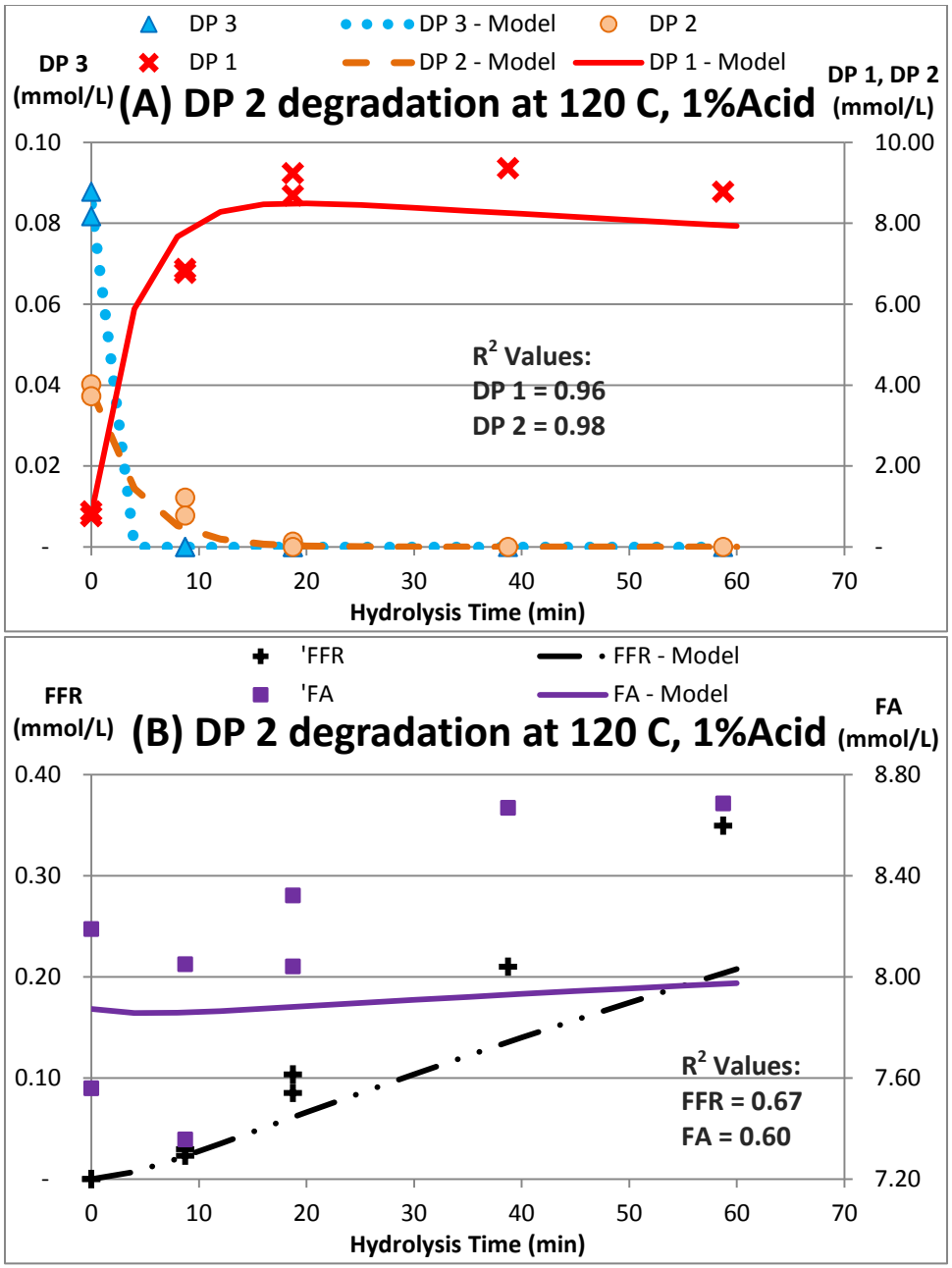

Figure 43: The best-fit model prediction and data of **(A)** DP 2 containing some DP 3 impurities and DP 1, **(B)** furfural (FFR) formic acid (FA) for the hydrolysis of DP 2 at 120 ˚C using 1 v/v% sulfuric acid.

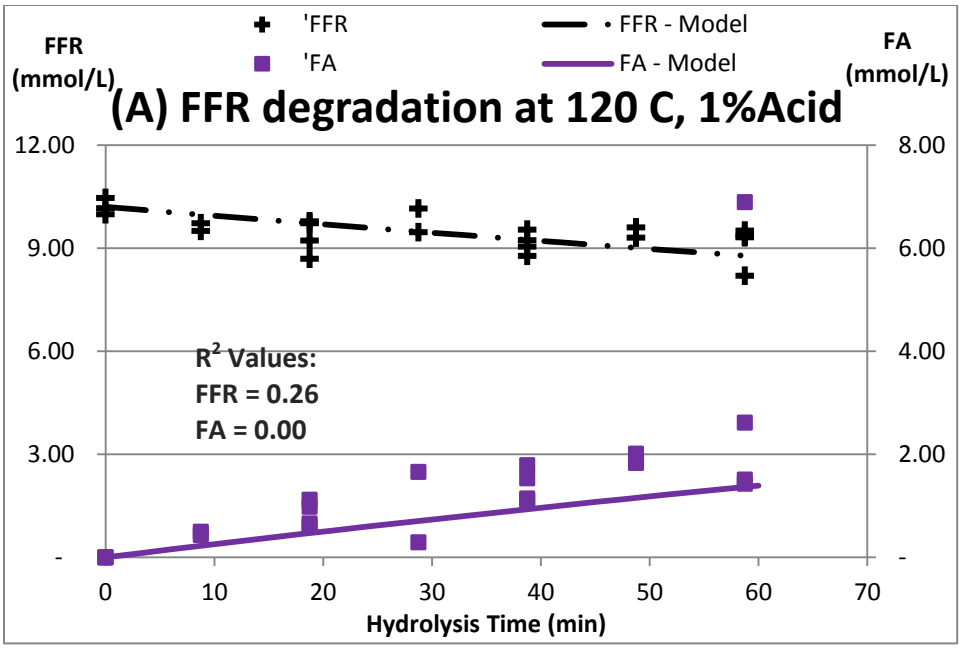

Figure 44: The best-fit model prediction and data of **(A)** furfural (FFR) and formic acid (FA) for the hydrolysis of furfural at 120 ˚C using 1 v/v% sulfuric acid.

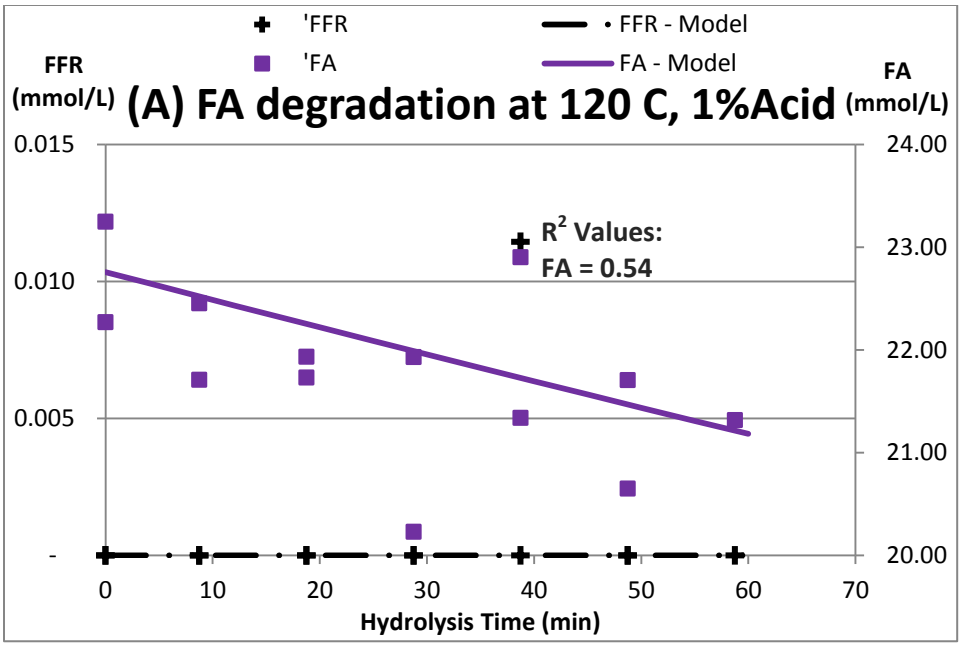

Figure 45: The best-fit model prediction and data of **(A)** formic acid (FA) and furfural (FFR) for the hydrolysis of formic acid at 120 ˚C using 1 v/v% sulfuric acid.

Table 17: The R^2 values of the changes of DP 1, DP 2, formic acid (FA), and furfural (FFR), in mmol/L, as a function of hydrolysis time in 120 ˚C using 1 v/v% sulfuric acid, as shown **Figures 42- 45**.

	Hydrolysis of DP 1	Hydrolysis of DP 2	Hydrolysis of FA	Hydrolysis of FFR
DP 1	0.75	0.96		
DP 2		0.98		
FA	NA[#]	0.60	0.54	0.00
FFR	0.49	0.67		0.26

The R^2 values were not calculated because the experimental value was zero, i.e. the concentration of the compound was below the detection limit.

5.5.2.4 Hydrolysis Condition at 160 ˚C Using Water

The degradation rate constants for DP 1 (k_1), DP 2 (k_2), DP 3 (k_3), DP 4 (k_4), furfural (k_F), and formic acid (k_A), were calculated as 0.0054, 0.0030, 0.0103, 0.0032, 0.0027 and 0.0004 min^{-1}, respectively. The individual formation rate constants k_{41}, k_{42}, k_{31}, k_{21}, k_{1F}, k_{1A}, and k_{FA} were determined to be 0.0001, 0.0031, 0.0103, 0.0030, 0.0014, 0.0040, and 0.0027 min^{-1}, respectively, while the decomposition rate of furfural and formic acid, k_{FL} and k_{AL} were determined to be 0.0000 and 0.0004 min^{-1}, respectively. The data and the best-fit model predictions for each compound are presented in **Figures 46 - 51**. The R^2 values of the model fits are presented in **Table 18**.

The model provided a reasonable fit to the experimental data for the concentrations of DP 1, as shown by the R^2 values of 0.92, 0.72, and 0.92, respectively for the hydrolysis of DP 1, DP 2, and DP 4. However, during the hydrolysis of DP 3, the R^2 value for the concentration of DP 1 was only -0.65, which indicated a poor model fit. Similarly, the concentrations of DP 2 were not well represented by the model, as shown by the R^2 values of -1.37 and -0.07 during the hydrolysis of DP 2 and DP 4, respectively, although the model predicted the concentration of DP 2 better during the hydrolysis of DP 3, as shown by the R^2 value of 0.89. The model did not provide a good fit to the concentration of DP 3 during the hydrolysis of DP 3, and the concentration of DP 4 during the hydrolysis of DP 4, as reflected by the R^2 values of -0.73 and -3.53, respectively, although the model performed better in predicting the concentration of DP 3 during the hydrolysis of DP 4, as shown by the R^2 value of 0.64.

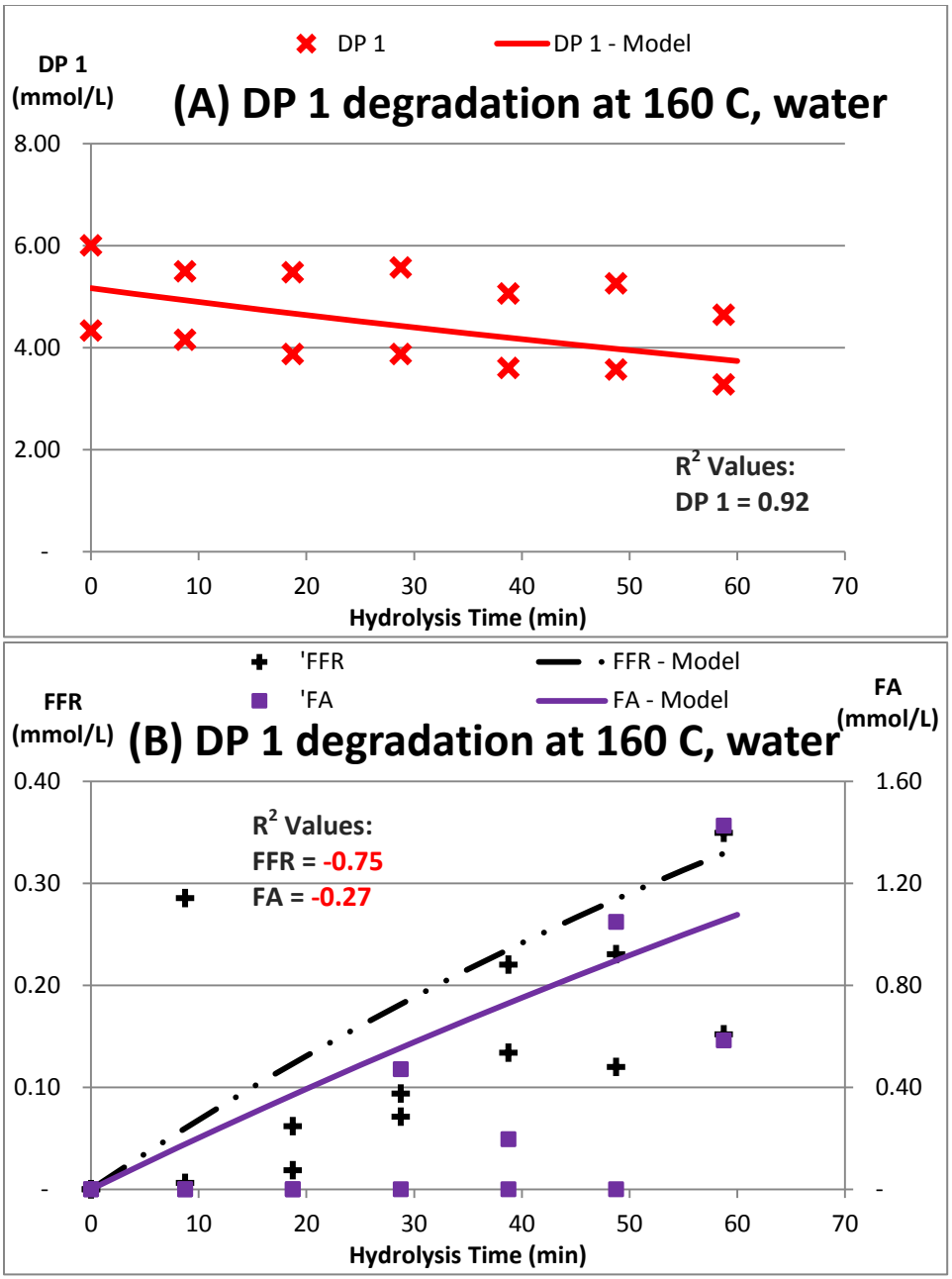

Figure 46: The best-fit model prediction and data of **(A)** DP 1, **(B)** furfural (FFR) and formic acid (FA) for the hydrolysis of DP 1 at 160 ˚C using water.

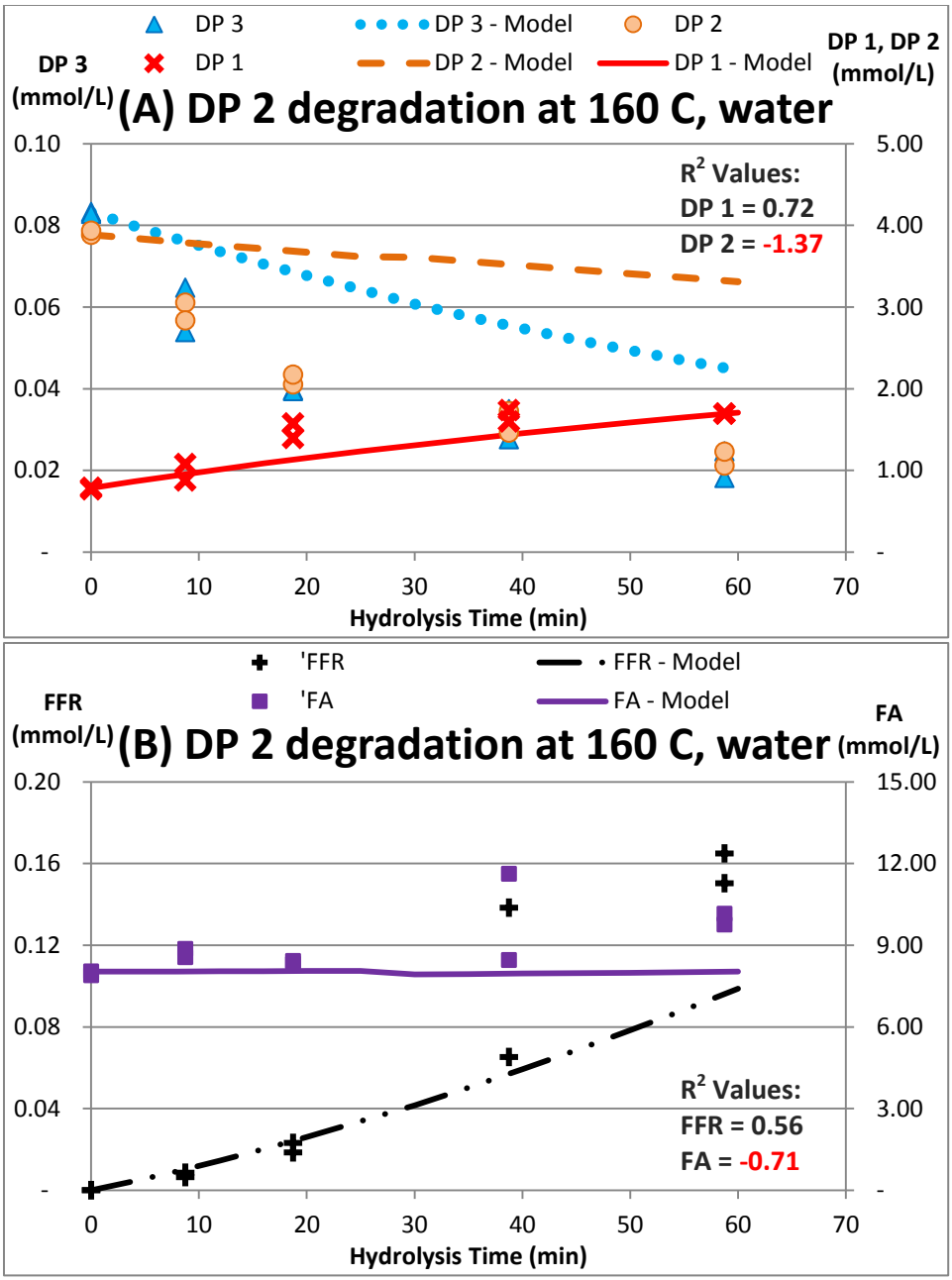

Figure 47: The best-fit model prediction and data of **(A)** DP 2 containing some DP 3 impurities and DP 1, **(B)** furfural (FFR) and formic acid (FA) for the hydrolysis of DP 2 at 160 ˚C using water.

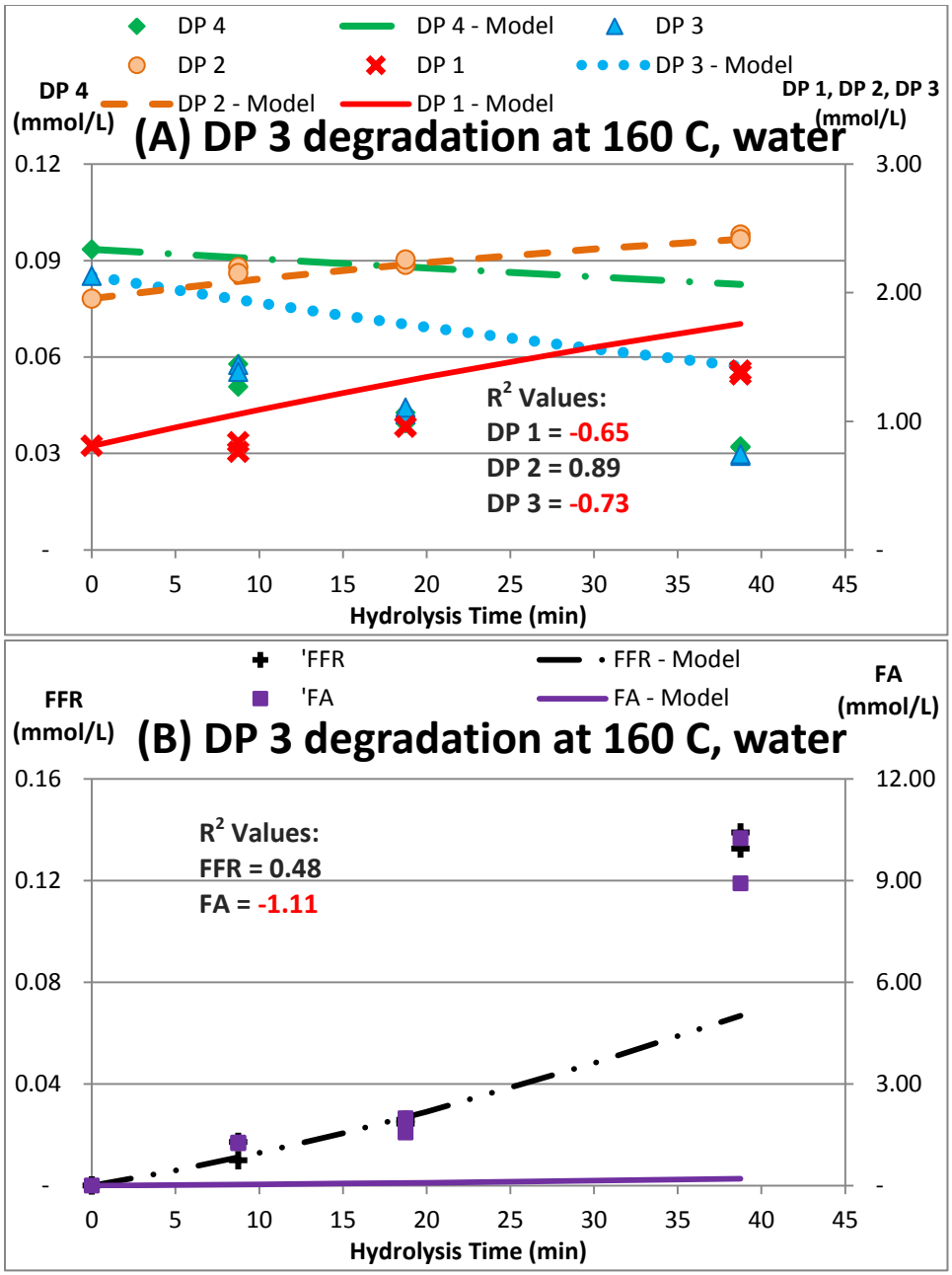

Figure 48: The best-fit model prediction and data of **(A)** DP 3 containing some DP 4 impurities, DP 2, and DP1, **(B)** furfural (FFR) and formic acid (FA) for the hydrolysis of DP 3 at 160 ˚C using water.

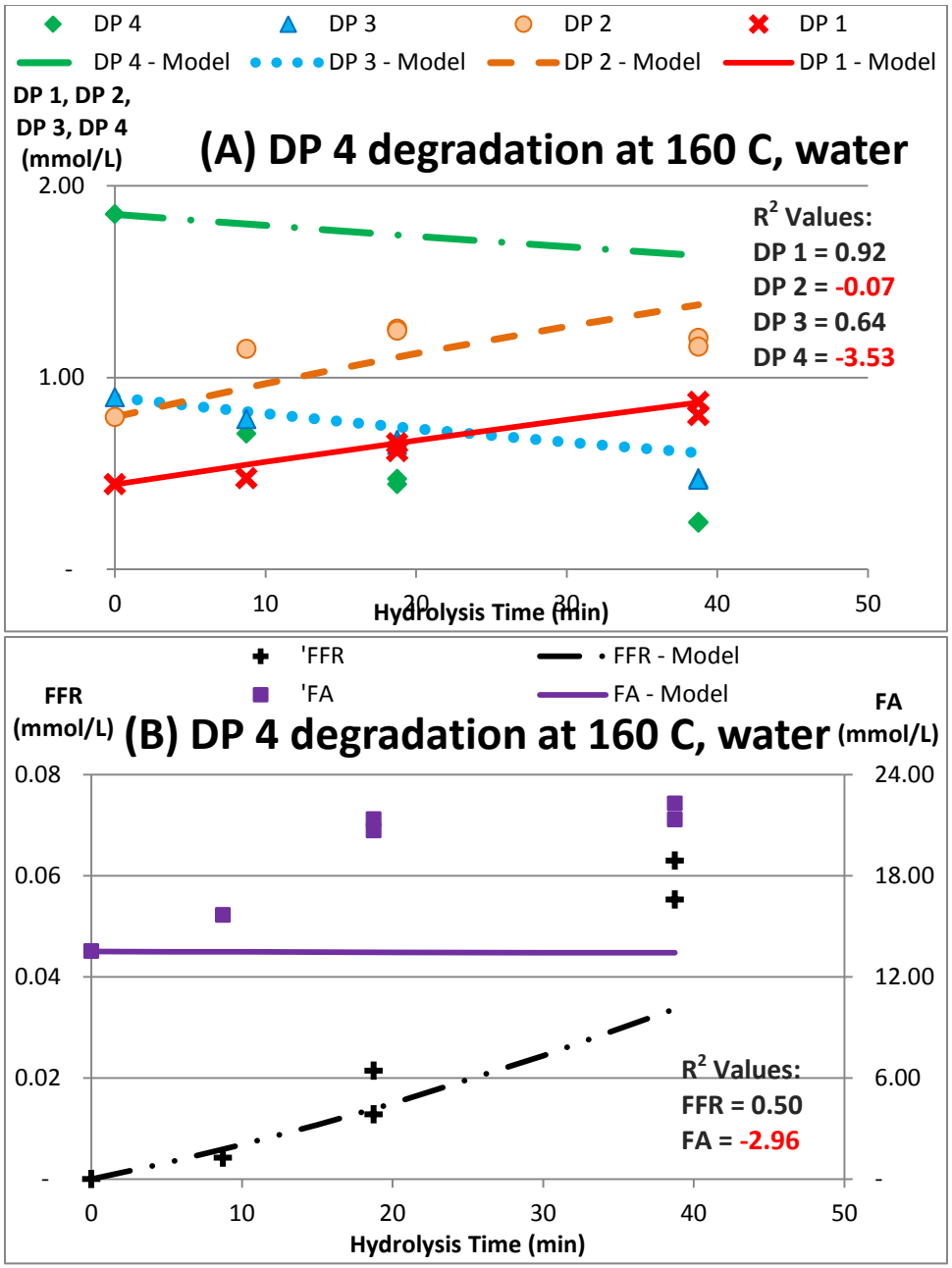

Figure 49: The best-fit model prediction and data of **(A)** DP 4, DP 3, DP2, and DP 1, **(B)** furfural (FFR) and formic acid (FA) for the hydrolysis of DP 3 at 160 ˚C using water.

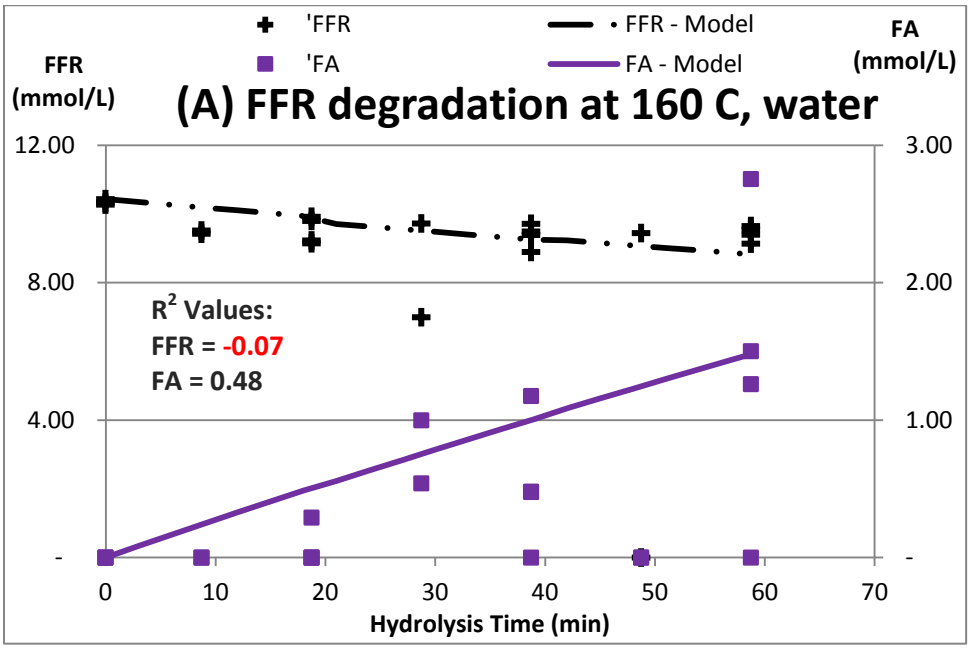

Figure 50: The best-fit model prediction and data of **(A)** furfural (FFR) and formic acid (FA) for the hydrolysis of furfural at 160 ˚C using water.

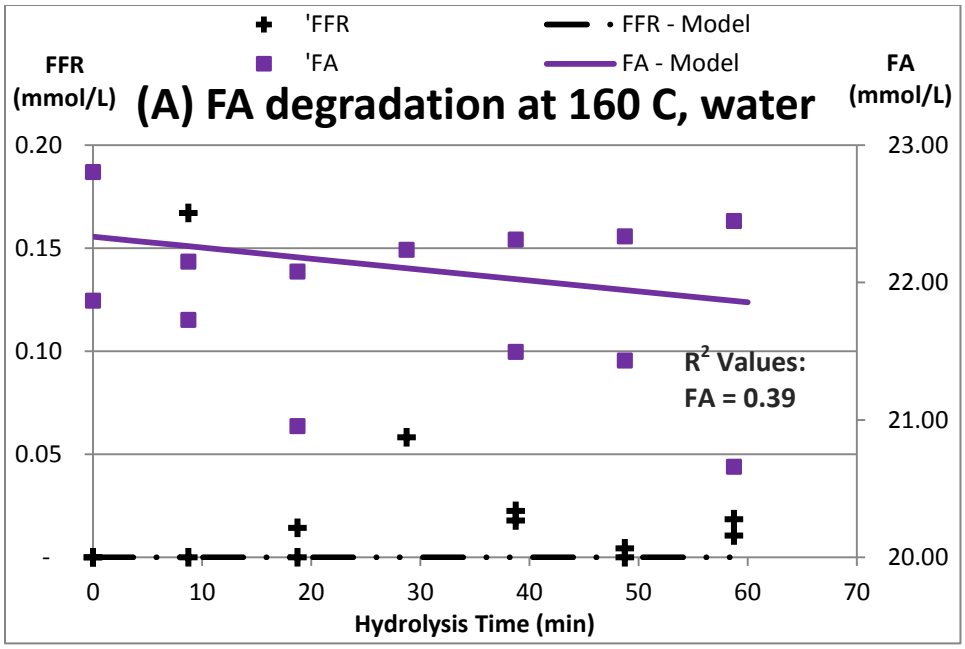

Figure 51: The best-fit model prediction and data of **(A)** formic acid (FA) and furfural (FFR) for the hydrolysis of formic acid at 160 ˚C using water.

Table 18: The R^2 values of the changes of DP 1, DP 2, DP 3, DP 4, formic acid (FA), and furfural (FFR), in mmol/L, as a function of hydrolysis time in 160 ˚C water, as shown **Figures 46- 51**.

	Hydrolysis of DP 1	Hydrolysis of DP 2	Hydrolysis of DP 3	Hydrolysis of DP 4	Hydrolysis of FA	Hydrolysis of FFR
DP 1	0.92	0.72	(0.65)	0.92		
DP 2		(1.37)	0.89	(0.07)		
DP 3			(0.73)	0.64		
DP 4				(3.53)		
FA	(0.27)	(0.71)	(1.11)	(2.96)	0.39	0.48
FFR	(0.75)	0.56	0.48	0.50		(0.07)

The concentrations of formic acid were not accurately predicted by the model during the hydrolysis of DP 1, DP 2, DP 3, and DP 4, as pointed by the R^2 values of -0.27, -0.71, -1.11 and -2.96, respectively, although the model predictions were better during the hydrolysis of formic acid and furfural, as indicated by the R^2 values of 0.39 and 0.48, respectively. In comparison to formic acid, furfural concentrations were better represented by the model, as shown by the R^2 values of 0.56, 0.48, and 0.50 during the hydrolysis of DP 2, DP 3, and DP 4, although the R^2 values were only -0.75 and -0.07, respectively during the hydrolysis of DP 1, and furfural.

5.5.2.5 Hydrolysis Condition at 160 ˚C Using 0.1 v/v% Sulfuric Acid

The degradation rate constants for DP 1 (k_1), DP 2 (k_2), DP 3 (k_3), DP 4 (k_4), furfural (k_F), and formic acid (k_A), were calculated as 0.0057, 0.0439, 0.1048, 0.1049, 0.0014 and 0.0013 min^{-1}, respectively. The individual formation rate constants k_{41}, k_{42}, k_{31}, k_{21}, k_{1F}, k_{1A}, and k_{FA} were determined to be 0.0699, 0.0350, 0.1048, 0.0439, 0.0020, 0.0037, and 0.0014 min^{-1}, respectively, while the decomposition rate of furfural and formic acid k_{FL} and k_{AL} were determined to be 0.0000 and 0.0013 min^{-1}, respectively. The data and the best-fit model predictions for each compound are presented in **Figures 52 - 57**. The R^2 values of the model fits are presented in **Table 19**.

The model provided a good fit to the experimental data for the concentrations of DP 1, DP 2, DP 3, DP 4, and furfural concentrations, except for two instances, as reflected by the R^2 values of 0.63 – 0.99. The exceptions were the concentration of DP 1 during the hydrolysis of DP 3, and the concentration of furfural during the hydrolysis of furfural, where the R^2 values were -0.18 and -0.43, respectively. The concentrations of formic acid were poorly represented by the model during the hydrolysis of DP 3, DP 4, and furfural, as shown by the R^2 values of -3.25, -3.17, and -0.91, respectively, although the model performed better in predicting the formic acid concentrations during the hydrolysis of DP 1, DP 2, and formic acid, as shown by the R^2 values of 0.47, 0.15, and 0.22, respectively.

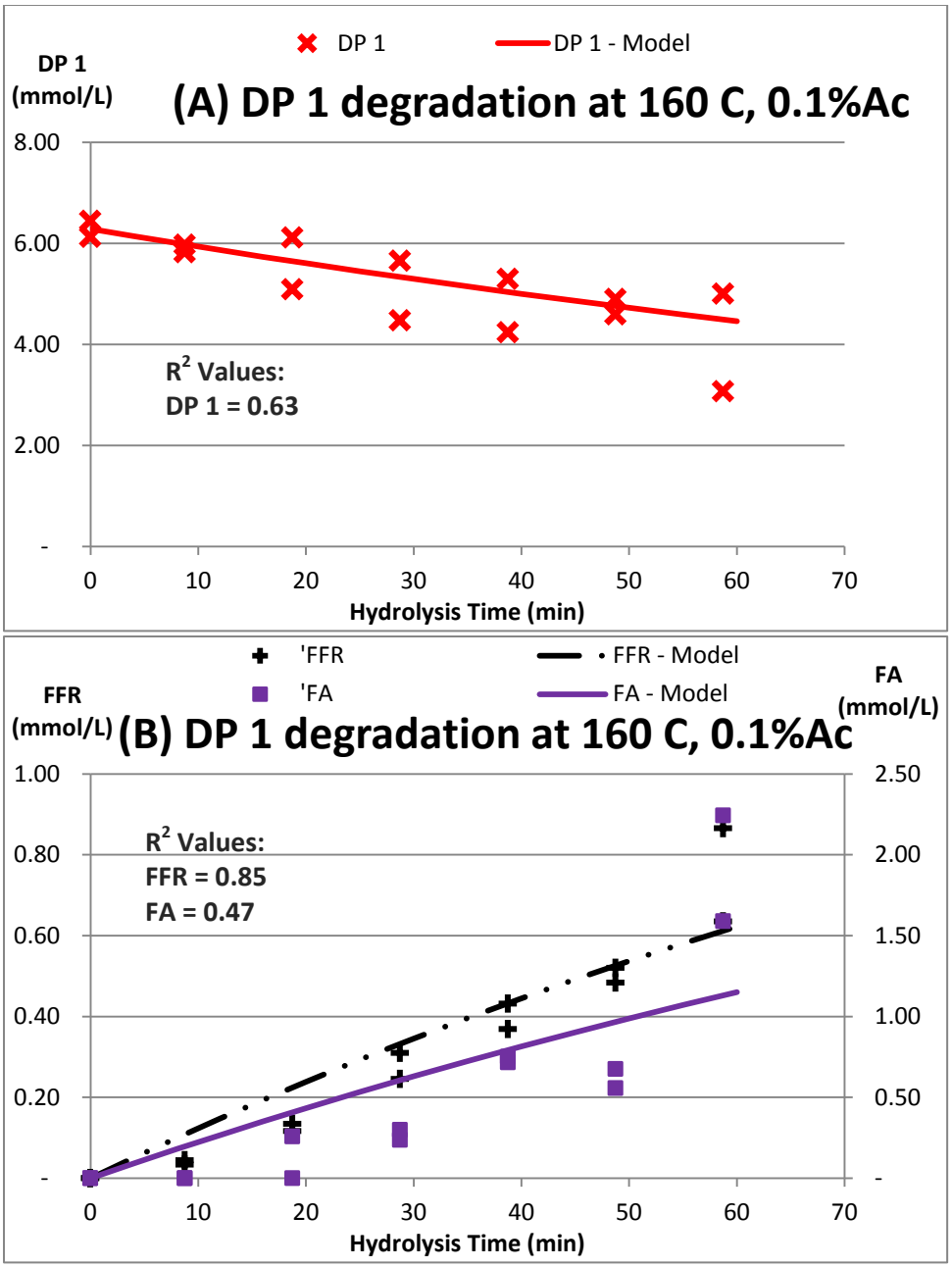

Figure 52: The best-fit model prediction and data of **(A)** DP 1, **(B)** furfural (FFR) and formic acid (FA) for the hydrolysis of DP 1 at 160 ˚C using 0.1 v/v% sulfuric acid.

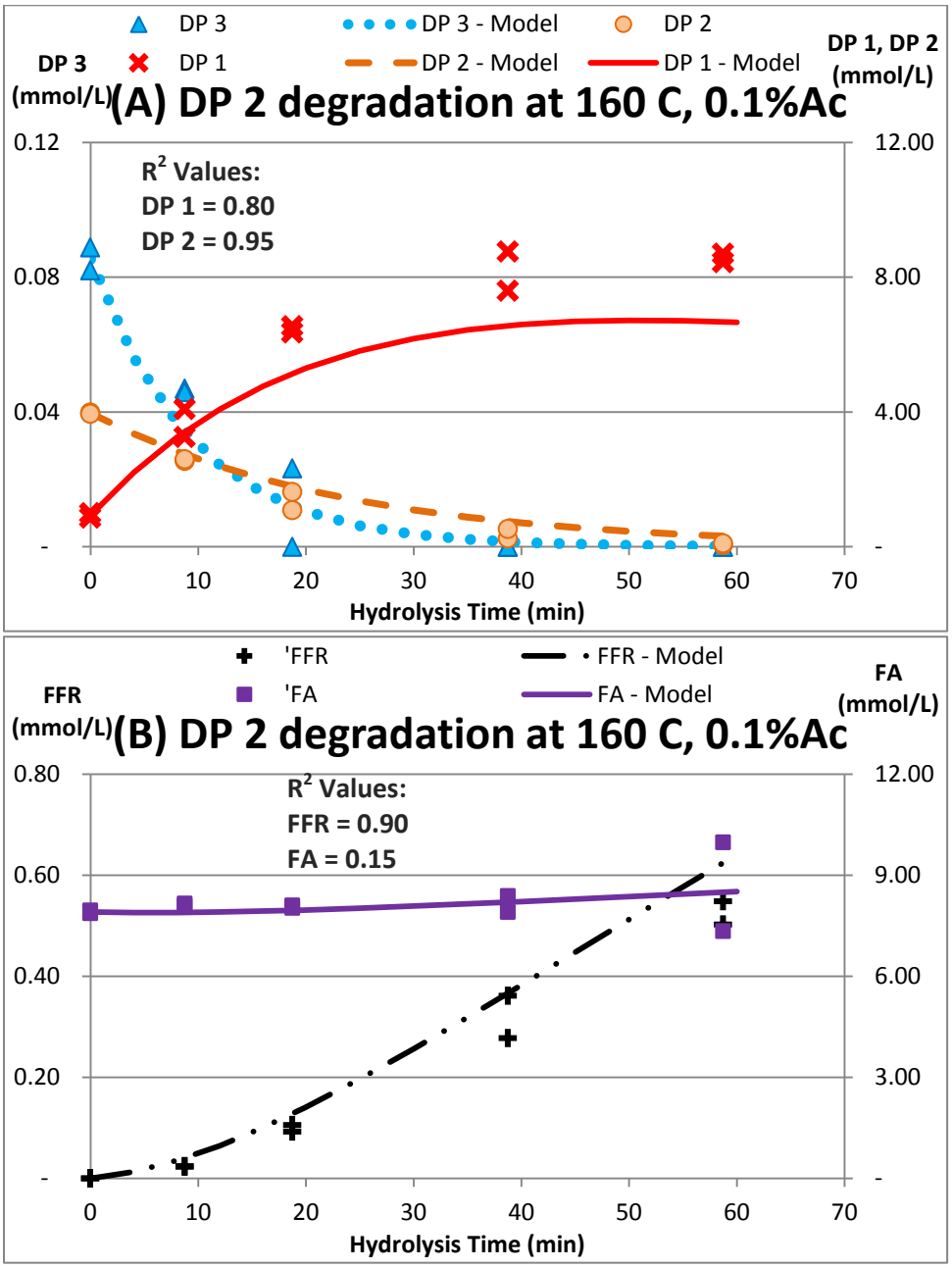

Figure 53: The best-fit model prediction and data of **(A)** DP 2 containing some DP 3 impurities and DP 1, **(B)** furfural (FFR) and formic acid (FA) for the hydrolysis of DP 2 at 160 ˚C using 0.1 v/v% sulfuric acid.

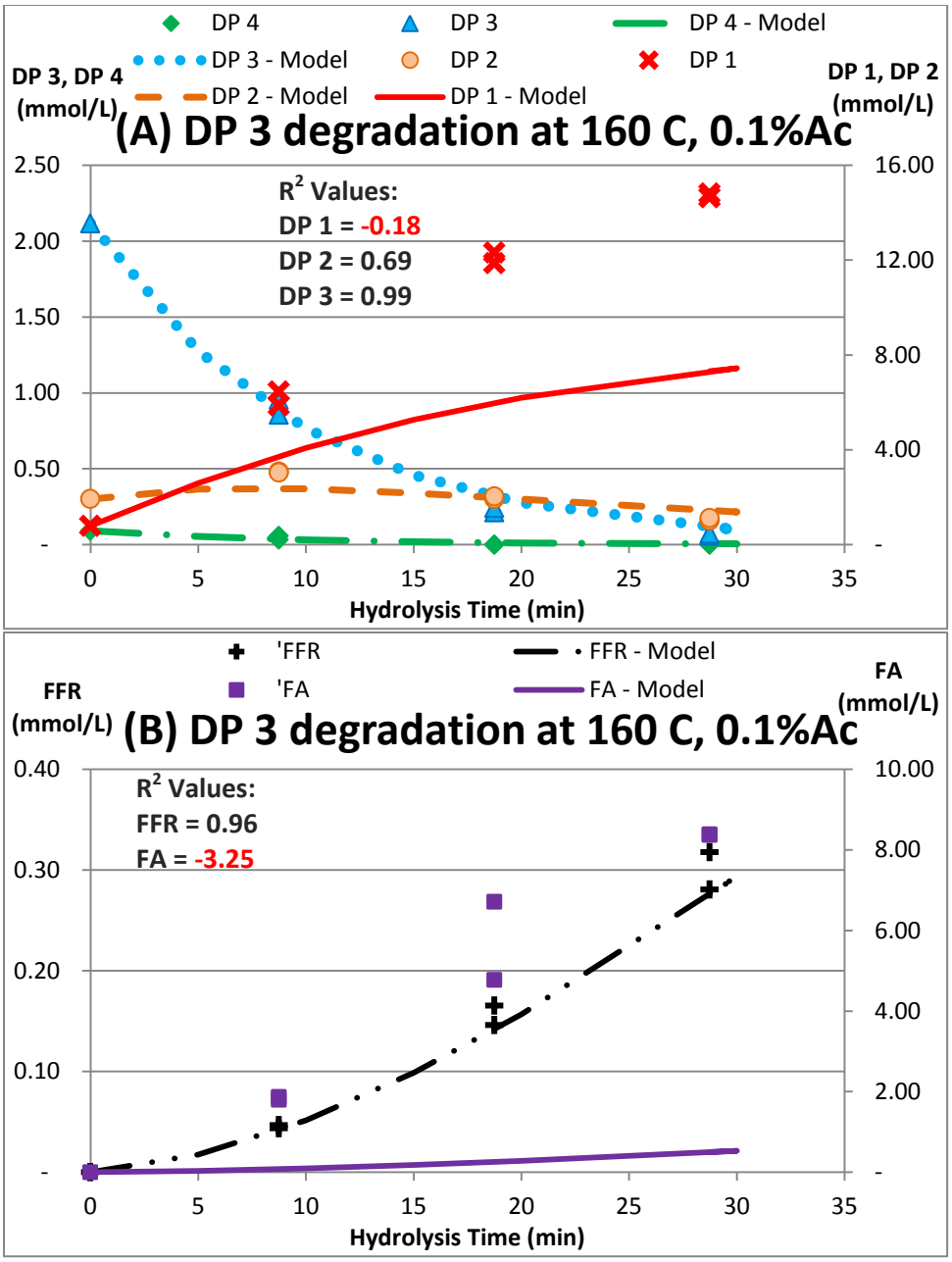

Figure 54: The best-fit model prediction and data of **(A)** DP 3 containing some DP 4 impurities, DP 2, and DP1, **(B)** furfural (FFR) and formic acid (FA) for the hydrolysis of DP 3 at 160 ˚C using 0.1 v/v% sulfuric acid.

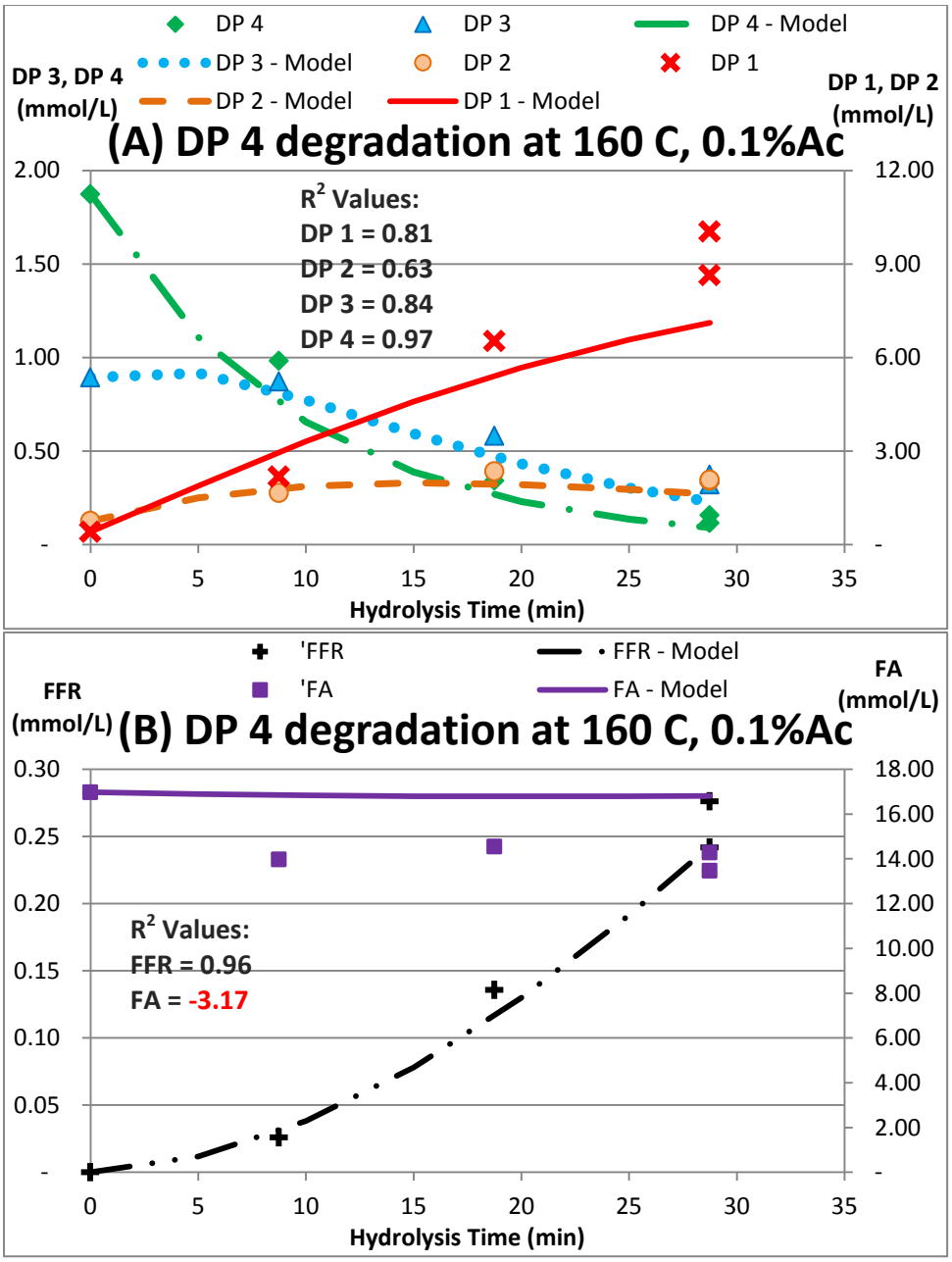

Figure 55: The best-fit model prediction and data of **(A)** DP 4, DP 3, DP2, and DP 1, **(B)** furfural (FFR) and formic acid (FA) for the hydrolysis of DP 4 at 160 ˚C using 0.1 v/v% sulfuric acid.

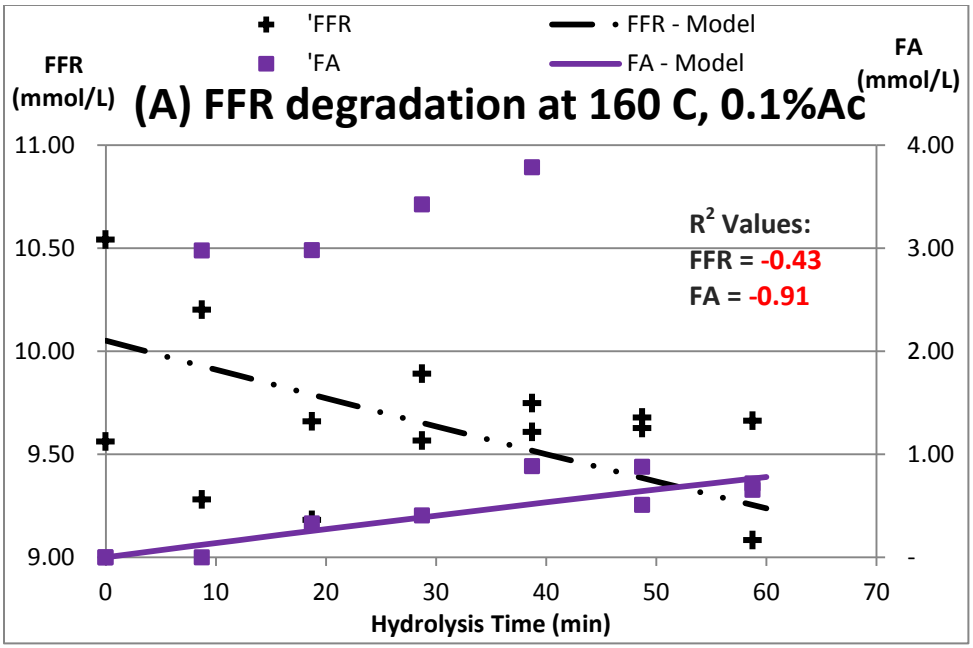

Figure 56: The best-fit model prediction and data of **(A)** furfural and formic acid (FA) for the hydrolysis of furfural (FFR) at 160 ˚C using 0.1 v/v% sulfuric acid.

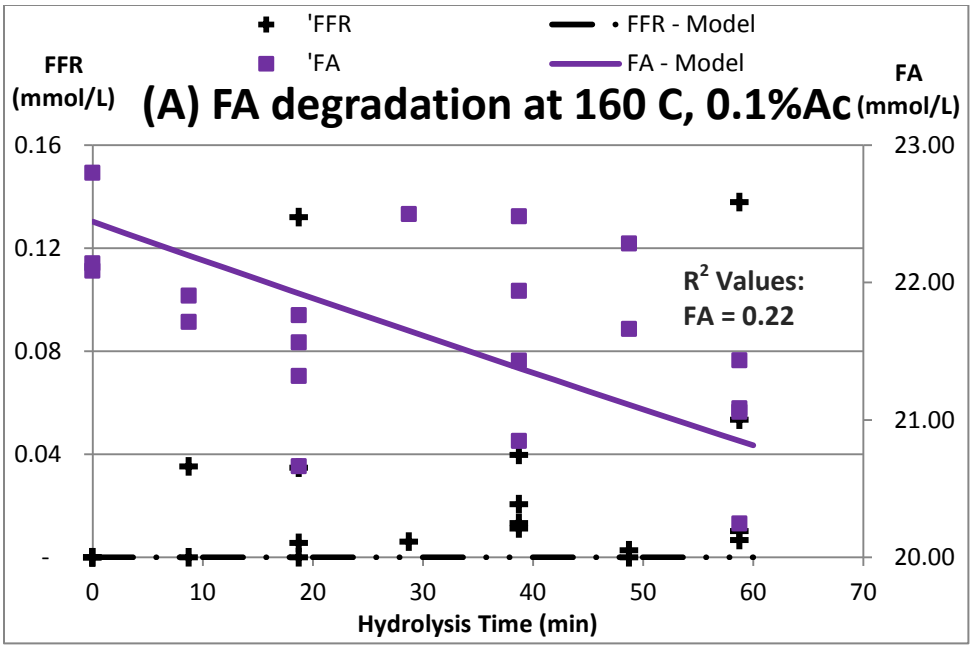

Figure 57: The best-fit model prediction and data of **(A)** formic acid (FA) and furfural (FFR) for the hydrolysis of formic acid 160 ˚C using 0.1 v/v% sulfuric acid.

Table 19: The R^2 values of the changes of DP 1, DP 2, DP 3, DP 4, formic acid (FA), and furfural (FFR), in mmol/L, as a function of hydrolysis time in 160 ˚C using 0.1 v/v% sulfuric acid, as shown **Figures 52- 57**.

	Hydrolysis of DP 1	Hydrolysis of DP 2	Hydrolysis of DP 3	Hydrolysis of DP 4	Hydrolysis of FA	Hydrolysis of FFR
DP 1	0.63	0.80	(0.18)	0.81		
DP 2		0.95	0.69	0.63		
DP 3			0.99	0.84		
DP 4				0.97		
FA	0.47	0.15	(3.25)	(3.17)	0.22	(0.91)
FFR	0.85	0.90	0.96	0.96		(0.43)

5.5.2.6 Hydrolysis Condition at 160 ˚C Using 1 v/v% Sulfuric Acid

The degradation rate constants for DP 1 (k_1), DP 2 (k_2), DP 3 (k_3), DP 4 (k_4), furfural (k_F), and formic acid (k_A), were calculated as 0.0363, 1.0152, 1.9862, 3.8453, 0.0040 and 0.0008 min^{-1}, respectively. The individual formation rate constants k_{41}, k_{42}, k_{31}, k_{21}, k_{1F}, k_{1A}, and k_{FA} were determined to be 3.8453, 0.000, 1.9862, 1.0152, 0.0128, 0.0235, and 0.0040 min^{-1}, respectively, while the decomposition rate of furfural and formic acid k_{FL} and k_{AL} were determined to be 0.0000 and 0.0008 min^{-1}, respectively. The data and the best-fit model predictions for each compound are presented in **Figures 58 - 63**. The R^2 values of the model fits are presented in **Table 20**.

The model provided a good fit to the experimental data for the concentrations of DP 1 and DP 2, as reflected by the R^2 values of 0.35 – 0.97. Similarly, the concentration of furfural was well predicted by the model as shown by the R^2 values of 0.39 – 0.98, except during the hydrolysis of DP 1, which had an R^2 value of -1.10 for the concentration of furfural. The concentration of DP 3 and DP 4 were not well represented by the model, as shown by the R^2 values of 0.21, 0.21, and -0.33 for the concentration of DP 3 during the hydrolysis of DP 3, the concentration of DP 3 during the hydrolysis of DP 4, and the concentration of DP 4 during the hydrolysis of DP 4, respectively. The R^2 values for formic acid were low during the hydrolysis of DP 1, DP 3, DP 4, and furfural, at -1.28, 0.02, 0.24, and -2.58, respectively, although the R^2 values were better during the hydrolysis of DP 2 and formic acid, at 0.95 and 0.47, respectively.

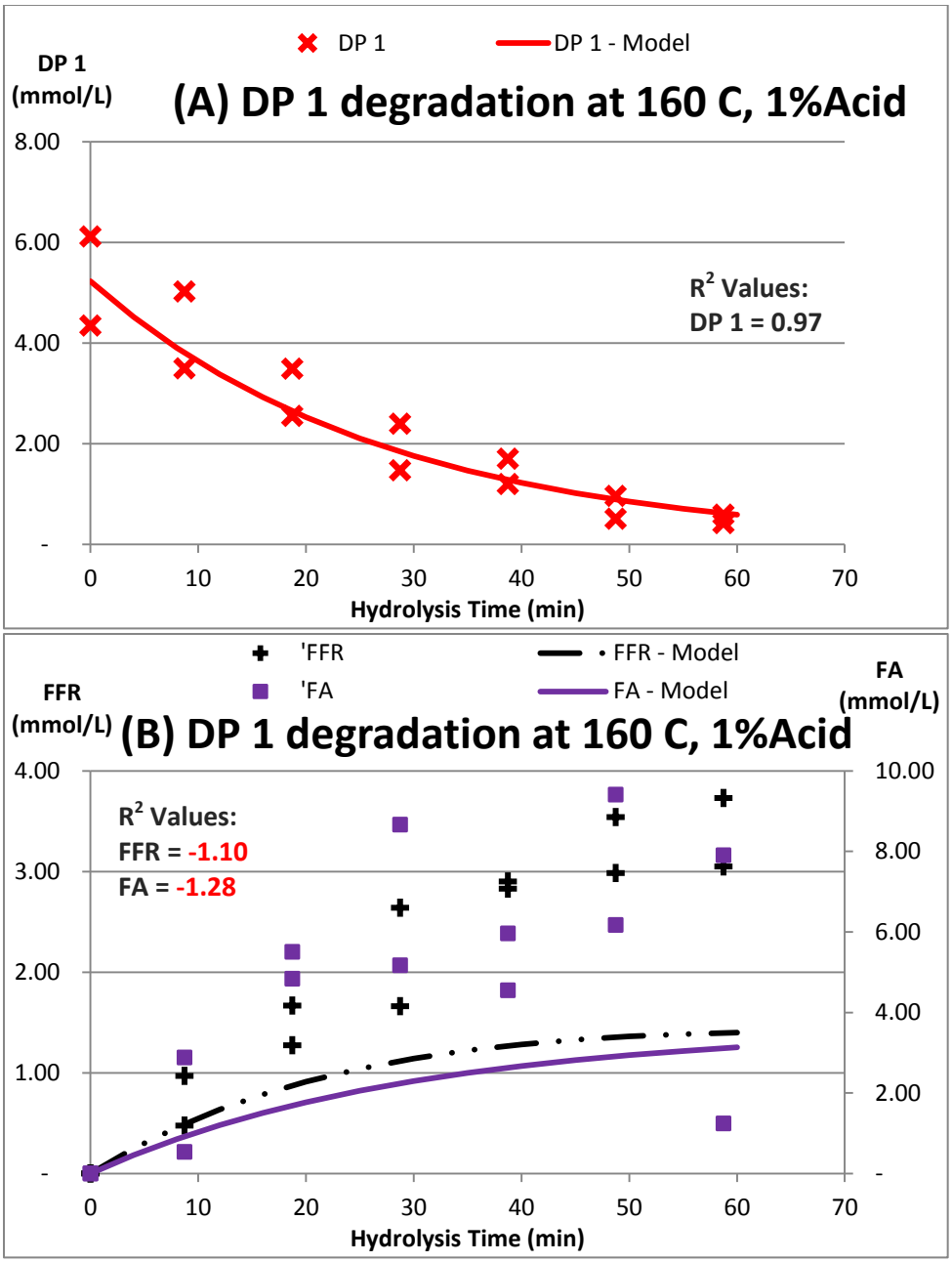

Figure 58: The best-fit model prediction and data of **(A)** DP 1, **(B)** furfural (FFR) and formic acid (FA) for the hydrolysis of DP 1 at 160 ˚C using 1 v/v% sulfuric acid.

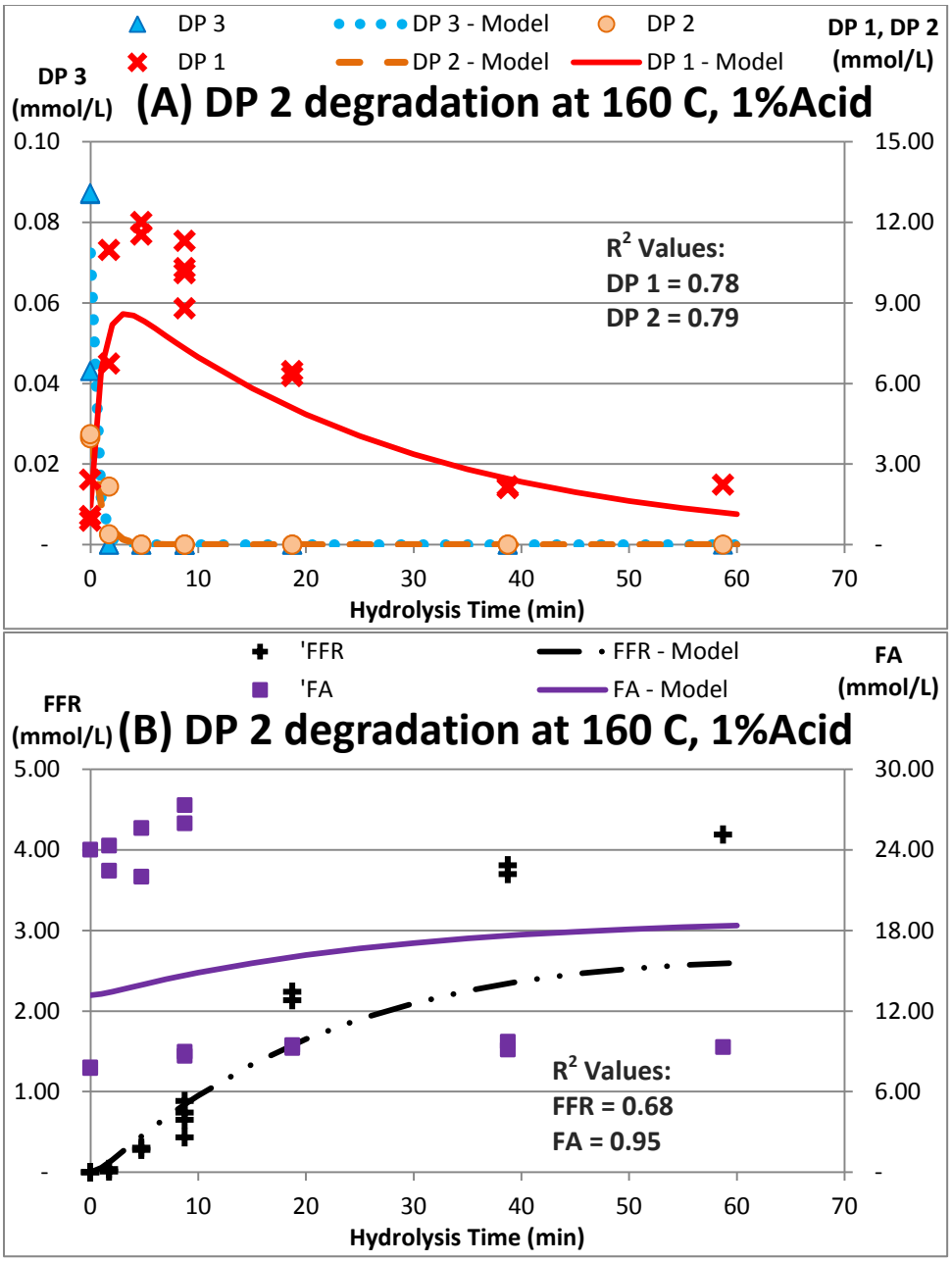

Figure 59: The best-fit model prediction and data of **(A)** DP 2 containing some DP 3 impurities and DP 1, **(B)** furfural (FFR) and formic acid (FA) for the hydrolysis of DP 2 at 160 ˚C using 1 v/v% sulfuric acid.

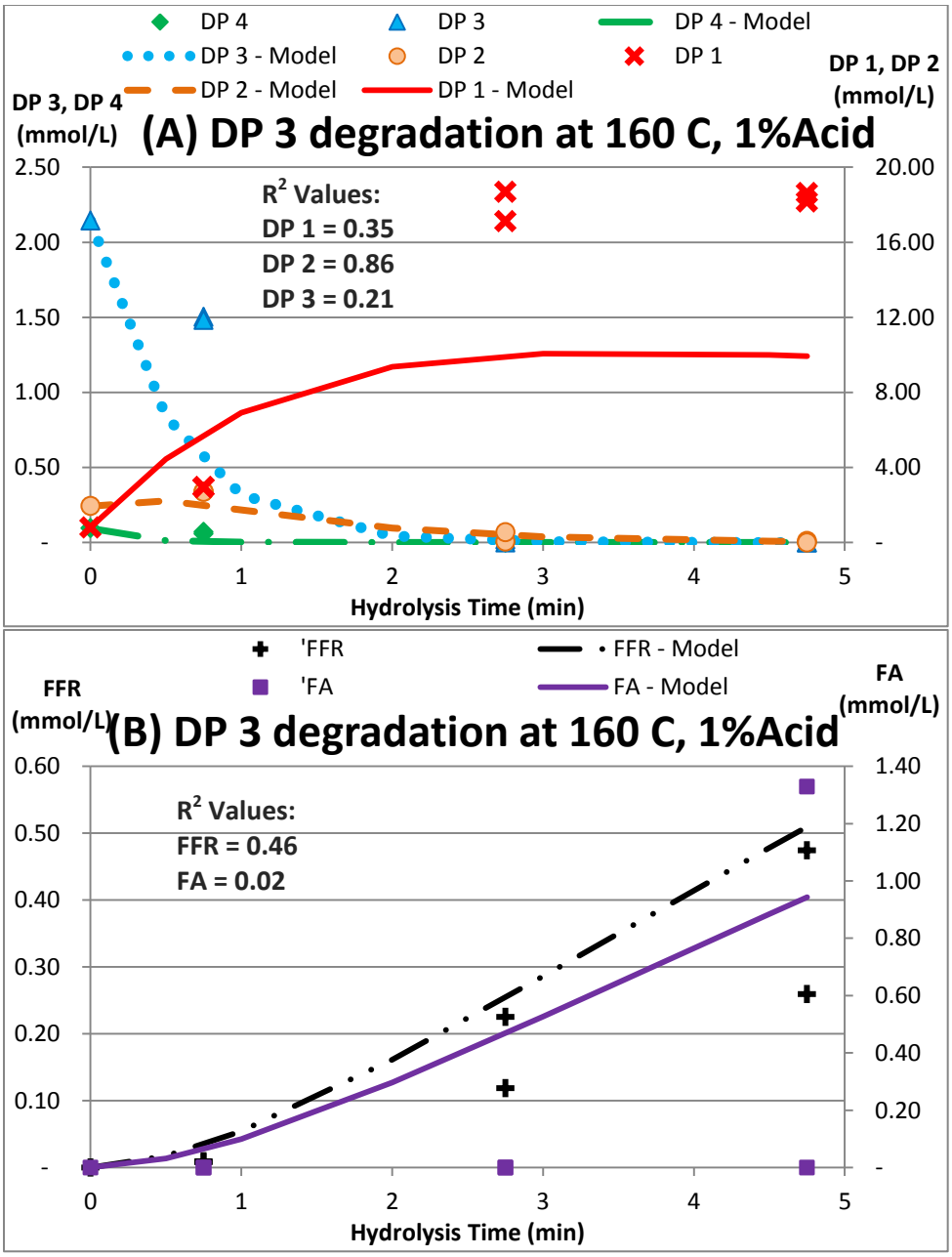

Figure 60: The best-fit model prediction and data of **(A)** DP 3 containing some DP 4 impurities, DP 2, and DP1, **(B)** furfural (FFR) and formic acid (FA) for the hydrolysis of DP 3 at 160 ˚C using 1 v/v% sulfuric acid.

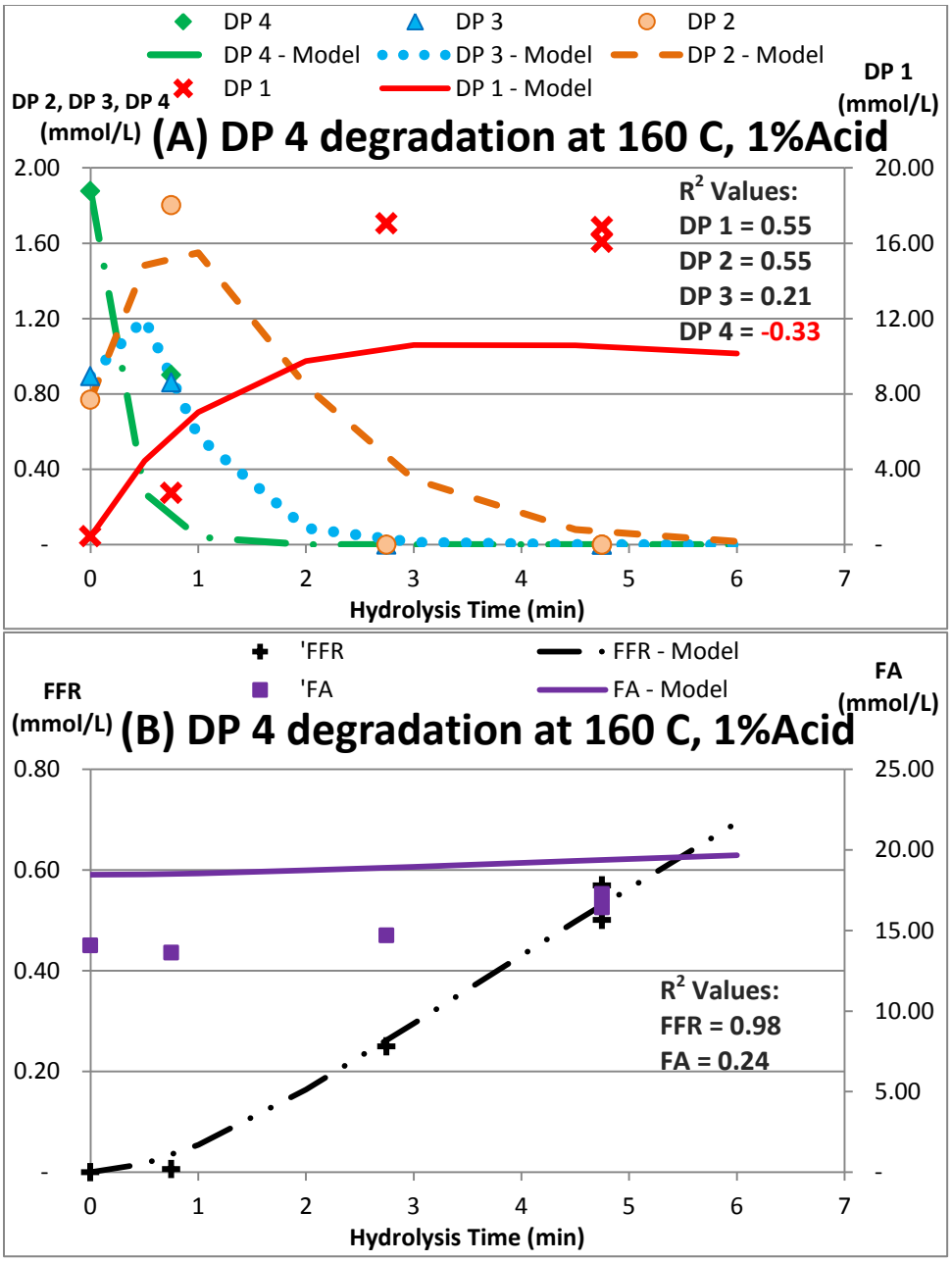

Figure 61: The best-fit model prediction and data of **(A)** DP 4, DP 3, DP2, and DP 1, **(B)** furfural (FFR) and formic acid (FA) for the hydrolysis of DP 4 at 160 ˚C using 1 v/v% sulfuric acid.

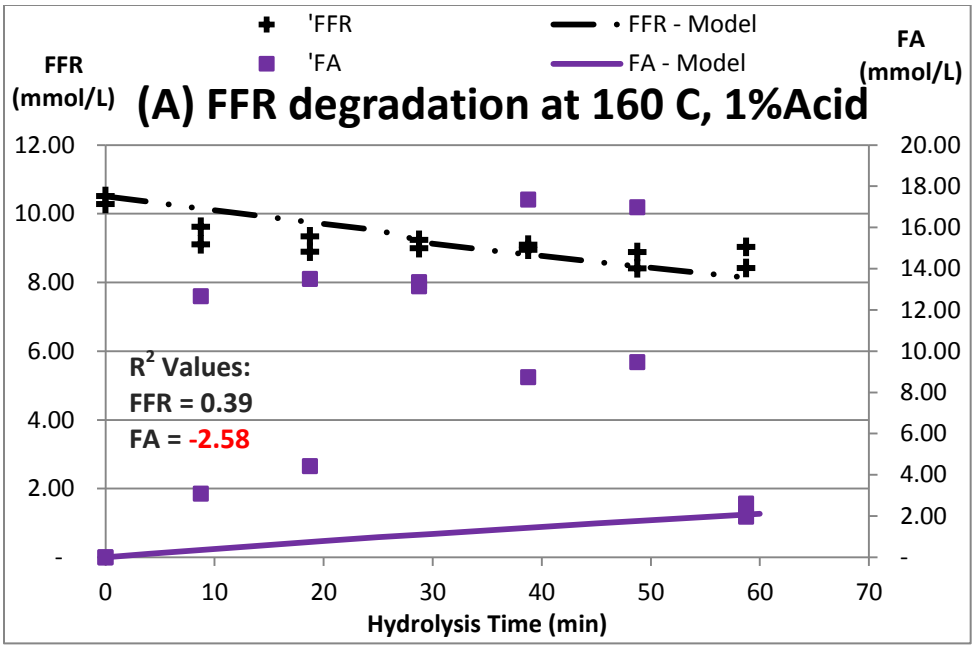

Figure 62: The best-fit model prediction and data of **(A)** furfural and formic acid (FA) for the hydrolysis of furfural (FFR) at 160 ˚C using 1 v/v% sulfuric acid.

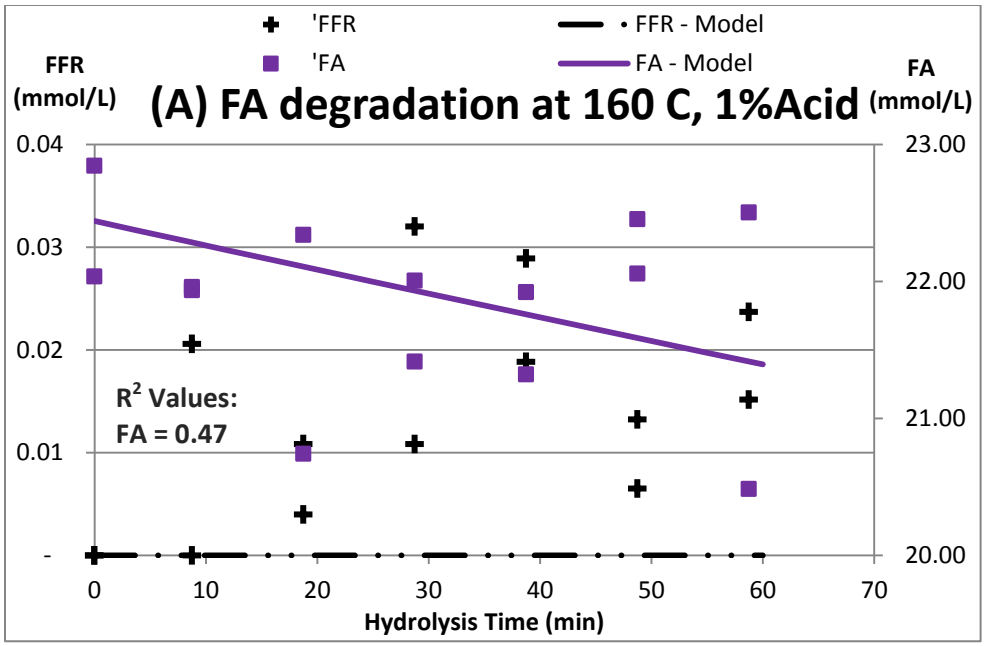

Figure 63: The best-fit model prediction and data of **(A)** formic acid (FA) and furfural (FFR) for the hydrolysis of formic acid at 160 ˚C using 1 v/v% sulfuric acid.

Table 20: The R^2 values of the changes of DP 1, DP 2, DP 3, DP 4, formic acid (FA), and furfural (FFR), in mmol/L, as a function of hydrolysis time in 160 ˚C using 1 v/v% sulfuric acid, as shown **Figures 58 - 63**.

	Hydrolysis of DP 1	Hydrolysis of DP 2	Hydrolysis of DP 3	Hydrolysis of DP 4	Hydrolysis of FA	Hydrolysis of FFR
DP 1	0.97	0.78	0.35	0.55		
DP 2		0.79	0.86	0.55		
DP 3			0.21	0.21		
DP 4				(0.33)		
FA	(1.28)	0.95	0.02	0.24	0.47	(2.58)
FFR	(1.10)	0.68	0.46	0.98		0.39

5.5.2.7 Hydrolysis Condition at 200 ˚C Using Water

The degradation rate constants for DP 1 (k_1), DP 2 (k_2), DP 3 (k_3), DP 4 (k_4), furfural (k_F), and formic acid (k_A), were calculated as 0.2396, 0.0414, 0.0681, 0.0161, 0.0044, and 0.0020 min^{-1}, respectively. The individual formation rate constants k_{41}, k_{42}, k_{31}, k_{21}, k_{1F}, k_{1A}, and k_{FA} were determined to be 0.0026, 0.0136, 0.0681, 0.0414, 0.0112, 0.2284, and 0.0038 min^{-1}, respectively, while the decomposition rate of furfural and formic acid k_{FL} and k_{AL} were determined to be 0.0000 and 0.0020 min^{-1}, respectively. The data and the best-fit model predictions for each compound are presented in **Figures 64 - 69**. The R^2 values of the model fits are presented in **Table 21**.

The model provided a reasonable fit to the experimental data for the concentrations of DP 2, as reflected by the R^2 values of 0.36 – 0.42. However, the model, in general, provided a poor data fit to the concentrations of DP 1, DP 3, and DP 4, as shown by the R^2 values of less than zero, except for the concentrations of DP 1 during the hydrolysis of DP 3 and DP 4, with the R^2 values of 0.07 and 0.60, respectively. The concentration of formic acid was well predicted by the model during the hydrolysis of DP 2 and formic acid, as shown by the R^2 values of 0.44 and 0.27, respectively. However, during the hydrolysis of DP 1, DP 3, DP 4, and furfural, the R^2 values for the concentration of formic acid were -0.64, -0.46, -1.33, and 0.07, respectively, indicating poor model predictions. Similarly, the model did not predict the concentrations of furfural well during the hydrolysis of DP 1, DP 2, and DP 4, as reflected by the R^2 values of -3.98, 0.15, and -0.07, respectively, although the model performed better in predicting the concentrations of furfural during the hydrolysis of DP 3 and furfural, as shown by the R^2 values of 0.69 and 0.55, respectively.

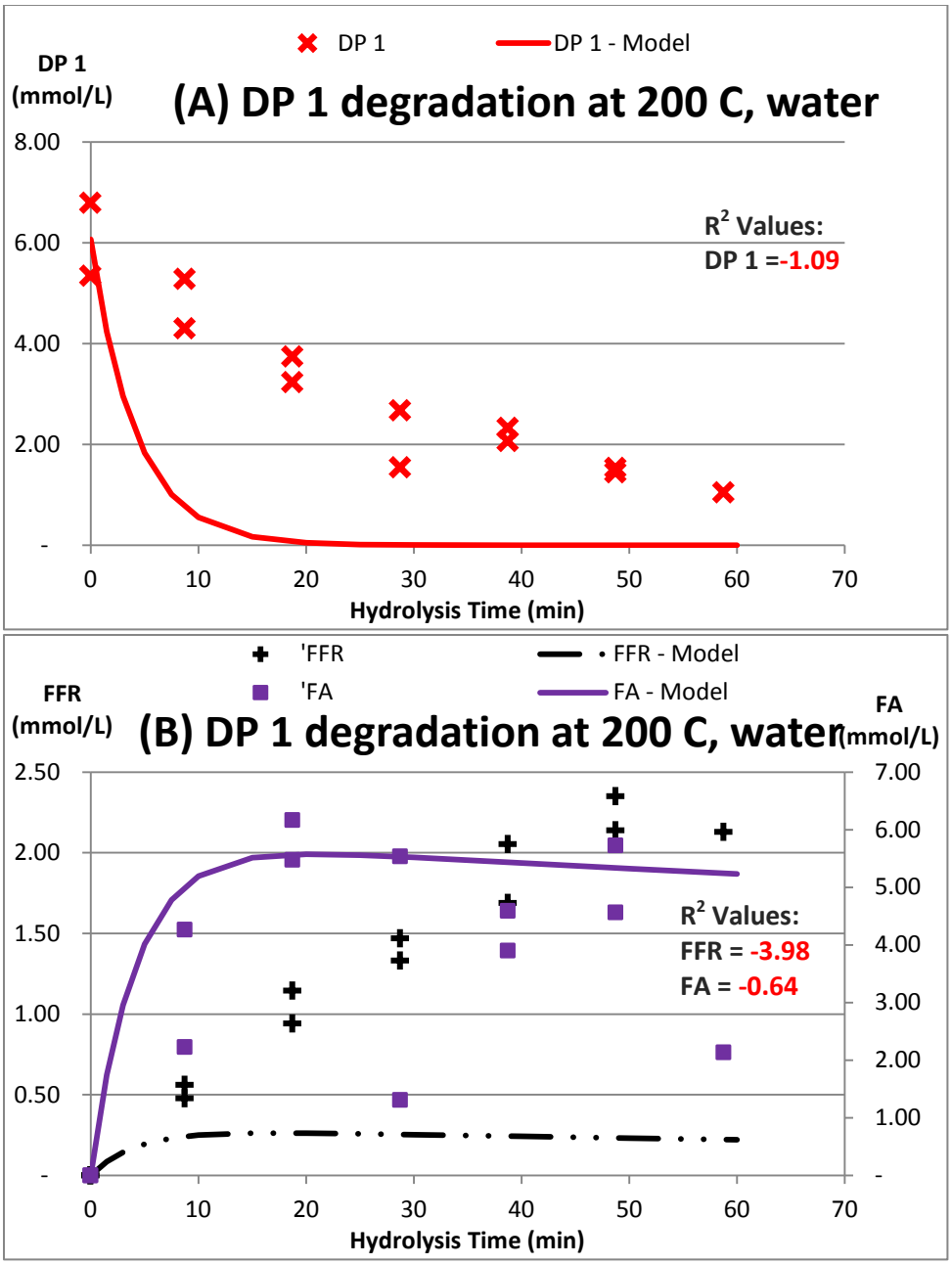

Figure 64: The best-fit model prediction and data of **(A)** DP 1, **(B)** furfural (FFR) and formic acid (FA) for the hydrolysis of DP 1 at 200 ˚C using water.

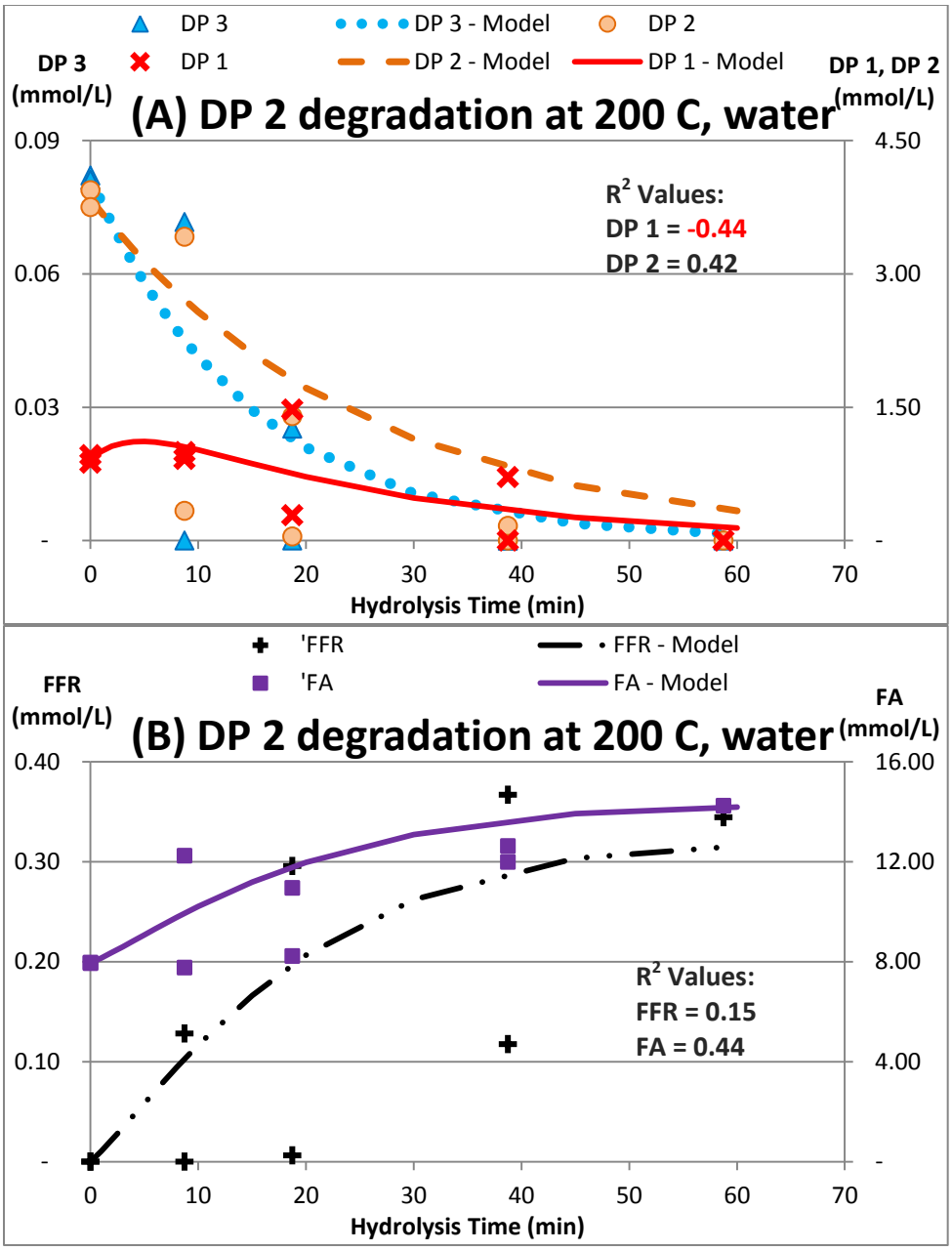

Figure 65: The best-fit model prediction and data of **(A)** DP 2 containing some DP 3 impurities and DP 1, **(B)** furfural (FFR) and formic acid (FA) for the hydrolysis of DP 2 at 200 ˚C using water.

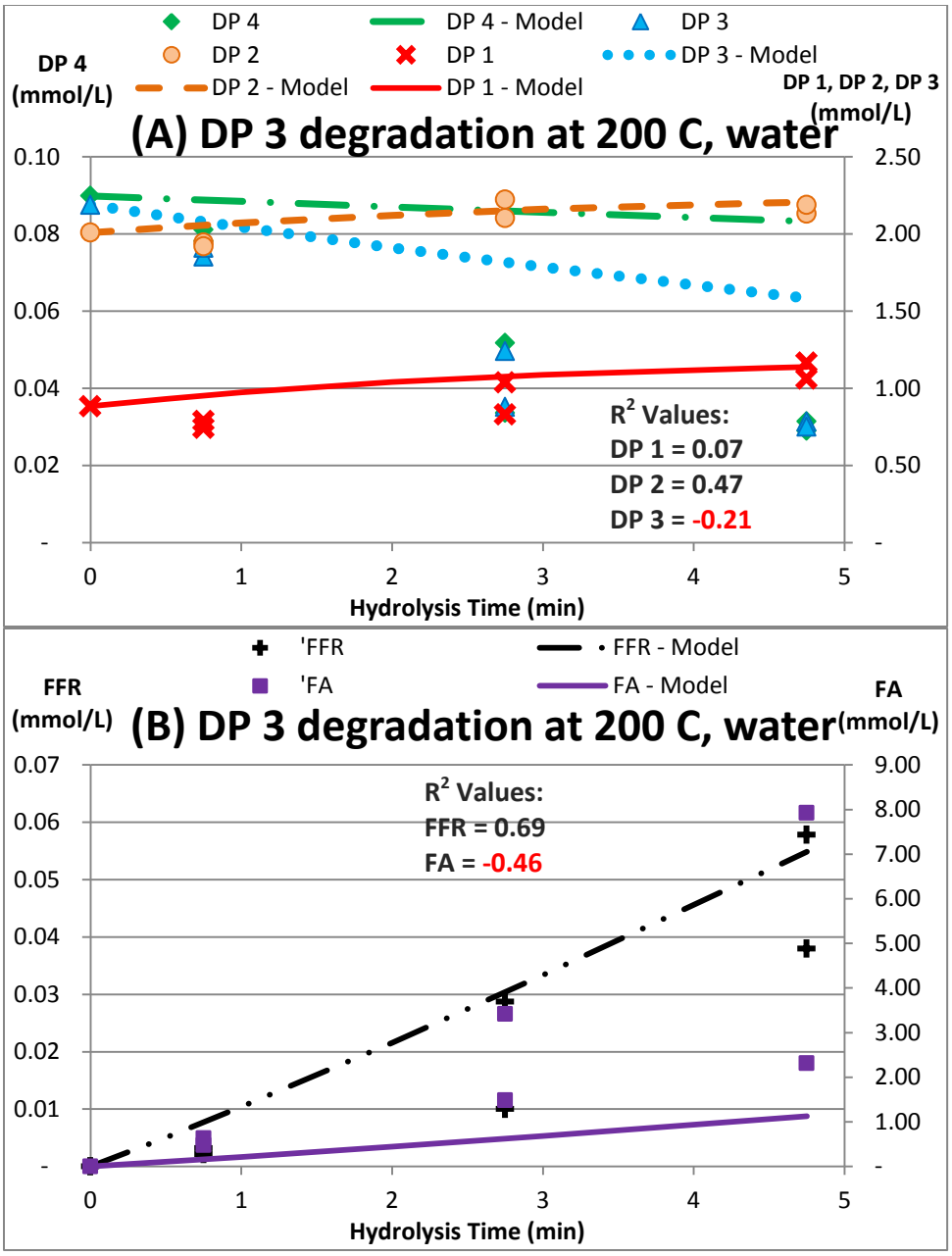

Figure 66: The best-fit model prediction and data of **(A)** DP 3 containing some DP 4 impurities, DP 2, and DP1, **(B)** furfural (FFR) and formic acid (FA) for the hydrolysis of DP 3 at 200 ˚C using water.

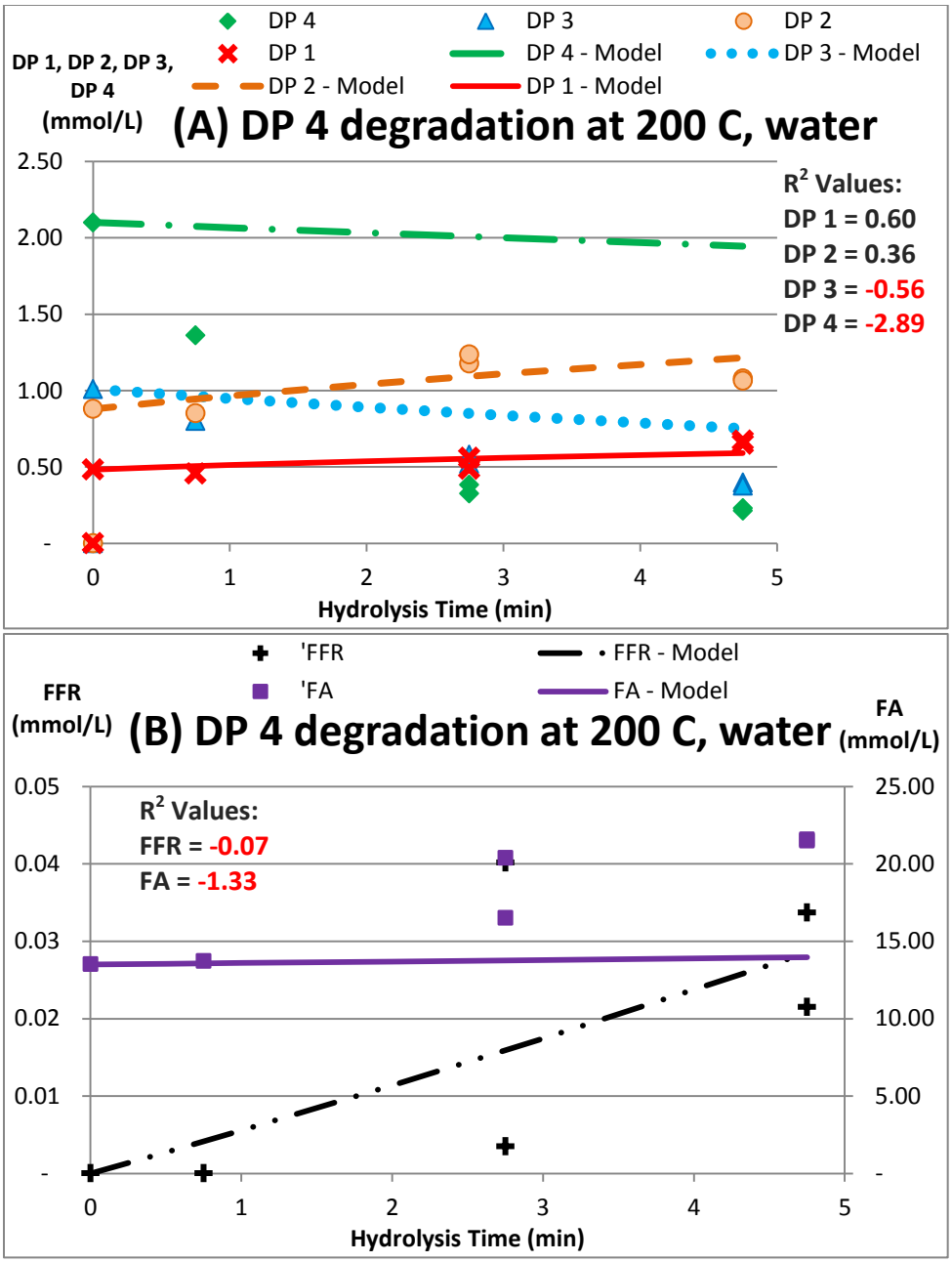

Figure 67: The best-fit model prediction and data of **(A)** DP 4, DP 3, DP2, and DP 1, **(B)** furfural (FFR) and formic acid (FA) for the hydrolysis of DP 4 at 200 ˚C using water.

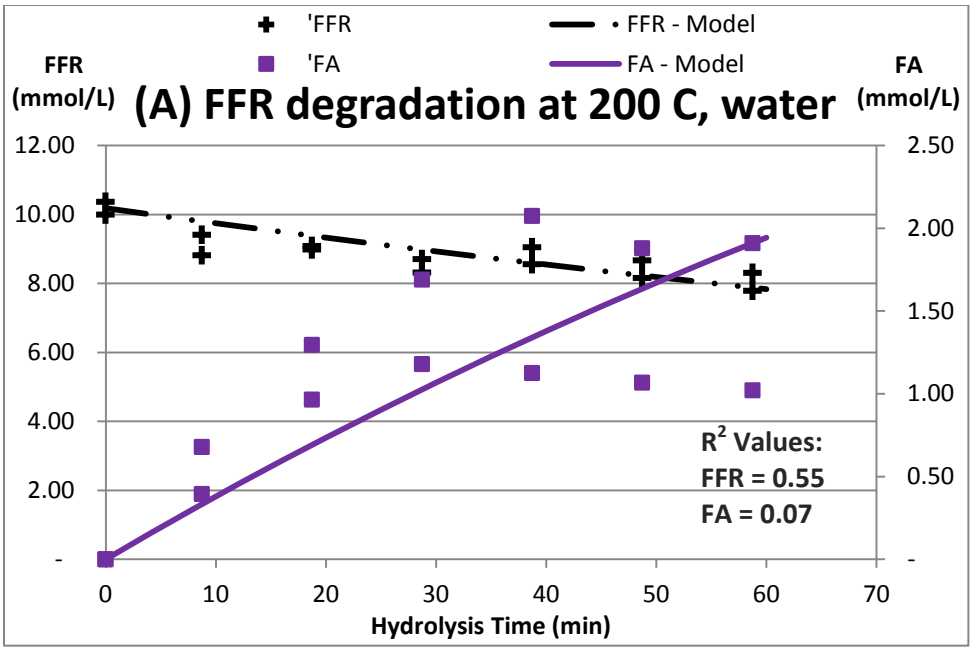

Figure 68: The best-fit model prediction and data of **(A)** furfural (FFR) and formic acid (FA) for the hydrolysis of furfural at 200 ˚C using water.

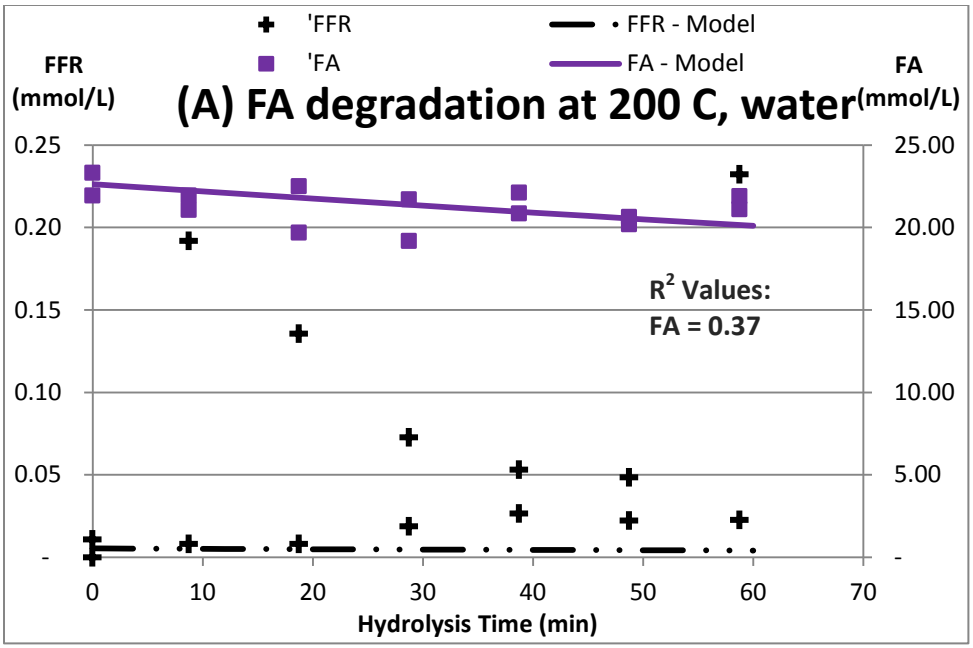

Figure 69: The best-fit model prediction and data of **(A)** formic acid (FA) and furfural (FFR) for the hydrolysis of formic acid at 200 ˚C using water.

Table 21: The R^2 values of the changes of DP 1, DP 2, DP 3, DP 4, formic acid (FA), and furfural (FFR), in mmol/L, as a function of hydrolysis time in 200 ˚C water, as shown **Figures 64- 69**.

	Hydrolysis of DP 1	Hydrolysis of DP 2	Hydrolysis of DP 3	Hydrolysis of DP 4	Hydrolysis of FA	Hydrolysis of FFR
DP 1	(1.09)	(0.44)	0.07	0.60		
DP 2		0.42	0.47	0.36		
DP 3			(0.21)	(0.56)		
DP 4				(2.89)		
FA	(0.64)	0.44	(0.46)	(1.33)	0.37	0.07
FFR	(3.98)	0.15	0.69	(0.07)		0.55

5.5.2.8 Hydrolysis Condition at 200 ˚C Using 0.1 v/v% Sulfuric Acid.

The degradation rate constants for DP 1 (k_1), DP 2 (k_2), DP 3 (k_3), furfural (k_F), and formic acid (k_A), were calculated as 0.0343, 0.2431, 0.4787, 0.0079, and 0.0020 min^{-1}, respectively. The individual formation rate constants k_{31}, k_{21}, k_{1F}, k_{1A}, and k_{FA} were determined to be 0.4787, 0.2431, 0.0234, 0.0109, and 0.0079 min^{-1}, respectively, while the decomposition rate of furfural and formic acid k_{FL} and k_{AL} were determined to be 0.0000 and 0.0020 min^{-1}, respectively. The data and the best-fit model predictions for each compound are presented in **Figures 70 - 74**. The R^2 values of the model fits are presented in **Table 22**.

The model provided a reasonable fit to the experimental data for the concentrations of DP 1, DP 2 and DP 3, except for one instance, as reflected by the R^2 values of 0.52 – 0.98. The model over predicted the degradation rate of DP 1 during the hydrolysis of DP 1, resulted in a R^2 value of only 0.08. Similarly, the concentrations of furfural were fairly represented by the model, as reflected by the R^2 values of 0.30 - 0.96. However, the concentrations of formic acid were not well presented by the model, as shown by the R^2 values of -1.44 to -0.17.

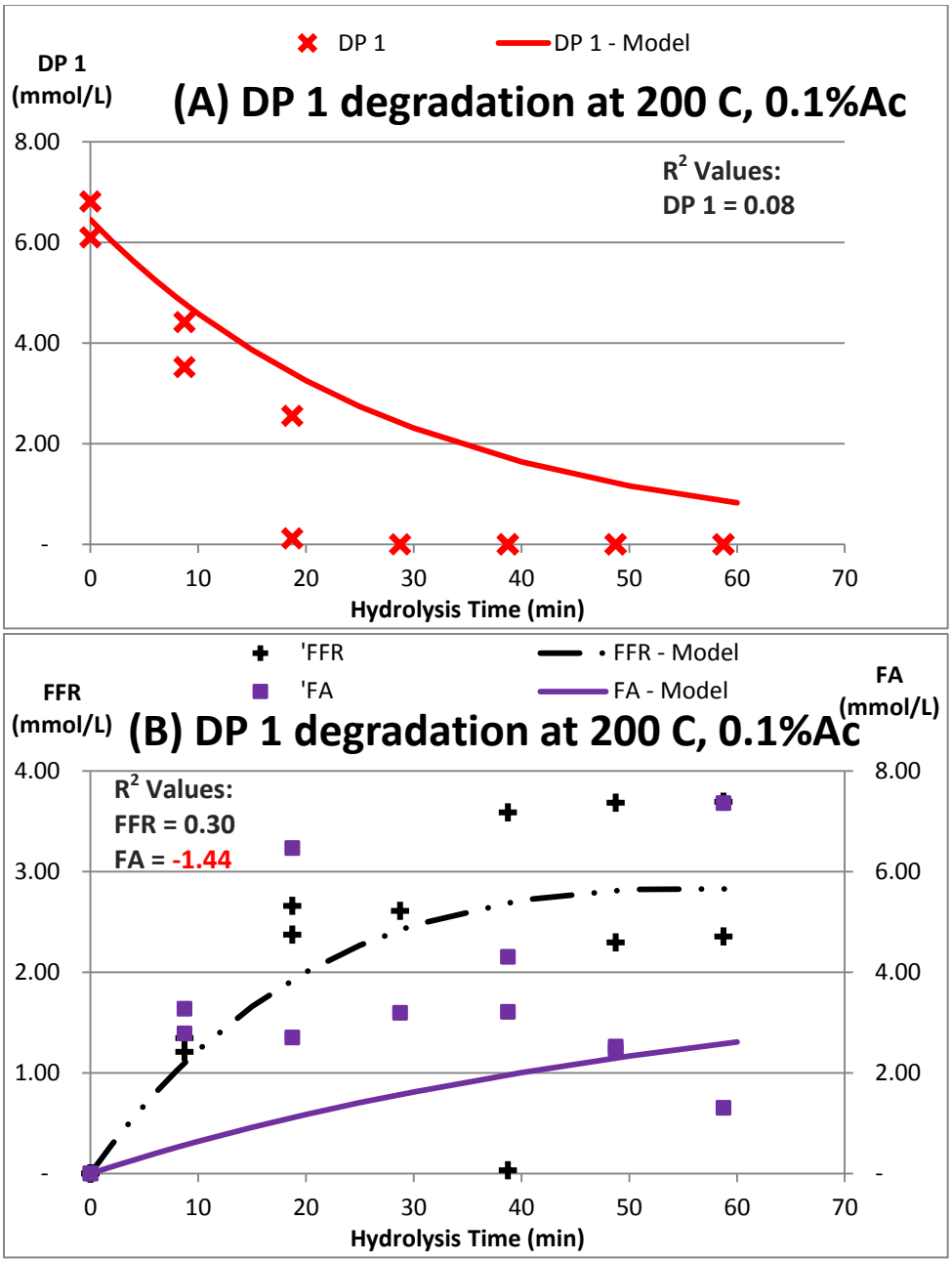

Figure 70: The best-fit model prediction and data of **(A)** DP 1, **(B)** furfural (FFR) and formic acid (FA) for the hydrolysis of DP 1 at 200 ˚C using 0.1 v/v% sulfuric acid.

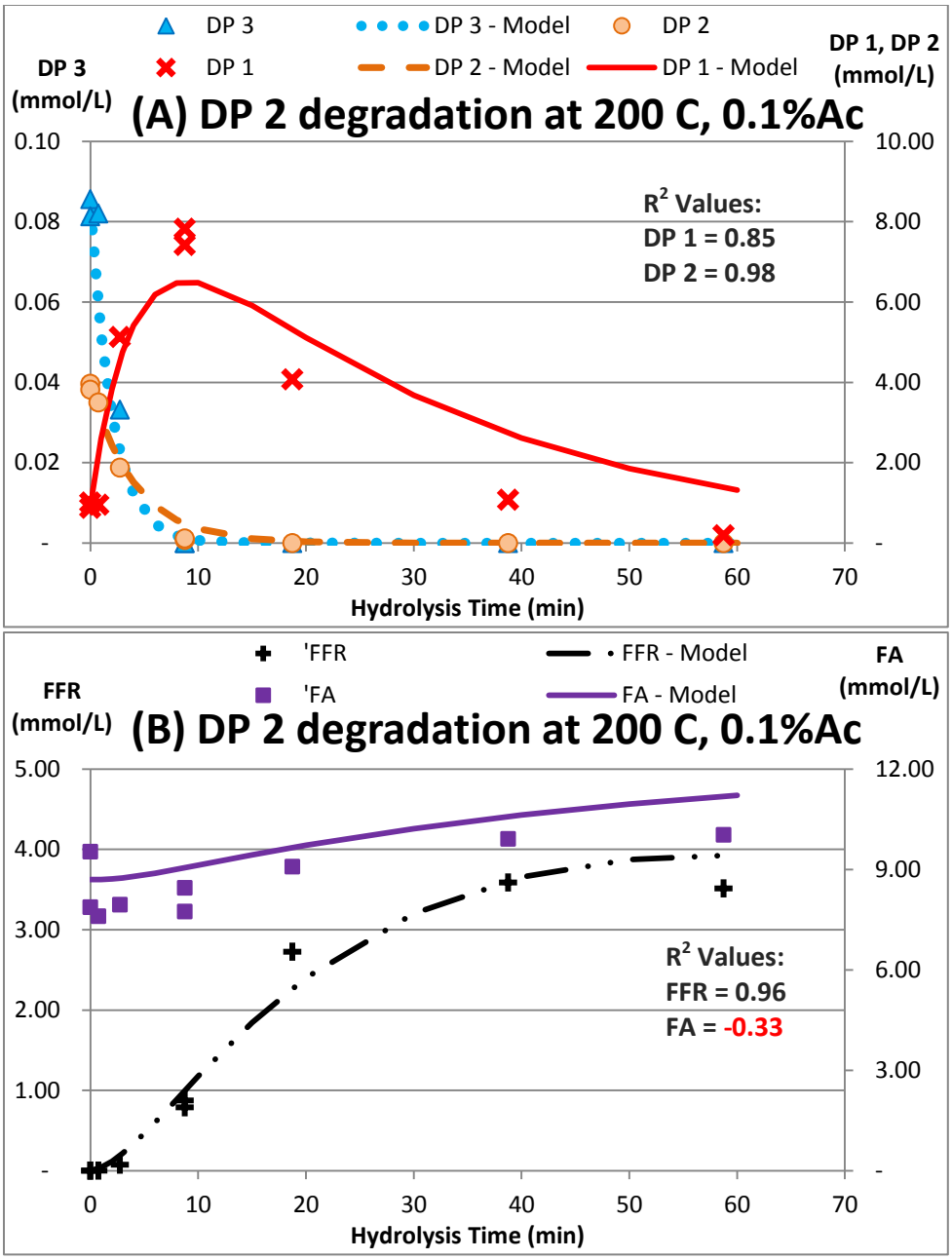

Figure 71: The best-fit model prediction and data of **(A)** DP 2 containing some DP 3 impurities and DP 1, **(B)** furfural (FFR) and formic acid (FA) for the hydrolysis of DP 2 at 200 ˚C using 0.1 v/v% sulfuric acid.

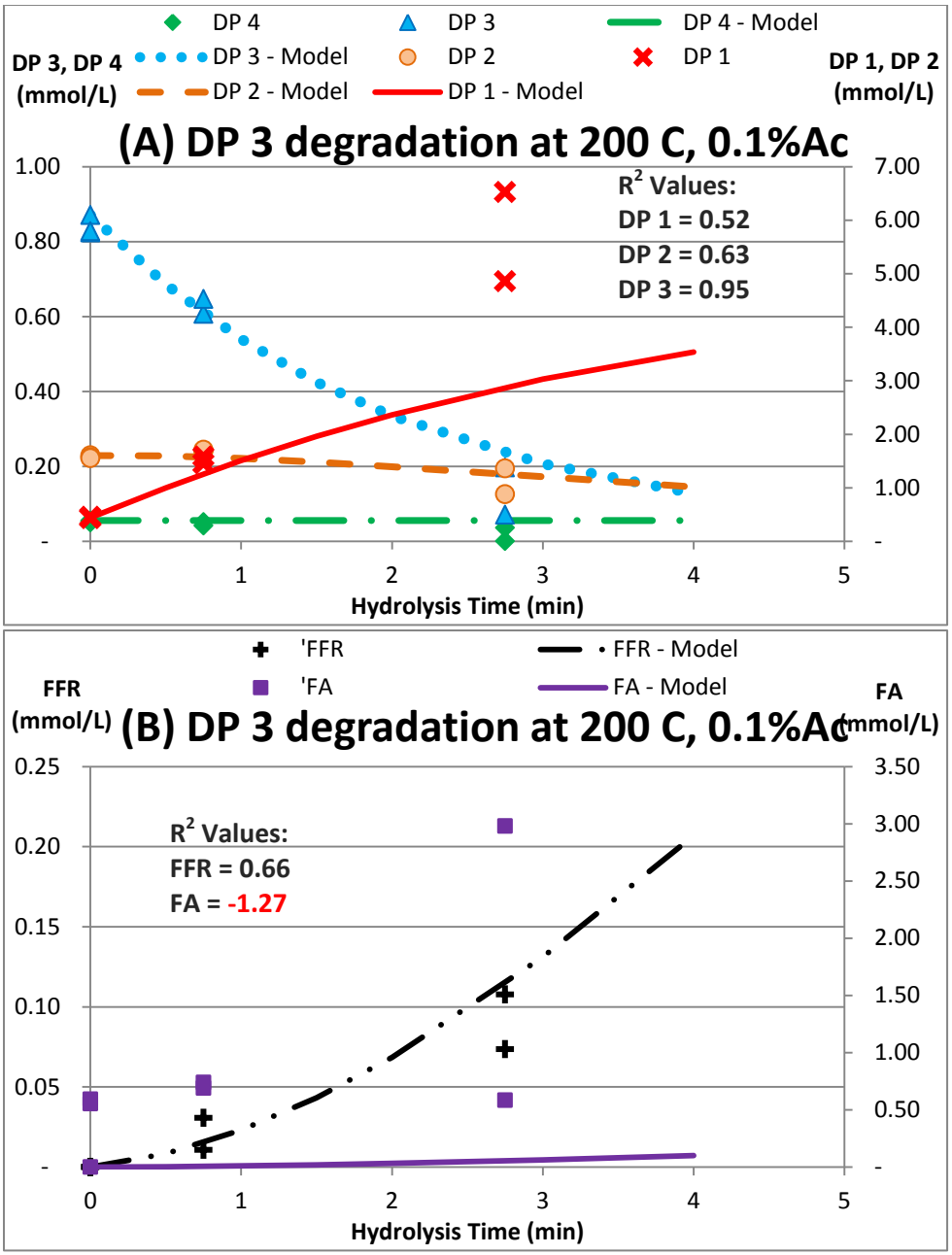

Figure 72: The best-fit model prediction and data of **(A)** DP 3 containing some DP 4 impurities, DP 2, and DP1, **(B)** furfural (FFR) and formic acid (FA) for the hydrolysis of DP 3 at 200 ˚C using 0.1 v/v% sulfuric acid.

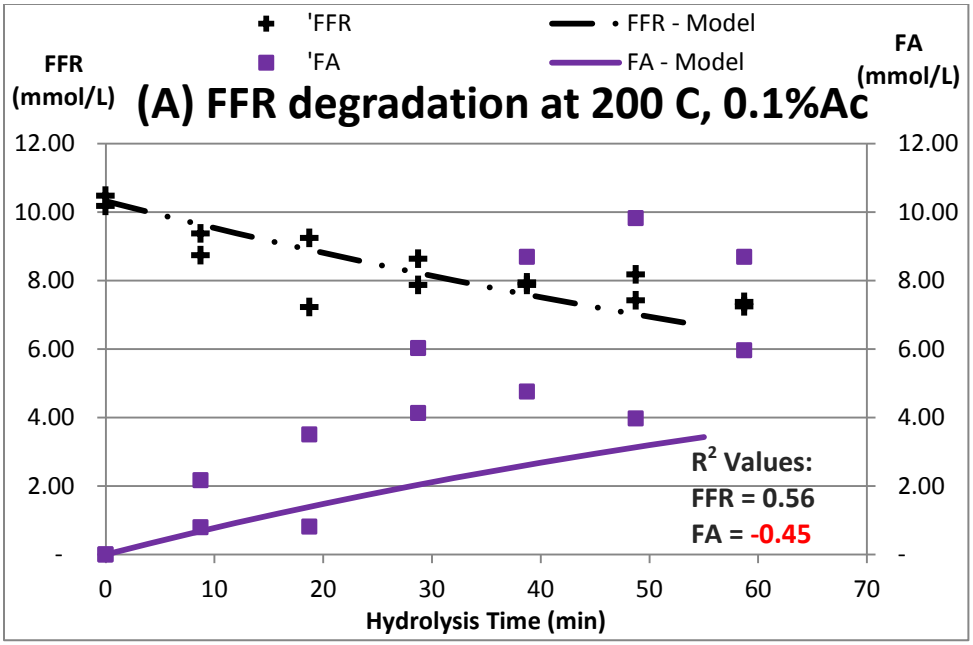

Figure 73: The best-fit model prediction and data of **(A)** furfural (FFR) and formic acid (FA) for the hydrolysis of furfural at 200 ˚C using 0.1 v/v% sulfuric acid.

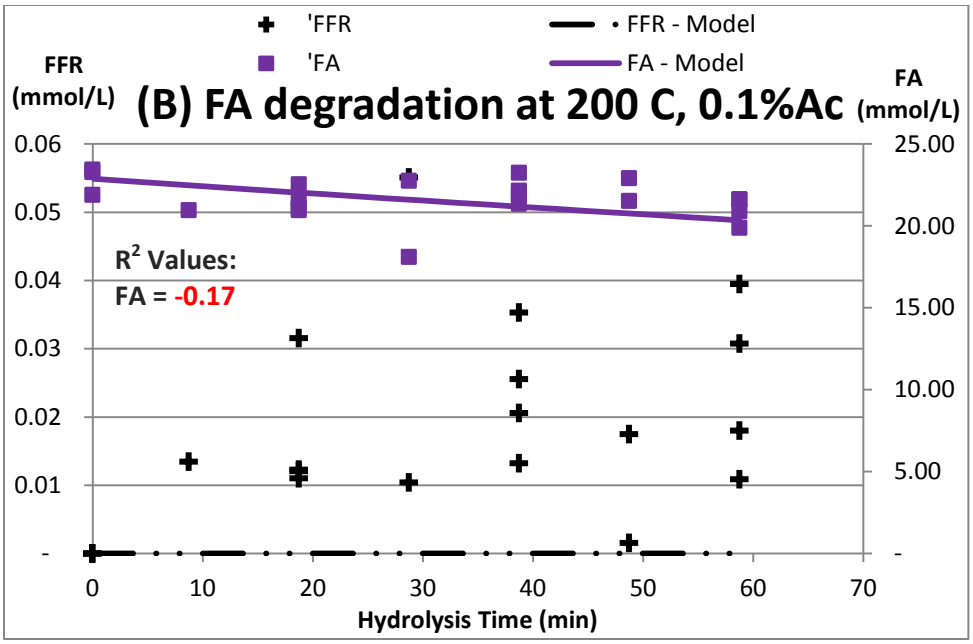

Figure 74: The best-fit model prediction and data of **(A)** formic acid (FA) and furfural (FFR) for the hydrolysis of formic acid at 200 ˚C using 0.1 v/v% sulfuric acid.

Table 22: The R^2 values of the changes of DP 1, DP 2, DP 3, formic acid (FA), and furfural (FFR), in mmol/L, as a function of hydrolysis time in 200 ˚C using 0.1 v/v% sulfuric acid, as shown **Figures 70 - 74**.

	Hydrolysis of DP 1	Hydrolysis of DP 2	Hydrolysis of DP 3	Hydrolysis of FA	Hydrolysis of FFR
DP 1	0.08	0.85	0.52		
DP 2		0.98	0.63		
DP 3			0.95		
FA	(1.44)	(0.33)	(1.27)	(0.17)	(0.45)
FFR	0.30	0.96	0.66		0.56

5.5.2.9 Hydrolysis Condition at 200 ˚C Using 1 v/v% Sulfuric Acid.

The degradation rate constants for DP 1 (k_1), DP 2 (k_2), furfural (k_F), and formic acid (k_A), were calculated as 0.3055, 2.2762, 0.0154, and 0.0021 min^{-1}, respectively. The individual formation rate constants k_{21}, k_{1F}, k_{1A}, and k_{FA} were determined to be 2.2762, 0.1428, 0.1627, and 0.0154 min^{-1}, respectively, while the decomposition rate of furfural and formic acid k_{FL} and k_{AL} were determined to be 0.0000 and 0.0021 min^{-1}, respectively. The data and the best-fit model predictions for each compound are presented in **Figures 75 - 78**. The R^2 values of the model fits are presented in **Table 23**.

The model provided an acceptable fit to the experimental data for the concentrations of DP 1 and DP 2, as reflected by the R^2 values of 0.54 – 0.89. Similarly, the concentrations of furfural and formic acid were reasonably predicted by the model, except for one instance, as shown by the R^2 values of 0.32 – 0.83. However, the concentration of formic acid during the hydrolysis of DP 1 was under predicted, resulting in an R^2 value of -0.28.

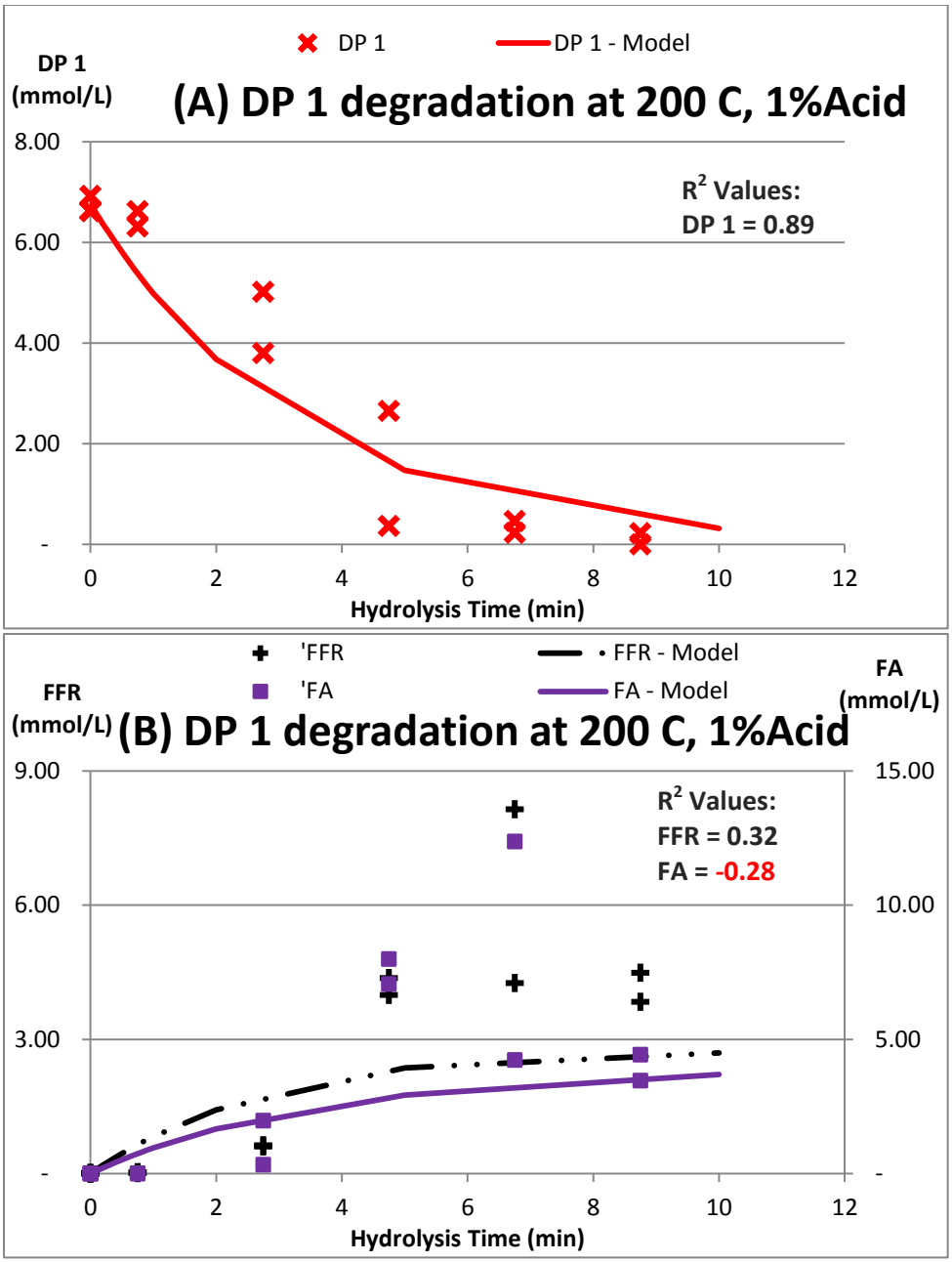

Figure 75: The best-fit model prediction and data of **(A)** DP 1, **(B)** furfural (FFR) and formic acid (FA) for the hydrolysis of DP 1 at 200 ˚C using 1 v/v% sulfuric acid.

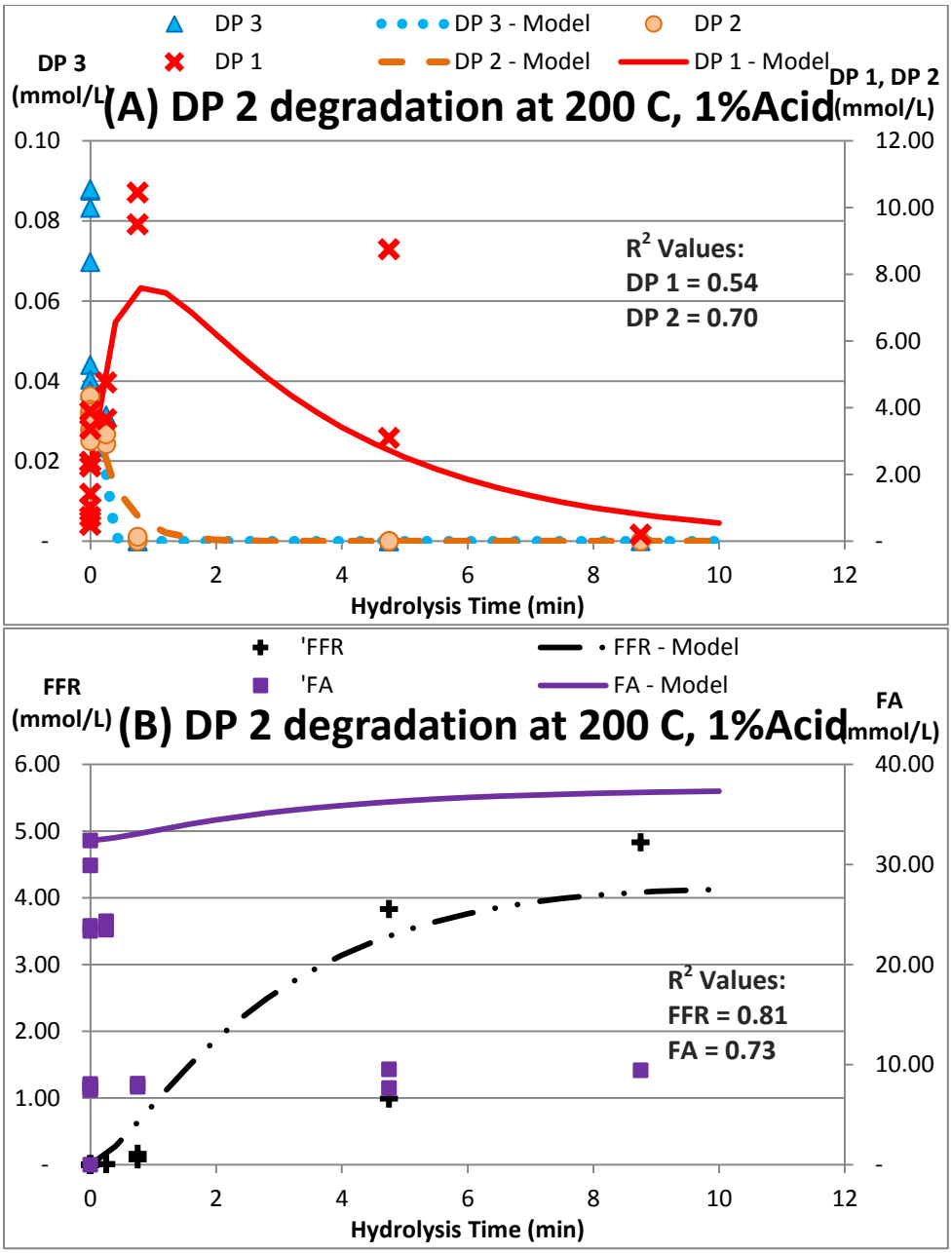

Figure 76: The best-fit model prediction and data of **(A)** DP 2 containing some DP 3 impurities and DP 1, **(B)** furfural (FFR) and formic acid (FA) for the hydrolysis of DP 2 at 200 ˚C using 1 v/v% sulfuric acid.

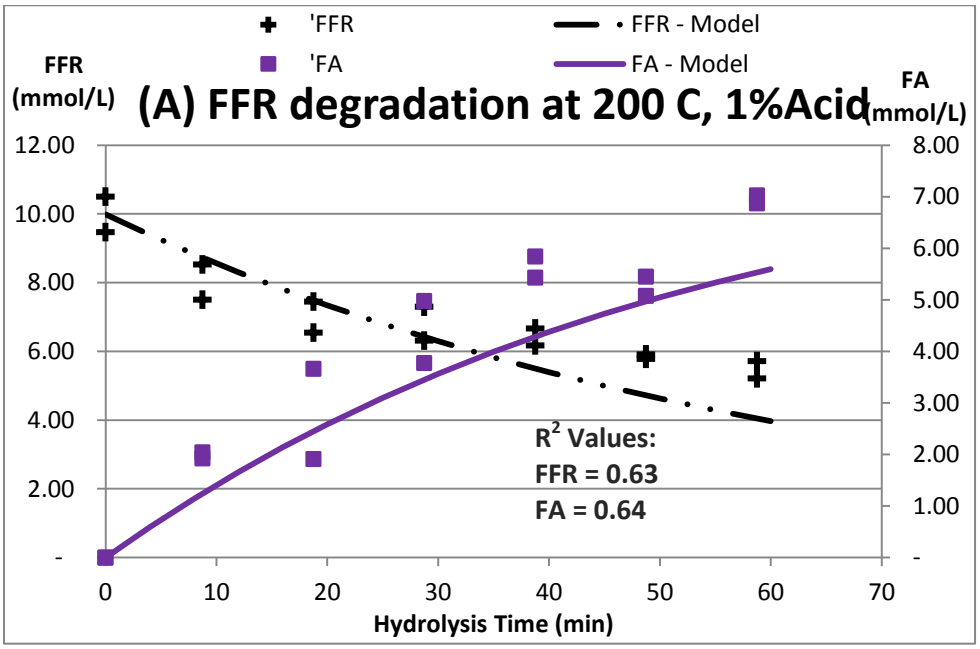

Figure 77: The best-fit model prediction and data of **(A)** furfural (FFR) and formic acid (FA) for the hydrolysis of furfural at 200 ˚C using 1 v/v% sulfuric acid.

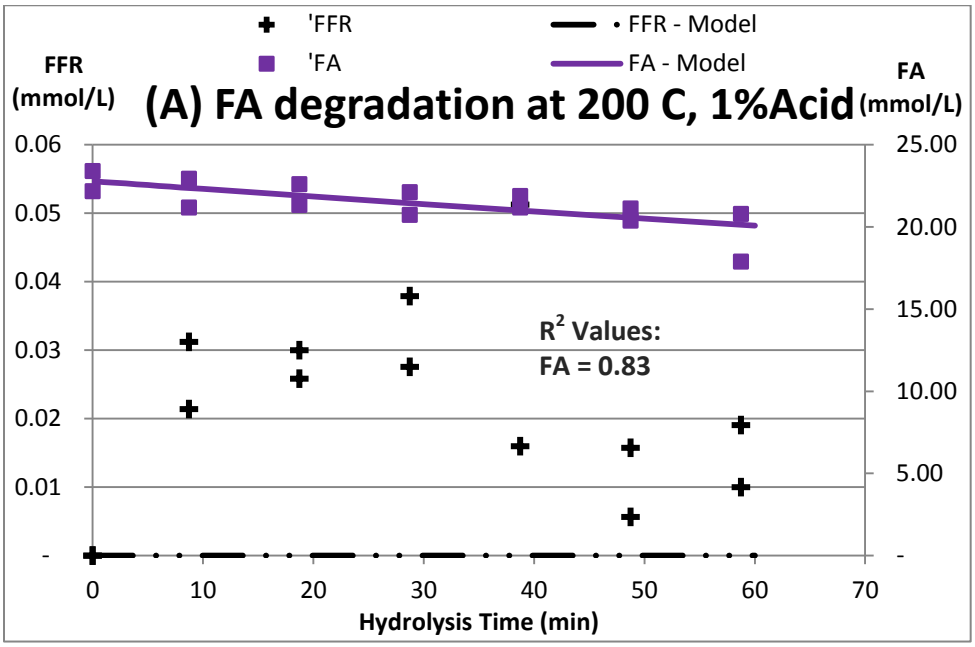

Figure 78: The best-fit model prediction and data of **(A)** formic acid (FA) and furfural (FFR) for the hydrolysis of formic acid at 200 ˚C using 1 v/v% sulfuric acid.

Table 23: The R^2 values of the changes of DP 1, DP 2, formic acid (FA), and furfural (FFR), in mmol/L, as a function of hydrolysis time in 200 ˚C using 1 v/v% sulfuric acid, as shown **Figures 75 - 78**.

	Hydrolysis of DP 1	Hydrolysis of DP 2	Hydrolysis of FA	Hydrolysis of FFR
DP 1	0.89	0.54		
DP 2		0.70		
FA	(0.28)	0.73	0.83	0.64
FFR	0.32	0.81		0.63

5.5.2.10 Inferences from Main Experiments

The best-fit kinetic constants, k_i, according to the proposed model in **Equations 18 - 23** for the entire experimental set are listed in **Table 24**. In general, the model predictions improved as the hydrolysis conditions became more severe, as shown in **Table 14** by the increases of the average R^2 values as the acid concentration increases. At the 120 ˚C hydrolysis condition, the average R^2 values were 0.08, 0.21, and 0.58 for water, 0.1% acid, and 1% acid, respectively. Similarly, the average R^2 values improved from -0.27 to 0.21 at 160 ˚C hydrolysis condition, and from -0.36 to 0.58 at 200 ˚C hydrolysis condition, as the acid concentration increased from 0 to 1%.

At the 120 ˚C hydrolysis condition, the model predicted the concentrations of DP 1 and DP 2 reasonably well, as reflected by the R^2 values of 0.61 – 0.98. However, the prediction for the concentrations of formic acid and furfural were spotty, as in some scenarios resulted in the low R^2 values. At the 160 ˚C hydrolysis condition, the model prediction for DP 1, DP 2, DP 3, and DP 4 was better in 0.1 and 1% acid conditions, as compared to the water condition. The model, in general, did not predict the concentrations of furfural and formic acid well during the 160 ˚C hydrolysis conditions, as evidenced by several scenarios where the R^2 values of less than zero. The model performed poorly in predicting the concentrations of most compounds during the hydrolysis in 200 ˚C water. Therefore, the model prediction has an average R^2 value of -0.36 in 200 ˚C water, the lowest among the nine hydrolysis conditions, as shown in **Table 14**. The model did, however, give a better prediction for the hydrolysis conditions of 0.1 and 1% acid at 200 ˚C, as reflected by the higher average R^2 values in both hydrolysis conditions.

Table 24: The summary of the degradation rate constants obtained in this study. k_1, k_2, k_3, k_4, k_F, k_A are the overall degradation rate constants of DP 1, DP 2, DP 3, DP 4, furfural, and formic acid, respectively, in min^{-1}; and k_{41}, k_{42}, k_{31}, k_{21}, k_{1F}, k_{1A}, k_{FA} are the formation rate constants of DP 1 from DP 4, DP 2 from DP 4, DP 1 from DP 3, DP 1 from DP 2, furfural from DP 1, formic acid from DP 1, and formic acid from furfural, respectively, in min^{-1}.

	120 ˚C, Water	**120 ˚C, 0.1% Acid**	**120 ˚C, 1% Acid**	**160 ˚C, Water**	**160 ˚C, 0.1% Acid**	**160 ˚C, 1% Acid**	**200 ˚C, Water**	**200 ˚C, 0.1% Acid**	**200 ˚C, 1% Acid**
k_1	0.0044	0.0013	0.0019	0.0054	0.0057	0.0363	0.2396	0.0343	0.3055
k_2	0.0003	0.0038	0.2513	0.0030	0.0439	1.0152	0.0414	0.2431	2.2762
k_3				0.0103	0.1048	1.9862	0.0681	0.4787	
k_4				0.0032	0.1049	3.8453	0.0161		
k_F	0.0014	0.0015	0.0026	0.0027	0.0014	0.0040	0.0044	0.0079	0.0154
k_A	0.0013	0.0015	0.0012	0.0004	0.0013	0.0008	0.0020	0.0020	0.0021
k_{41}				0.0001	0.0699	3.8453	0.0026		
k_{42}				0.0031	0.0350	0.0000	0.0136		
k_{31}				0.0103	0.1048	1.9862	0.0681	0.4787	
k_{21}	0.0003	0.0038	0.2513	0.0030	0.0439	1.0152	0.0414	0.2431	2.2762
k_{1F}	0.0001	0.0001	0.0005	0.0014	0.0020	0.0128	0.0112	0.0234	0.1428
k_{1A}	0.0043	0.0012	0.0014	0.0040	0.0037	0.0235	0.2284	0.0109	0.1627
k_{FA}	0.0014	0.0003	0.0025	0.0027	0.0014	0.0040	0.0038	0.0079	0.0154
k_{FL}	0.0000	0.0012	0.0000	0.0000	0.0000	0.0000	0.0005	0.0000	0.0000
k_{AL}	0.0013	0.0015	0.0012	0.0004	0.0013	0.0008	0.0020	0.0020	0.0021

The discrepancy between the predicted data and the experimental data was likely caused by a few factors. First, the CPC fractionated DP 2, DP 3, and DP 4 were not of commercial grade purity. The depolymerization of higher DP oligomers, although present at less than 10% of the total sugar concentration, resulted in higher than the expected concentrations of DP 2, DP 3, and DP 4 during the kinetic study. Equivalently, the presence of glucose and arabinose in birchwood xylan resulted in more furfural and formic acid formation than the alternative of using only xylose as the starting material, albeit xylose was at 93% sugar purity. Secondly, the sand bath reactor used in the kinetic study did not generate uniform heat to all reactor tubes, resulting in heat of various amounts that were transferred to the hydrolysates in the stainless steel tubes. Although replicates were taken for most of the samples, the variation in heat between different days and different reactor tubes from the sand bath reactor resulted in the experimental data behaving less than the ideal first order kinetic. Thirdly, the HPLC calibration of xylose oligomer standards was performed a few months to a year before the actual work was conducted on the kinetic study. Even though all the standards were kept at 4 ˚C (cold room conditions), some degradation occurred, and thus resulted in less accurate quantification of xylose oligomers during the kinetic study. The prohibitively expensive cost of the xylose oligomers, each at about $250 per purchase, prevented the restocking of the samples for the kinetic study. In spite of the factors contributing to the discrepancy between the experimental data and the model, the parameters in the kinetic model were optimized to be representative of the experimental conditions.

The calculated kinetic constants were subsequently used in solving for parameters in the Arrhenius relationship. Also, when comparing to the degradation values obtained from the study by Kumar and Wyman (2008), the results obtained from the current study are within reasonable ranges, as shown in **Table 25**.

Table 25: The comparison of the degradation rate constants obtained from the current study and the degradation rate constants obtained from the study by Kumar and Wyman. Both sets of values are conducted at 160 ˚C using water. All the rate constants are in min^{-1}.

SUMMARY	Current study	Literature[#]
k_1	0.0054	0.0059
k_2	0.0030	0.0121
k_3	0.0103	0.0240
k_4	0.0032	0.0184
k_{21}	0.0030	0.0059
k_{31}	0.0103	0.0180
k_{41}	0.0001	0.0148
k_{42}	0.0031	0.0032

In reference to the study by Kumar and Wyman (2008).

Several observations can be drawn from the experimental data. First, the assumption in the kinetic model of one-way formation of furfural to formic acid was valid. The later assumption was based on the observation that the degradation of furfural produced a higher concentration of formic acid than when formic acid was used as the substrate in the degradation studies. The data showed that in acidic degradation studies using furfural as the substrate at 10 mmol/L, the concentration of formic acid formed from furfural degradation was as high as 7 mmol/L. In water conditions, furfural still degraded to formic acid, but to lower concentrations in the range of 2 mmol/L. On the other hand, in all hydrolysis conditions using 23 mmol/L of formic acid as the starting substrate, furfural formed from formic acid degradation did not exceed 0.06 mmol/L, indicating that the reaction path of formic acid to furfural was not very favorable. Formic acid yield from furfural reached a maximum of 70%, as compared to a maximum yield of 0.3% of furfural from formic acid degradation. Therefore the data supported the assumption that the degradation of furfural to formic acid was irreversible, which greatly reduced the complexity of the model.

Secondly, the degradation data for DP 4 was used to compare the likeliness of the cleaving of end bonds (k_{41}, into DP 1 and DP 3) as compared to that of the middle bonds (k_{42}, into DP 2 and DP 2). The degradation rate of DP 4 to DP 1, k_{41}, was predominant in the presence of sulfuric acid, as supported by the data collected during the hydrolysis at 160 ˚C, 0.1 v/v% acid and 160 ˚C, 1 v/v% acid. At both conditions, the ratio between the hydrolysis rate constants (k_{41} / k_{42}) were 2 and 384,526, respectively, as shown in **Table 26**. On the other hand, the cleavage of middle bonds was faster in the hydrolysis with water, as calculated by the ratio of k_{41} / k_{42} at 160 ˚C, and 200 ˚C water, as 0.03, and 0.19, respectively.

Table 26: Comparison of end cleavage and middle cleavage of the bonds in DP 4 from the current study.

SUMMARY	160 ˚C, water	160 ˚C, 0.1%Acid	160 ˚C, 1% Acid	200 ˚C, water
$k_4 = k_{41} + k_{42}$	0.0032	0.1049	3.8453	0.0161
k_{41}	0.0001	0.0699	3.8453	0.0026
k_{42}	0.0031	0.0350	0.0000	0.0136
k_{41} / k_{42}	0.03	2.00	384,526.79	0.19

The observation was in contrast with the data obtained by Kumar and Wyman (2008) where the ratio between the two degradation rate constants, k_{41} / $k_{42,}$ were 4.63, 3.25, 3.07. 1.27, and 0.41, respectively for pH 7, 4.75, 3.75, 2.75, and pH 1.45, as shown in **Table 27.** The results obtained by Kumar and Wyman (2008) indicate that the middle bond cleavage is preferred in the presence of acid, as the ratio between k_{41} / k_{42} decreased. The discrepancy between this work and that of Kumar and Wyman (2008) could be attributed to two factors: 1) the use of DP 4 in this study contained DP 1, other xylose oligomers and by-products, as compared to the commercial grade DP 4 used in the study by Kumar and Wyman (2008); 2) by-products were monitored in this study, which took into consideration xylose degradation into the by-products. It is important to note that Kumar and Wyman (2008) did not specifically monitor formic acid formation, while the current study did. This implies that the generated model is very sensitive to formic acid mass balance, possibly skewing the degradation rates towards formic acid formation.

Table 27: Comparison of end cleavage and middle cleavage of the bonds in DP 4 from the study by Kumar and Wyman (2008).

SUMMARY	pH 7	pH 4.75	pH 3.75	pH 2.75	pH 1.45
k_{41}	0.0148	0.0166	0.0166	0.0805	1.7800
k_{42}	0.0032	0.0051	0.0054	0.0633	4.3510
k_{41} / k_{42}	4.63	3.25	3.07	1.27	0.41

The ability of the proposed model to predict reasonable trends in the formation of by-product indicated that the assumptions made in this study were valid. In other words, xylose oligomers have to depolymerize into xylose, before further degrading into by-products. The study by Kumar and Wyman (2008) used a general degradation term to represent xylose oligomers degrading into a lumped group of by-products. This general lumped term was created to account for the difference between the formation rate of xylose monomer from the depolymerization of xylose oligomers, and the disappearance rate of xylose oligomers. In the current study, the disappearance of xylose oligomers, DP 2 to DP 4, was accounted by the formation of xylose, while xylose was responsible for the formation of formic acid and furfural. In the current study, a complete mass balance was performed on each reaction step, eliminating the need to create an additional loss term to account for the rate difference, such as that used by Kumar and Wyman (2008).

The results presented in this study demonstrated that the formation of formic acid exceeded that of the predictions of the model. However, stoichiometrically, each mole of formic acid is formed by either one mole of xylose (Dunlop, 1948; Nimlos et al., 2006) or one mole of furfural (Dunlop, 1948). Similarly, one mole of xylose can degrade into one mole of furfural. Therefore, at the beginning of xylose degradation studies, the summation of the total number of moles of xylose, furfural and formic acid, should be at their maximum. As the hydrolysis progresses, more furfural degrades into humin, while formic acid decomposes into carbon dioxide, decreasing the summation of substrate moles. However, the current results indicate that the number of moles of formic acid, furfural and xylose increased after hydrolysis. Formic acid contributed to most of the mole increase, as shown in **Figure 79**.

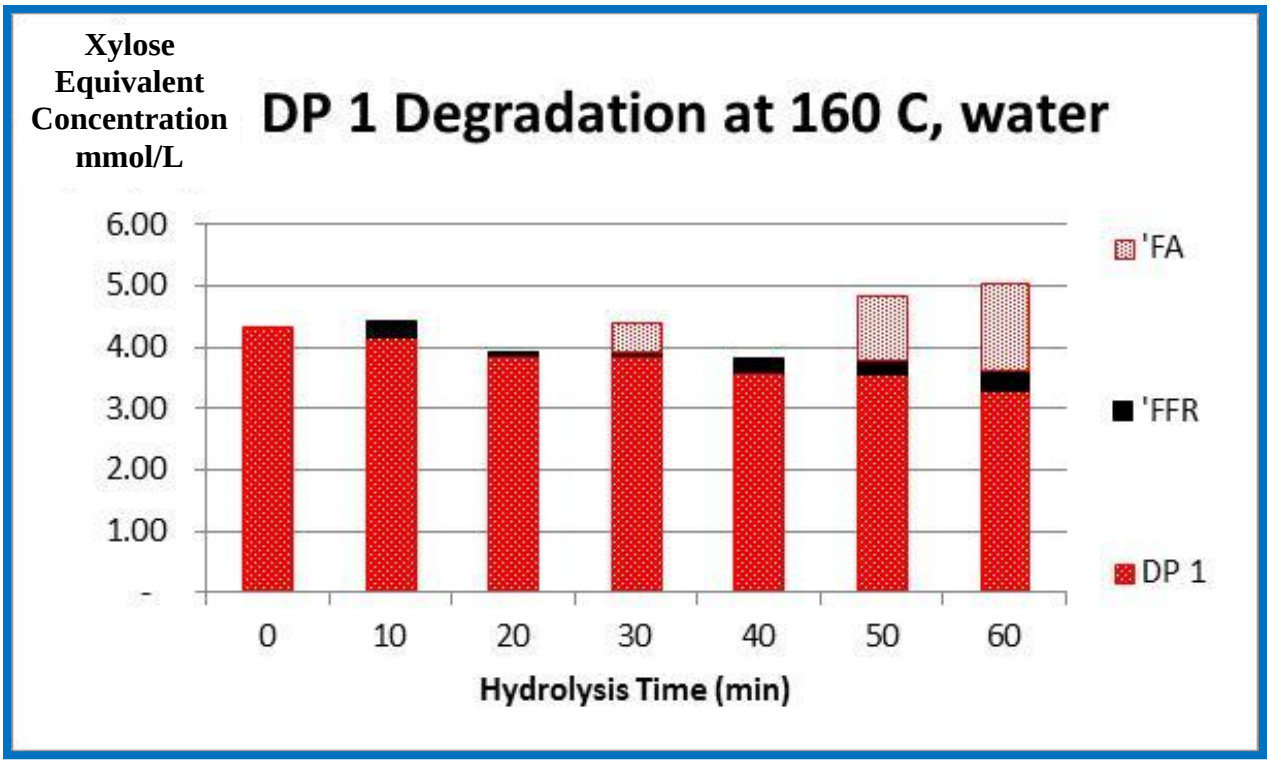

Figure 79: The total mole balance of all the compounds in involving in DP 1 degradation in160 ˚C water. FA, FFR, and DP 1 are the concentrations of formic acid, furfural, and xylose in mmol/L, respectively.

This could be attributed to the volume changes of the hydrolysates. The starting material of commercial grade xylose did not contain xylose oligomers impurities or other monosaccharides, confining the formation of furfural and formic acid solely from xylose.

The use of DP 4 as the starting material in the hydrolysis experiences more moles of xylose equivalents as the hydrolysis progressed. The total xylose equivalent was defined through the stoichiometry relationship, such that 1 mol of DP 2 would be 2 mol of DP 1 equivalent, similarly 1 mol of DP 3 would produce 3 mol equivalent of DP 1. As shown in **Figure 80**, the total number of moles prior to hydrolysis was less than that after 40 min of hydrolysis, indicating an increase of total moles of compounds. Formic acid accounted for most of the discrepancy. Possible changes in hydrolysate volumes could account for the discrepancy.

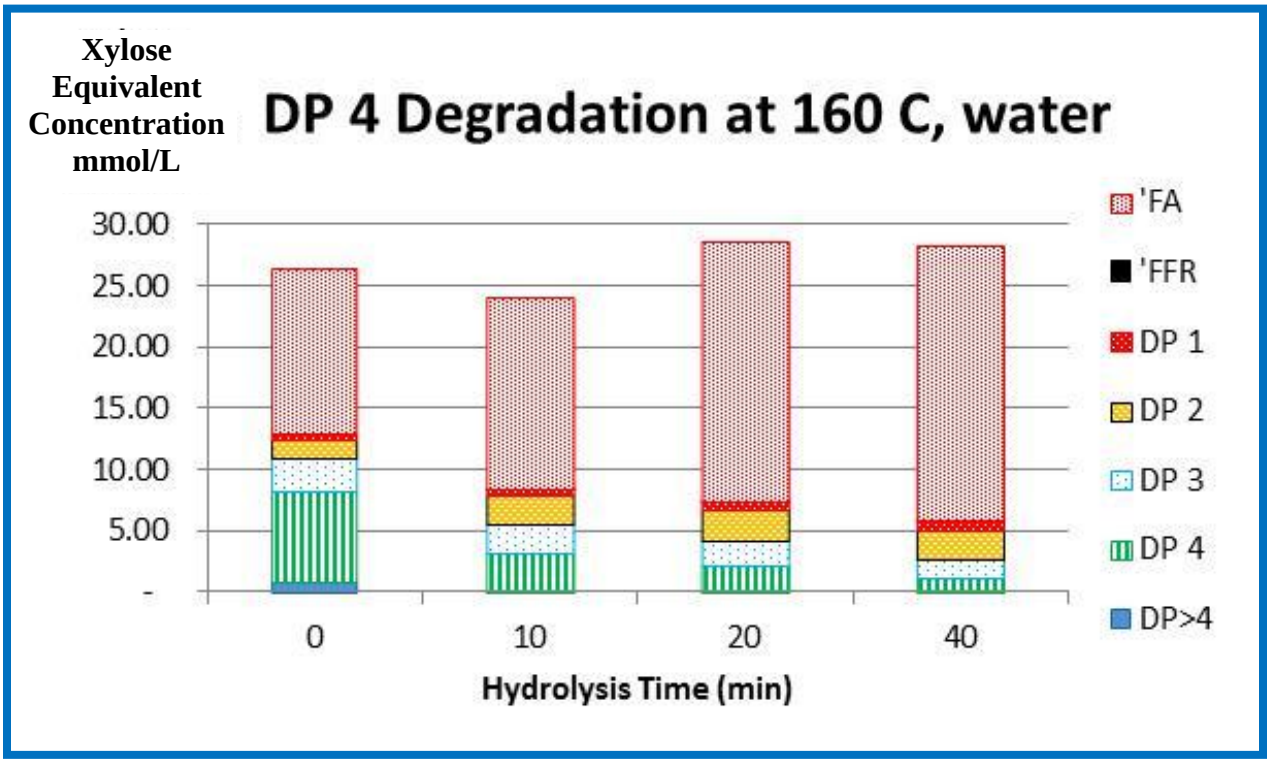

Figure 80: The total mole balance of all the compounds in involving in DP 4 degradation in160 ˚C water. FA, FFR, DP 1, DP 2, DP 3, DP 4, and DP >4 are the concentrations of formic acid, furfural, xylose, xylobiose, xylotriose, xylotetraose, and xylose oligomers greater than DP 4 in mmol/L, respectively.

In terms of xylose degradation, xylose degrades into formic acid at a faster rate, as compared to its degradation into furfural. This can be inferred by inspecting **Table 28**, k_{1A} (the degradation rates of xylose into formic acid) is consistently greater than k_{1F} (the degradation rates of xylose degradation into furfural), indicating a preference in formic acid formation during xylose degradation. The observation was supported by the experimental data, where the concentrations of formic acid were consistently higher than those of furfural during xylose degradation.

Similarly, in terms of furfural degradation, furfural rapidly degrades into formic acid, as opposed to its degradation into humin. This can be inferred by inspecting **Table 29**, where k_{FL} (the degradation rates of furfural into humin) is smaller than k_{FA} (the degradation rates of furfural into formic acid), indicating a preference of formic acid formation. This was true for all hydrolysis conditions, except 120 ˚C at 0.1% acid.

Table 28: The degradation of xylose into furfural and formic acid. The degradation rate constants k_{1F} and k_{1A} are the rate constants of furfural formation, and formic acid formation, respectively, from the degradation of xylose during the hydrolysis.

	120 ˚C, Water	**120 ˚C, 0.1% Acid**	**120 ˚C, 1% Acid**	**160 ˚C, Water**	**160 ˚C, 0.1% Acid**	**160 ˚C, 1% Acid**	**200 ˚C, Water**	**200 ˚C, 0.1% Acid**	**200 ˚C, 1% Acid**
k_{1F}	0.0001	0.0001	0.0005	0.0014	0.0020	0.0128	0.0112	0.0234	0.1428
k_{1A}	0.0043	0.0012	0.0014	0.0040	0.0037	0.0235	0.2284	0.0109	0.1627

Table 29: The degradation of furfural into humin and formic acid. The degradation rate constants k_{FL} and k_{FA} are the rate constants of humin formation, and formic acid formation, respectively, from the degradation of furfural during the hydrolysis.

	120 ˚C, Water	**120 ˚C, 0.1% Acid**	**120 ˚C, 1% Acid**	**160 ˚C, Water**	**160 ˚C, 0.1% Acid**	**160 ˚C, 1% Acid**	**200 ˚C, Water**	**200 ˚C, 0.1% Acid**	**200 ˚C, 1% Acid**
k_{FL}	0.0000	0.0012	0.0000	0.0000	0.0000	0.0000	0.0005	0.0000	0.0000
k_{FA}	0.0014	0.0003	0.0025	0.0027	0.0014	0.0040	0.0038	0.0079	0.0154

5.5.2.11 Arrhenius Equations

The Arrhenius equation was shown in **Equation 24**. The Arrhenius parameters presented in **Table 30** were estimated by best-fitting the kinetic rate constants shown in **Table 24** to solve the Arrhenius equation system. Additionally, the Arrhenius equation corresponding to each compound is summarized in the following equation:

$$k_1 = 6.63 \times 10^9 \times [H^+]^{0.95} \times \exp(-89.97 / RT) \quad \textbf{(29)}$$

$$k_2 = 8.68 \times 10^4 \times [H^+]^{1.02} \times \exp(-37.53 / RT) \quad \textbf{(30)}$$

$$k_3 = 4.34 \times 10^8 \times [H^+]^{1.28} \times \exp(-64.63 / RT) \quad \textbf{(31)}$$

$$k_4 = 4.43 \times 10^7 \times [H^+]^{1.57} \times \exp(-53.01 / RT) \quad \textbf{(32)}$$

$$k_F = 4.26 \times 10^3 \times [H^+]^{0.09} \times \exp(-49.55 / RT) \quad \textbf{(33)}$$

$$k_A = 3.91 \times 10^{-2} \times [H^+]^{0.01} \times \exp(-11.82 / RT) \quad \textbf{(34)}$$

The activation energy (E) of xylose and furfural calculated from the current study were compared to the values obtained from literature. The activation energy of xylose determined from the current study was comparable to the values found in the literature, while the activation energy for furfural degradation was lower than the values in the literature, but within reasonable range, as shown in **Table 31**.

Table 30: The Arrhenius parameters of the degradation of DP 1, DP 2, DP 3, DP 4, furfural, and formic acid. k_0, m, E are the pre-exponential factor, acid concentration exponent, and activation energy, respectively.

SUMMARY	k_0 (min^{-1})	m (unitless)	E (kJ/mol/K)
DP 1	6.63×10^9	0.95	89.97
DP 2	8.68×10^4	1.02	37.53
DP 3	4.34×10^8	1.28	64.63
DP 4	4.43×10^7	1.57	53.01
Furfural	4.26×10^3	0.09	49.55
Formic Acid	3.91×10^{-2}	0.01	11.82

Table 31: The activation energy of xylose and furfural in Arrhenius Equations.

	Feedstock	**Temperature (˚C)**	**Xylose**	**Furfural**
Morinelly et al. (2009)	Switchgrass	150 - 175	89.0	106.0
Esteghlalian et al. (1997)	Switchgrass	140 - 180	99.5	
Jin et al. (2011)	Xylose	90	95.7	
Qi et al. (2008)	Xylose	150 - 200	114.4	
Weingarten et al. (2010)	Furfural	150 - 170	123.9	67.6
Rose et al. (2000)	Furfural	130 - 170		83.6
Current Study	Birchwood xylan	120 - 200	90.0	49.6

5.5.2.12 Recommendations from Arrhenius Data

The degradation of all compounds was affected by acid concentration and temperature, as shown by non-zero values of k_0 and E for all compounds. Xylose monomer and oligomers were particularly sensitive to acid degradation as compared to the by-products, namely formic acid and furfural, as shown by the high m values. Similarly, the degradation of DP 1 was most affected by the elevated temperature, as shown by high E value. Among the six compounds, the degradation of formic acid was least affected by the temperature and acid concentration, as shown by the lowest k_0 and E values.

Using the k values obtained from **Table 24**, the degradation of compounds was presented in **Figure 81**.

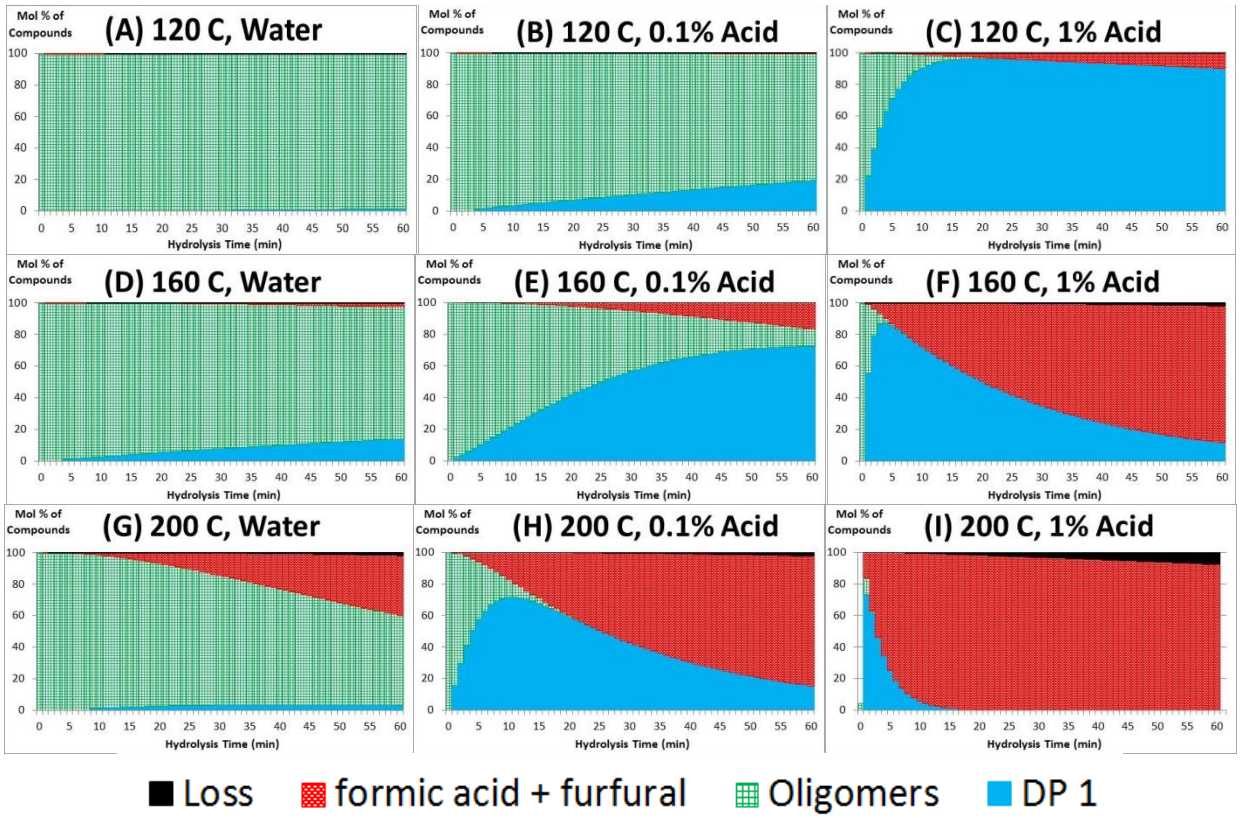

Figure 81: Kinetic model summarizing the molar composition of xylose oligomers during dilute acid hydrolysis at nine different hydrolysis conditions for 60 min. The y-axis is the molar composition of compounds presented in mol of xylose equivalent. The degradation rates obtained from the experiment were used to calculate molar composition, with the initial composition consisting of only xylose oligomers: the hydrolysis conditions **(A)** 120 ˚C water, **(B)** 0.1 v/v% acid at 120 ˚C, **(C)** 1 v/v% acid at 120 ˚C, and **(I)** 1 v/v% acid at 200 ˚C consisting of only DP 2; the hydrolysis conditions **(D)** 160 ˚C water, **(E)** 0.1 v/v% acid at 160 ˚C, **(F)** 1 v/v% acid at 160 ˚C, and **(G)** 200 ˚C water consisting of only DP 4; and the hydrolysis condition **(H)** 0.1 v/v% acid at 200 ˚C consisting of only DP 3.

As shown in **Figure 81**, in the water hydrolysis at all three temperatures conducted in this study, the depolymerization rate of xylose oligomers was not as fast as the degradation rate of DP 1, resulting in little accumulation of DP 1. At low temperature such as in 120 and 160 ˚C water, 98 and 83% moles of xylose equivalent, respectively, of xylose oligomers did not depolymerize completely after 60 min of hydrolysis, and thus both hydrolysis conditions are not favorable for DP 1 accumulation. At high temperature such as in 200 ˚C water, 57% of xylose oligomers remained as xylose oligomers, but the total production of furfural and formic acid were 38% after 60 min of hydrolysis. In all three hydrolysis conditions using water, the maximum accumulation of DP 1 was less than 15% after 60 min of hydrolysis. The addition of sulfuric acid improved the yield of DP 1 during the hydrolysis at 120 ˚C, as shown by 19% and 90% DP 1 after 60 min, in 0.1 and 1 v/v% acid hydrolysis, respectively. However, at elevated temperatures, the addition of sulfuric acid also resulted in the formation of more formic acid and furfural. At 160 ˚C, the hydrolysis using 0.1 and 1 v/v% acid resulted in 16 and 86% of total formic acid and furfural formation, which would create problem to the downstream fermentation process. Similarly, at 200 ˚C, the hydrolysis using 0.1 and 1 v/v% acid resulted in 82 and 92% of total formic acid and furfural formation.

Although the results draw towards the conclusions that the hydrolysis should be at 120 ˚C using 1 v/v% acid because of the highest DP 1 accumulation after 60 min, several precautions are needed when interpreting the results from this study. First, the study was based on low molecular weight xylose oligomers, such as DP 4. The presence of higher molecular weight xylose oligomers and hemicellulose, as the case in the real biomass treatment, could possibly require a longer depolymerization time and more severe hydrolysis conditions to achieve the same degree of hydrolysis as shown in this study. Secondly, the presence of neutralizing

compounds in real biomass could affect the hydrolysate pH, and thus require more acid than was experienced in this study to achieve the same hydrolysis rate. Third, the setup of each hydrolysis apparatus have some intrinsic variations, which must be accounted when comparing the hydrolysis rates between different experimental setup. The current study used fluidized sand bath as the heating medium, which might not produce the same heating rate as in the real biomass treatment, and thus must be carefully compared before adopting the results from this study.

Therefore, this study indicated that an optimum pretreatment condition should not reach 200 ˚C, as at this temperature, the xylose degradation rate is higher than the depolymerization rates of oligomers, resulting in a net loss of xylose.

6.0 Conclusions

Birchwood xylan was used as the starting material to produce xylose oligomers. The hydrolysis of birchwood xylan was conducted in 200 ˚C water for 60 min. The resulting hydrolysate, which contained a variety of xylose oligomers, was fractionated using CPC with the solvent system of butanol: methanol: water at a 5:1:4 volumetric ratio. The CPC was operated in ascending mode, with water-rich lower phase as the stationary phase, and butanol-rich upper phase as the mobile phase. The elution of oligomers using CPC was conducted at 2300 rpm, with 8.8 mL/min flow rate, ELSD as the detector, for a total run time of 200 min. The oligomers in the fractionated CPC were identified and quantified using HPLC and HPAEC-PAD, with the calibration curves setup based on the analysis of the commercial grade xylose oligomers. The identity of fractionated xylose oligomers was also confirmed using MS analysis.

After 10 runs of CPC, 350 mg of DP 2, 150 mg of DP 3, and 100 mg of DP 4, at 91%, 71%, and 49% sugar purity, respectively, were collected. The impurities in the CPC-fractionated oligomers included other xylose oligomers and formic acid. The kinetic study involved the degradation rates of six compounds: DP 1, DP 2, DP 3, DP 4, furfural, and formic acid, at pH 7, pH 1.43 (0.1 v/v% sulfuric acid), and pH 0.43 (1 v/v% sulfuric acid), at temperatures of 120, 160, and 200 ˚C. The initial concentration of all compounds used in the study was 1 mg/mL.

The kinetic model revealed that all compounds can be predicted using first order kinetics. The depolymerization of xylose oligomers resulted in the formation of xylose monomer, while xylose was responsible for the formation of formic acid and furfural. At all hydrolysis conditions, xylose degraded mostly into formic acid, rather than into furfural. In addition, the dissociation of bonds in DP 4 was pH dependent: at low pH (0.43 – 1.43), the end bonds were cleaved faster

resulting in the formation of DP 1 and DP 3; at high pH (7), the middle bonds were cleaved at a faster rates, resulting in the formation of DP 2.

The degradation rates of DP 1 and formic acid were determined to be most influenced by temperature and pH, as reflected by the Arrhenius Equations of the respective compounds. Pretreatment condition was more favorable for maximizing the yield of xylose monomer at the temperatures between 120 and 160 ˚C, at a pH between 0.43 and 7, because of lower degradation rate of DP 1, and higher degradation rates of xylose oligomers, resulting in a net accumulation of DP 1.

7.0 Future Work

This study provided an understanding of the degradation rates of xylose oligomers, and the influence of temperature and pH on the degradation rates. However, because of the limitation in the scale of the experiments, the study contained several weaknesses that can be improved upon in future studies.

First, the purity of xylose oligomers can be further improved. While the presence of lower DP oligomers, monomer, and formic acid should not change the degradation rates of the xylose oligomers, the presence of higher DP oligomers, even in small concentrations, can change the degradation rates of xylose oligomers in a significant manner because of the reaction stoichiometry in which each mole of higher DP oligomer produces several moles of lower DP oligomers. This suggestion can be implemented during the CPC fractionation by lowering the tolerance of higher DP oligomers as impurities rather than using current collection method, which was based on the purity cutoff of each desired compound.

Second, the study of the oligomers bond dissociation would need to include higher DP oligomers. This study used DP 4 to determine the preference of bond cleavage. Although this study exhibited consistent results, a sufficient conclusion cannot be drawn on whether end bonds or middle bonds are preferentially cleaved during acid pretreatment. The inclusion of DP 5 and higher DP oligomers would provide more support to the results obtained from this study.

Third, the presence of formic acid in this study was higher than the anticipated amount based on the reaction stoichiometry. Based on the observation that the formic acid problem occurs in both the degradation of commercial-grade xylose and CPC-fractionated xylose oligomers, although not fully comprehended, the discrepancy was believed to be caused by

experimental error. Future studies should verify if similar results would be obtained to determine the cause of the problem.

Finally, this study uses high purity xylan, although an improvement over previous studies using commercial-grade xylose oligomers, is not representative of the processed biomass. Future studies should include the presence of other sugars, cellulose, and lignin. Based on the results from the current study, the inclusion of other impurities in future studies would determine if the current kinetic model remains valid in a more complicated biomass hydrolysis.

Literature Cited

1. Akiya, N., and Savage, P. E. (1998). Role of water in formic acid decomposition. *AIChE Journal, 44*, 405-415.

2. Antal, M., Leesomboon, T., Mok, W., and Richards, G. (1991). Mechanism of formation of 2-furaldehyde from D-xylose. *Carbohydrate Research, 217*, 71-85.

3. Berthod, A., Friesen, J. B., Inui, T., and Pauli, G. F. (2007). Elution-extrusion countercurrent chromatography: Theory and concepts in metabolic analysis. *Analytical Chemistry, 79*, 3371-3382.

4. Brodeur, G., Yau, E., Badal, K., Collier, J., Ramachandran, K., and Ramakrishnan, S. (2011). Chemical and physicochemical pretreatment of lignocellulosic biomass: A review. *Enzyme Research.* Doi:10.4061/2011/787532.

5. Bruker Corporation. (2004). *MALDI theory mass spectrometry.*

6. Burke, K. J. M., Berry, M. C., and Cooke, M. (1987). Improved method for the determination of sugars using capillary gas chromatography with flame-ionisation and nitrogen-selective detection. *The Analyst, 112*, 1427-1431.

7. Camilleri, P., Tolson, D., and Birrell, H. (1998). Direct structural analysis of 2-aminoacridone derivatized oligosaccharides by high-performance liquid chromatography/mass spectrometric detection. *Rapid Communications in Mass Spectrometry, 12*, 144-148.

8. Cataldi, T. R. I., Angelotti, M., and Bianco, G. (2003). Determination of mono-and disaccharides in milk and milk products by high-performance anion-exchange chromatography with pulsed amperometric detection. *Analytica Chimica Acta, 485*, 43-49.

9. Cataldi, T. R. I., Campa, C., and De Benedetto, G. E. (2000). Carbohydrate analysis by high-performance anion-exchange chromatography with pulsed amperometric detection: The potential is still growing. *Fresenius' Journal of Analytical Chemistry, 368*, 739-758.

10. Chen, S. F., Mowery, R. A., Chambliss, C. K., and van Walsum, G. P. (2007). Pseudo reaction kinetics of organic degradation products in dilute-acid-catalyzed corn stover pretreatment hydrolysates. *Biotechnology and Bioengineering, 98*, 1135-1145.

11. Chum, H. L., Johnson, D. K., and Black, S. K. (1990). Organosolv pretreatment for enzymic hydrolysis of poplars. 2. catalyst effects and the combined severity parameter. *Industrial and Engineering Chemistry Research, 29*, 156-162.

12. Crowell, E. P., and Burnett, B. B. (1967). Determination of the carbohydrate composition of wood pulps by gas chromatography of the alditol acetates. *Analytical Chemistry, 39*, 121-124.

13. Dias, A. S., Pillinger, M., and Valente, A. A. (2005). Dehydration of xylose into furfural over micro-mesoporous sulfonic acid catalysts. *Journal of Catalysis, 229,* 414-423.

14. Dionex Corporation. (2004). Technical note 20: Analysis of carbohydrates by high performance anion exchange chromatography with pulsed amperometric detection (HPAE-PAD). http://www.dionex.com/en-us/webdocs/5023-TN20_LPN032857-04.pdf. Accessed May 2012.

15. Dionex Corporation. (2011). Technical note 110: Carbohydrate determination by HPAE-PAD with disposable au on PTFE working electrodes. http://www.dionex.com/en-us/webdocs/111176-TN110-IC-Carb-HPAEPADdisposAuPTFE-12Oct2011-LPN2952.pdf. Accessed May 2012.

16. DOE (2006). Breaking the biological barriers to cellulosic ethanol: A joint research agenda. http://genomicscience.energy.gov/biofuels/2005workshop/b2blowres63006.pdf. Accessed May 2012.

17. Draper, N. R., and Smith, H. (1998). Applied regression analysis (wiley series in probability and statistics). Wiley-Interscience, third edition.

18. Dunlop, A. (1948). Furfural formation and behavior. *Industrial and Engineering Chemistry, 40,* 204-209.

19. Engelberth, A. S., Carrier, D. J., and Clausen, E. C. (2008). Separation of silymarins from milk thistle (*Silybum marianum* L.) extracted with pressurized hot water using fast centrifugal partition chromatography. *Journal of Liquid Chromatography and Related Technologies, 31,* 3001-3011.

20. Esteghlalian, A., Hashimoto, A. G., Fenske, J. J., and Penner, M. H. (1997). Modeling and optimization of the dilute-sulfuric-acid pretreatment of corn stover, poplar and switchgrass. *Bioresource Technology, 59,* 129-136.

21. Foucault, A. P., and Chevolot, L. (1998). Counter-current chromatography: Instrumentation, solvent selection and some recent applications to natural product purification. *Journal of Chromatography A, 808,* 3-22.

22. Foucault, A., Durand, P., Frias, E. C., and Le Goffic, F. (1993). Biphasic mixture of water, dimethyl sulfoxide, and tetrahydrofuran for use in centrifugal partition chromatography. *Analytical Chemistry, 65,* 2150-2154.

23. Fox, A. (1999). Carbohydrate profiling of bacteria by gas chromatography-mass spectrometry and their trace detection in complex matrices by gas chromatography-tandem mass spectrometry. *Journal of Chromatography A, 843,* 287-300.

24. Hodge, D. B., Karim, M. N., Schell, D. J., and McMillan, J. D. (2008). Soluble and insoluble solids contributions to high-solids enzymatic hydrolysis of lignocellulose. *Bioresource Technology, 99,* 8940-8948.

25. Jensen, J., Morinelly, J., Aglan, A., Mix, A., and Shonnard, D. R. (2008). Kinetic characterization of biomass dilute sulfuric acid hydrolysis: Mixtures of hardwoods, softwood, and switchgrass. *AIChE Journal, 54*, 1637-1645.

26. Jin, Q., Zhang, H., Yan, L., Qu, L., and Huang, H. (2011). Kinetic characterization for hemicellulose hydrolysis of corn stover in a dilute acid cycle spray flow-through reactor at moderate conditions. *Biomass and Bioenergy, 35*, 4158-4164.

27. Johnson, D. C., Dobberpuhl, D., Roberts, R., and Vandeberg, P. (1993). Pulsed amperometric detection of carbohydrates, amines and sulfur species in ion chromatography--the current state of research. *Journal of Chromatography A, 640*, 79-96.

28. Jørgensen, H., Kristensen, J. B., and Felby, C. (2007). Enzymatic conversion of lignocellulose into fermentable sugars: Challenges and opportunities. *Biofuels, Bioproducts and Biorefining, 1*, 119-134.

29. Kim, Y. M., Kreke, T., and Ladisch, M. R. (2012). Reaction mechanisms and kinetics of xylo-oligosaccharide hydrolysis by dicarboxylic acids. *AIChE Journal*. Doi:10.1002/aic.13807.

30. Kumar, P., Barrett, D. M., Delwiche, M. J., and Stroeve, P. (2009). Methods for pretreatment of lignocellulosic biomass for efficient hydrolysis and biofuel production. *Industrial and Engineering Chemistry Research, 48*, 3713-3729.

31. Kumar, R., and Wyman, C. E. (2008). The impact of dilute sulfuric acid on the selectivity of xylooligomer depolymerization to monomers. *Carbohydrate Research, 343*, 290-300.

32. Kumar, R., and Wyman, C. (2009). Effect of enzyme supplementation at moderate cellulase loadings on initial glucose and xylose release from corn stover solids pretreated by leading technologies. *Biotechnology and Bioengineering, 102*, 457-467.

33. Lau, C. S., Bunnell, K. A., Clausen, E. C., Thoma, G. J., Lay, J. O., Gidden, J., Carrier, D. J. (2011). Separation and purification of xylose oligomers using centrifugal partition chromatography. *Journal of Industrial Microbiology and Biotechnology, 38*, 363-370.

34. Levy, D. E., and Fügedi, P. (2006). *The organic chemistry of sugars*, CRC Press.

35. Li, X., Converse, A. O., and Wyman, C. E. (2003). Characterization of molecular weight distribution of oligomers from autocatalyzed batch hydrolysis of xylan. *Applied Biochemistry and Biotechnology, 107*, 515-522.

36. Lloyd, T. A., and Wyman, C. E. (2004). Predicted effects of mineral neutralization and bisulfate formation on hydrogen ion concentration for dilute sulfuric acid pretreatment. *Applied Biochemistry and Biotechnology, 115*, 1013-1022.

37. Lloyd, T. A., and Wyman, C. E. (2005). Combined sugar yields for dilute sulfuric acid pretreatment of corn stover followed by enzymatic hydrolysis of the remaining solids. *Bioresource Technology, 96*, 1967-1977.

38. Marchal, L., Legrand, J., and Foucault, A. (2002). Mass transport and flow regimes in centrifugal partition chromatography. *AIChE Journal, 48*, 1692-1704.

39. Marchal, L., Legrand, J., and Foucault, A. (2003). Centrifugal partition chromatography: A survey of its history, and our recent advances in the field. *The Chemical Record, 3*, 133-143.

40. Marston, A., and Hostettmann, K. (2006). Developments in the application of counter-current chromatography to plant analysis. *Journal of Chromatography A, 1112*, 181-194.

41. Martin, E., Duke, J., Pelkki, M., Clausen, E. C., and Carrier, D. J. (2010). Sweetgum (*Liquidambar styraciflua* L.): Extraction of shikimic acid coupled to dilute acid pretreatment. *Applied Biochemistry and Biotechnology, 162,* 1660–1668.

42. Morinelly, J. E., Jensen, J. R., Browne, M., Co, T. B., and Shonnard, D. R. (2009). Kinetic characterization of xylose monomer and oligomer concentrations during dilute acid pretreatment of lignocellulosic biomass from forests and switchgrass. *Industrial and Engineering Chemistry Research, 48,* 9877-9884.

43. Mosier, N., Hendrickson, R., Ho, N., Sedlak, M., and Ladisch, M. R. (2005). Optimization of pH controlled liquid hot water pretreatment of corn stover. *Bioresource Technology, 96*, 1986-1993.

44. Mosier, N., Wyman, C., Dale, B., Elander, R., Lee, Y., Holtzapple, M., and Ladisch, M. R. (2005). Features of promising technologies for pretreatment of lignocellulosic biomass. *Bioresource Technology, 96*, 673-686.

45. Nabarlatz, D., Farriol, X., and Montané, D. (2004). Kinetic modeling of the autohydrolysis of lignocellulosic biomass for the production of hemicellulose-derived oligosaccharides. *Industrial and Engineering Chemistry Research, 43*, 4124-4131.

46. Nimlos, M. R., Qian, X., Davis, M., Himmel, M. E., and Johnson, D. K. (2006). Energetics of xylose decomposition as determined using quantum mechanics modeling. *The Journal of Physical Chemistry. A, 110*, 11824-11838.

47. Olk, D. C. (2008). Improved analytical techniques for carbohydrates, amino compounds, and phenols: Tools for understanding soil processes. *Soil Science Society of America Journal, 72*, 1672-1682.

48. O'Neill, R., Ahmad, M. N., Vanoye, L., and Aiouache, F. (2009). Kinetics of aqueous phase dehydration of xylose into furfural catalyzed by ZSM-5 zeolite. *Industrial and Engineering Chemistry Research, 48*, 4300-4306.

49. Palmqvist, E., Almeida, J. S., and Hahn-Hägerdal, B. (1999). Influence of furfural on anaerobic glycolytic kinetics of *Saccharomyces cerevisiae* in batch culture. *Biotechnology and Bioengineering, 62*, 447-454.

50. Palmqvist, E., and Hahn-Hägerdal, B. (2000). Fermentation of lignocellulosic hydrolysates. II: Inhibitors and mechanisms of inhibition. *Bioresource Technology, 74*, 25-33.

51. Pedersen, M., and Meyer, A. S. (2010). Lignocellulose pretreatment severity–relating pH to biomatrix opening. *New Biotechnology, 27*, 739-750.

52. Qi, W., Zhang, S. P., Xu, Q. L., Ren, Z. W., Yan, Y. J. (2008). Degradation kinetics of xylose and glucose in hydrolysate containing dilute sulfuric acid. *The Chinese Journal of Process Engineering, 8*, 1132-1137.

53. Qing, Q., and Wyman, C. E. (2011). Hydrolysis of different chain length xylooligomers by cellulase and hemicellulase. *Bioresource Technology, 102*, 1359-1366.

54. Rose, I. C., Epstein, N., and Watkinson, A. P. (2000). Acid-catalyzed 2-furaldehyde (furfural) decomposition kinetics. *Industrial and Engineering Chemistry Research, 39*, 843-845.

55. Saeman, J. F. (1945). Kinetics of wood saccharification - hydrolysis of cellulose and decompositio of sugars in dilute acid at high temperature. *Industrial and Engineering Chemistry, 37*, 43-52.

56. Saha, B. C. (2003). Hemicellulose bioconversion. *Journal of Industrial Microbiology and Biotechnology, 30*, 279-291.

57. Sharara, M. A., Clausen, E. C., and Carrier, D. J. (2012). Chapter 1: An overview of biorefinery technology. In C. Bergeron, D. J. Carrier and S. Ramaswamy (Eds.), *Biorefinery co-products: Phytochemicals, primary metabolites and value-added biomass processing* (pp. 1-18) Wiley.

58. Shibusawa, Y., Yanagida, A., Shindo, H., and Ito, Y. (2003). Separation of apple catechin oligomers by CCC. *Journal of Liquid Chromatography and Related Technologies, 26*, 1609-1621.

59. Shinomiya, K., Kabasawa, Y., and Ito, Y. (1999). Countercurrent chromatographic separation of sugars and their p-nitrophenyl derivatives by cross-axis coil planet centrifuge. *Journal of Liquid Chromatography and Related Technologies, 22*, 579-592.

60. Sluiter, A., Hames, B., Ruiz, R., Scarlata, C., Sluiter, J., and Templeton, D. (2006). Determination of sugars, byproducts, and degradation products in liquid fraction process samples. *Golden, CO: National Renewable Energy Laboratory Analytical Procedure.* http://www.nrel.gov/biomass/pdfs/42623.pdf. Assessed May 2012.

61. Wang-Fan, W., Küsters, E., Mak, C. P., and Wang, Y. (2000). Application of centrifugal counter-current chromatography to the separation of macrolide antibiotic analogues. II. Determination of partition coefficients in comparison with the shake-flask method. *Journal of Liquid Chromatography and Related Technologies, 23*, 1365-1376.

62. Wei, Y., and Ding, M. Y. (2000). Analysis of carbohydrates in drinks by high-performance liquid chromatography with a dynamically modified amino column and evaporative light scattering detection. *Journal of Chromatography A, 904*, 113-117.

63. Weil, J., Brewer, M., Hendrickson, R., Sarikaya, A., and Ladisch, M. R. (1998). Continuous pH monitoring during pretreatment of yellow poplar wood sawdust by pressure cooking in water. *Applied Biochemistry and Biotechnology, 70*, 99-111.

64. Weingarten, R., Cho, J., Conner, W. C., and Huber, G. W. (2010). Kinetics of furfural production by dehydration of xylose in a biphasic reactor with microwave heating. *Green Chemistry, 12*, 1423-1429.

65. Wyman, C. E. (1999). Biomass ethanol: Technical progress, opportunities, and commercial challenges. *Annual Review of Energy and the Environment, 24*, 189-226.

66. Xiang, Q., Lee, Y. Y., and Torget, R. W. (2004). Kinetics of glucose decomposition during dilute-acid hydrolysis of lignocellulosic biomass. *Applied Biochemistry and Biotechnology, 115*, 1127-1138.

67. Ximenes, E., Kim, Y., Mosier, N., Dien, B., and Ladisch, M. (2010). Inhibition of cellulases by phenols. *Enzyme and Microbial Technology, 46*, 170-176.

68. Yang, B., and Wyman, C. E. (2008). Pretreatment: The key to unlocking low-cost cellulosic ethanol. *Biofuels, Bioproducts and Biorefining, 2*, 26-40.

69. Yat, S. C., Berger, A., and Shonnard, D. R. (2008). Kinetic characterization for dilute sulfuric acid hydrolysis of timber varieties and switchgrass. *Bioresource Technology, 99*, 3855-3863.

70. Yu, J., and Savage, P. E. (1998). Decomposition of formic acid under hydrothermal conditions. *Industrial and Engineering Chemistry Research, 37*, 2-10.

Appendices

Appendix 1: The expression of individual compound concentration with respect to the hydrolysis time. The calculation was completed by solving **Equations 12** – **17** manually.

$X_A = (2*k_{FA}*k_{1F}*k_{21}*k_{31}*k_{41}*X_{4O}/(k_3-k_4)/(k_2-k_4)/(k_1-k_4)/(k_F-k_4)/(k_A-k_4))*EXP(-k_4*t)+(2*k_{FA}*k_{21}*k_{31}*k_{1F}*A/(k_2-k_3)/(k_1-k_3)/(k_F-k_3)/(k_A-k_3))*EXP(-k_3*t)+(4*k_{FA}*k_{1F}*k_{21}*k_{42}*X_{4O}/(k_2-k_4)/(k_1-k_4)/(k_F-k_4)/(k_A-k_4))*EXP(-k_4*t)+(2*k_{FA}*k_{1F}*k_{21}*B/(k_1-k_2)/(k_F-k_2)/(k_A-k_2))*EXP(-k_2*t)+(k_{FA}*k_{1F}*k_{31}*k_{41}*X_{4O}/(k_3-k_4)/(k_1-k_4)/(k_F-k_4)/(k_A-k_4))*EXP(-k_4*t)+(A*k_{FA}*k_{1F}*k_{31}/(k_1-k_3)/(k_F-k_3)/(k_A-k_3))*EXP(-k_3*t)+(k_{FA}*k_{1F}*k_{41}*X_{4O}/(k_1-k_4)/(k_F-k_4)/(k_A-k_4))*EXP(-k_4*t)+(k_{FA}*k_{1F}*C/(k_F-k_1)/(k_A-k_1))*EXP(-k_1*t)+(k_{FA}*D/(k_A-k_F))*EXP(-k_F*t)+E*EXP(-k_A*t)+(2*k_{41}*k_{31}*k_{21}*k_{1A}*X_{4O}/(k_3-k_4)/(k_2-k_4)/(k_1-k_4)/(k_A-k_4)*EXP(-k_4*t))+(2*k_{31}*k_{21}*_A*k_{1A}/(k_2-k_3)/(k_1-k_3)/(k_A-k_3)*EXP(-k_3*t))+(4*k_{21}*k_{42}*X_{4O}*k_{1A}/(k_2-k_4)/(k_1-k_4)/(k_A-k_4)*EXP(-k_4*t))+(2*k_{21}*B*k_{1A}/(k_1-k_2)/(k_A-k_2)*EXP(-k_2*t))+(k_{31}*k_{41}*X_{4O}*k_{1A}/(k_3-k_4)/(k_1-k_4)/(k_A-k_4)*EXP(-k_4*t))+(A*k_{31}*k_{1A}/(k_1-k_3)/(k_A-k_3)*EXP(-k_3*t))+(k_{41}*X_{4O}*k_{1A}/(k_1-k_4)/(k_A-k_4)*EXP(-k_4*t))+(C*k_{1A}/(k_A-k_1)*EXP(-k_1*t))$

$X_F = (2*k_{1F}*k_{21}*k_{31}*k_{41}*X_{4O}/(k_3-k_4)/(k_2-k_4)/(k_1-k_4)/(k_F-k_4))*EXP(-k_4*t)+(2*k_{21}*k_{31}*k_{1F}*_A/(k_2-k_3)/(k_1-k_3)/(k_F-k_3))*EXP(-k_3*t)+(4*k_{1F}*k_{21}*k_{42}*X_{4O}/(k_2-k_4)/(k_1-k_4)/(k_F-k_4))*EXP(-k_4*t)+(2*k_{1F}*k_{21}*B/(k_1-k_2)/(k_F-k_2))*EXP(-k_2*t)+(k_{1F}*k_{31}*k_{41}*X_{4O}/(k_3-k_4)/(k_1-k_4)/(k_F-k_4))*EXP(-k_4*t)+(A*k_{1F}*k_{31}/(k_1-k_3)/(k_F-k_3))*EXP(-k_3*t)+(k_{1F}*k_{41}*X_{4O}/(k_1-k_4)/(k_F-k_4))*EXP(-k_4*t)+(k_{1F}*C/(k_F-k_1))*EXP(-k_1*t)+D*EXP(-k_F*t)$

$X_1 = (2*k_{21}*k_{31}*k_{41}*X_{4O}/(k_3-k_4)/(k_2-k_4)/(k_1-k_4))*EXP(-k_4*t)+(2*k_{21}*k_{31}*_A/(k_2-k_3)/(k_1-k_3))*EXP(-k_3*t)+(4*k_{21}*k_{42}*X_{4O}/(k_2-k_4)/(k_1-k_4))*EXP(-k_4*t)+(2*k_{21}*B/(k_1-k_2))*EXP(-k_2*t)+(k_{31}*k_{41}*X_{4O}/(k_3-k_4)/(k_1-k_4))*EXP(-k_4*t)+(A*k_{31}/(k_1-k_3))*EXP(-k_3*t)+(k_{41}*X_{4O}/(k_1-k_4))*EXP(-k_4*t)+C*EXP(-k_1*t)$

$X_2 = (k_{31}*k_{41}*X_{4O}/(k_3-k_4)/(k_2-k_4)*EXP(-k_4*t))+(k_{31}*_A/(k_2-k_3)*EXP(-k_3*t))+(2*k_{42}*X_{4O}/(k_2-k_4)*EXP(-k_4*t))+(B*EXP(-k_2*t))$

$X_3 = k_{41}*X_{4O}/(k_3-k_4)*EXP(-k_4*t)+A*EXP(-k_3*t)$

$X_4 = X_{4O}*EXP(-k_4*t)$

$A = X_{3O}-(k_{41}*X_{4O}/(k_3-k_4))$

$B = X_{2O}-(k_{31}*k_{41}*X_{4O}/(k_3-k_4)/(k_2-k_4))-(k_{31}*_A/(k_2-k_3))-(_2*k_{42}*X_{4O}/(k_2-k_4))$

$$C = X_{1O}-(_2*k_{21}*k_{31}*k_{41}*X_{4O}/(k_3-k_4)/(k_2-k_4)/(k_1-k_4))-(_2*k_{21}*k_{31}*_A/(k_2-k_3)/(k_1-k_3))-(_4*k_{21}*k_{42}*X_{4O}/(k_2-k_4)/(k_1-k_4))-(_2*k_{21}*B/(k_1-k_2))-(k_{31}*k_{41}*X_{4O}/(k_3-k_4)/(k_1-k_4))-(_A*k_{31}/(k_1-k_3))-(k_{41}*X_{4O}/(k_1-k_4))$$

$$D = X_{FO}-(2*k_{1F}*k_{21}*k_{31}*k_{41}*X_{4O}/(k_3-k_4)/(k_2-k_4)/(k_1-k_4)/(k_F-k_4))-(2*k_{31}*k_{21}*k_{1F}*_A/(k_2-k_3)/(k_1-k_3)/(k_F-k_3))-(_4*k_{1F}*k_{21}*k_{42}*X_{4O}/(k_2-k_4)/(k_1-k_4)/(k_F-k_4))-(2*k_{1F}*k_{21}*B/(k_1-k_2)/(k_F-k_2))-(k_{1F}*k_{31}*k_{41}*X_{4O}/(k_3-k_4)/(k_1-k_4)/(k_F-k_4))-(A*k_{1F}*k_{31}/(k_1-k_3)/(k_F-k_3))-(k_{1F}*k_{41}*X_{4O}/(k_1-k_4)/(k_F-k_4))-(k_{1F}*C/(k_F-k_1))$$

$$E = X_{AO}-(2*k_{FA}*k_{1F}*k_{21}*k_{31}*k_{41}*X_{4O}/(k_3-k_4)/(k_2-k_4)/(k_1-k_4)/(k_F-k_4)/(k_A-k_4))-(2*k_{FA}*k_{21}*k_{31}*k_{1F}*_A/(k_2-k_3)/(k_1-k_3)/(k_F-k_3)/(k_A-k_3))-(4*k_{FA}*k_{1F}*k_{21}*k_{42}*X_{4O}/(k_2-k_4)/(k_1-k_4)/(k_F-k_4)/(k_A-k_4))-(2*k_{FA}*k_{1F}*k_{21}*B/(k_1-k_2)/(k_F-k_2)/(k_A-k_2))-(k_{FA}*k_{1F}*k_{31}*k_{41}*X_{4O}/(k_3-k_4)/(k_1-k_4)/(k_F-k_4)/(k_A-k_4))-(A*k_{FA}*k_{1F}*k_{31}/(k_1-k_3)/(k_F-k_3)/(k_A-k_3))-(k_{FA}*k_{1F}*k_{41}*X_{4O}/(k_1-k_4)/(k_F-k_4)/(k_A-k_4))-(k_{FA}*k_{1F}*C/(k_F-k_1)/(k_A-k_1))-(k_{FA}*D/(k_A-k_F))-((2*k_{41}*k_{31}*k_{21}*k_{1A}*X_{4O}/(k_3-k_4)/(k_2-k_4)/(k_1-k_4)/(k_A-k_4)+(2*k_{31}*k_{21}*_A*k_{1A}/(k_2-k_3)/(k_1-k_3)/(k_A-k_3)+(4*k_{21}*k_{42}*X_{4O}*k_{1A}/(k_2-k_4)/(k_1-k_4)/(k_A-k_4))+(2*k_{21}*B*k_{1A}/(k_1-k_2)/(k_A-k_2))+(k_{31}*k_{41}*X_{4O}*k_{1A}/(k_3-k_4)/(k_1-k_4)/(k_A-k_4))+(A*k_{31}*k_{1A}/(k_1-k_3)/(k_A-k_3))+(k_{41}*X_{4O}*k_{1A}/(k_1-k_4)/(k_A-k_4))+(C*k_{1A}/(k_A-k_1)))))$$

Appendix 2: The expression of individual compound concentration with respect to the hydrolysis time. The calculation was completed by solving **Equations 12** – **17** using Matlab software.

Input function:

>> [X_1,X2,X_3,X_4]=dsolve('DX_1=-k_1*X_1+2*k_{21}*X_2+k_{31}*X_3+k_{41}*k_4','X_1(0)=X_{10}', 'DX_2=-k_2*X_2+k_{32}*X_3+2*k_{42}*X_4', 'X_2(0)=X_{20}', 'DX_3=-k_3*X_3+k_{41}*X_4', 'X_3(0)=X_{30}', 'DX_4=-k_4*X_4', 'X_4(0)=X_{40}','t')

Results:

[X_1,X2,X_3,X_4]=dsolve('DX_1=-k_1*X_1+2*k_{21}*X2+k_{31}*X_3+k_{41}*k_4','X_1(0)=X_{10}','DX2=-k_2*X2+k_{32}*X_3+2*k_{42}*X_4','X2(0)=X_{20}','DX_3=-k_3*X_3+k_{41}*X_4','X_3(0)=X_{30}','DX_4=-k_4*X_4','X_4(0)=X_{40}','t')

X_1 = (2*X2*k_{21}*k_3^2*EXP(k_1*t + k_3*t + k_4*t))/(k_1*k_3^2*EXP(k_1*t + k_3*t + k_4*t) - $k_1^{2*}k_3$*EXP(k_1*t + k_3*t + k_4*t) - k_1*k_4^2*EXP(k_1*t + k_3*t + k_4*t) + $k_1^{2*}k_4$*EXP(k_1*t + k_3*t + k_4*t) + k_3*k_4^2*EXP(k_1*t + k_3*t + k_4*t) - $k_3^{2*}k_4$*EXP(k_1*t + k_3*t + k_4*t)) - (k_3*k_4^$_3$*k_{41}*EXP(k_1*t + k_3*t + k_4*t))/(k_1^$_3$*k_3*EXP(k_1*t + k_3*t + k_4*t) - k_1^$_3$*k_4*EXP(k_1*t + k_3*t + k_4*t) - $k_1^{2*}k_3$^2*EXP(k_1*t + k_3*t + k_4*t) + $k_1^{2*}k_4$^2*EXP(k_1*t + k_3*t + k_4*t) - k_1*k_3*k_4^2*EXP(k_1*t + k_3*t + k_4*t) + k_1*$k_3^{2*}k_4$*EXP(k_1*t + k_3*t + k_4*t)) - (k_4^$_3$*k_{41}*EXP(k_1*t + k_3*t + k_4*t))/(k_1*k_3^2*EXP(k_1*t + k_3*t + k_4*t) - $k_1^{2*}k_3$*EXP(k_1*t + k_3*t + k_4*t) - k_1*k_4^2*EXP(k_1*t + k_3*t + k_4*t) + $k_1^{2*}k_4$*EXP(k_1*t + k_3*t + k_4*t) + k_3*k_4^2*EXP(k_1*t + k_3*t + k_4*t) - $k_3^{2*}k_4$*EXP(k_1*t + k_3*t + k_4*t)) - (2*X2*k_{21}*k_4^2*EXP(k_1*t + k_3*t + k_4*t))/(k_1*k_3^2*EXP(k_1*t + k_3*t + k_4*t) - $k_1^{2*}k_3$*EXP(k_1*t + k_3*t + k_4*t) - k_1*k_4^2*EXP(k_1*t + k_3*t + k_4*t) + $k_1^{2*}k_4$*EXP(k_1*t + k_3*t + k_4*t) + k_3*k_4^2*EXP(k_1*t + k_3*t + k_4*t) - $k_3^{2*}k_4$*EXP(k_1*t + k_3*t + k_4*t)) + ($k_3^{2*}k_4^{2*}k_{41}$*EXP(k_1*t + k_3*t + k_4*t))/(k_1^$_3$*k_3*EXP(k_1*t + k_3*t + k_4*t) - k_1^$_3$*k_4*EXP(k_1*t + k_3*t + k_4*t) - $k_1^{2*}k_3$^2*EXP(k_1*t + k_3*t + k_4*t) + $k_1^{2*}k_4$^2*EXP(k_1*t + k_3*t + k_4*t) - k_1*k_3*k_4^2*EXP(k_1*t + k_3*t + k_4*t) + k_1*$k_3^{2*}k_4$*EXP(k_1*t + k_3*t + k_4*t)) + (k_1*$k_4^{2*}k_{41}$*EXP(k_1*t + k_3*t + k_4*t))/(k_1*k_3^2*EXP(k_1*t + k_3*t + k_4*t) - $k_1^{2*}k_3$*EXP(k_1*t + k_3*t + k_4*t) - k_1*k_4^2*EXP(k_1*t + k_3*t + k_4*t) + $k_1^{2*}k_4$*EXP(k_1*t + k_3*t + k_4*t) + k_3*k_4^2*EXP(k_1*t + k_3*t + k_4*t) - $k_3^{2*}k_4$*EXP(k_1*t + k_3*t + k_4*t)) + ($k_3^{2*}k_4$*k_{41}*EXP(k_1*t + k_3*t + k_4*t))/(k_1*k_3^2*EXP(k_1*t + k_3*t + k_4*t) - $k_1^{2*}k_3$*EXP(k_1*t + k_3*t + k_4*t) - k_1*k_4^2*EXP(k_1*t + k_3*t + k_4*t) + $k_1^{2*}k_4$*EXP(k_1*t + k_3*t + k_4*t) + k_3*k_4^2*EXP(k_1*t + k_3*t + k_4*t) - $k_3^{2*}k_4$*EXP(k_1*t + k_3*t + k_4*t)) - (k_1*k_3^2*EXP(k_3*t + k_4*t)*(k_1^$_3$*X_{10} + k_1*$k_4^{2*}k_{41}$ - $k_1^{2*}k_4$*k_{41} - k_3*$k_4^{2*}k_{41}$ - $k_1^{2*}k_3$*X_{10} - $k_1^{2*}k_4$*X_{10} - $k_1^{2*}k_{31}$*X_{30} - 2*X2*$k_1^{2*}k_{21}$ + k_1*k_3*k_4*k_{41} + k_1*k_3*k_4*X_{10} +

$k_1*k_{31}*k_4*X_{30} + k_1*k_{31}*k_{41}*X_{40} + 2*X2*k_1*k_{21}*k_3 + 2*X2*k_1*k_{21}*k_4 - 2*X2*k_{21}*k_3*k_4))/((k_1\text{^}2*k_3 + k_1\text{^}2*k_4 - k_1\text{^}_3 - k_1*k_3*k_4)*(k_1*k_3\text{^}2*EXP(k_1*t + k_3*t + k_4*t) - k_1\text{^}2*k_3*EXP(k_1*t + k_3*t + k_4*t) - k_1*k_4\text{^}2*EXP(k_1*t + k_3*t + k_4*t) + k_1\text{^}2*k_4*EXP(k_1*t + k_3*t + k_4*t) + k_3*k_4\text{^}2*EXP(k_1*t + k_3*t + k_4*t) - k_3\text{^}2*k_4*EXP(k_1*t + k_3*t + k_4*t))) + (k_1\text{^}2*k_3*EXP(k_3*t + k_4*t)*(k_1\text{^}_3*X_{10} + k_1*k_4\text{^}2*k_{41} - k_1\text{^}2*k_4*k_{41} - k_3*k_4\text{^}2*k_{41} - k_1\text{^}2*k_3*X_{10} - k_1\text{^}2*k_4*X_{10} - k_1\text{^}2*k_{31}*X_{30} - 2*X2*k_1\text{^}2*k_{21} + k_1*k_3*k_4*k_{41} + k_1*k_3*k_4*X_{10} + k_1*k_{31}*k_4*X_{30} + k_1*k_{31}*k_{41}*X_{40} + 2*X2*k_1*k_{21}*k_3 + 2*X2*k_1*k_{21}*k_4 - 2*X2*k_{21}*k_3*k_4))/((k_1\text{^}2*k_3 + k_1\text{^}2*k_4 - k_1\text{^}_3 - k_1*k_3*k_4)*(k_1*k_3\text{^}2*EXP(k_1*t + k_3*t + k_4*t) - k_1\text{^}2*k_3*EXP(k_1*t + k_3*t + k_4*t) - k_1*k_4\text{^}2*EXP(k_1*t + k_3*t + k_4*t) + k_1\text{^}2*k_4*EXP(k_1*t + k_3*t + k_4*t) + k_3*k_4\text{^}2*EXP(k_1*t + k_3*t + k_4*t) - k_3\text{^}2*k_4*EXP(k_1*t + k_3*t + k_4*t))) + (k_1*k_4\text{^}2*EXP(k_3*t + k_4*t)*(k_1\text{^}_3*X_{10} + k_1*k_4\text{^}2*k_{41} - k_1\text{^}2*k_4*k_{41} - k_3*k_4\text{^}2*k_{41} - k_1\text{^}2*k_3*X_{10} - k_1\text{^}2*k_4*X_{10} - k_1\text{^}2*k_{31}*X_{30} - 2*X2*k_1\text{^}2*k_{21} + k_1*k_3*k_4*k_{41} + k_1*k_3*k_4*X_{10} + k_1*k_{31}*k_4*X_{30} + k_1*k_{31}*k_{41}*X_{40} + 2*X2*k_1*k_{21}*k_3 + 2*X2*k_1*k_{21}*k_4 - 2*X2*k_{21}*k_3*k_4))/((k_1\text{^}2*k_3 + k_1\text{^}2*k_4 - k_1\text{^}_3 - k_1*k_3*k_4)*(k_1*k_3\text{^}2*EXP(k_1*t + k_3*t + k_4*t) - k_1\text{^}2*k_3*EXP(k_1*t + k_3*t + k_4*t) - k_1*k_4\text{^}2*EXP(k_1*t + k_3*t + k_4*t) + k_1\text{^}2*k_4*EXP(k_1*t + k_3*t + k_4*t) + k_3*k_4\text{^}2*EXP(k_1*t + k_3*t + k_4*t) - k_3\text{^}2*k_4*EXP(k_1*t + k_3*t + k_4*t))) - (k_1\text{^}2*k_4*EXP(k_3*t + k_4*t)*(k_1\text{^}_3*X_{10} + k_1*k_4\text{^}2*k_{41} - k_1\text{^}2*k_4*k_{41} - k_3*k_4\text{^}2*k_{41} - k_1\text{^}2*k_3*X_{10} - k_1\text{^}2*k_4*X_{10} - k_1\text{^}2*k_{31}*X_{30} - 2*X2*k_1\text{^}2*k_{21} + k_1*k_3*k_4*k_{41} + k_1*k_3*k_4*X_{10} + k_1*k_{31}*k_4*X_{30} + k_1*k_{31}*k_{41}*X_{40} + 2*X2*k_1*k_{21}*k_3 + 2*X2*k_1*k_{21}*k_4 - 2*X2*k_{21}*k_3*k_4))/((k_1\text{^}2*k_3 + k_1\text{^}2*k_4 - k_1\text{^}_3 - k_1*k_3*k_4)*(k_1*k_3\text{^}2*EXP(k_1*t + k_3*t + k_4*t) - k_1\text{^}2*k_3*EXP(k_1*t + k_3*t + k_4*t) - k_1*k_4\text{^}2*EXP(k_1*t + k_3*t + k_4*t) + k_1\text{^}2*k_4*EXP(k_1*t + k_3*t + k_4*t) + k_3*k_4\text{^}2*EXP(k_1*t + k_3*t + k_4*t) - k_3\text{^}2*k_4*EXP(k_1*t + k_3*t + k_4*t))) - (k_3*k_4\text{^}2*EXP(k_3*t + k_4*t)*(k_1\text{^}_3*X_{10} + k_1*k_4\text{^}2*k_{41} - k_1\text{^}2*k_4*k_{41} - k_3*k_4\text{^}2*k_{41} - k_1\text{^}2*k_3*X_{10} - k_1\text{^}2*k_4*X_{10} - k_1\text{^}2*k_{31}*X_{30} - 2*X2*k_1\text{^}2*k_{21} + k_1*k_3*k_4*k_{41} + k_1*k_3*k_4*X_{10} + k_1*k_{31}*k_4*X_{30} + k_1*k_{31}*k_{41}*X_{40} + 2*X2*k_1*k_{21}*k_3 + 2*X2*k_1*k_{21}*k_4 - 2*X2*k_{21}*k_3*k_4))/((k_1\text{^}2*k_3 + k_1\text{^}2*k_4 - k_1\text{^}_3 - k_1*k_3*k_4)*(k_1*k_3\text{^}2*EXP(k_1*t + k_3*t + k_4*t) - k_1\text{^}2*k_3*EXP(k_1*t + k_3*t + k_4*t) - k_1*k_4\text{^}2*EXP(k_1*t + k_3*t + k_4*t) + k_1\text{^}2*k_4*EXP(k_1*t + k_3*t + k_4*t) + k_3*k_4\text{^}2*EXP(k_1*t + k_3*t + k_4*t) - k_3\text{^}2*k_4*EXP(k_1*t + k_3*t + k_4*t))) + (k_3\text{^}2*k_4*EXP(k_3*t + k_4*t)*(k_1\text{^}_3*X_{10} + k_1*k_4\text{^}2*k_{41} - k_1\text{^}2*k_4*k_{41} - k_3*k_4\text{^}2*k_{41} - k_1\text{^}2*k_3*X_{10} - k_1\text{^}2*k_4*X_{10} - k_1\text{^}2*k_{31}*X_{30} - 2*X2*k_1\text{^}2*k_{21} + k_1*k_3*k_4*k_{41} + k_1*k_3*k_4*X_{10} + k_1*k_{31}*k_4*X_{30} + k_1*k_{31}*k_{41}*X_{40} + 2*X2*k_1*k_{21}*k_3 + 2*X2*k_1*k_{21}*k_4 - 2*X2*k_{21}*k_3*k_4))/((k_1\text{^}2*k_3 + k_1\text{^}2*k_4 - k_1\text{^}_3 - k_1*k_3*k_4)*(k_1*k_3\text{^}2*EXP(k_1*t + k_3*t + k_4*t) - k_1\text{^}2*k_3*EXP(k_1*t + k_3*t + k_4*t) - k_1*k_4\text{^}2*EXP(k_1*t + k_3*t + k_4*t) + k_1\text{^}2*k_4*EXP(k_1*t + k_3*t + k_4*t) + k_3*k_4\text{^}2*EXP(k_1*t + k_3*t + k_4*t) - k_3\text{^}2*k_4*EXP(k_1*t + k_3*t + k_4*t))) + (k_{31}*k_4\text{^}2*EXP(k_1*t + k_4*t)*(k_4*X_{30} - k_3*X_{30} + k_{41}*X_{40}))/((k_3 - k_4)*(k_1*k_3\text{^}2*EXP(k_1*t + k_3*t + k_4*t) - k_1\text{^}2*k_3*EXP(k_1*t + k_3*t + k_4*t) - k_1*k_4\text{^}2*EXP(k_1*t + k_3*t + k_4*t) + k_1\text{^}2*k_4*EXP(k_1*t + k_3*t + k_4*t) + k_3*k_4\text{^}2*EXP(k_1*t + k_3*t + k_4*t) - k_3\text{^}2*k_4*EXP(k_1*t + k_3*t + k_4*t))) - (k_1*k_{31}*k_{41}*X_{40}*EXP(k_1*t + k_3*t))/(k_1*k_3\text{^}2*EXP(k_1*t + k_3*t + k_4*t) - k_1\text{^}2*k_3*EXP(k_1*t + k_3*t + k_4*t) - k_1*k_4\text{^}2*EXP(k_1*t + k_3*t + k_4*t) + k_1\text{^}2*k_4*EXP(k_1*t + k_3*t + k_4*t) + k_3*k_4\text{^}2*EXP(k_1*t + k_3*t + k_4*t) - k_3\text{^}2*k_4*EXP(k_1*t + k_3*t + k_4*t)) + (k_3*k_{31}*k_{41}*X_{40}*EXP(k_1*t + k_3*t))/(k_1*k_3\text{^}2*EXP(k_1*t +$

k3*t + k4*t) - k1^2*k3*EXP(k1*t + k3*t + k4*t) - k1*k4^2*EXP(k1*t + k3*t + k4*t) + k1^2*k4*EXP(k1*t + k3*t + k4*t) + k3*k4^2*EXP(k1*t + k3*t + k4*t) - k3^2*k4*EXP(k1*t + k3*t + k4*t)) - (2*X2*k21*k3*k4^2*EXP(k1*t + k3*t + k4*t))/(k1^3*k3*EXP(k1*t + k3*t + k4*t) - k1^3*k4*EXP(k1*t + k3*t + k4*t) - k1^2*k3^2*EXP(k1*t + k3*t + k4*t) + k1^2*k4^2*EXP(k1*t + k3*t + k4*t) - k1*k3*k4^2*EXP(k1*t + k3*t + k4*t) + k1*k3^2*k4*EXP(k1*t + k3*t + k4*t)) + (2*X2*k21*k3^2*k4*EXP(k1*t + k3*t + k4*t))/(k1^3*k3*EXP(k1*t + k3*t + k4*t) - k1^3*k4*EXP(k1*t + k3*t + k4*t) - k1^2*k3^2*EXP(k1*t + k3*t + k4*t) + k1^2*k4^2*EXP(k1*t + k3*t + k4*t) - k1*k3*k4^2*EXP(k1*t + k3*t + k4*t) + k1*k3^2*k4*EXP(k1*t + k3*t + k4*t)) - (2*X2*k1*k21*k3*EXP(k1*t + k3*t + k4*t))/(k1*k3^2*EXP(k1*t + k3*t + k4*t) - k1^2*k3*EXP(k1*t + k3*t + k4*t) - k1*k4^2*EXP(k1*t + k3*t + k4*t) + k1^2*k4*EXP(k1*t + k3*t + k4*t) + k3*k4^2*EXP(k1*t + k3*t + k4*t) - k3^2*k4*EXP(k1*t + k3*t + k4*t)) + (2*X2*k1*k21*k4*EXP(k1*t + k3*t + k4*t))/(k1*k3^2*EXP(k1*t + k3*t + k4*t) - k1^2*k3*EXP(k1*t + k3*t + k4*t) - k1*k4^2*EXP(k1*t + k3*t + k4*t) + k1^2*k4*EXP(k1*t + k3*t + k4*t) + k3*k4^2*EXP(k1*t + k3*t + k4*t) - k3^2*k4*EXP(k1*t + k3*t + k4*t)) - (k1*k3*k4*k41*EXP(k1*t + k3*t + k4*t))/(k1*k3^2*EXP(k1*t + k3*t + k4*t) - k1^2*k3*EXP(k1*t + k3*t + k4*t) - k1*k4^2*EXP(k1*t + k3*t + k4*t) + k1^2*k4*EXP(k1*t + k3*t + k4*t) + k3*k4^2*EXP(k1*t + k3*t + k4*t) - k3^2*k4*EXP(k1*t + k3*t + k4*t)) + (k1*k3*k31*EXP(k1*t + k4*t)*(k4*X30 - k3*X30 + k41*X40))/((k3 - k4)*(k1*k3^2*EXP(k1*t + k3*t + k4*t) - k1^2*k3*EXP(k1*t + k3*t + k4*t) - k1*k4^2*EXP(k1*t + k3*t + k4*t) + k1^2*k4*EXP(k1*t + k3*t + k4*t) + k3*k4^2*EXP(k1*t + k3*t + k4*t) - k3^2*k4*EXP(k1*t + k3*t + k4*t))) - (k1*k31*k4*EXP(k1*t + k4*t)*(k4*X30 - k3*X30 + k41*X40))/((k3 - k4)*(k1*k3^2*EXP(k1*t + k3*t + k4*t) - k1^2*k3*EXP(k1*t + k3*t + k4*t) - k1*k4^2*EXP(k1*t + k3*t + k4*t) + k1^2*k4*EXP(k1*t + k3*t + k4*t) + k3*k4^2*EXP(k1*t + k3*t + k4*t) - k3^2*k4*EXP(k1*t + k3*t + k4*t))) - (k3*k31*k4*EXP(k1*t + k4*t)*(k4*X30 - k3*X30 + k41*X40))/((k3 - k4)*(k1*k3^2*EXP(k1*t + k3*t + k4*t) - k1^2*k3*EXP(k1*t + k3*t + k4*t) - k1*k4^2*EXP(k1*t + k3*t + k4*t) + k1^2*k4*EXP(k1*t + k3*t + k4*t) + k3*k4^2*EXP(k1*t + k3*t + k4*t) - k3^2*k4*EXP(k1*t + k3*t + k4*t)))

X2= (2*k3^2*k42*X40*EXP(k2*t + k3*t))/(k2*k3^2*EXP(k2*t + k3*t + k4*t) - k2^2*k3*EXP(k2*t + k3*t + k4*t) - k2*k4^2*EXP(k2*t + k3*t + k4*t) + k2^2*k4*EXP(k2*t + k3*t + k4*t) + k3*k4^2*EXP(k2*t + k3*t + k4*t) - k3^2*k4*EXP(k2*t + k3*t + k4*t)) - (k2*k3^2*EXP(k3*t + k4*t)*(k2^2*X20 - k2*k3*X20 - k2*k4*X20 - k2*k32*X30 + k3*k4*X20 - 2*k2*k42*X40 + k32*k4*X30 + 2*k3*k42*X40 + k32*k41*X40))/((k2*k3 + k2*k4 - k3*k4 - k2^2)*(k2*k3^2*EXP(k2*t + k3*t + k4*t) - k2^2*k3*EXP(k2*t + k3*t + k4*t) - k2*k4^2*EXP(k2*t + k3*t + k4*t) + k2^2*k4*EXP(k2*t + k3*t + k4*t) + k3*k4^2*EXP(k2*t + k3*t + k4*t) - k3^2*k4*EXP(k2*t + k3*t + k4*t))) + (k2^2*k3*EXP(k3*t + k4*t)*(k2^2*X20 - k2*k3*X20 - k2*k4*X20 - k2*k32*X30 + k3*k4*X20 - 2*k2*k42*X40 + k32*k4*X30 + 2*k3*k42*X40 + k32*k41*X40))/((k2*k3 + k2*k4 - k3*k4 - k2^2)*(k2*k3^2*EXP(k2*t + k3*t + k4*t) - k2^2*k3*EXP(k2*t + k3*t + k4*t) - k2*k4^2*EXP(k2*t + k3*t + k4*t) + k2^2*k4*EXP(k2*t + k3*t + k4*t) + k3*k4^2*EXP(k2*t + k3*t + k4*t) - k3^2*k4*EXP(k2*t + k3*t + k4*t))) + (k2*k4^2*EXP(k3*t + k4*t)*(k2^2*X20 - k2*k3*X20 -

$k_2*k_4*X_{20} - k_2*k_{32}*X_{30} + k_3*k_4*X_{20} - 2*k_2*k_{42}*X_{40} + k_{32}*k_4*X_{30} + 2*k_3*k_{42}*X_{40} + k_{32}*k_{41}*X_{40}))/((k_2*k_3 + k_2*k_4 - k_3*k_4 - k_2\wedge 2)*(k_2*k_3\wedge 2*EXP(k_2*t + k_3*t + k_4*t) - k_2\wedge 2*k_3*EXP(k_2*t + k_3*t + k_4*t) - k_2*k_4\wedge 2*EXP(k_2*t + k_3*t + k_4*t) + k_2\wedge 2*k_4*EXP(k_2*t + k_3*t + k_4*t) + k_3*k_4\wedge 2*EXP(k_2*t + k_3*t + k_4*t) - k_3\wedge 2*k_4*EXP(k_2*t + k_3*t + k_4*t))) - (k_2\wedge 2*k_4*EXP(k_3*t + k_4*t)*(k_2\wedge 2*X_{20} - k_2*k_3*X_{20} - k_2*k_4*X_{20} - k_2*k_{32}*X_{30} + k_3*k_4*X_{20} - 2*k_2*k_{42}*X_{40} + k_{32}*k_4*X_{30} + 2*k_3*k_{42}*X_{40} + k_{32}*k_{41}*X_{40}))/((k_2*k_3 + k_2*k_4 - k_3*k_4 - k_2\wedge 2)*(k_2*k_3\wedge 2*EXP(k_2*t + k_3*t + k_4*t) - k_2\wedge 2*k_3*EXP(k_2*t + k_3*t + k_4*t) - k_2*k_4\wedge 2*EXP(k_2*t + k_3*t + k_4*t) + k_2\wedge 2*k_4*EXP(k_2*t + k_3*t + k_4*t) + k_3*k_4\wedge 2*EXP(k_2*t + k_3*t + k_4*t) - k_3\wedge 2*k_4*EXP(k_2*t + k_3*t + k_4*t))) - (k_3*k_4\wedge 2*EXP(k_3*t + k_4*t)*(k_2\wedge 2*X_{20} - k_2*k_3*X_{20} - k_2*k_4*X_{20} - k_2*k_{32}*X_{30} + k_3*k_4*X_{20} - 2*k_2*k_{42}*X_{40} + k_{32}*k_4*X_{30} + 2*k_3*k_{42}*X_{40} + k_{32}*k_{41}*X_{40}))/((k_2*k_3 + k_2*k_4 - k_3*k_4 - k_2\wedge 2)*(k_2*k_3\wedge 2*EXP(k_2*t + k_3*t + k_4*t) - k_2\wedge 2*k_3*EXP(k_2*t + k_3*t + k_4*t) - k_2*k_4\wedge 2*EXP(k_2*t + k_3*t + k_4*t) + k_2\wedge 2*k_4*EXP(k_2*t + k_3*t + k_4*t) + k_3*k_4\wedge 2*EXP(k_2*t + k_3*t + k_4*t) - k_3\wedge 2*k_4*EXP(k_2*t + k_3*t + k_4*t))) + (k_{32}*k_4\wedge 2*EXP(k_2*t + k_4*t)*(k_4*X_{30} - k_3*X_{30} + k_{41}*X_{40}))/((k_3 - k_4)*(k_2*k_3\wedge 2*EXP(k_2*t + k_3*t + k_4*t) - k_2\wedge 2*k_3*EXP(k_2*t + k_3*t + k_4*t) - k_2*k_4\wedge 2*EXP(k_2*t + k_3*t + k_4*t) + k_2\wedge 2*k_4*EXP(k_2*t + k_3*t + k_4*t) + k_3*k_4\wedge 2*EXP(k_2*t + k_3*t + k_4*t) - k_3\wedge 2*k_4*EXP(k_2*t + k_3*t + k_4*t))) - (2*k_2*k_3*k_{42}*X_{40}*EXP(k_2*t + k_3*t))/(k_2*k_3\wedge 2*EXP(k_2*t + k_3*t + k_4*t) - k_2\wedge 2*k_3*EXP(k_2*t + k_3*t + k_4*t) - k_2*k_4\wedge 2*EXP(k_2*t + k_3*t + k_4*t) + k_2\wedge 2*k_4*EXP(k_2*t + k_3*t + k_4*t) + k_3*k_4\wedge 2*EXP(k_2*t + k_3*t + k_4*t) - k_3\wedge 2*k_4*EXP(k_2*t + k_3*t + k_4*t)) - (k_2*k_{32}*k_{41}*X_{40}*EXP(k_2*t + k_3*t))/(k_2*k_3\wedge 2*EXP(k_2*t + k_3*t + k_4*t) - k_2\wedge 2*k_3*EXP(k_2*t + k_3*t + k_4*t) - k_2*k_4\wedge 2*EXP(k_2*t + k_3*t + k_4*t) + k_2\wedge 2*k_4*EXP(k_2*t + k_3*t + k_4*t) + k_3*k_4\wedge 2*EXP(k_2*t + k_3*t + k_4*t) - k_3\wedge 2*k_4*EXP(k_2*t + k_3*t + k_4*t)) + (2*k_2*k_4*k_{42}*X_{40}*EXP(k_2*t + k_3*t))/(k_2*k_3\wedge 2*EXP(k_2*t + k_3*t + k_4*t) - k_2\wedge 2*k_3*EXP(k_2*t + k_3*t + k_4*t) - k_2*k_4\wedge 2*EXP(k_2*t + k_3*t + k_4*t) + k_2\wedge 2*k_4*EXP(k_2*t + k_3*t + k_4*t) + k_3*k_4\wedge 2*EXP(k_2*t + k_3*t + k_4*t) - k_3\wedge 2*k_4*EXP(k_2*t + k_3*t + k_4*t)) + (k_3*k_{32}*k_{41}*X_{40}*EXP(k_2*t + k_3*t))/(k_2*k_3\wedge 2*EXP(k_2*t + k_3*t + k_4*t) - k_2\wedge 2*k_3*EXP(k_2*t + k_3*t + k_4*t) - k_2*k_4\wedge 2*EXP(k_2*t + k_3*t + k_4*t) + k_2\wedge 2*k_4*EXP(k_2*t + k_3*t + k_4*t) + k_3*k_4\wedge 2*EXP(k_2*t + k_3*t + k_4*t) - k_3\wedge 2*k_4*EXP(k_2*t + k_3*t + k_4*t)) - (2*k_3*k_4*k_{42}*X_{40}*EXP(k_2*t + k_3*t))/(k_2*k_3\wedge 2*EXP(k_2*t + k_3*t + k_4*t) - k_2\wedge 2*k_3*EXP(k_2*t + k_3*t + k_4*t) - k_2*k_4\wedge 2*EXP(k_2*t + k_3*t + k_4*t) + k_2\wedge 2*k_4*EXP(k_2*t + k_3*t + k_4*t) + k_3*k_4\wedge 2*EXP(k_2*t + k_3*t + k_4*t) - k_3\wedge 2*k_4*EXP(k_2*t + k_3*t + k_4*t)) + (k_2*k_3*k_{32}*EXP(k_2*t + k_4*t)*(k_4*X_{30} - k_3*X_{30} + k_{41}*X_{40}))/((k_3 - k_4)*(k_2*k_3\wedge 2*EXP(k_2*t + k_3*t + k_4*t) - k_2\wedge 2*k_3*EXP(k_2*t + k_3*t + k_4*t) - k_2*k_4\wedge 2*EXP(k_2*t + k_3*t + k_4*t) + k_2\wedge 2*k_4*EXP(k_2*t + k_3*t + k_4*t) + k_3*k_4\wedge 2*EXP(k_2*t + k_3*t + k_4*t) - k_3\wedge 2*k_4*EXP(k_2*t + k_3*t + k_4*t))) - (k_2*k_{32}*k_4*EXP(k_2*t + k_4*t)*(k_4*X_{30} - k_3*X_{30} + k_{41}*X_{40}))/((k_3 - k_4)*(k_2*k_3\wedge 2*EXP(k_2*t + k_3*t + k_4*t) - k_2\wedge 2*k_3*EXP(k_2*t + k_3*t + k_4*t) - k_2*k_4\wedge 2*EXP(k_2*t + k_3*t + k_4*t) + k_2\wedge 2*k_4*EXP(k_2*t$

$+ k_3*t + k_4*t) + k_3*k_4\text{^}2*EXP(k_2*t + k_3*t + k_4*t) - k_3\text{^}2*k_4*EXP(k_2*t + k_3*t + k_4*t))) - (k_3*k_{32}*k_4*EXP(k_2*t + k_4*t)*(k_4*X_{30} - k_3*X_{30} + k_{41}*X_{40}))/((k_3 - k_4)*(k_2*k_3\text{^}2*EXP(k_2*t + k_3*t + k_4*t) - k_2\text{^}2*k_3*EXP(k_2*t + k_3*t + k_4*t) - k_2*k_4\text{^}2*EXP(k_2*t + k_3*t + k_4*t) + k_2\text{^}2*k_4*EXP(k_2*t + k_3*t + k_4*t) + k_3*k_4\text{^}2*EXP(k_2*t + k_3*t + k_4*t) - k_3\text{^}2*k_4*EXP(k_2*t + k_3*t + k_4*t)))$

$X_3 = (k_{41}*X_{40}*EXP(k_3*t))/(k_3*EXP(k_3*t + k_4*t) - k_4*EXP(k_3*t + k_4*t)) - (k_3*EXP(k_4*t)*(k_4*X_{30} - k_3*X_{30} + k_{41}*X_{40}))/((k_3*EXP(k_3*t + k_4*t) - k_4*EXP(k_3*t + k_4*t))*(k_3 - k_4)) + (k_4*EXP(k_4*t)*(k_4*X_{30} - k_3*X_{30} + k_{41}*X_{40}))/((k_3*EXP(k_3*t + k_4*t) - k_4*EXP(k_3*t + k_4*t))*(k_3 - k_4))$

$X_4 = X_{40}/EXP(k_4*t)$

Appendix 3: The effect of concentration on the degradation rates of xylose (DP 1).

Theory (Drapper and Smith, 1998):

F-Test on the model of 1 g/L vs. 2 g/L.

For 2 g/L model: $Y = \beta_0 + \beta_1 X$

For 1 g/L model: $Y = \alpha_0 + \alpha_1 X$

Combined model: $Y = \delta_0 * Z + \beta_0 + \delta_1 * X * Z + \beta_1 * X$

where $\delta_0 = \alpha_0 - \beta_0$

$\delta_1 = \alpha_1 - \beta_1$

Z = 0 for 1 g/L data; Z = 1 for 2 g/L data.

Hypothesis test:

Null hypothesis: $\delta_0 = \delta_1 = 0$

Full regression model = $[\beta_0, \beta_1 , \delta_0 , \delta_1]$

Reduced regression model = $[\beta_0, \beta_1]$

$$F = \frac{(SSReg, Full – SSReg, Red)/2}{(SSRes, Full) / (n-4)}$$

where SSReg, Full, SSReg, Red, and SSRes, Full are the sum of the squares of the regression of the full model, the sum of the squares of the regression of the reduced model, and the sum of the squares of the residual of the full model, respectively.

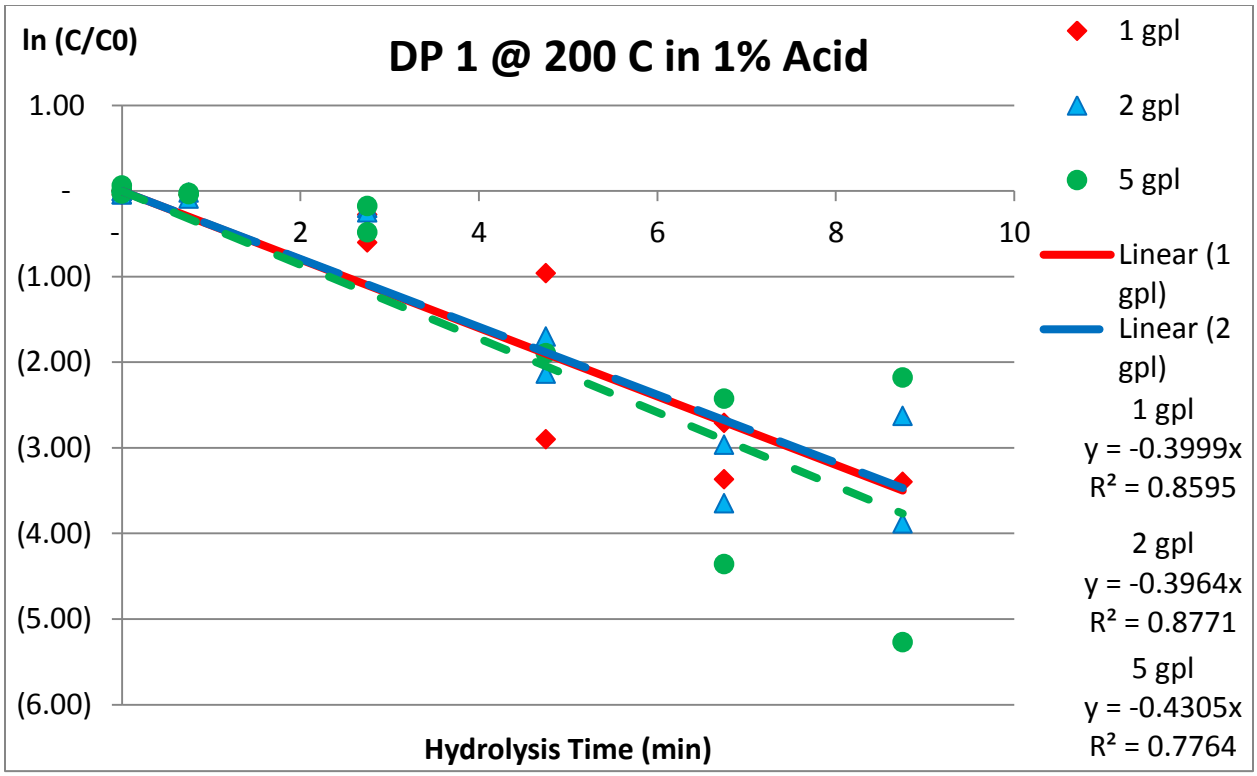

Hydrolysis Time (min)	ln (C/C$_0$)		
	1 gpl	2 gpl	5 gpl
0	-	-	-
1	0.00	(0.04)	(0.03)
2	(0.05)	(0.09)	(0.04)
4	(0.28)	(0.20)	(0.48)
6	(2.90)	(2.13)	-
8	(3.37)	(2.96)	(4.36)
10	(3.40)	(2.63)	(5.27)
0	-	-	-
6	(0.96)	(1.70)	(1.90)
8	(2.71)	(3.65)	(2.43)
10	-	(3.88)	(2.18)
1	(0.04)	(0.04)	0.06
2	(0.04)	(0.02)	(0.02)
4	(0.60)	(0.25)	(0.17)

Data for 1 vs. 2 gpL

Data	X	Z	X*Z	Y = ln (C/C_0)
1 gpL	0	0	0	-
	1	0	0	0.00
	2	0	0	(0.05)
	4	0	0	(0.28)
	6	0	0	(2.90)
	8	0	0	(3.37)
	10	0	0	(3.40)
	0	0	0	-
	6	0	0	(0.96)
	8	0	0	(2.71)
	1	0	0	(0.04)
	2	0	0	(0.04)
	4	0	0	(0.60)
2 gpL	0	1	0	-
	1	1	1	(0.04)
	2	1	2	(0.09)
	4	1	4	(0.20)
	6	1	6	(2.13)
	8	1	8	(2.96)
	10	1	10	(2.63)
	0	1	0	-
	6	1	6	(1.70)
	8	1	8	(3.65)
	10	1	10	(3.88)
	1	1	1	(0.04)
	2	1	2	(0.02)
	4	1	4	(0.25)

Full regression model, used X, Z, and X*Z vs. Y

Reduced regression model, used only X vs. Y

Full Model (1 vs. 2 gpl)								
SUMMARY OUTPUT								
Regression Statistics								
Multiple F	0.949076293							
R Square	0.90074581							
Adjusted I	0.850807961							
Standard E	0.615762751							
Observati	27							
ANOVA								
	df	*SS*	*MS*	*F*	*gnificance F*			
Regressio	3	82.58316	27.52772	72.60113	7.04E-12			
Residual	24	9.09993	0.379164					
Total	27	91.68309						
	Coefficients	*andard Err*	*t Stat*	*P-value*	*Lower 95%*	*Upper 95%*	*ower 95.0%*	*pper 95.0%*
Intercept	0	#N/A	#N/A	#N/A	#N/A	#N/A	#N/A	#N/A
X Variable	-0.32026307	0.033297	-9.61848	1.04E-09	-0.38898	-0.25154	-0.38898	-0.25154
X Variable	0.467234973	0.26739	1.747389	0.093356	-0.08463	1.019102	-0.08463	1.019102
X Variable	-0.06909379	0.05808	-1.18963	0.245828	-0.18897	0.050778	-0.18897	0.050778

Reduced Model (1 vs. 2 gpl)								
SUMMARY OUTPUT								
Regression Statistics								
Multiple F	0.942386							
R Square	0.888092							
Adjusted I	0.84963							
Standard E	0.628187							
Observati	27							
ANOVA								
	df	*SS*	*MS*	*F*	*nificance F*			
Regressio	1	81.4229932	81.423	206.333211	1.4E-13			
Residual	26	10.2600924	0.39462					
Total	27	91.6830856						
	Coefficients	*tandard Erro*	*t Stat*	*P-value*	*ower 95%*	*Upper 95%*	*ver 95.*	*Upper 95.0%*
Intercept	0	#N/A	#N/A	#N/A	#N/A	#N/A	#N/A	#N/A
X Variable	-0.32227	0.02243525	-14.364	7.0684E-14	-0.3684	-0.276150432	-0.37	-0.27615

$$F = \frac{(SSReg, Full - SSReg, Red)/2}{(SSRes, Full) / (n-4)}$$

SSReg, Full = 82.58

SSReg, Red = 81.42

(SSRes, Full) / (n-4) = 0.37

Thus, F = 1.53

P-value of the F-test based on F value of 1.53, and the degrees of freedom of 2 and 24 = 24%

Appendix 4: Model using non-normalized least sum of the squares method.

Table 32: The summary of the degradation rate constants obtained using non-normalized least sum of the squares method, as shown by **Equation 25**.

	120 ˚C, Water	**120 ˚C, 0.1% Acid**	**120 ˚C, 1% Acid**	**160 ˚C, Water**	**160 ˚C, 0.1% Acid**	**160 ˚C, 1% Acid**	**200 ˚C, Water**	**200 ˚C, 0.1% Acid**	**200 ˚C, 1% Acid**
k_1	0.0017	0.0013	0.0015	0.0542	0.0043	0.0262	2.3001	0.0488	0.2514
k_2	0.0004	0.0036	0.1722	0.0192	0.0870	1.2766	0.0432	0.3111	2.3457
k_3				0.1797	10.0000	1.6397	0.4852	5.1440	
k_4				2.0000	0.0760	1.7585	1.2244		
k_F	0.0014	0.0015	0.0036	0.0026	0.0023	0.0232	0.0043	0.0131	0.0158
k_A	0.0013	0.0013	0.0014	0.0003	0.0013	0.0007	0.0020	0.0015	0.0021
k_{41}				2.0000	0.0000	0.0001	1.2244		
k_{42}				0.0000	0.0760	1.7584	0.0000		
k_{31}				0.1797	10.0000	1.6397	0.4852	5.1440	
k_{21}	0.0004	0.0036	0.1722	0.0192	0.0870	1.2766	0.0432	0.3111	2.3457
k_{1F}	0.0001	0.0003	0.0001	0.0024	0.0000	0.0141	0.3762	0.0330	0.1320
k_{1A}	0.0016	0.0010	0.0014	0.0518	0.0043	0.0121	1.9238	0.0158	0.1194
k_{FA}	0.0014	0.0003	0.0036	0.0026	0.0023	0.0232	0.0037	0.0131	0.0158
k_{FL}	0.0000	0.0012	0.0000	0.0000	0.0000	0.0000	0.0006	0.0000	0.0000
k_{AL}	0.0013	0.0013	0.0014	0.0003	0.0013	0.0007	0.0020	0.0015	0.0021

1. Hydrolysis Condition at 120 ˚C, Water (Model using non-normalized least sum of the squares method)

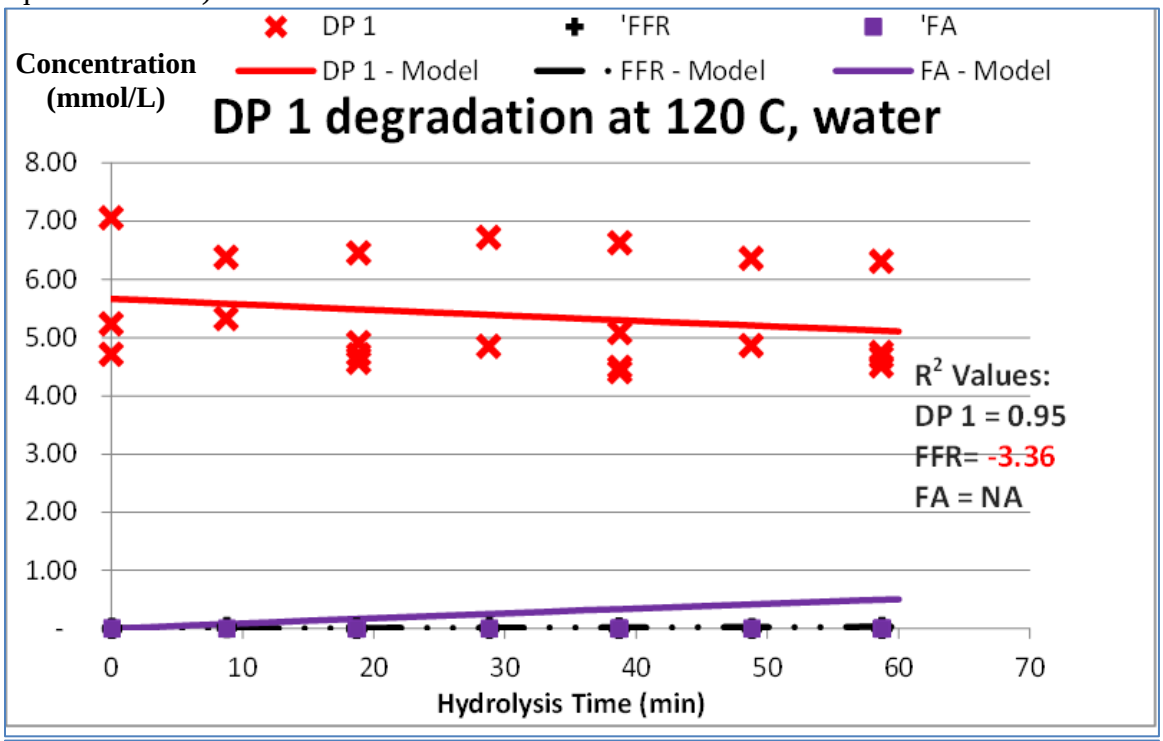

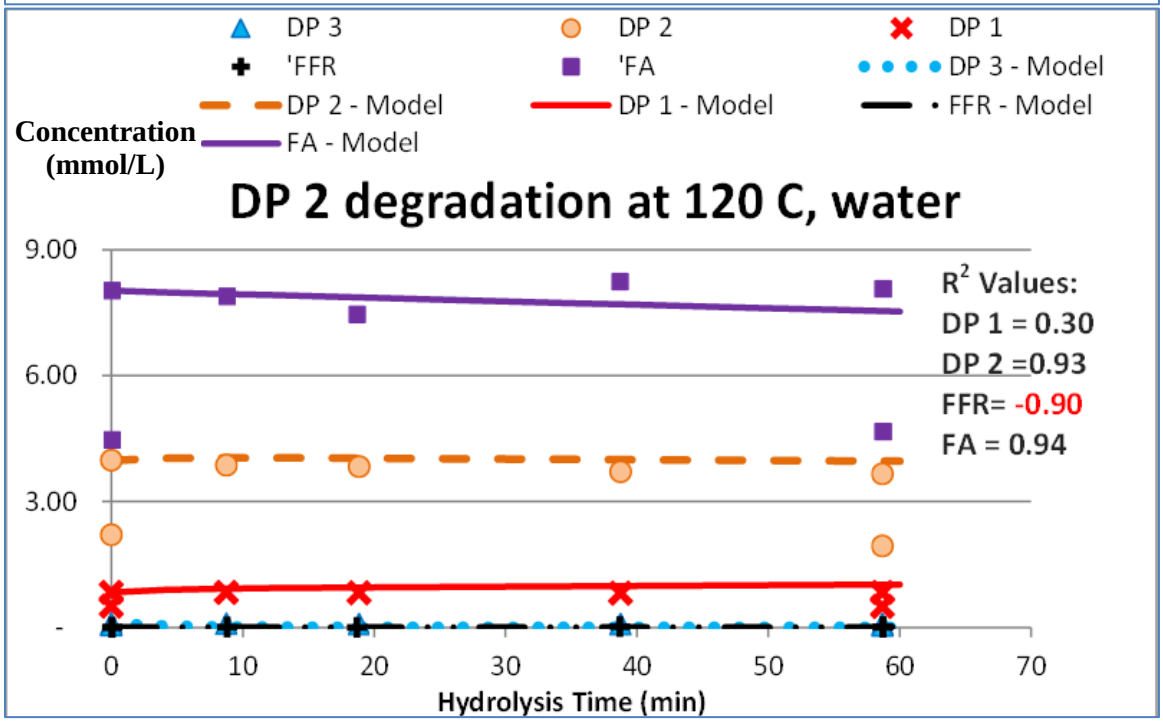

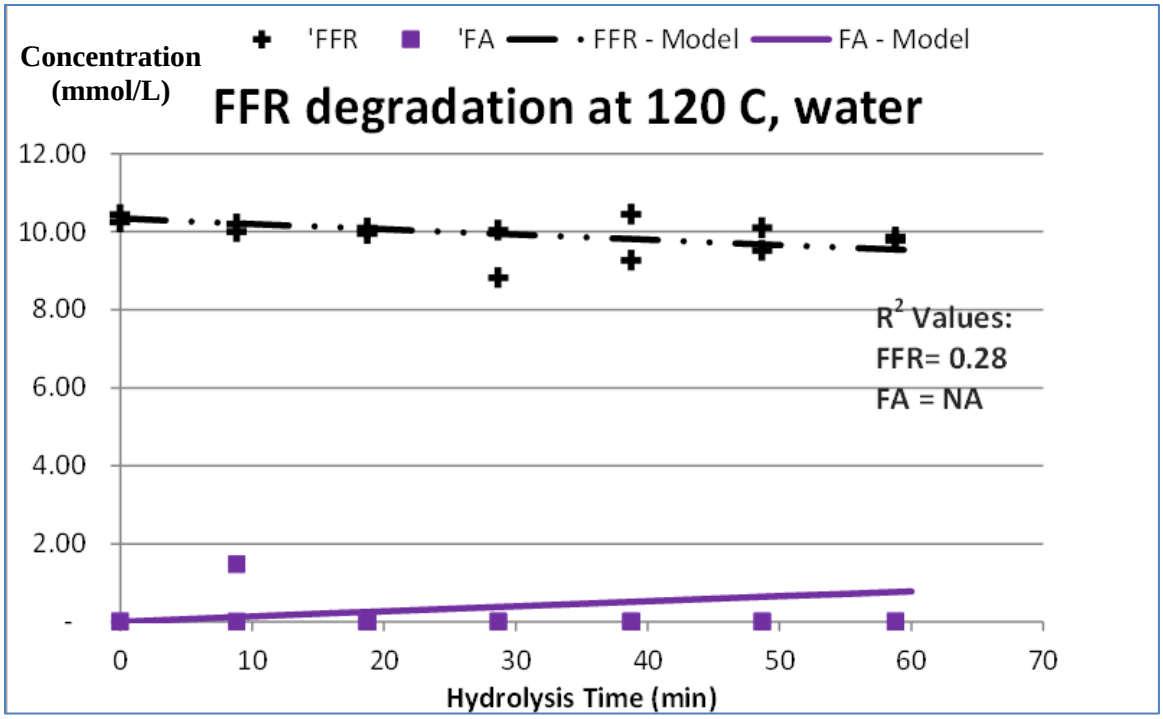
'FFR
'FA
FFR - Model
FA - Model
Concentration (mmol/L)
FFR degradation at 120 C, water
12.00
10.00
8.00
6.00
4.00
2.00
-
0
10
20
30
40
50
60
70
Hydrolysis Time (min)
R2 Values:
FFR= 0.28
FA = NA

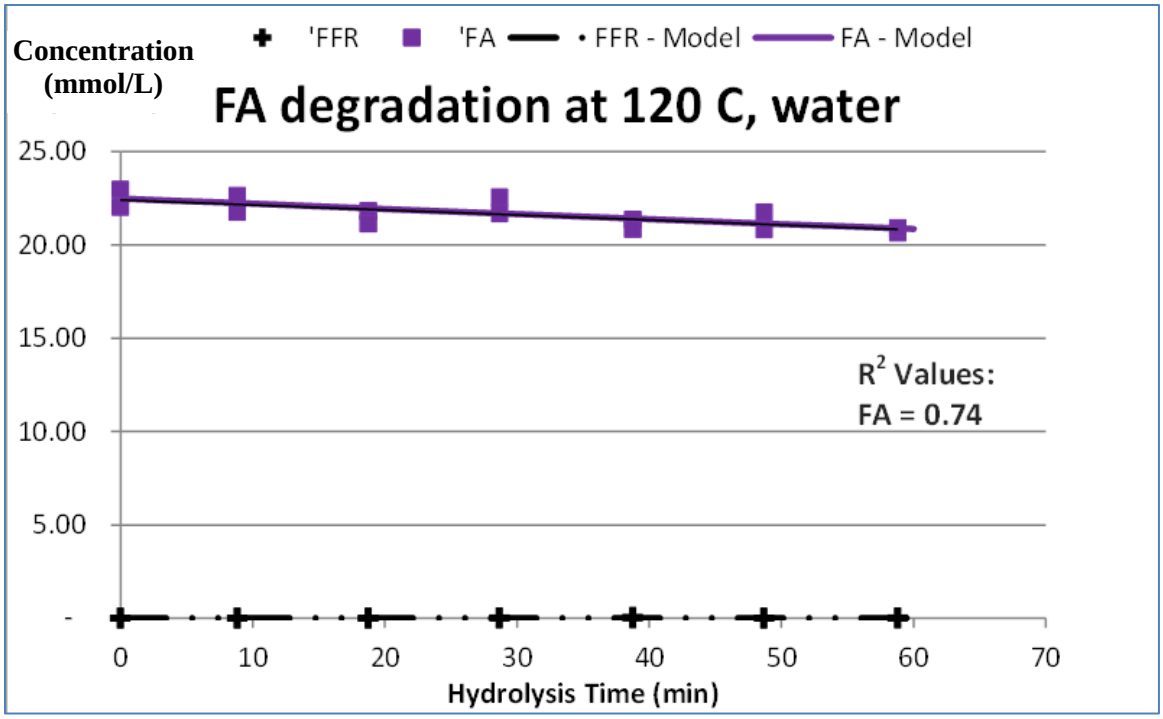
'FFR
'FA
FFR - Model
FA - Model
Concentration (mmol/L)
FA degradation at 120 C, water
25.00
20.00
15.00
10.00
5.00
-
0
10
20
30
40
50
60
70
Hydrolysis Time (min)
R2 Values:
FA = 0.74

2. Hydrolysis Condition at 120 ˚C, 0.1% Acid (Model using non-normalized least sum of the squares method)

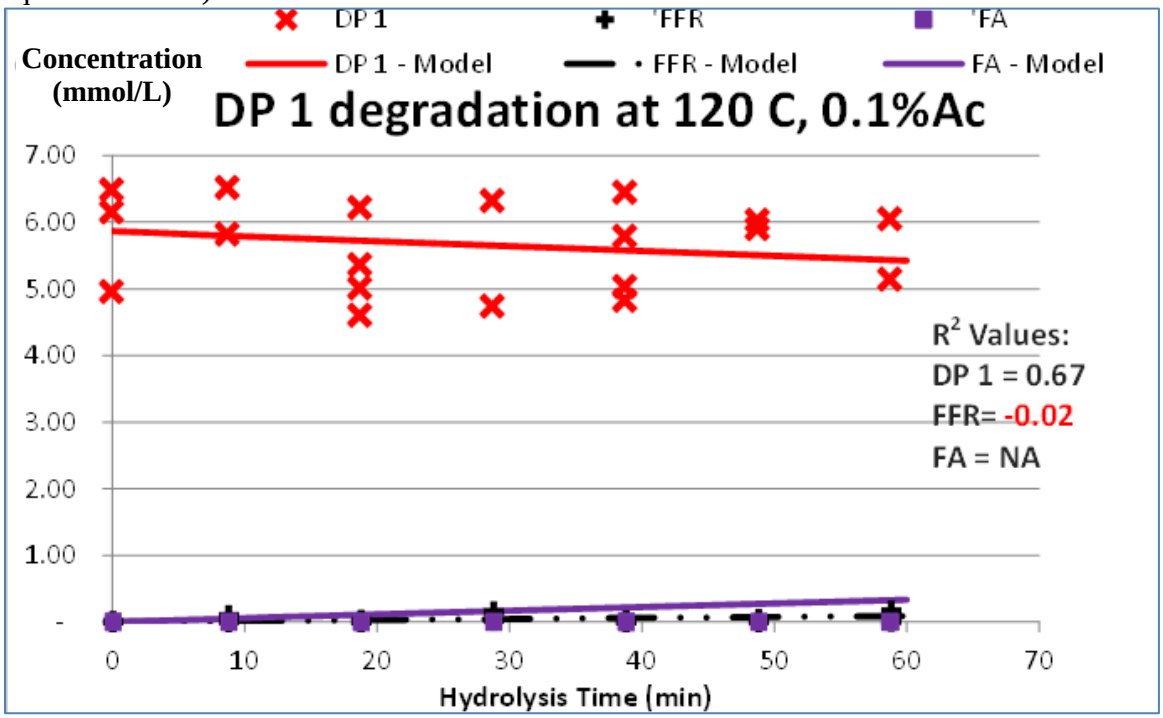

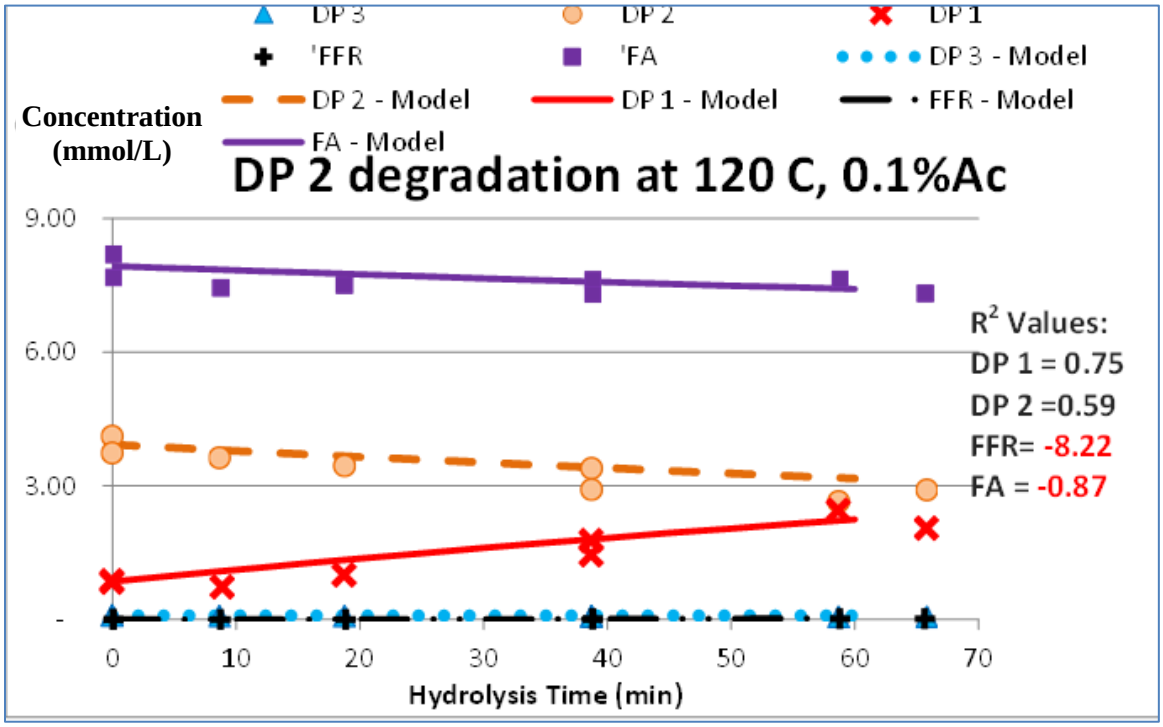

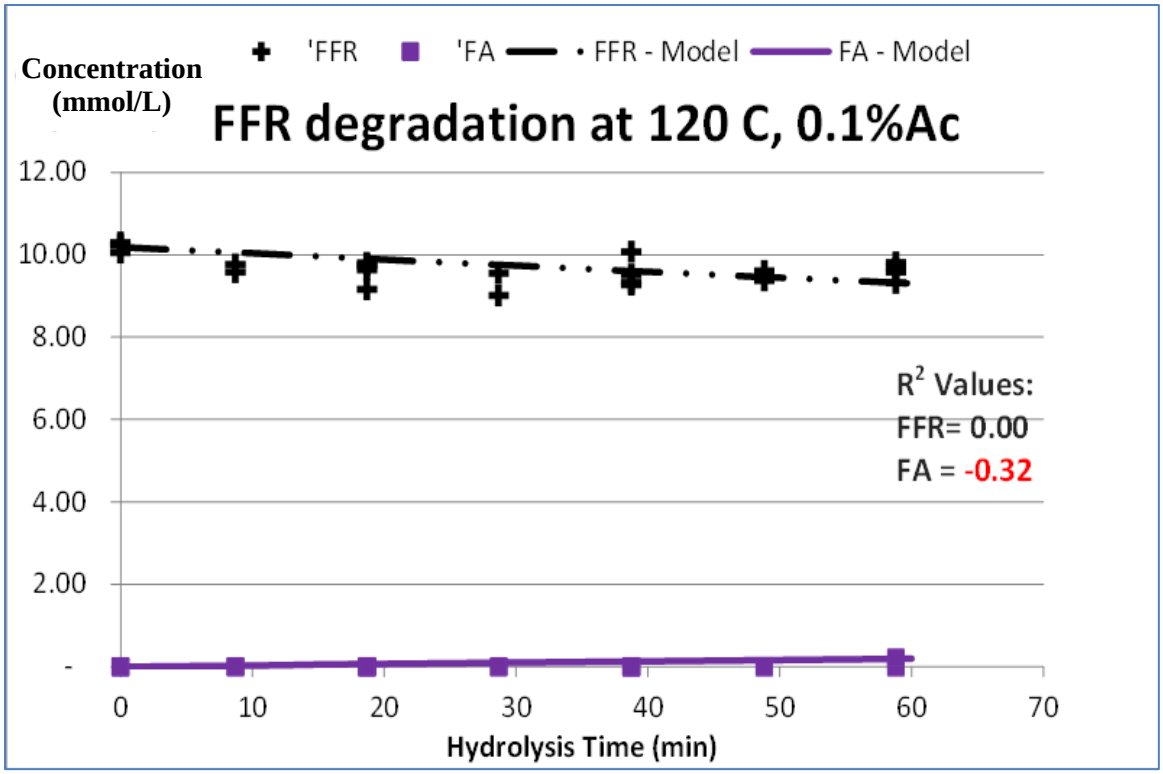
Concentration (mmol/L)
'FFR
'FA
FFR - Model
FA - Model
FFR degradation at 120 C, 0.1%Ac
12.00
10.00
8.00
6.00
4.00
2.00
-
0
10
20
30
40
50
60
70
Hydrolysis Time (min)
R2 Values:
FFR= 0.00
FA = -0.32

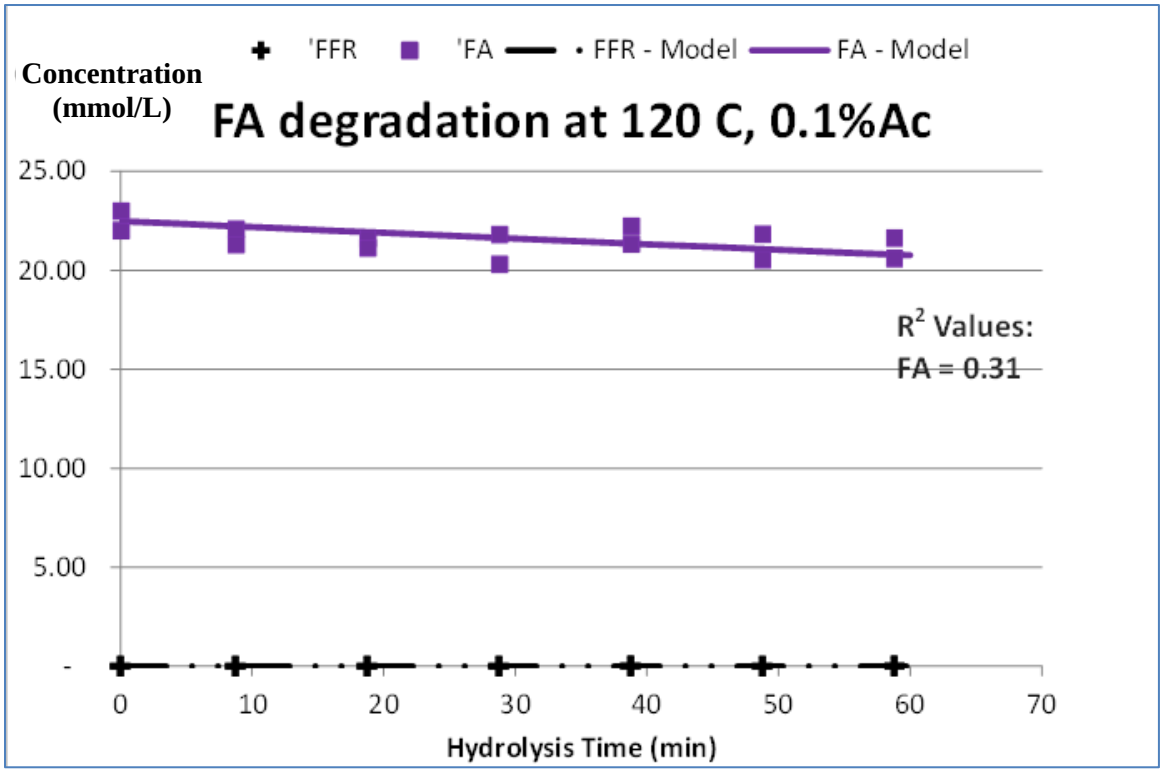
Concentration (mmol/L)
'FFR
'FA
FFR - Model
FA - Model
FA degradation at 120 C, 0.1%Ac
25.00
20.00
15.00
10.00
5.00
-
0
10
20
30
40
50
60
70
Hydrolysis Time (min)
R2 Values:
FA = 0.31

3. Hydrolysis Condition at 120 ˚C, 1% Acid (Model using non-normalized least sum of the squares method)

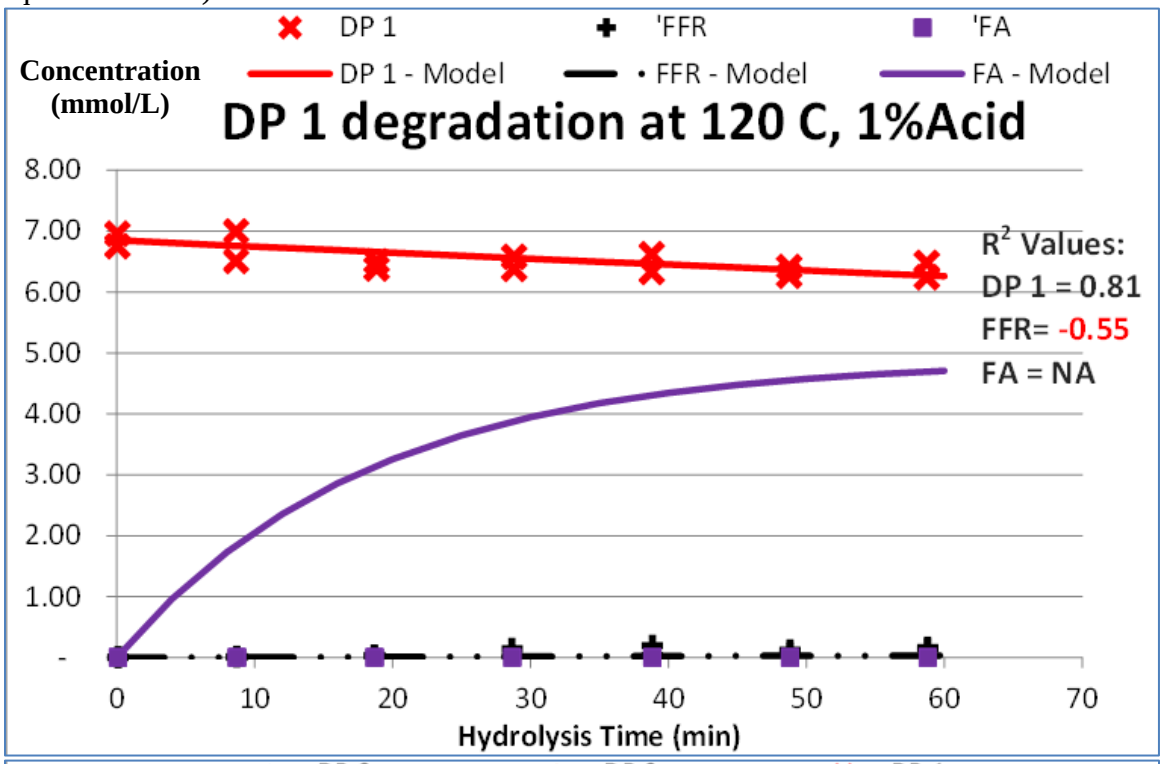

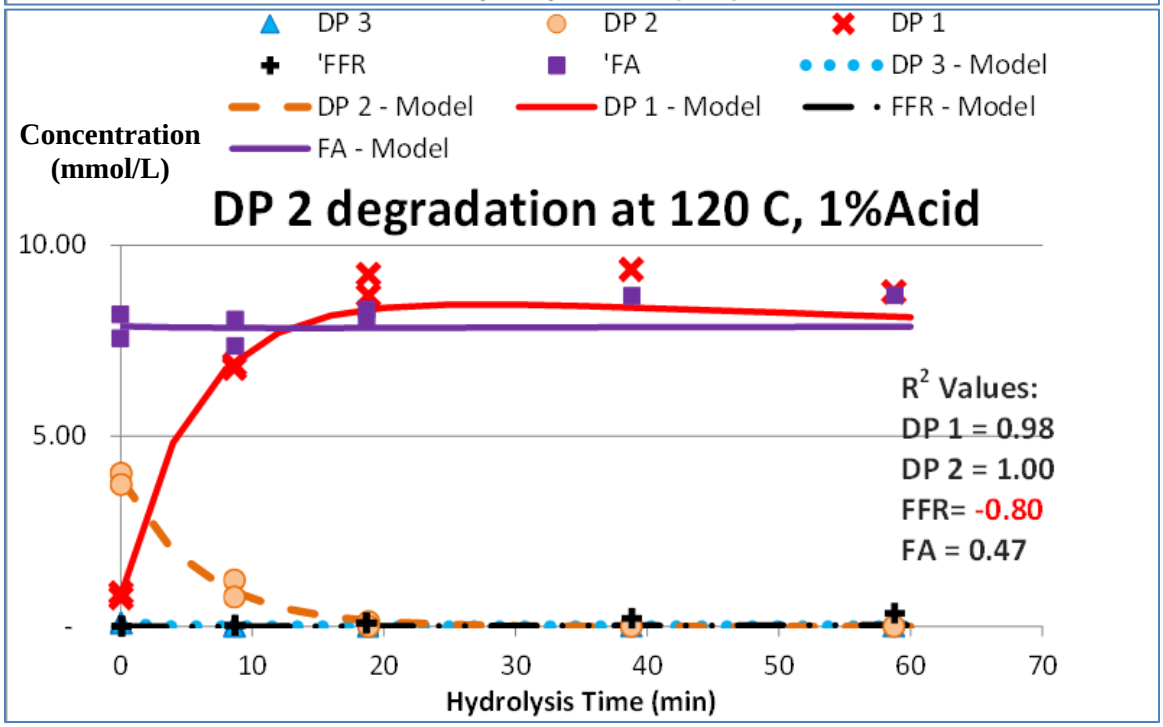

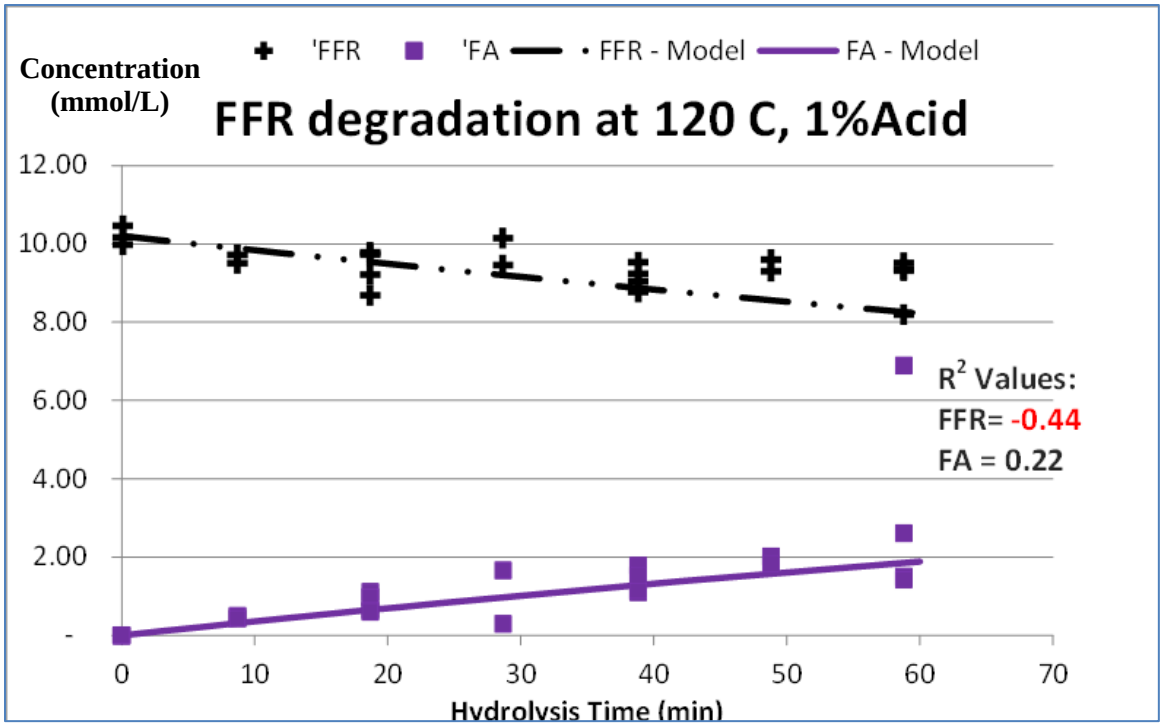
Concentration (mmol/L)
'FFR
'FA
FFR - Model
FA - Model
FFR degradation at 120 C, 1%Acid
12.00
10.00
8.00
6.00
4.00
2.00
-
0
10
20
30
40
50
60
70
R² Values:
FFR= -0.44
FA = 0.22
Hydrolysis Time (min)

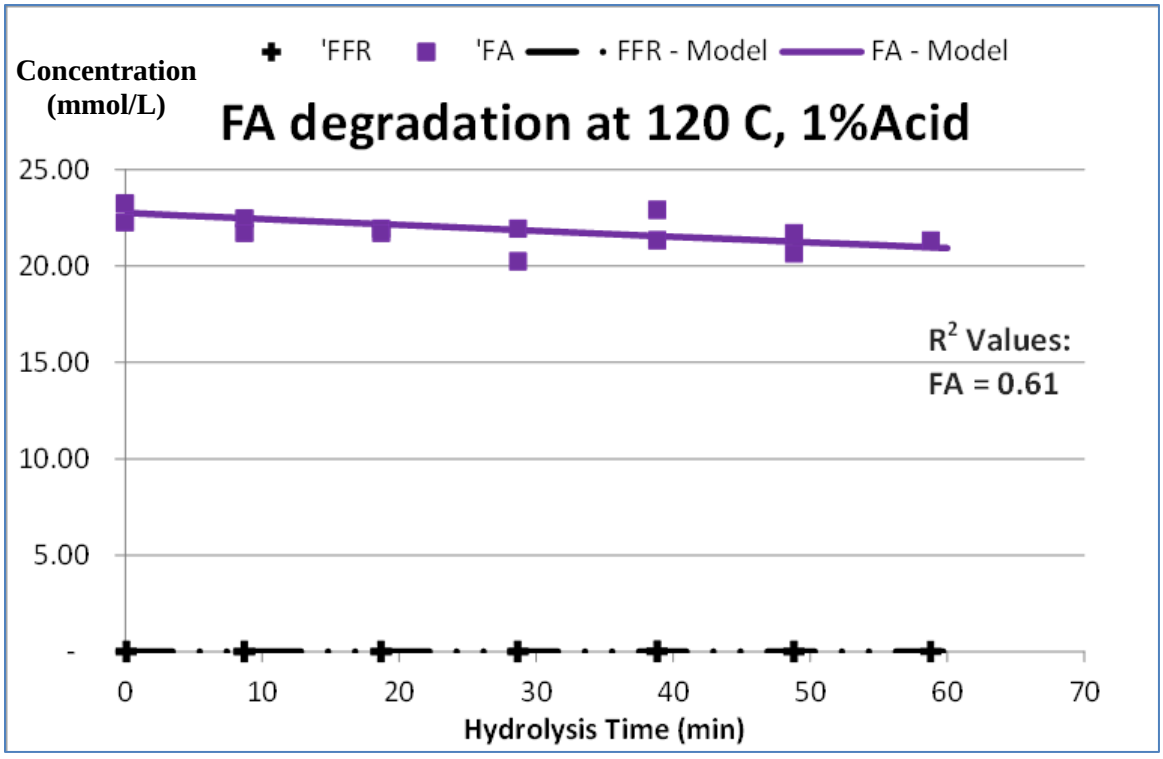
Concentration (mmol/L)
'FFR
'FA
FFR - Model
FA - Model
FA degradation at 120 C, 1%Acid
25.00
20.00
15.00
10.00
5.00
-
0
10
20
30
40
50
60
70
R² Values:
FA = 0.61
Hydrolysis Time (min)

4. Hydrolysis Condition at 160 ˚C, Water (Model using non-normalized least sum of the squares method)

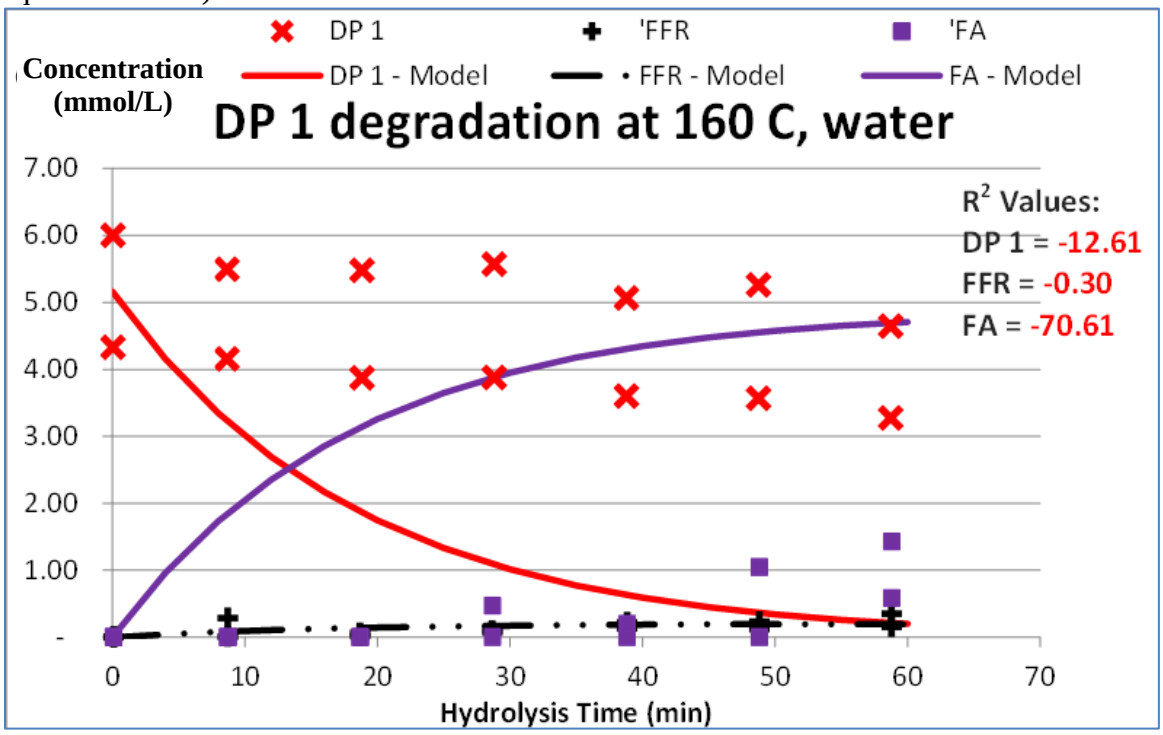

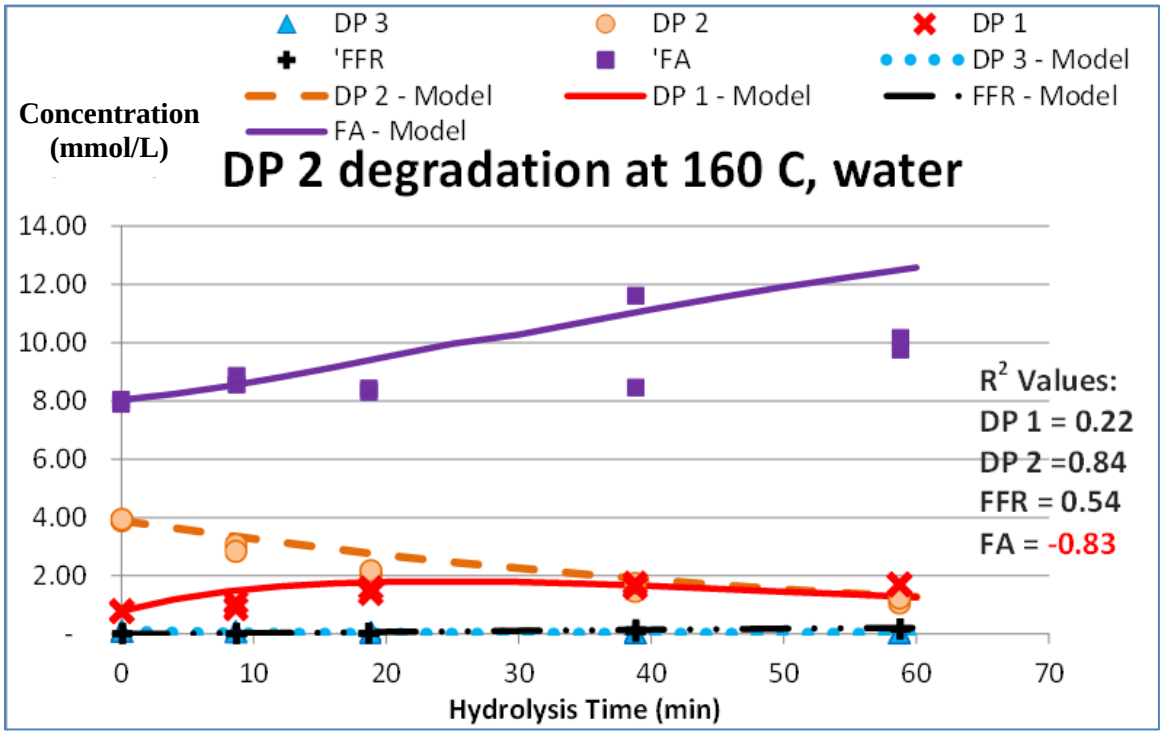

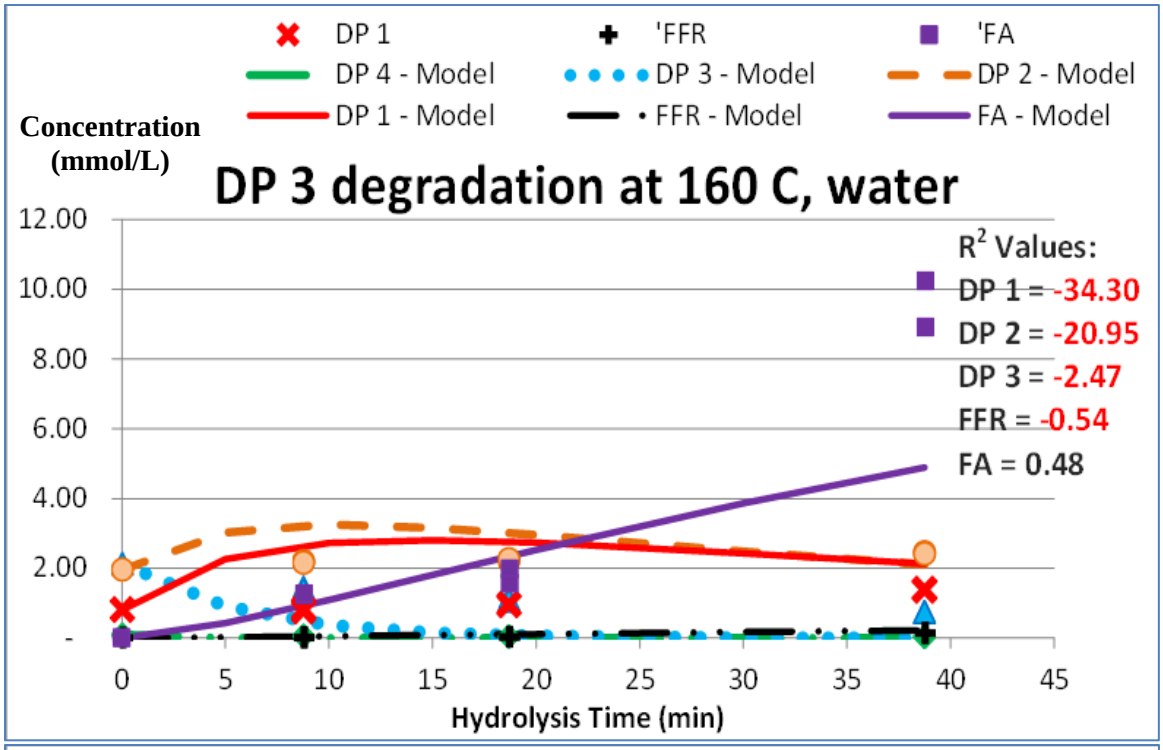
DP 1
'FFR
'FA
DP 4 - Model
DP 3 - Model
DP 2 - Model
DP 1 - Model
FFR - Model
FA - Model
Concentration (mmol/L)
DP 3 degradation at 160 C, water
12.00
10.00
8.00
6.00
4.00
2.00
-
0
5
10
15
20
25
30
35
40
45
Hydrolysis Time (min)
R2 Values:
DP 1 = -34.30
DP 2 = -20.95
DP 3 = -2.47
FFR = -0.54
FA = 0.48

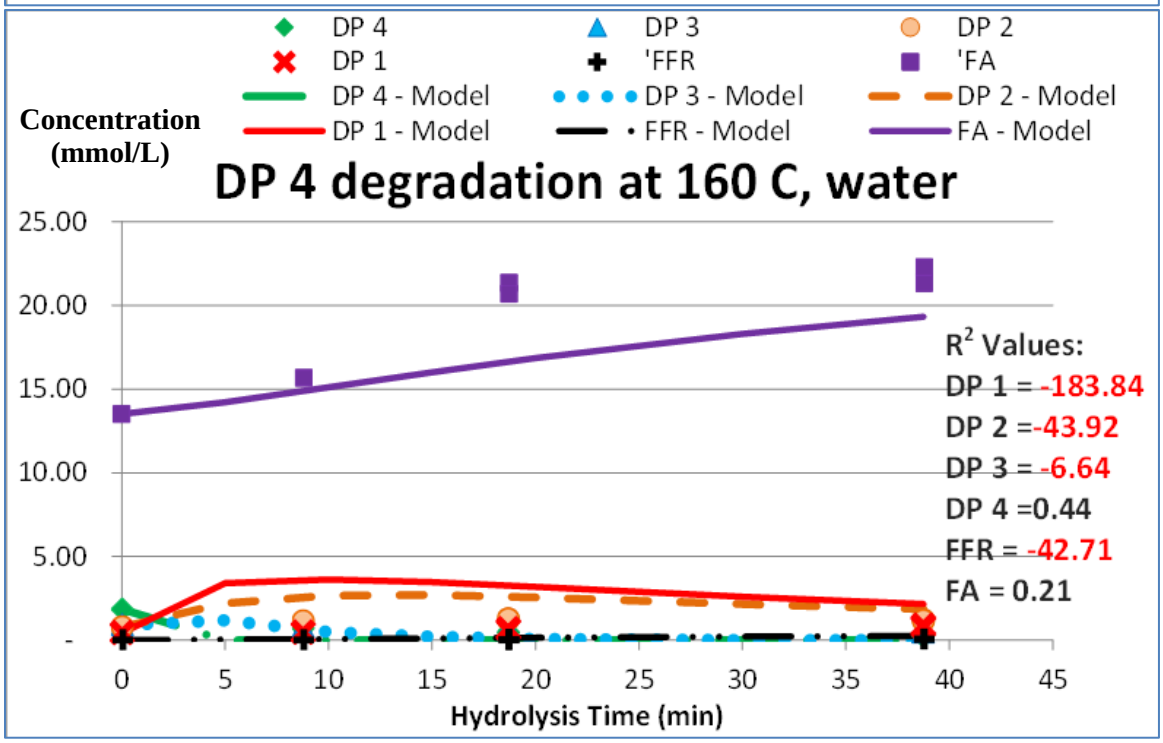
DP 4
DP 3
DP 2
DP 1
'FFR
'FA
DP 4 - Model
DP 3 - Model
DP 2 - Model
DP 1 - Model
FFR - Model
FA - Model
Concentration (mmol/L)
DP 4 degradation at 160 C, water
25.00
20.00
15.00
10.00
5.00
-
0
5
10
15
20
25
30
35
40
45
Hydrolysis Time (min)
R2 Values:
DP 1 = -183.84
DP 2 =-43.92
DP 3 = -6.64
DP 4 =0.44
FFR = -42.71
FA = 0.21

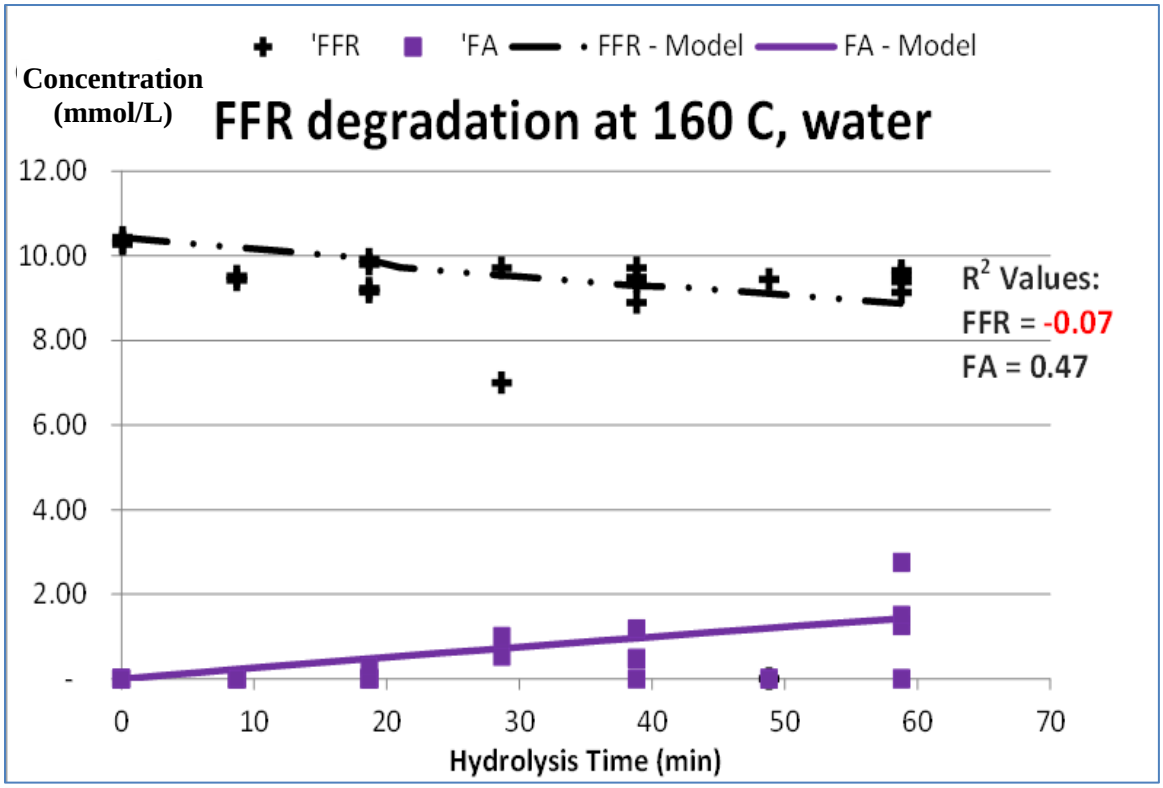
'FFR
'FA
FFR - Model
FA - Model
Concentration (mmol/L)
FFR degradation at 160 C, water
12.00
10.00
8.00
6.00
4.00
2.00
-
0
10
20
30
40
50
60
70
Hydrolysis Time (min)
R2 Values:
FFR = -0.07
FA = 0.47

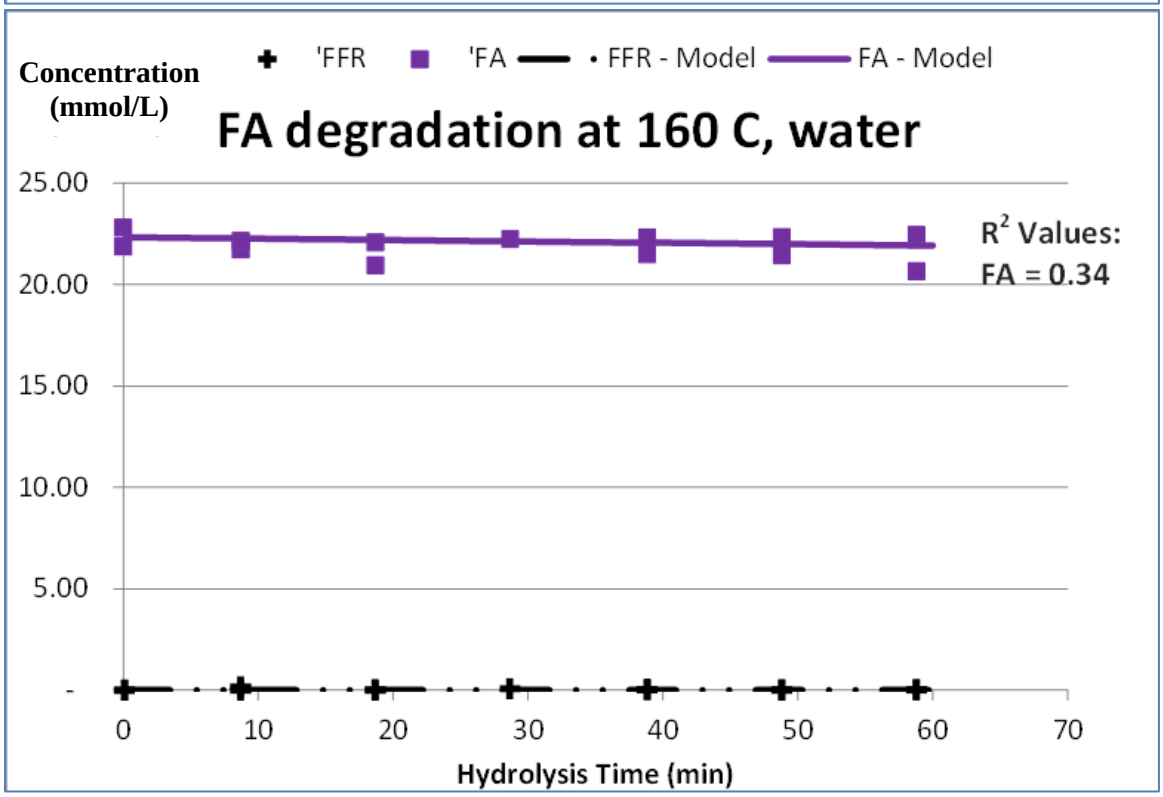
'FFR
'FA
FFR - Model
FA - Model
Concentration (mmol/L)
FA degradation at 160 C, water
25.00
20.00
15.00
10.00
5.00
-
0
10
20
30
40
50
60
70
Hydrolysis Time (min)
R2 Values:
FA = 0.34

5. Hydrolysis Condition at 160 ˚C, 0.1% Acid (Model using non-normalized least sum of the squares method)

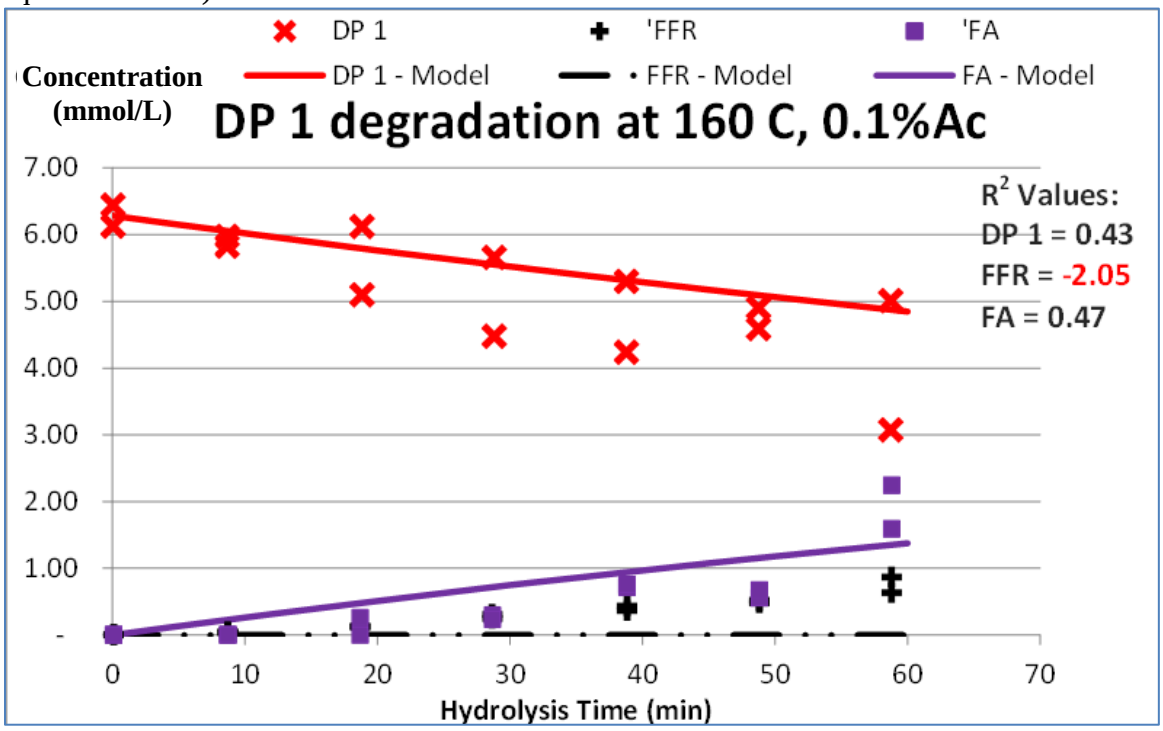

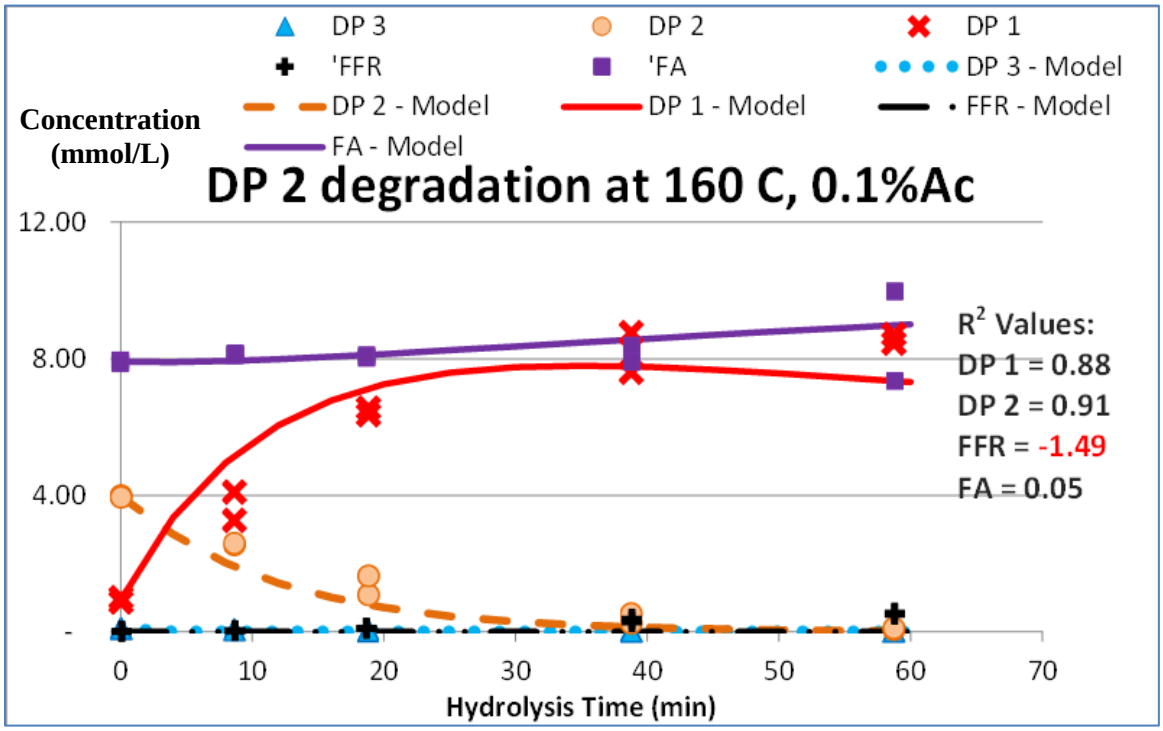

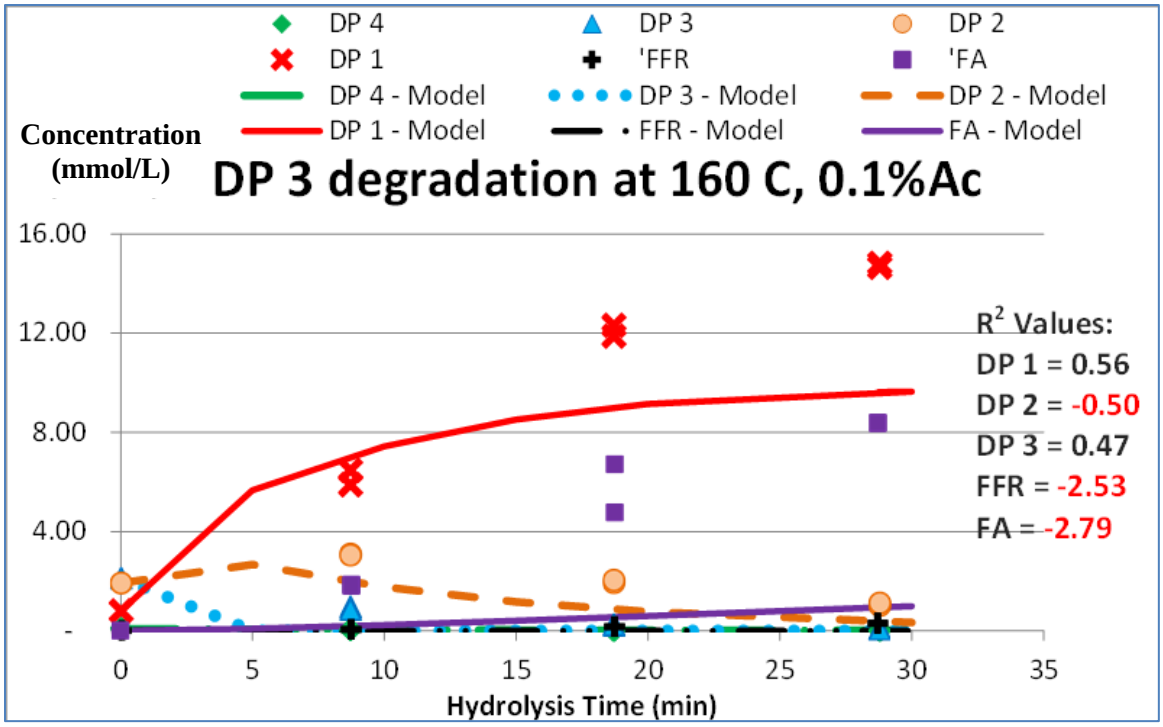
DP 4
DP 3
DP 2
DP 1
'FFR
'FA
DP 4 - Model
DP 3 - Model
DP 2 - Model
DP 1 - Model
FFR - Model
FA - Model
Concentration (mmol/L)
DP 3 degradation at 160 C, 0.1%Ac
16.00
12.00
8.00
4.00
-
0
5
10
15
20
25
30
35
Hydrolysis Time (min)
R² Values:
DP 1 = 0.56
DP 2 = -0.50
DP 3 = 0.47
FFR = -2.53
FA = -2.79

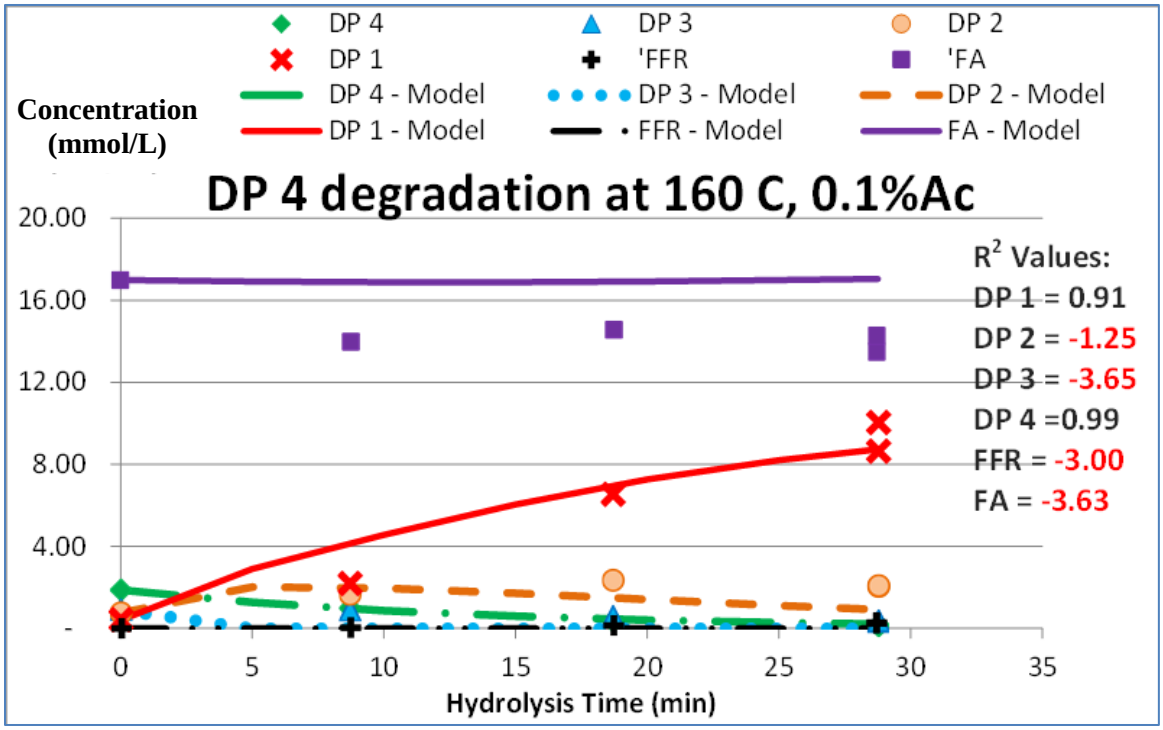
DP 4
DP 3
DP 2
DP 1
'FFR
'FA
DP 4 - Model
DP 3 - Model
DP 2 - Model
DP 1 - Model
FFR - Model
FA - Model
Concentration (mmol/L)
DP 4 degradation at 160 C, 0.1%Ac
20.00
16.00
12.00
8.00
4.00
-
0
5
10
15
20
25
30
35
Hydrolysis Time (min)
R² Values:
DP 1 = 0.91
DP 2 = -1.25
DP 3 = -3.65
DP 4 =0.99
FFR = -3.00
FA = -3.63

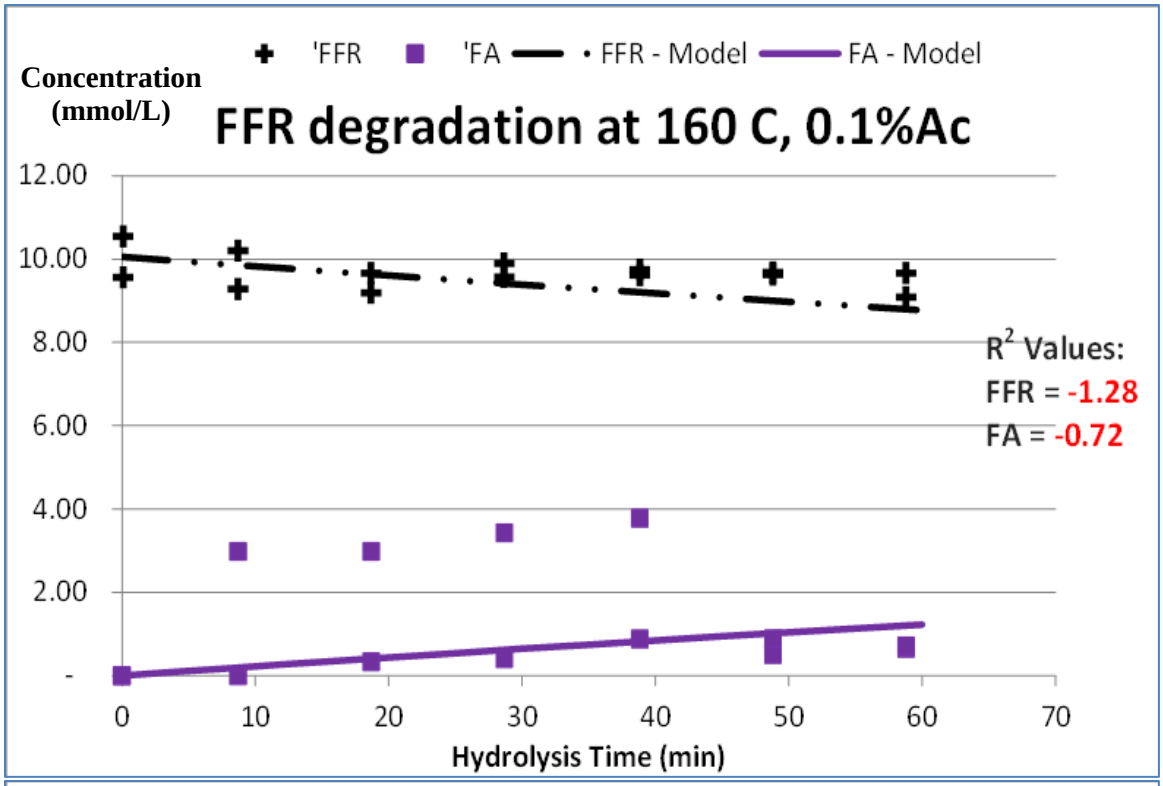
'FFR
'FA
FFR - Model
FA - Model
Concentration (mmol/L)
FFR degradation at 160 C, 0.1%Ac
12.00
10.00
8.00
6.00
4.00
2.00
-
0
10
20
30
40
50
60
70
Hydrolysis Time (min)
R2 Values:
FFR = -1.28
FA = -0.72

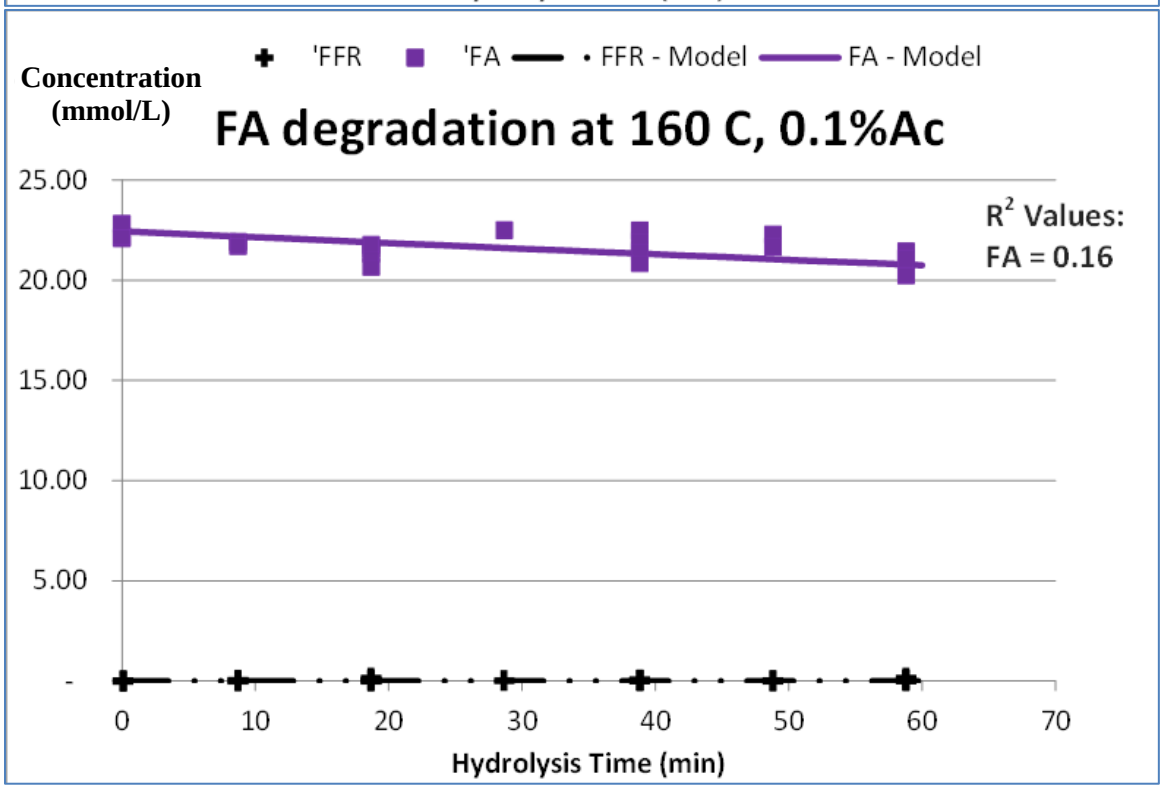
'FFR
'FA
FFR - Model
FA - Model
Concentration (mmol/L)
FA degradation at 160 C, 0.1%Ac
25.00
20.00
15.00
10.00
5.00
-
0
10
20
30
40
50
60
70
Hydrolysis Time (min)
R2 Values:
FA = 0.16

6. Hydrolysis Condition at 160 ˚C, 1% Acid (Model using non-normalized least sum of the squares method)

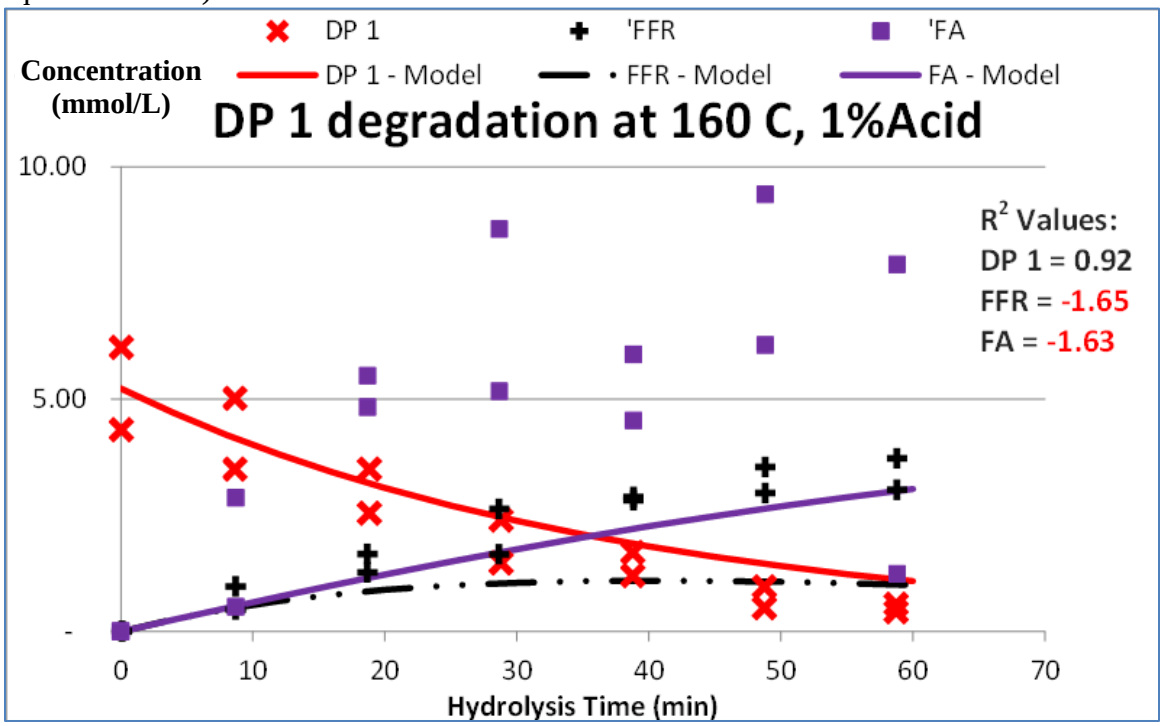

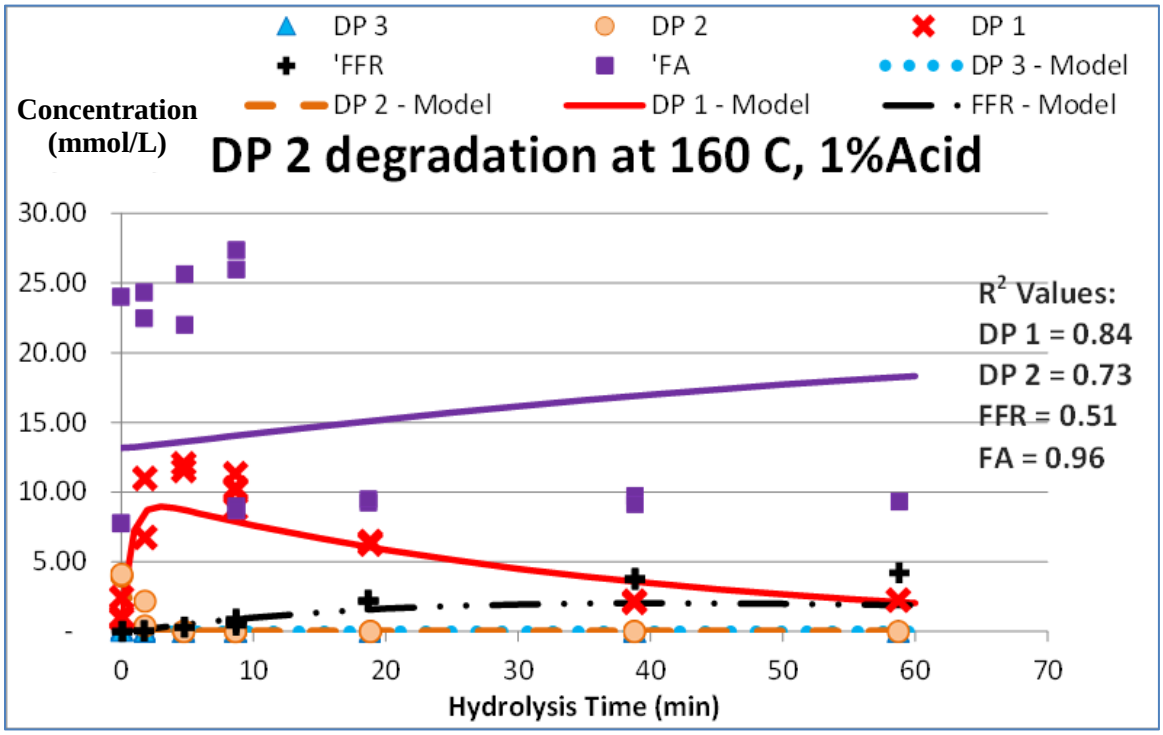

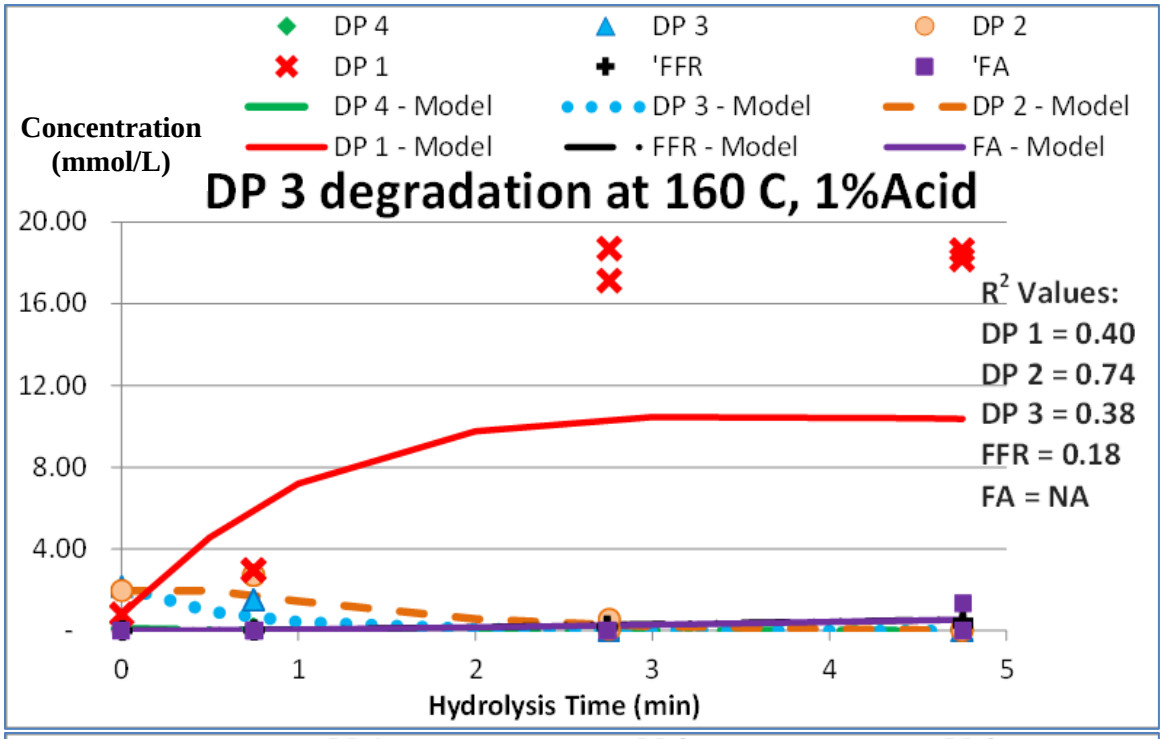
DP 4
DP 3
DP 2
DP 1
'FFR
'FA
DP 4 - Model
DP 3 - Model
DP 2 - Model
DP 1 - Model
FFR - Model
FA - Model
Concentration (mmol/L)
DP 3 degradation at 160 C, 1%Acid
20.00
16.00
12.00
8.00
4.00
-
0
1
2
3
4
5
Hydrolysis Time (min)
R2 Values:
DP 1 = 0.40
DP 2 = 0.74
DP 3 = 0.38
FFR = 0.18
FA = NA

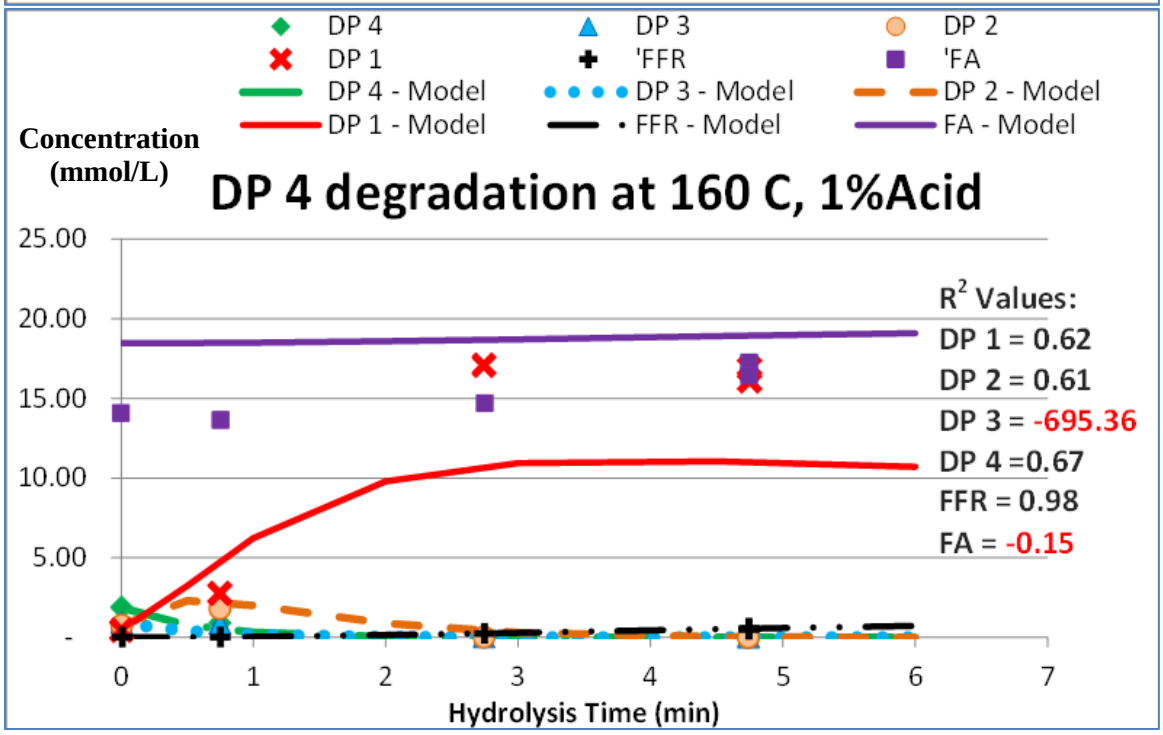
DP 4
DP 3
DP 2
DP 1
'FFR
'FA
DP 4 - Model
DP 3 - Model
DP 2 - Model
DP 1 - Model
FFR - Model
FA - Model
Concentration (mmol/L)
DP 4 degradation at 160 C, 1%Acid
25.00
20.00
15.00
10.00
5.00
-
0
1
2
3
4
5
6
7
Hydrolysis Time (min)
R2 Values:
DP 1 = 0.62
DP 2 = 0.61
DP 3 = -695.36
DP 4 =0.67
FFR = 0.98
FA = -0.15

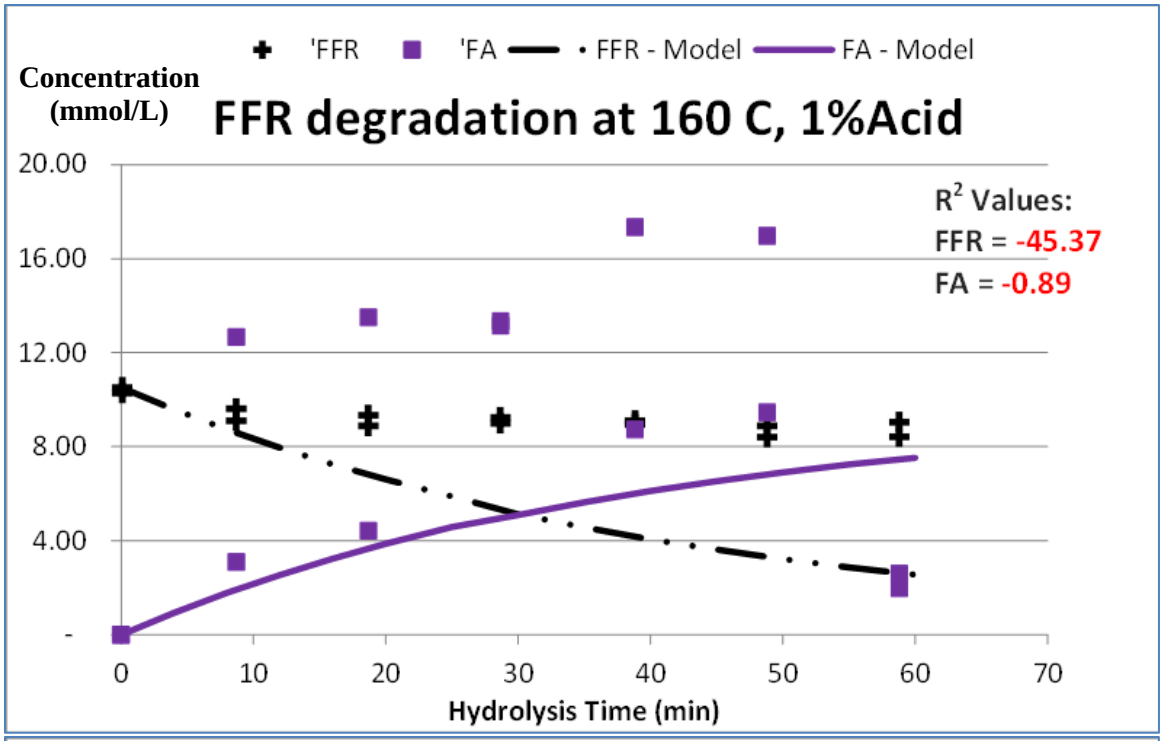
'FFR
'FA
FFR - Model
FA - Model
Concentration (mmol/L)
FFR degradation at 160 C, 1%Acid
20.00
16.00
12.00
8.00
4.00
-
0
10
20
30
40
50
60
70
Hydrolysis Time (min)
R2 Values:
FFR = -45.37
FA = -0.89

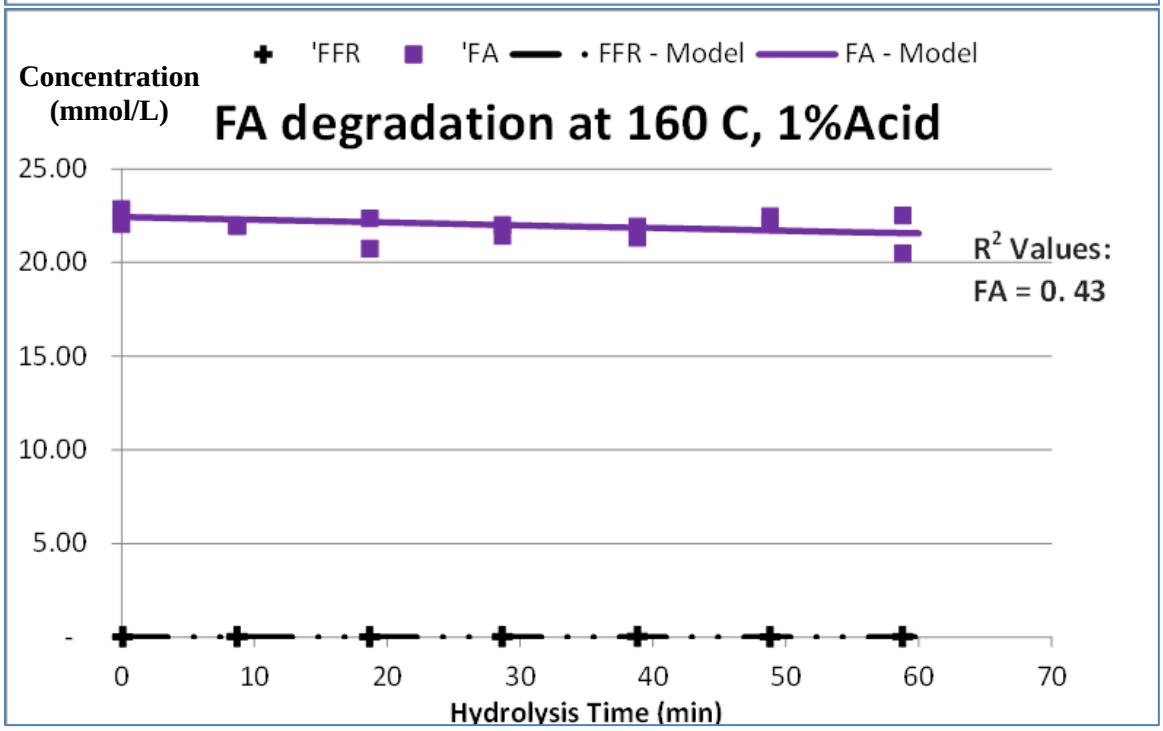
'FFR
'FA
FFR - Model
FA - Model
Concentration (mmol/L)
FA degradation at 160 C, 1%Acid
25.00
20.00
15.00
10.00
5.00
-
0
10
20
30
40
50
60
70
Hydrolysis Time (min)
R2 Values:
FA = 0. 43

7. Hydrolysis Condition at 200 ˚C, Water (Model using non-normalized least sum of the squares method)

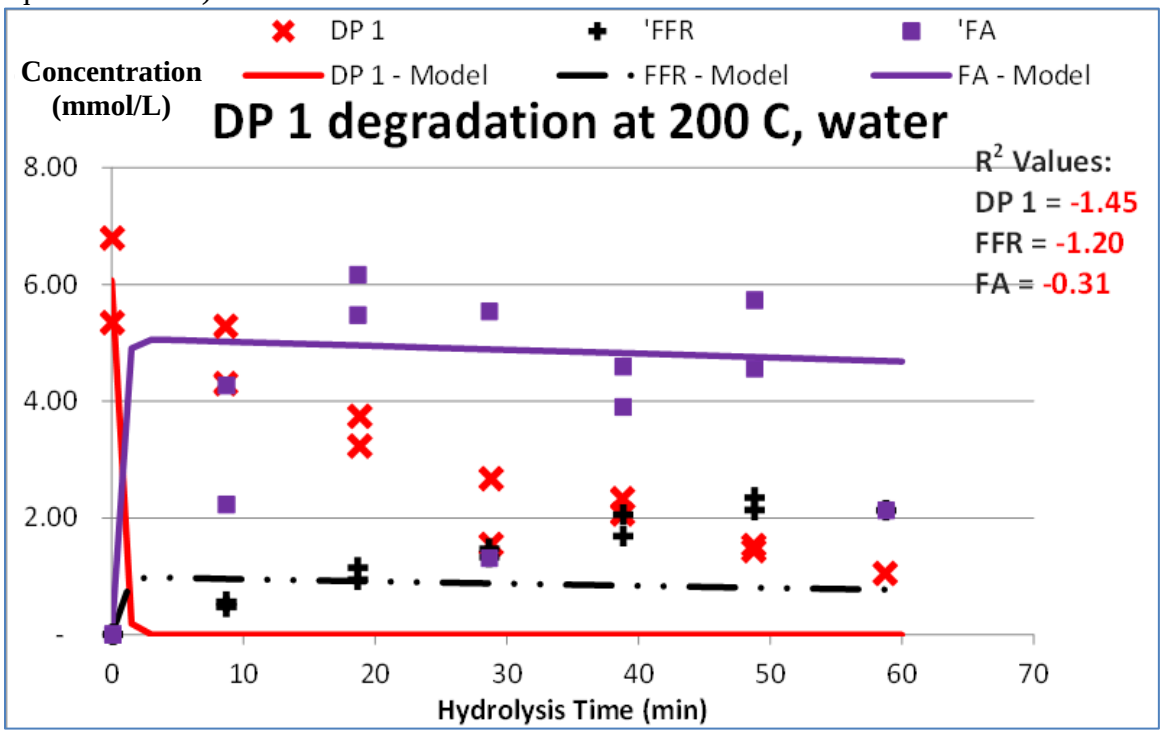

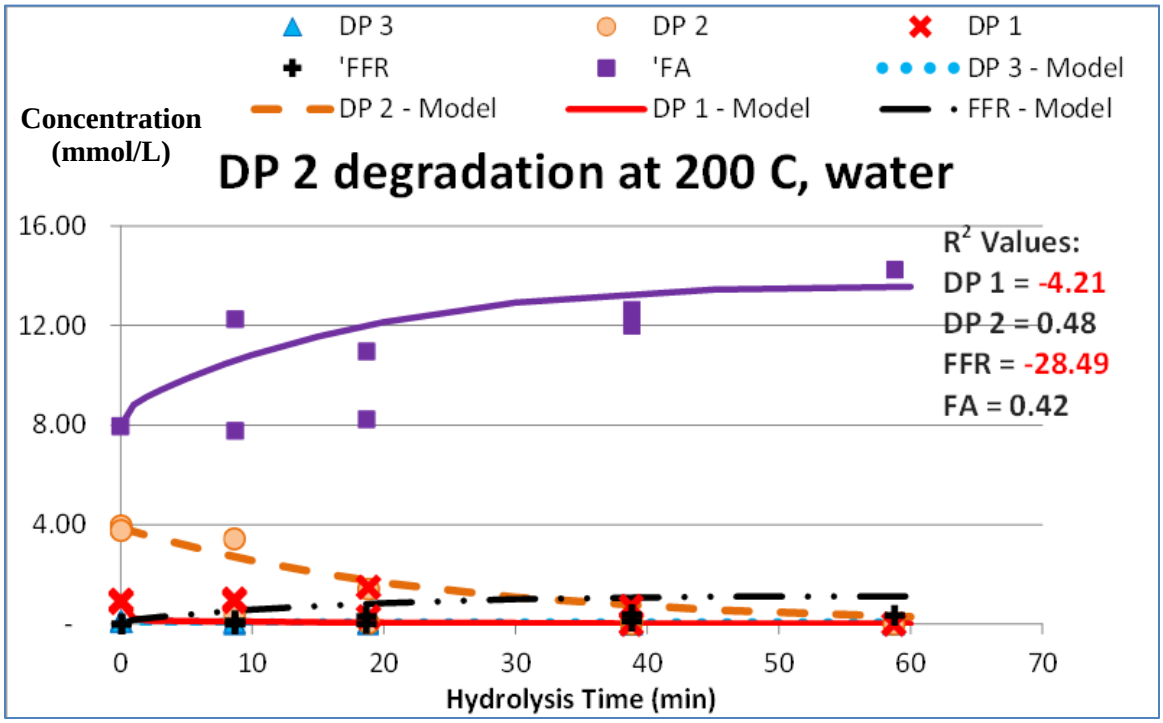

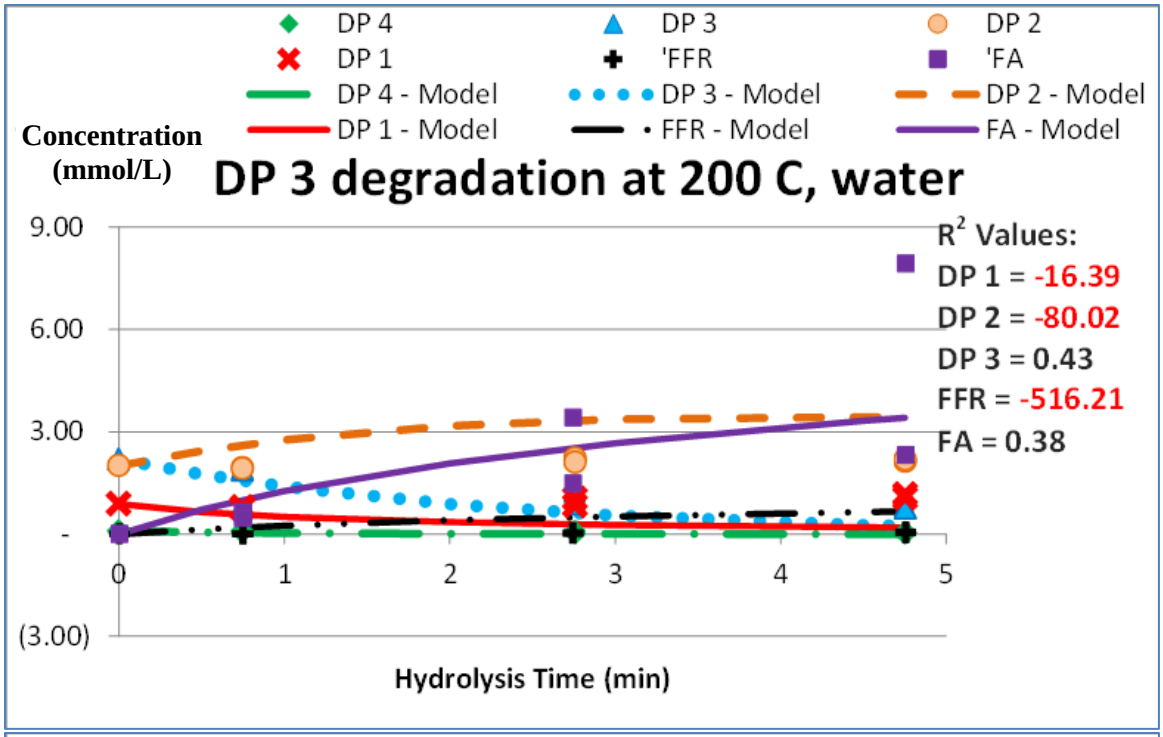
DP 4
DP 3
DP 2
DP 1
'FFR
'FA
DP 4 - Model
DP 3 - Model
DP 2 - Model
DP 1 - Model
FFR - Model
FA - Model
Concentration (mmol/L)
DP 3 degradation at 200 C, water
9.00
6.00
3.00
-
(3.00)
0
1
2
3
4
5
R² Values:
DP 1 = -16.39
DP 2 = -80.02
DP 3 = 0.43
FFR = -516.21
FA = 0.38
Hydrolysis Time (min)

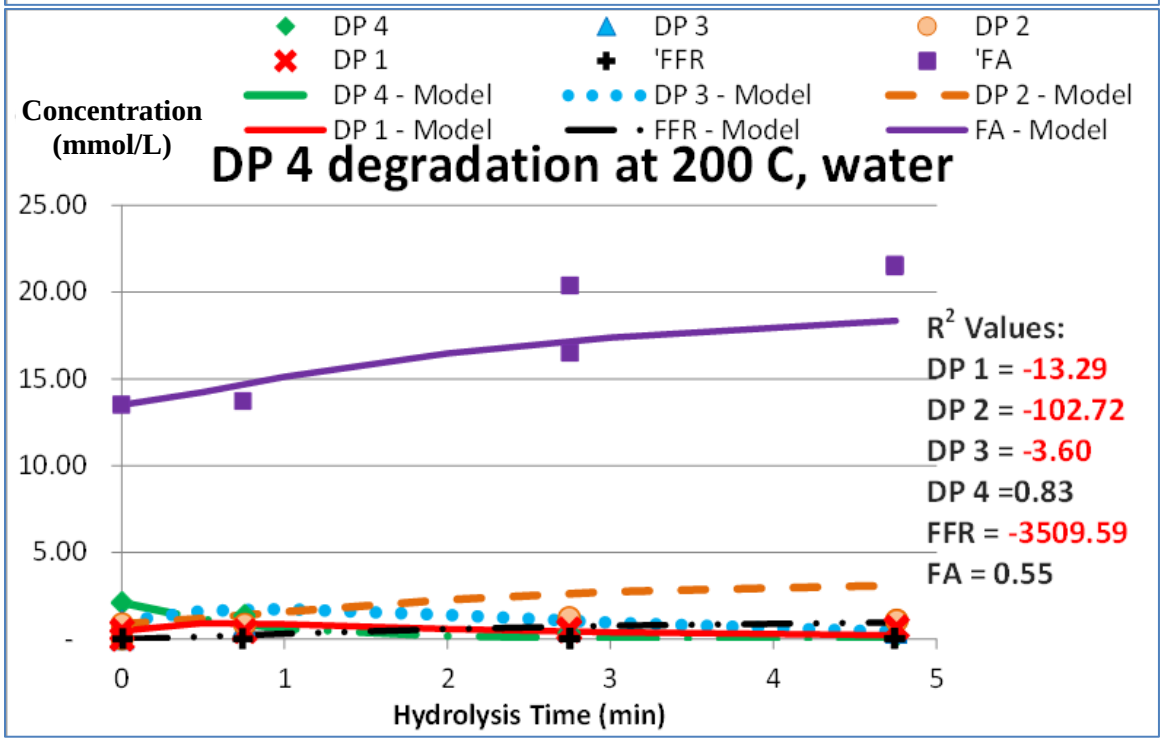
DP 4
DP 3
DP 2
DP 1
'FFR
'FA
DP 4 - Model
DP 3 - Model
DP 2 - Model
DP 1 - Model
FFR - Model
FA - Model
Concentration (mmol/L)
DP 4 degradation at 200 C, water
25.00
20.00
15.00
10.00
5.00
-
0
1
2
3
4
5
R² Values:
DP 1 = -13.29
DP 2 = -102.72
DP 3 = -3.60
DP 4 =0.83
FFR = -3509.59
FA = 0.55
Hydrolysis Time (min)

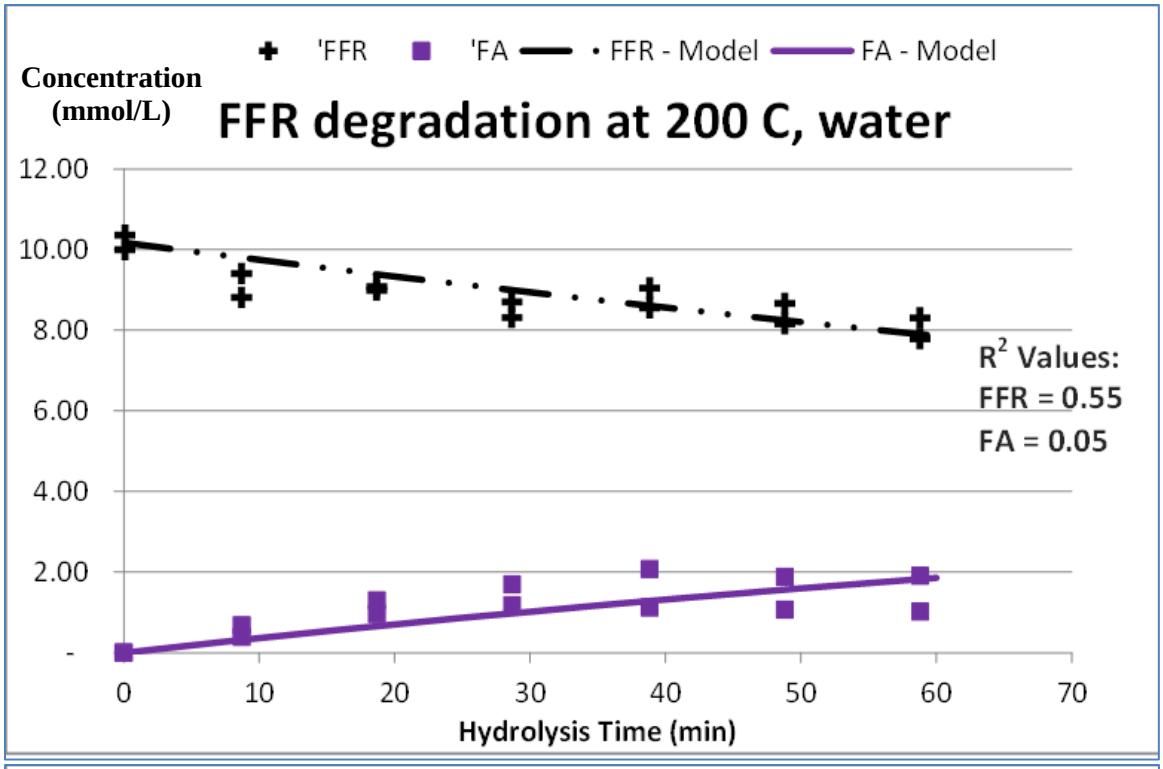
'FFR
'FA
FFR - Model
FA - Model
Concentration (mmol/L)
FFR degradation at 200 C, water
12.00
10.00
8.00
6.00
4.00
2.00
-
0
10
20
30
40
50
60
70
Hydrolysis Time (min)
R2 Values:
FFR = 0.55
FA = 0.05

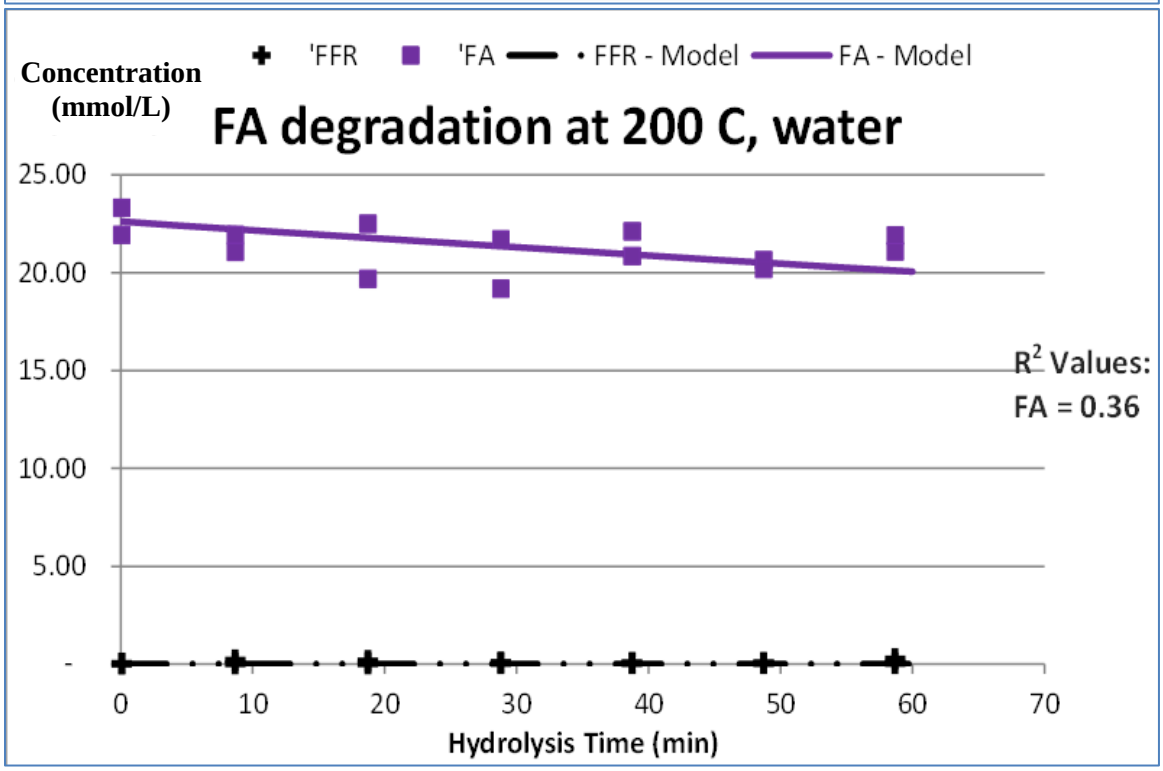
'FFR
'FA
FFR - Model
FA - Model
Concentration (mmol/L)
FA degradation at 200 C, water
25.00
20.00
15.00
10.00
5.00
-
0
10
20
30
40
50
60
70
Hydrolysis Time (min)
R2 Values:
FA = 0.36

8. Hydrolysis Condition at 200 ˚C, 0.1% Acid (Model using non-normalized least sum of the squares method)

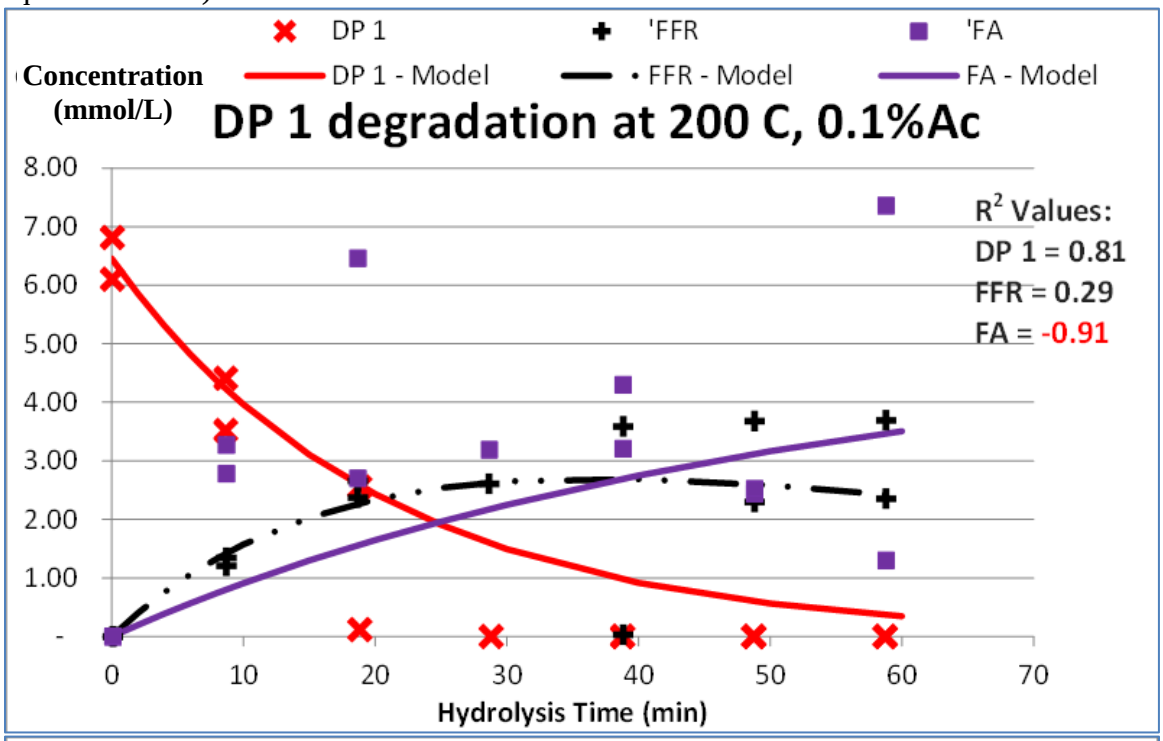

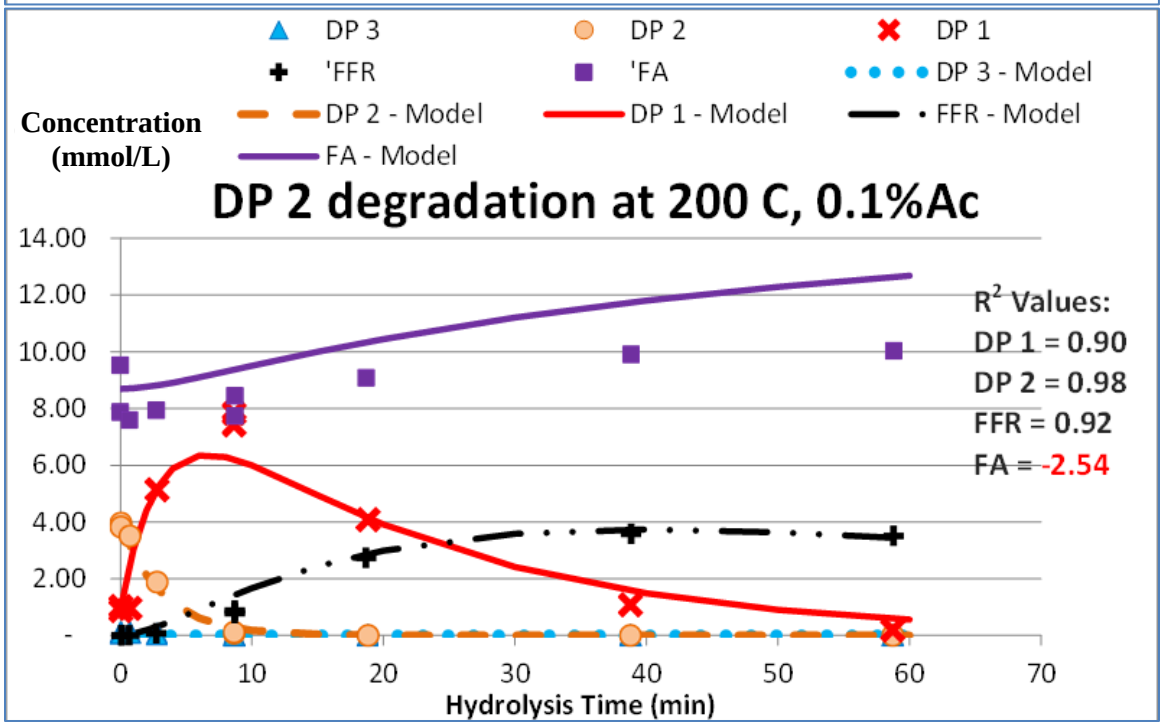

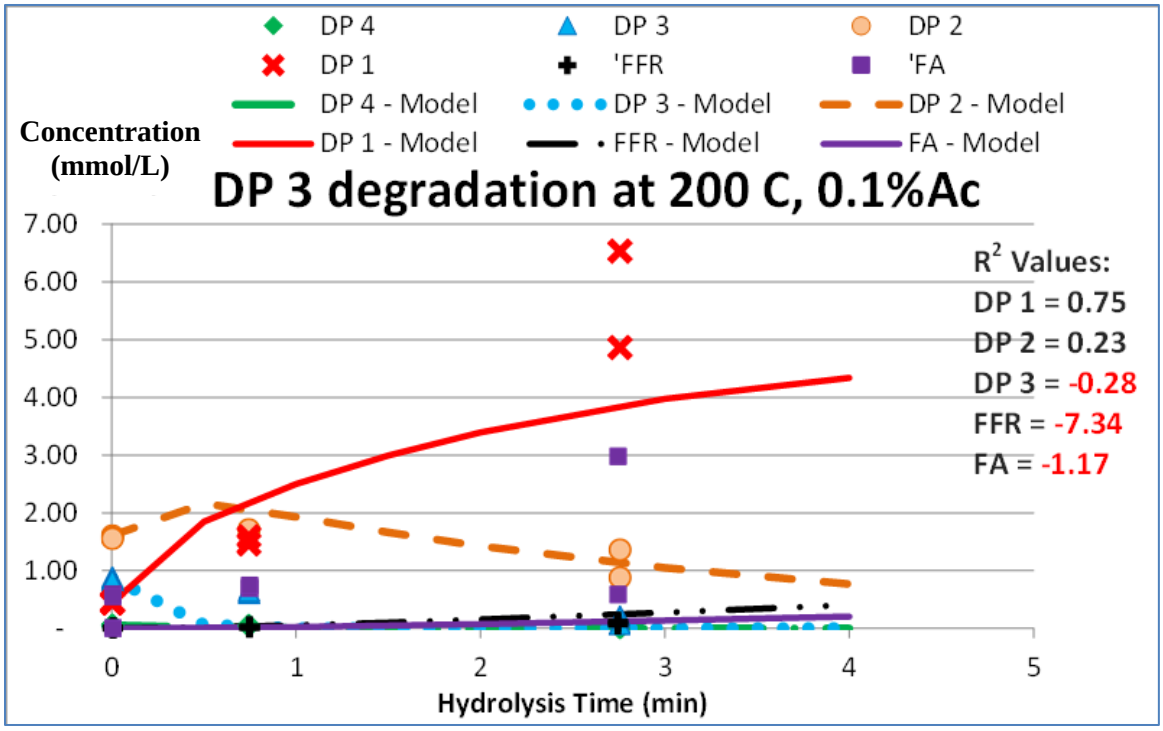
DP 4
DP 3
DP 2
DP 1
'FFR
'FA
DP 4 - Model
DP 3 - Model
DP 2 - Model
DP 1 - Model
FFR - Model
FA - Model
Concentration (mmol/L)
DP 3 degradation at 200 C, 0.1%Ac
7.00
6.00
5.00
4.00
3.00
2.00
1.00
-
0
1
2
3
4
5
Hydrolysis Time (min)
R2 Values:
DP 1 = 0.75
DP 2 = 0.23
DP 3 = -0.28
FFR = -7.34
FA = -1.17

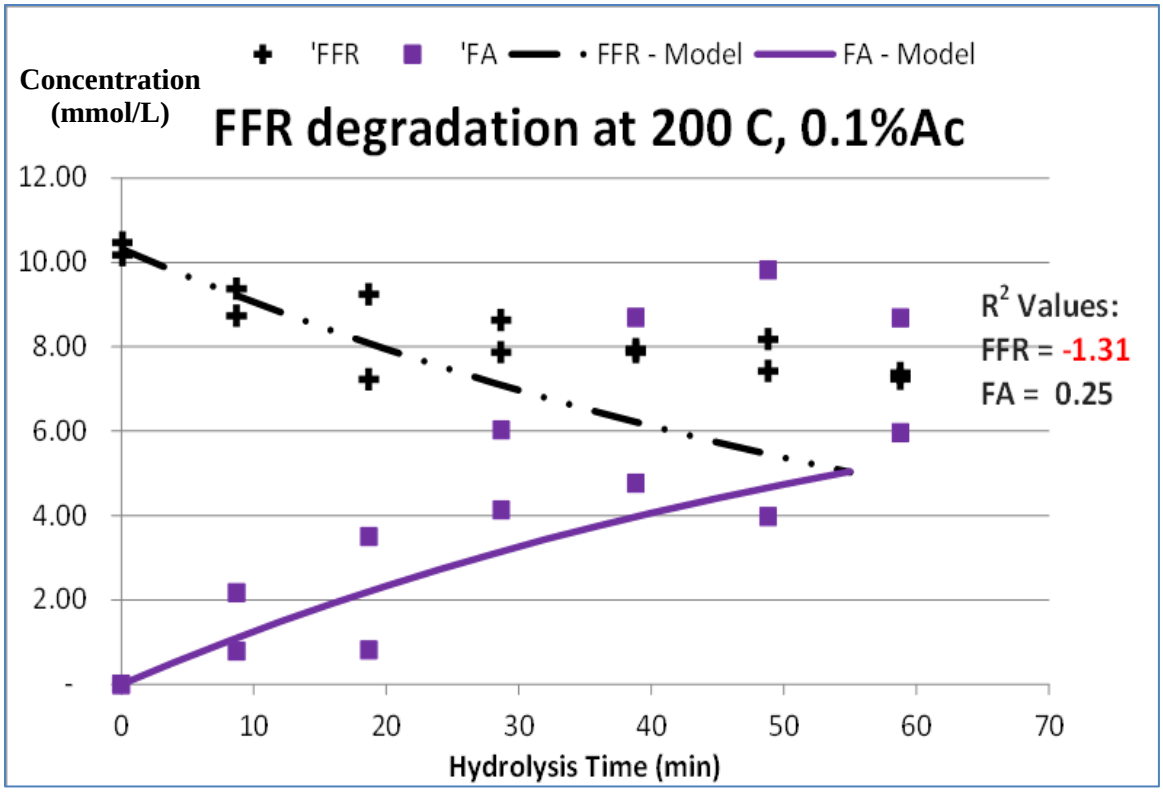
'FFR
'FA
FFR - Model
FA - Model
Concentration (mmol/L)
FFR degradation at 200 C, 0.1%Ac
12.00
10.00
8.00
6.00
4.00
2.00
-
0
10
20
30
40
50
60
70
Hydrolysis Time (min)
R2 Values:
FFR = -1.31
FA = 0.25

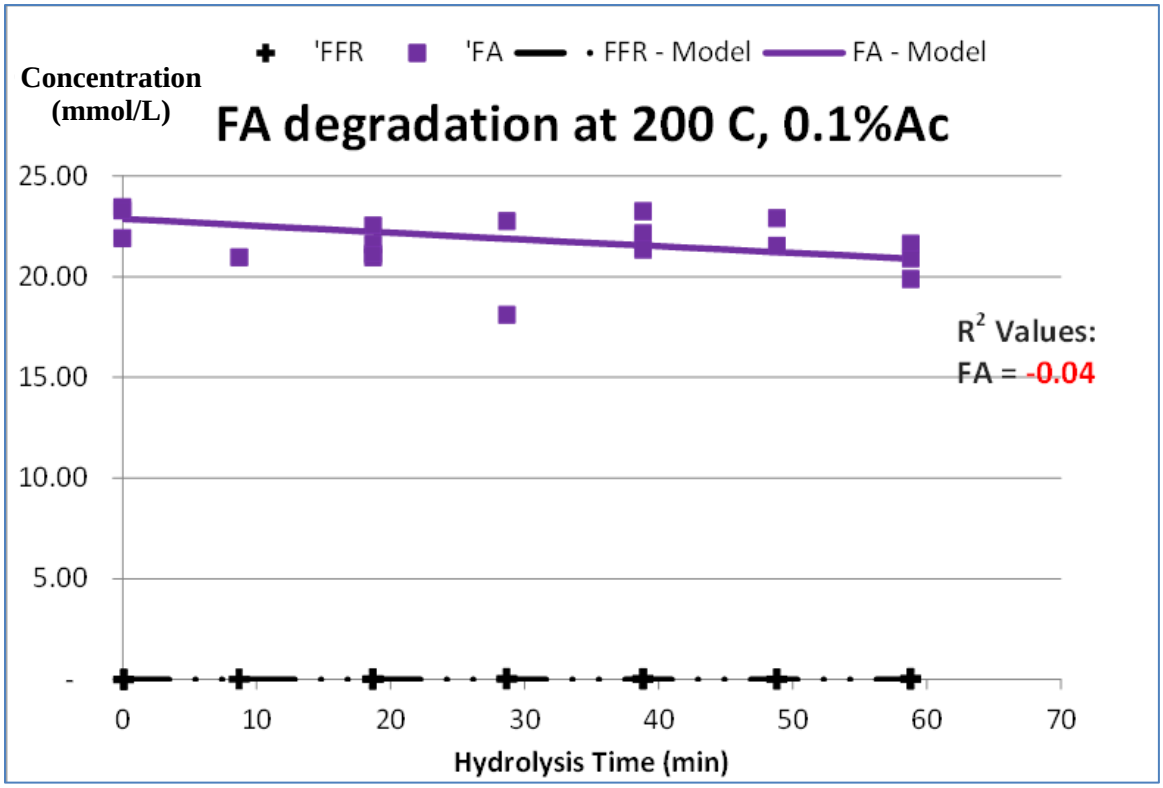
'FFR
'FA
FFR - Model
FA - Model
Concentration (mmol/L)
FA degradation at 200 C, 0.1%Ac
25.00
20.00
15.00
10.00
5.00
-
0
10
20
30
40
50
60
70
Hydrolysis Time (min)
R2 Values:
FA = -0.04

9. Hydrolysis Condition at 200 ˚C, 1% Acid (Model using non-normalized least sum of the squares method)

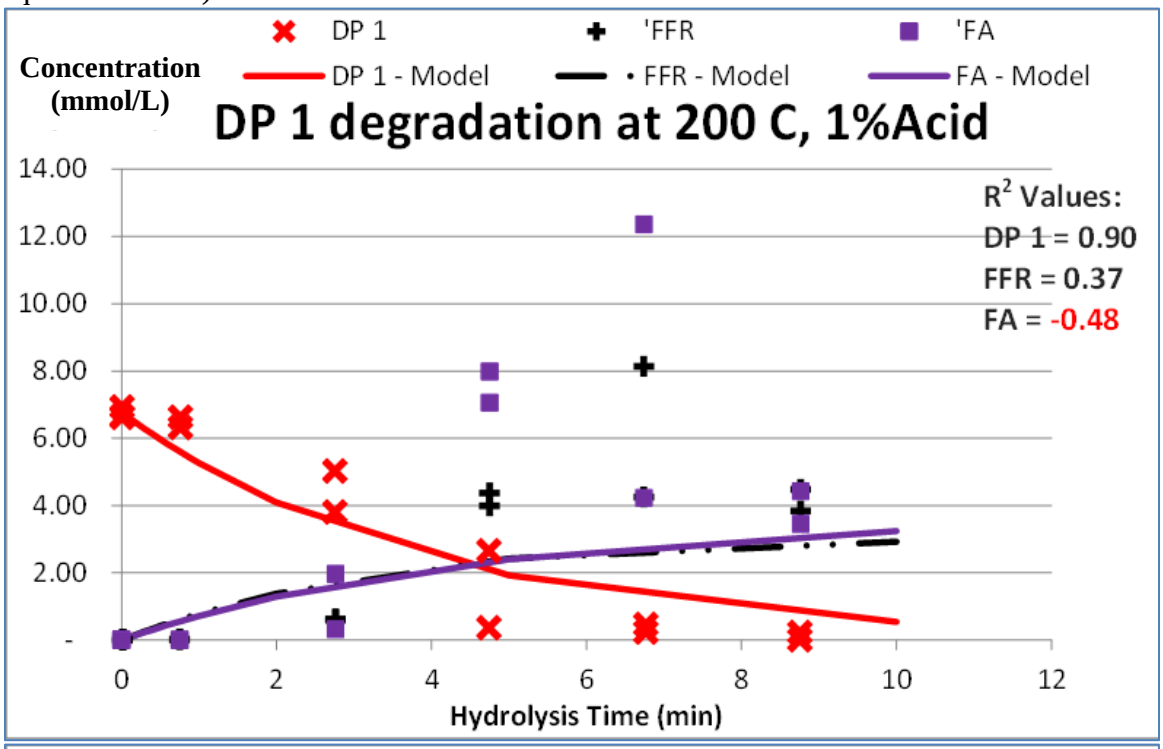

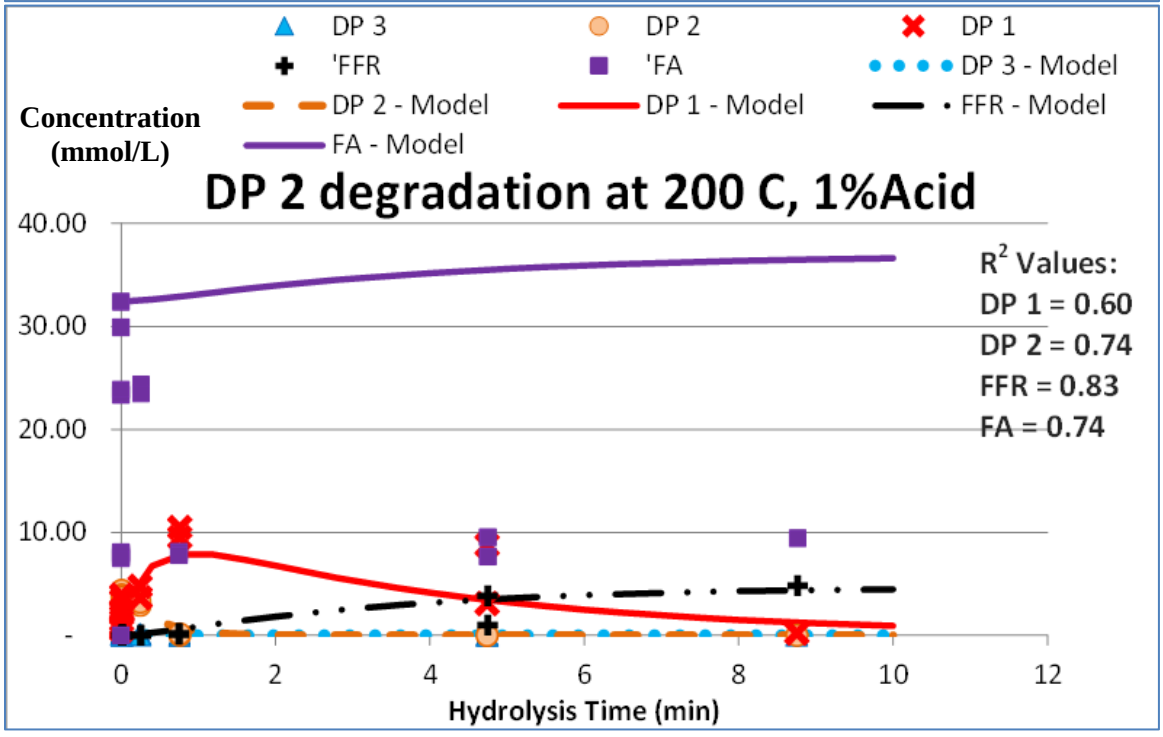

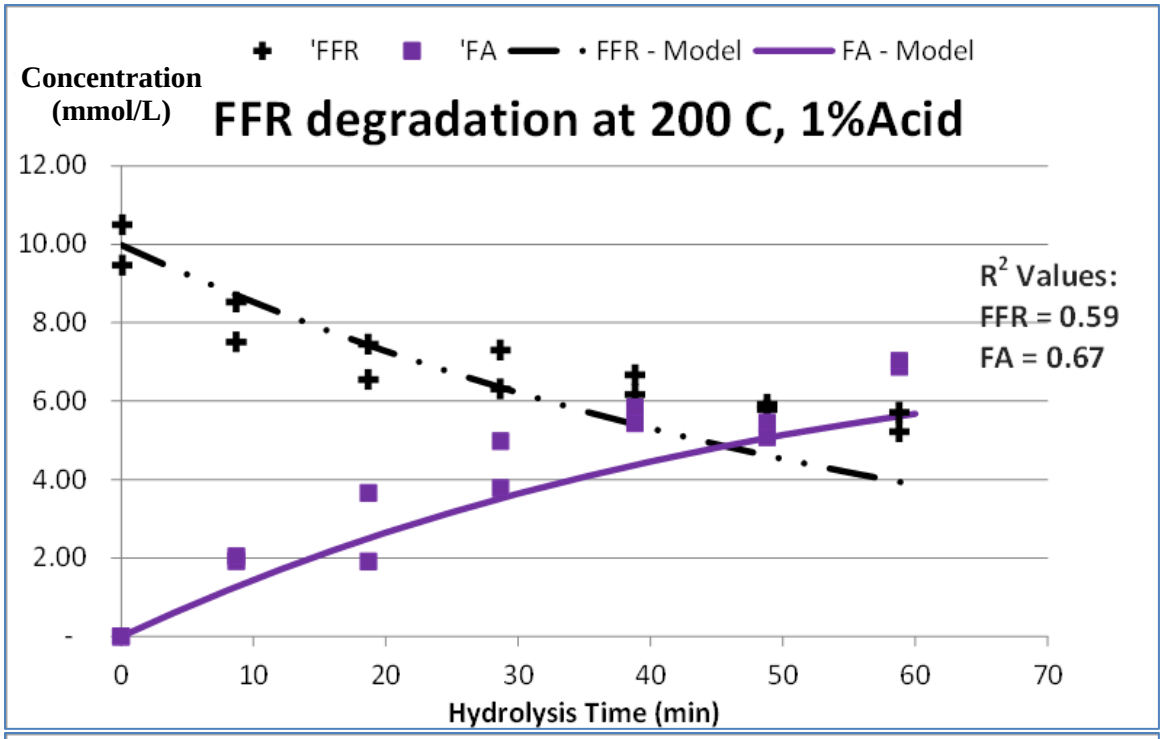
'FFR
'FA
FFR - Model
FA - Model
Concentration (mmol/L)
FFR degradation at 200 C, 1%Acid
12.00
10.00
8.00
6.00
4.00
2.00
-
0
10
20
30
40
50
60
70
Hydrolysis Time (min)
R2 Values:
FFR = 0.59
FA = 0.67

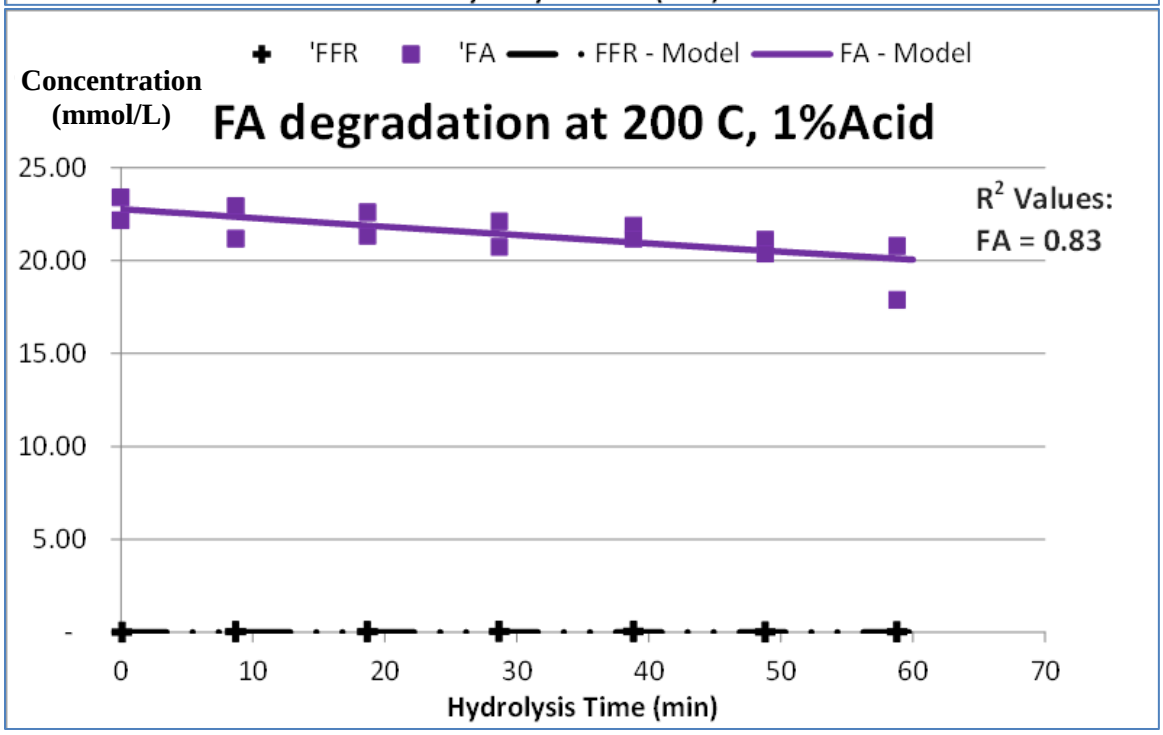
'FFR
'FA
FFR - Model
FA - Model
Concentration (mmol/L)
FA degradation at 200 C, 1%Acid
25.00
20.00
15.00
10.00
5.00
-
0
10
20
30
40
50
60
70
Hydrolysis Time (min)
R2 Values:
FA = 0.83

Appendix 5: Model using normalized least sum of the squares method.

Table 33: The summary of the degradation rate constants obtained using normalized least sum of the squares method, as shown by **Equation 26**.

	120 ˚C, Water	**120 ˚C, 0.1% Acid**	**120 ˚C, 1% Acid**	**160 ˚C, Water**	**160 ˚C, 0.1% Acid**	**160 ˚C, 1% Acid**	**200 ˚C, Water**	**200 ˚C, 0.1% Acid**	**200 ˚C, 1% Acid**
k_1	0.0267	0.0000	0.0013	0.0019	0.0035	0.0342	1.5040	0.1901	8.1059
k_2	0.0001	0.0000	0.1833	0.0042	0.0672	1.8048	0.2444	0.4032	4.5398
k_3				0.0164	0.1204	1.8188	0.1972	0.7808	
k_4				0.0381	0.0920	0.7849	0.4236		
k_F	0.0262	0.0001	0.0025	0.0017	0.0015	0.0815	0.0079	0.0106	0.0119
k_A	0.0001	0.0001	0.0007	0.0001	0.0015	0.0136	0.0468	0.0177	8.8924
k_{41}				0.0077	0.0788	0.7503	0.1083		
k_{42}				0.0304	0.0132	0.0347	0.3153		
k_{31}				0.0164	0.1204	1.8188	0.1972	0.7808	
k_{21}	0.0001	0.0000	0.1833	0.0042	0.0672	1.8048	0.2444	0.4032	4.5398
k_{1F}	0.0001	0.0000	0.0002	0.0003	0.0013	0.0016	0.0023	0.0024	0.0133
k_{1A}	0.0266	0.0000	0.0011	0.0016	0.0022	0.0326	1.5017	0.1878	8.0926
k_{FA}	0.0185	0.0001	0.0025	0.0017	0.0015	0.0500	0.0079	0.0106	0.0119
k_{FL}	0.0077	0.0000	0.0000	0.0000	0.0000	0.0315	0.0000	0.0000	0.0000
k_{AL}	0.0001	0.0001	0.0007	0.0001	0.0015	0.0136	0.0468	0.0177	8.8924

1. Hydrolysis Condition at 120 ˚C, Water (Model using normalized least sum of the squares method)

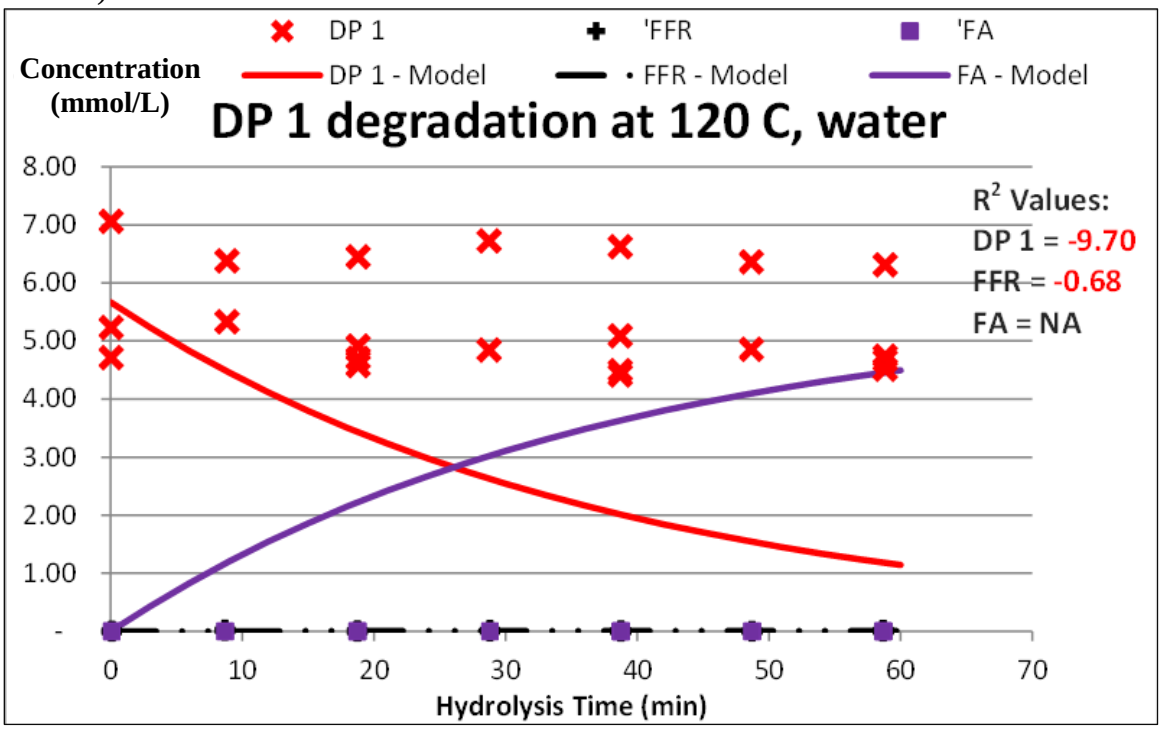

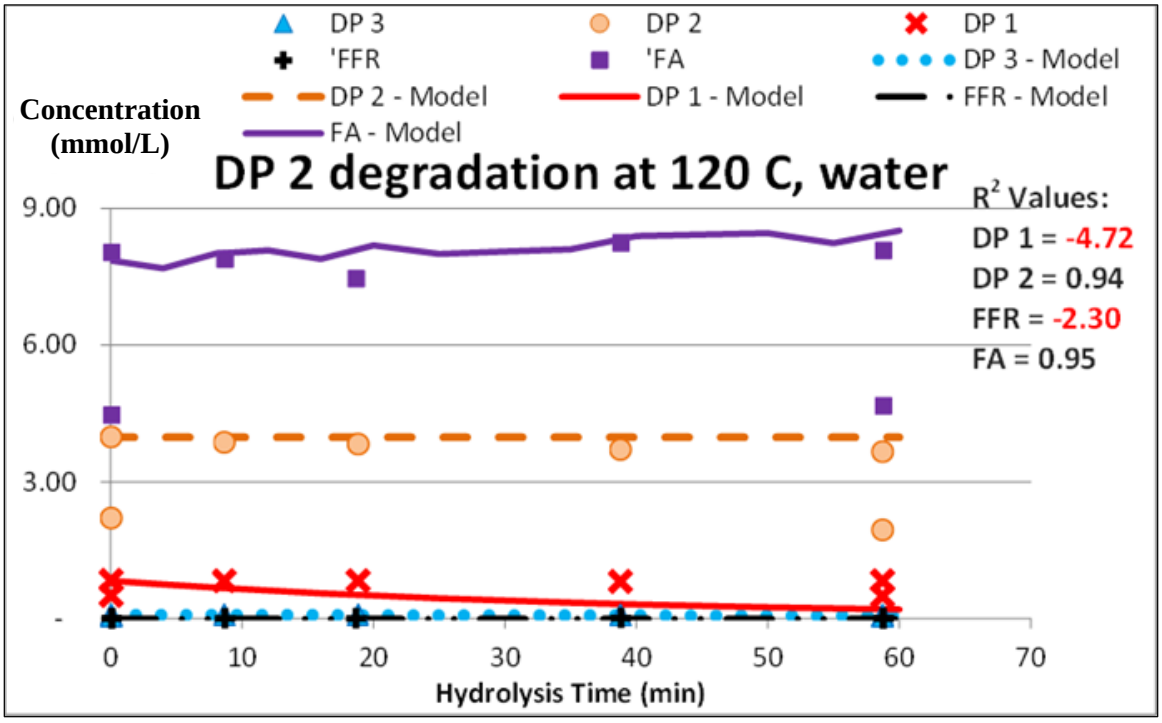

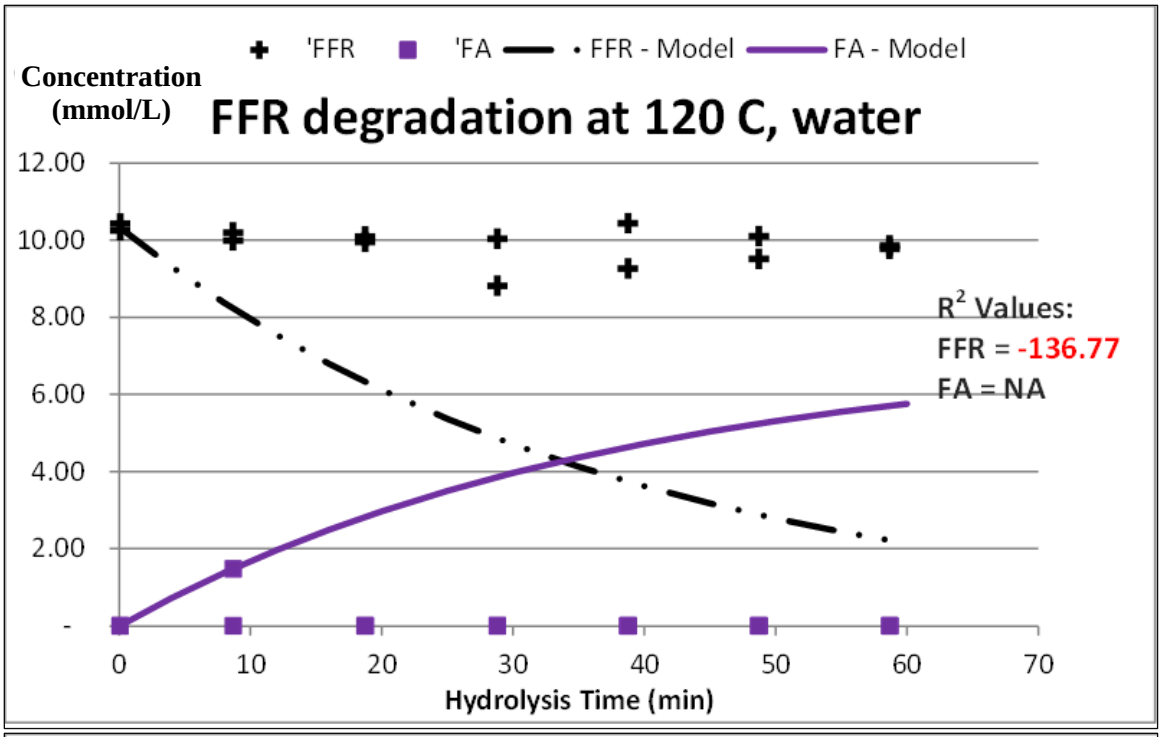
'FFR
'FA
FFR - Model
FA - Model
Concentration (mmol/L)
FFR degradation at 120 C, water
12.00
10.00
8.00
6.00
4.00
2.00
-
0
10
20
30
40
50
60
70
Hydrolysis Time (min)
R2 Values:
FFR = -136.77
FA = NA

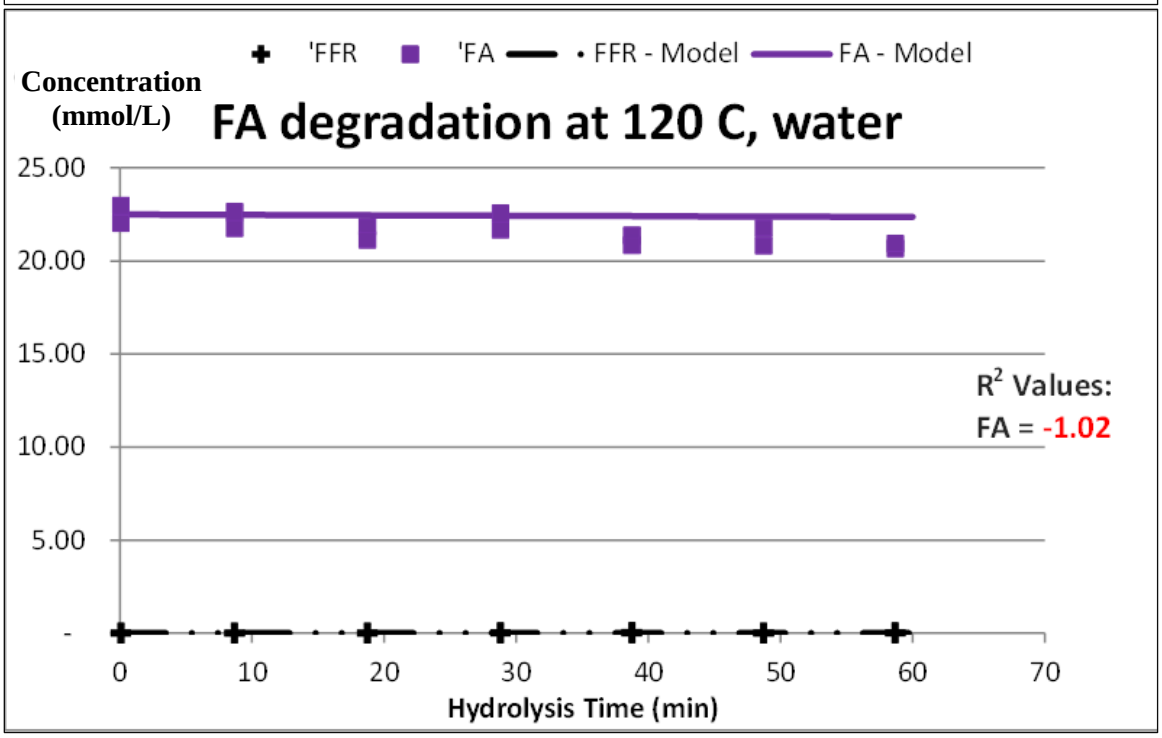
'FFR
'FA
FFR - Model
FA - Model
Concentration (mmol/L)
FA degradation at 120 C, water
25.00
20.00
15.00
10.00
5.00
-
0
10
20
30
40
50
60
70
Hydrolysis Time (min)
R2 Values:
FA = -1.02

2. Hydrolysis Condition at 120 ˚C, 0.1% Acid (Model using normalized least sum of the squares method)

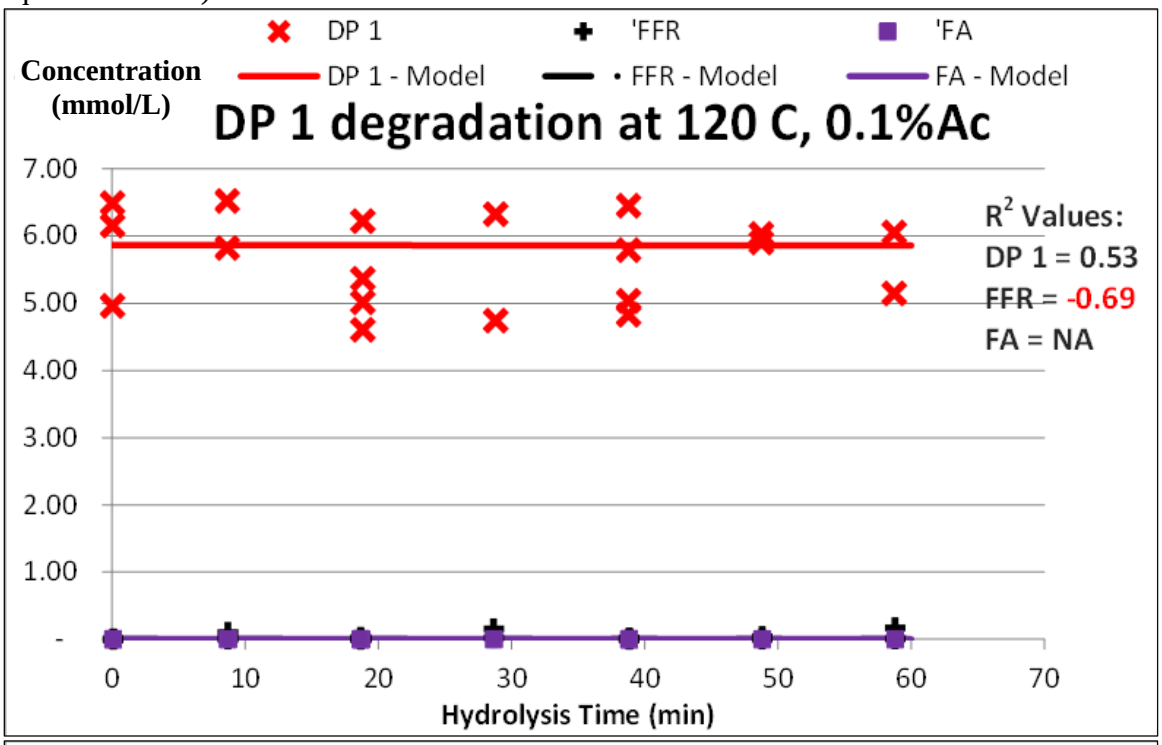

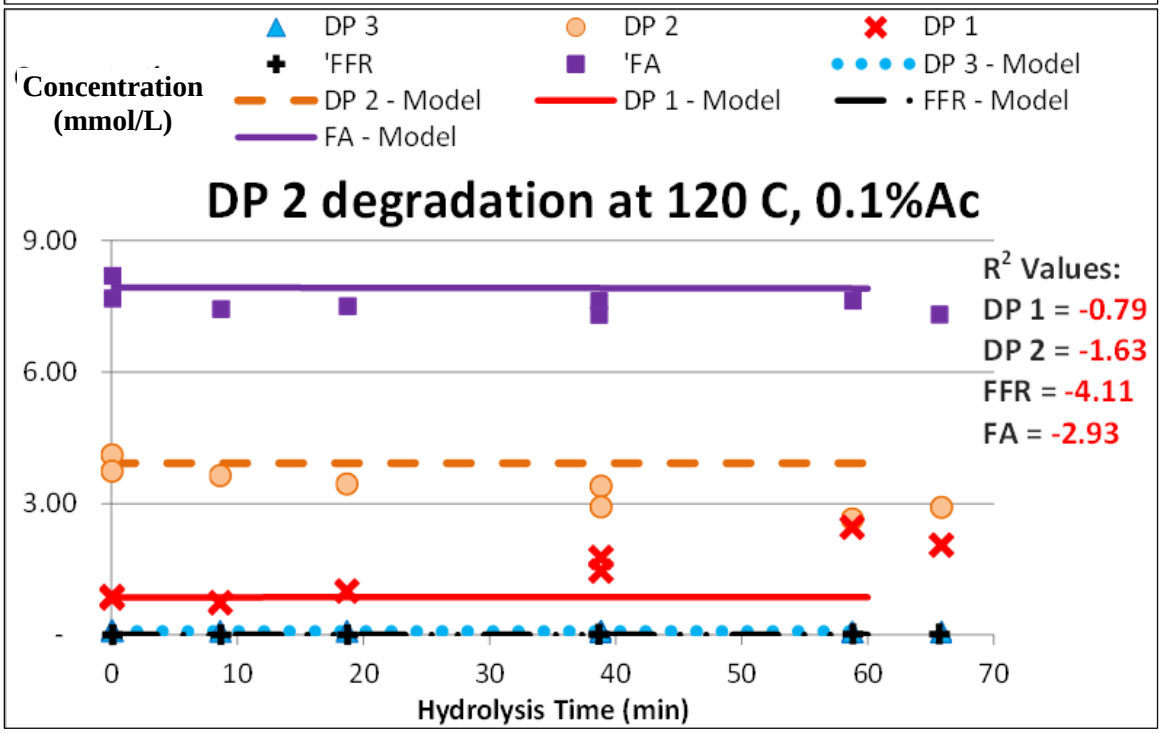

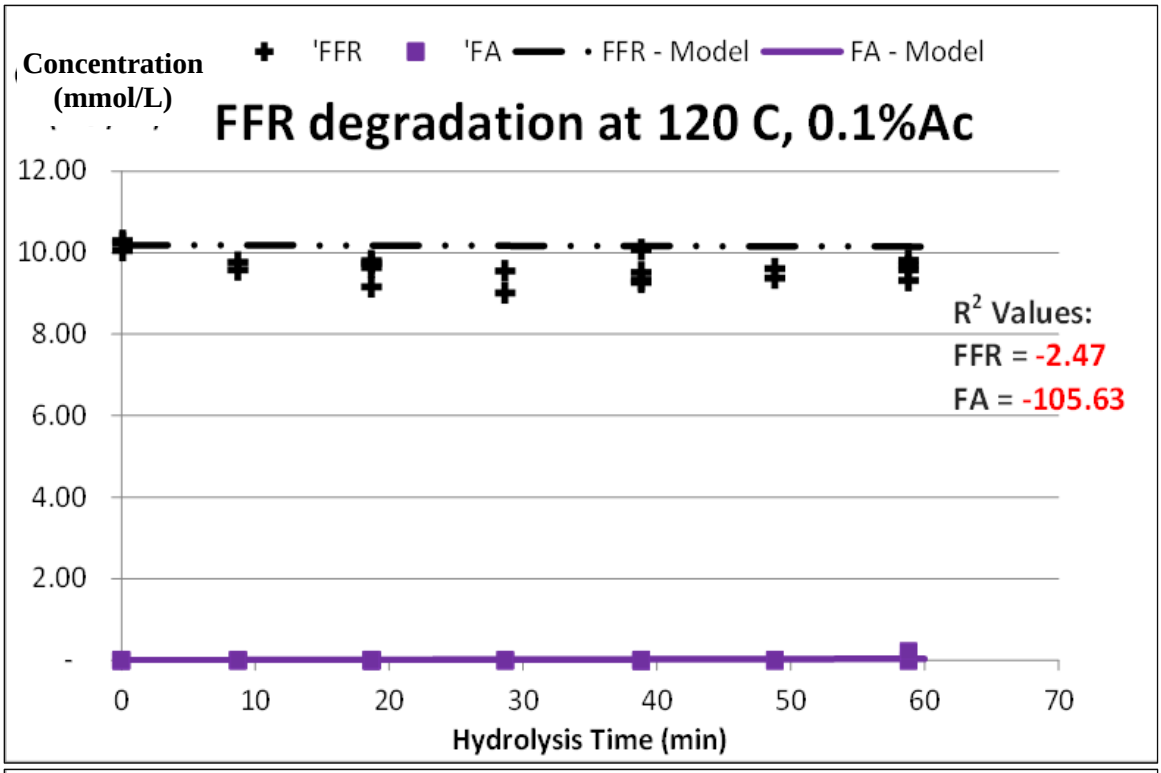
Concentration (mmol/L)
'FFR
'FA
FFR - Model
FA - Model
FFR degradation at 120 C, 0.1%Ac
12.00
10.00
8.00
6.00
4.00
2.00
-
0
10
20
30
40
50
60
70
Hydrolysis Time (min)
R² Values:
FFR = -2.47
FA = -105.63

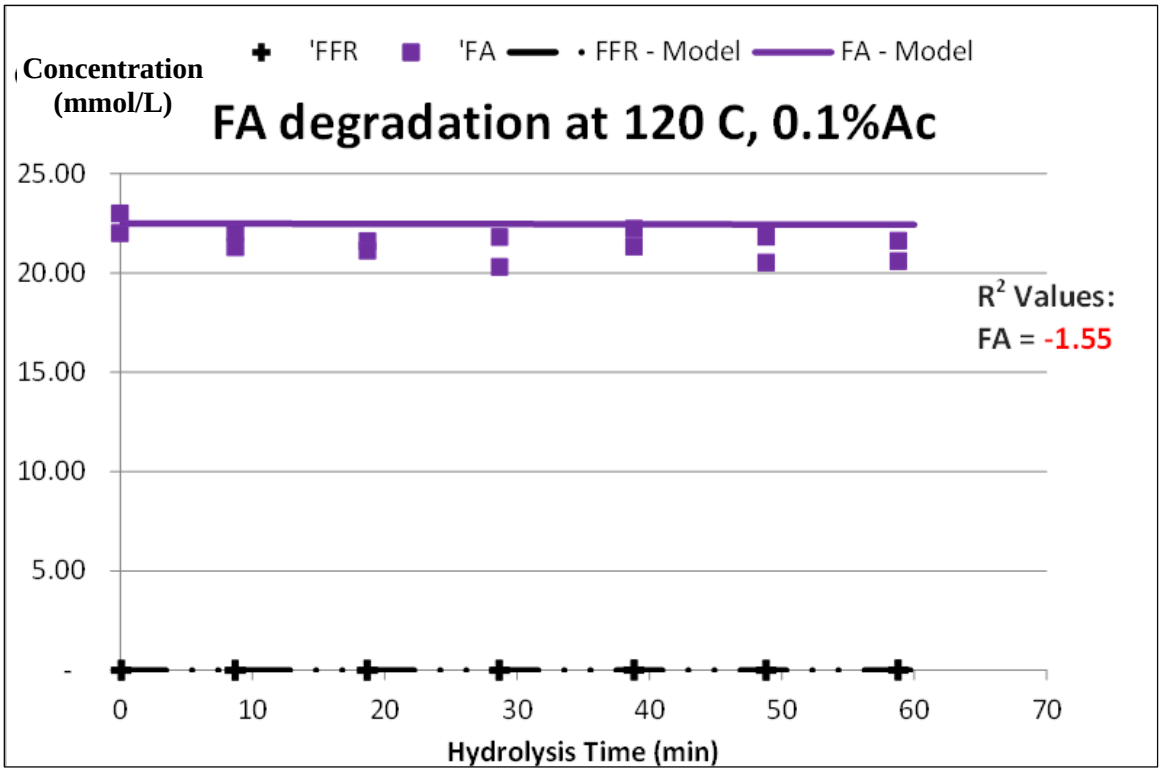
Concentration (mmol/L)
'FFR
'FA
FFR - Model
FA - Model
FA degradation at 120 C, 0.1%Ac
25.00
20.00
15.00
10.00
5.00
-
0
10
20
30
40
50
60
70
Hydrolysis Time (min)
R² Values:
FA = -1.55

3. Hydrolysis Condition at 120 ˚C, 1% Acid (Model using normalized least sum of the squares method)

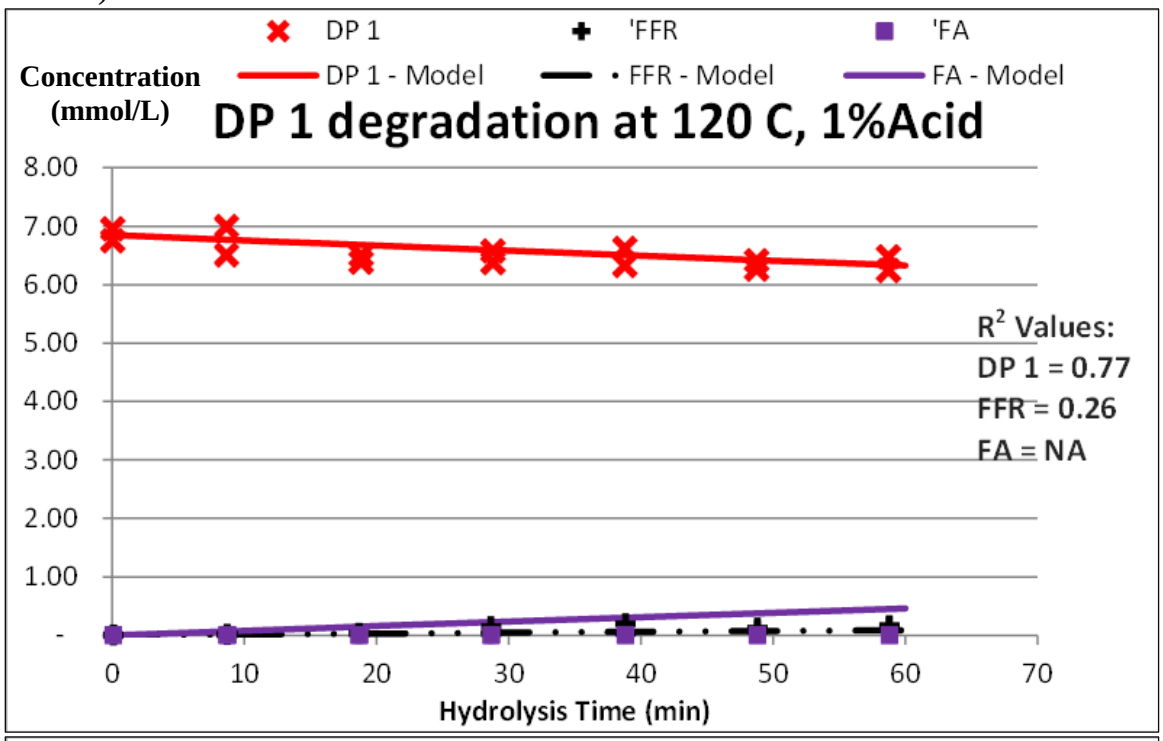

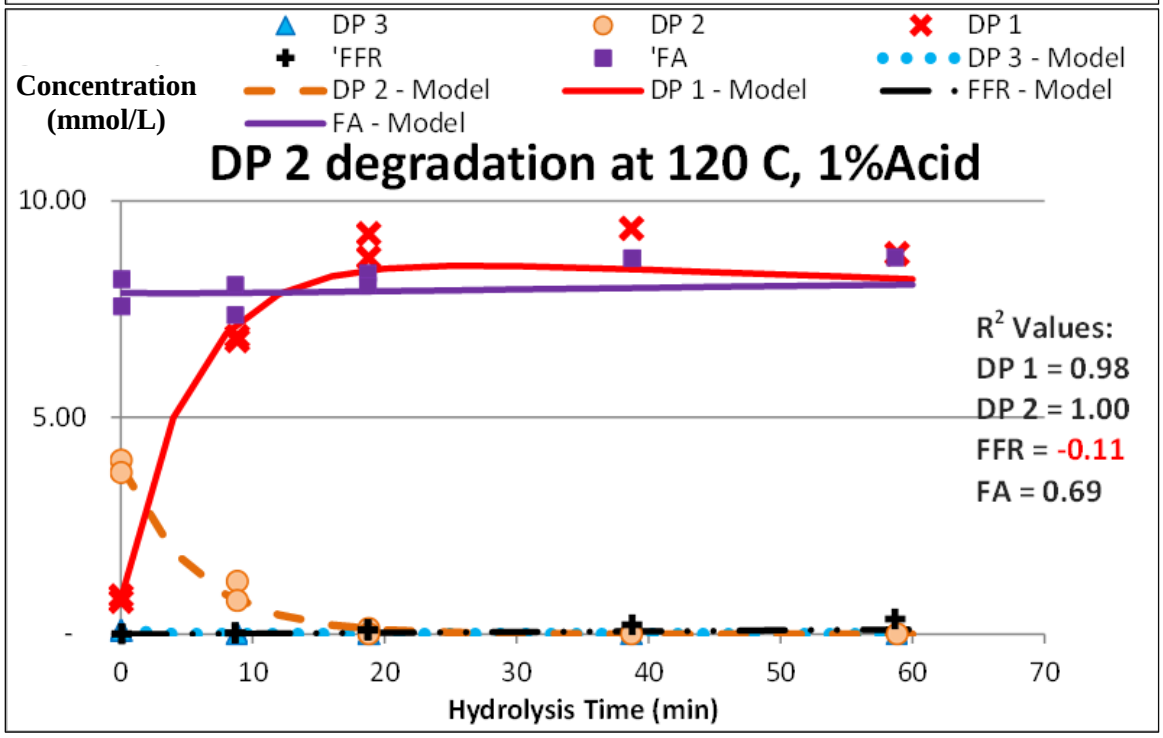

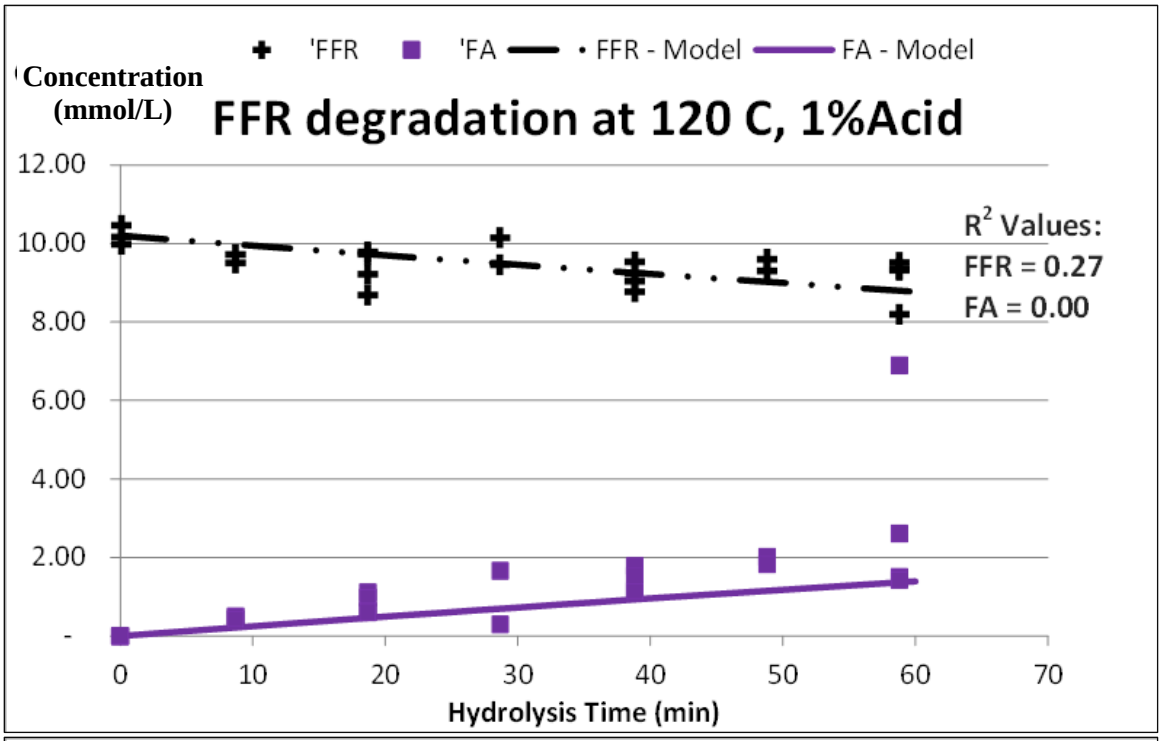
'FFR
'FA
FFR - Model
FA - Model
Concentration (mmol/L)
FFR degradation at 120 C, 1%Acid
12.00
10.00
8.00
6.00
4.00
2.00
-
0
10
20
30
40
50
60
70
Hydrolysis Time (min)
R2 Values:
FFR = 0.27
FA = 0.00

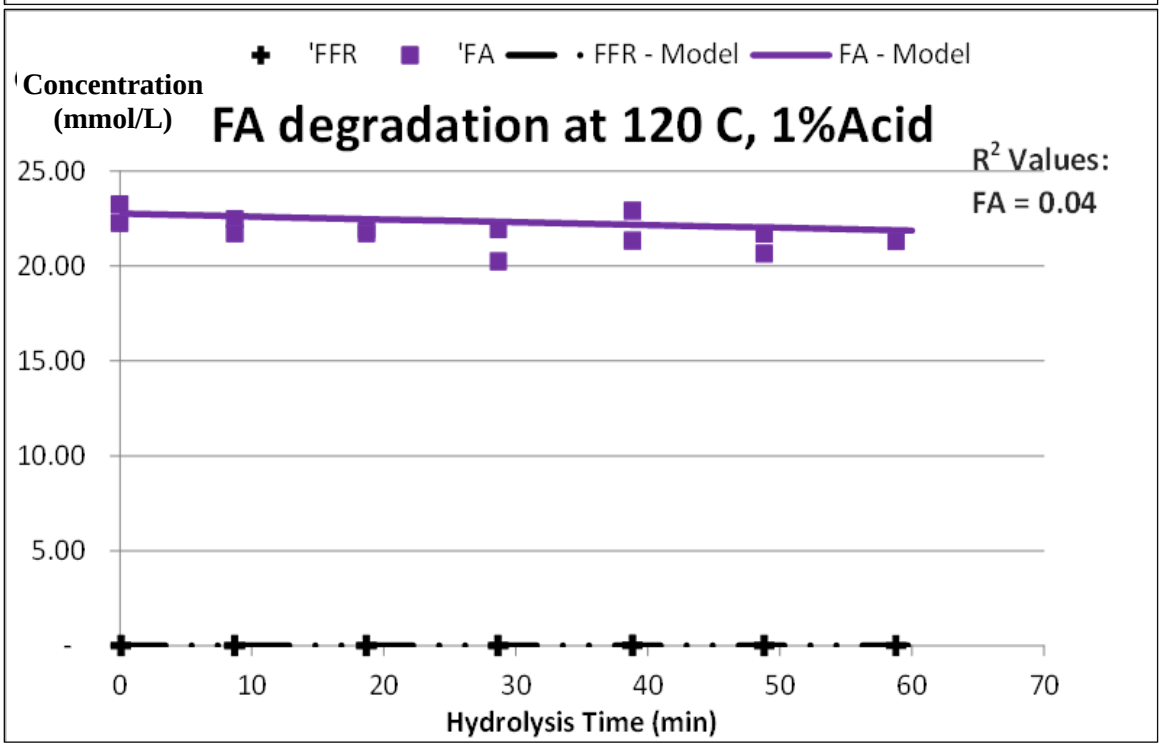
'FFR
'FA
FFR - Model
FA - Model
Concentration (mmol/L)
FA degradation at 120 C, 1%Acid
25.00
20.00
15.00
10.00
5.00
-
0
10
20
30
40
50
60
70
Hydrolysis Time (min)
R2 Values:
FA = 0.04

4. Hydrolysis Condition at 160 ˚C, Water (Model using normalized least sum of the squares method)

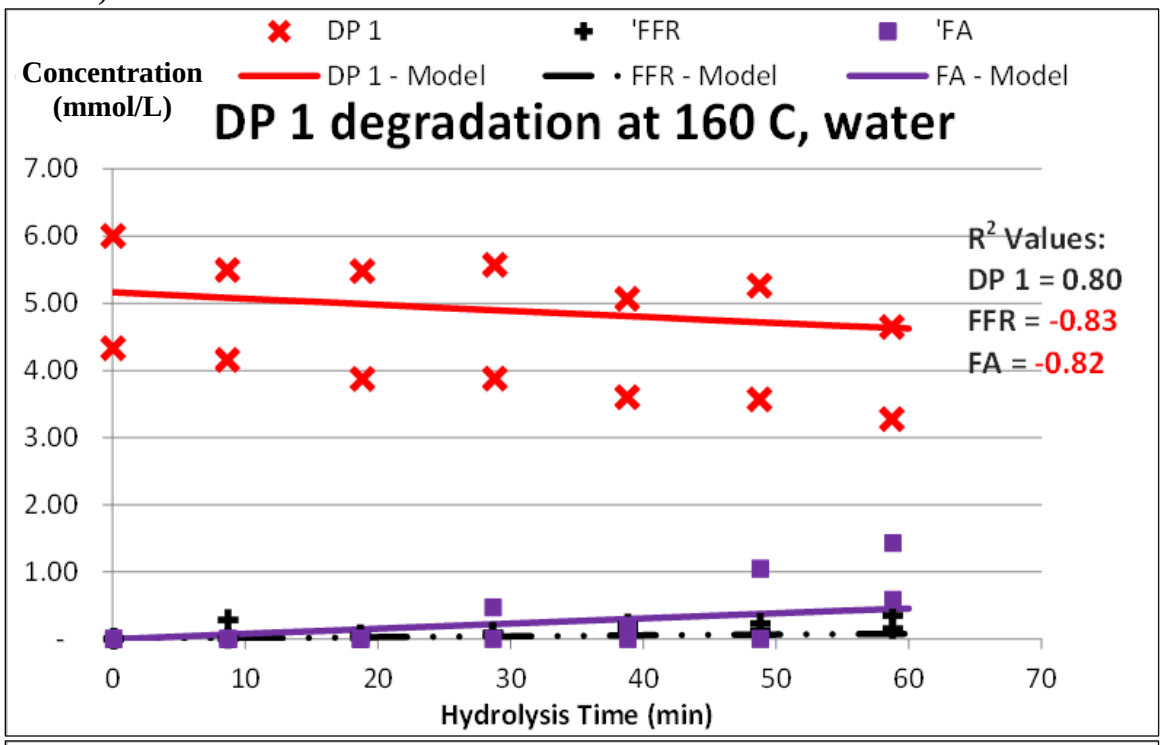

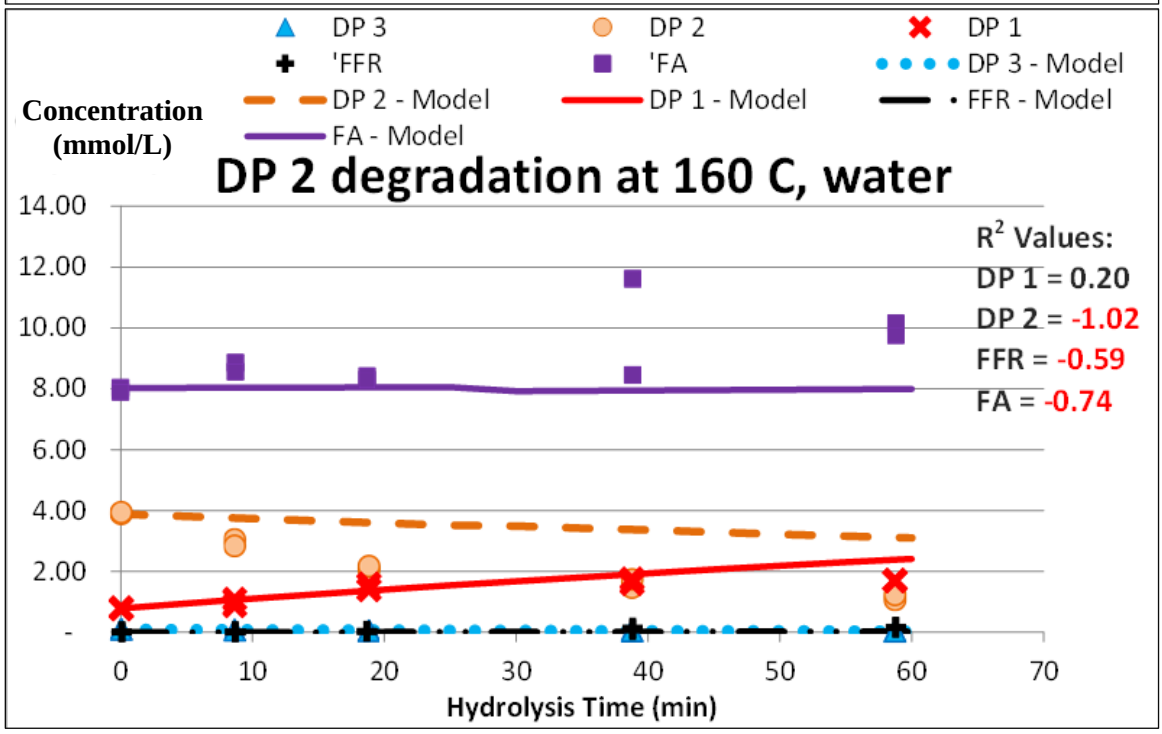

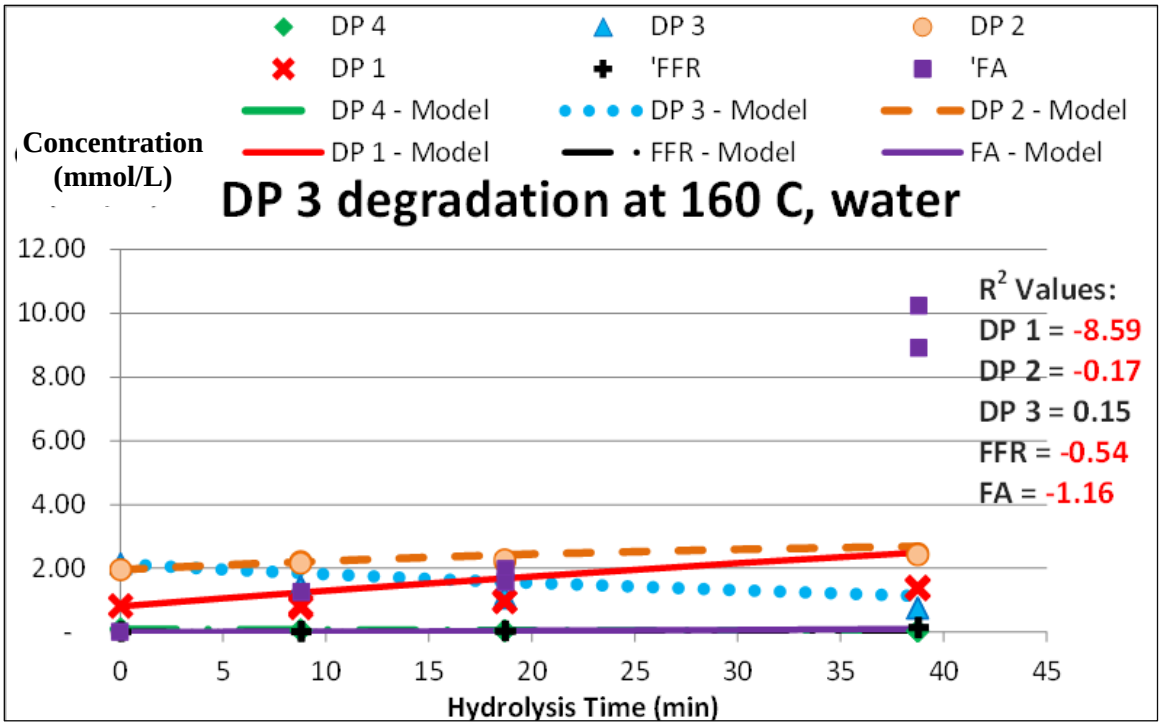
DP 4
DP 3
DP 2
DP 1
'FFR
'FA
DP 4 - Model
DP 3 - Model
DP 2 - Model
DP 1 - Model
FFR - Model
FA - Model
Concentration (mmol/L)
DP 3 degradation at 160 C, water
12.00
10.00
8.00
6.00
4.00
2.00
-
0
5
10
15
20
25
30
35
40
45
Hydrolysis Time (min)
R2 Values:
DP 1 = -8.59
DP 2 = -0.17
DP 3 = 0.15
FFR = -0.54
FA = -1.16

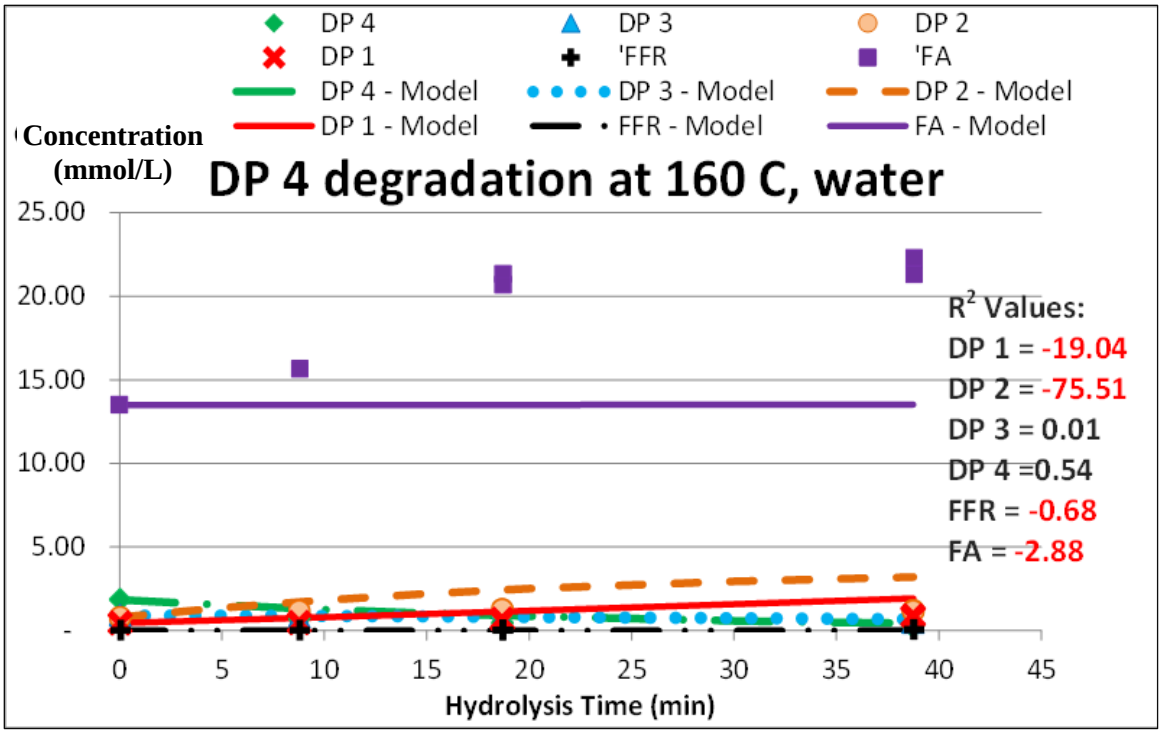
DP 4
DP 3
DP 2
DP 1
'FFR
'FA
DP 4 - Model
DP 3 - Model
DP 2 - Model
DP 1 - Model
FFR - Model
FA - Model
Concentration (mmol/L)
DP 4 degradation at 160 C, water
25.00
20.00
15.00
10.00
5.00
-
0
5
10
15
20
25
30
35
40
45
Hydrolysis Time (min)
R2 Values:
DP 1 = -19.04
DP 2 = -75.51
DP 3 = 0.01
DP 4 =0.54
FFR = -0.68
FA = -2.88

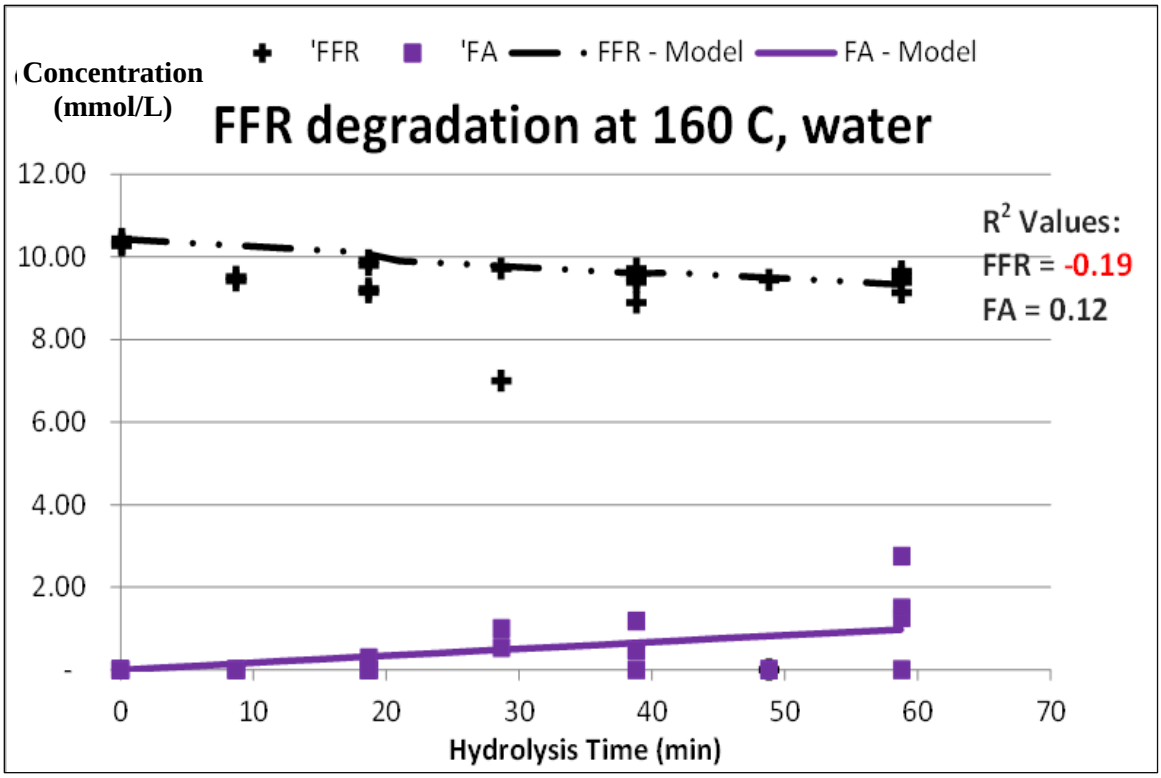
'FFR
'FA
FFR - Model
FA - Model
Concentration (mmol/L)
FFR degradation at 160 C, water
12.00
10.00
8.00
6.00
4.00
2.00
-
0
10
20
30
40
50
60
70
Hydrolysis Time (min)
R² Values:
FFR = -0.19
FA = 0.12

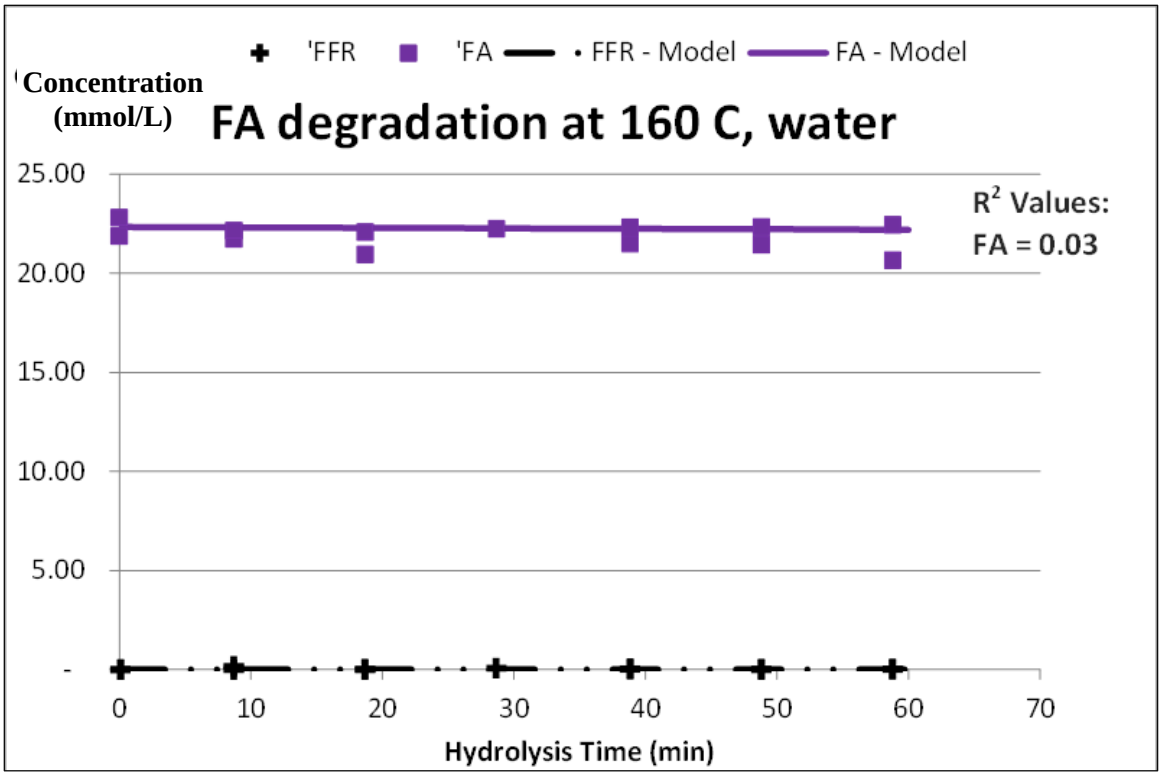
'FFR
'FA
FFR - Model
FA - Model
Concentration (mmol/L)
FA degradation at 160 C, water
25.00
20.00
15.00
10.00
5.00
-
0
10
20
30
40
50
60
70
Hydrolysis Time (min)
R² Values:
FA = 0.03

5. Hydrolysis Condition at 160 ˚C, 0.1% Acid (Model using normalized least sum of the squares method)

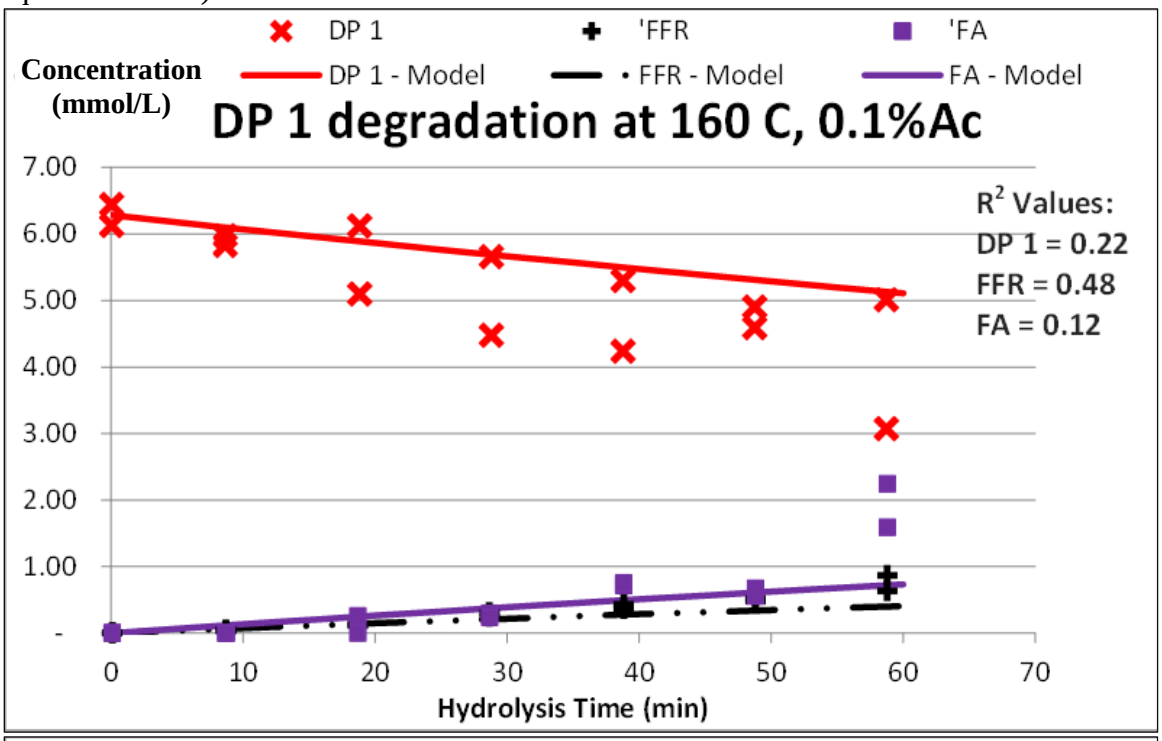

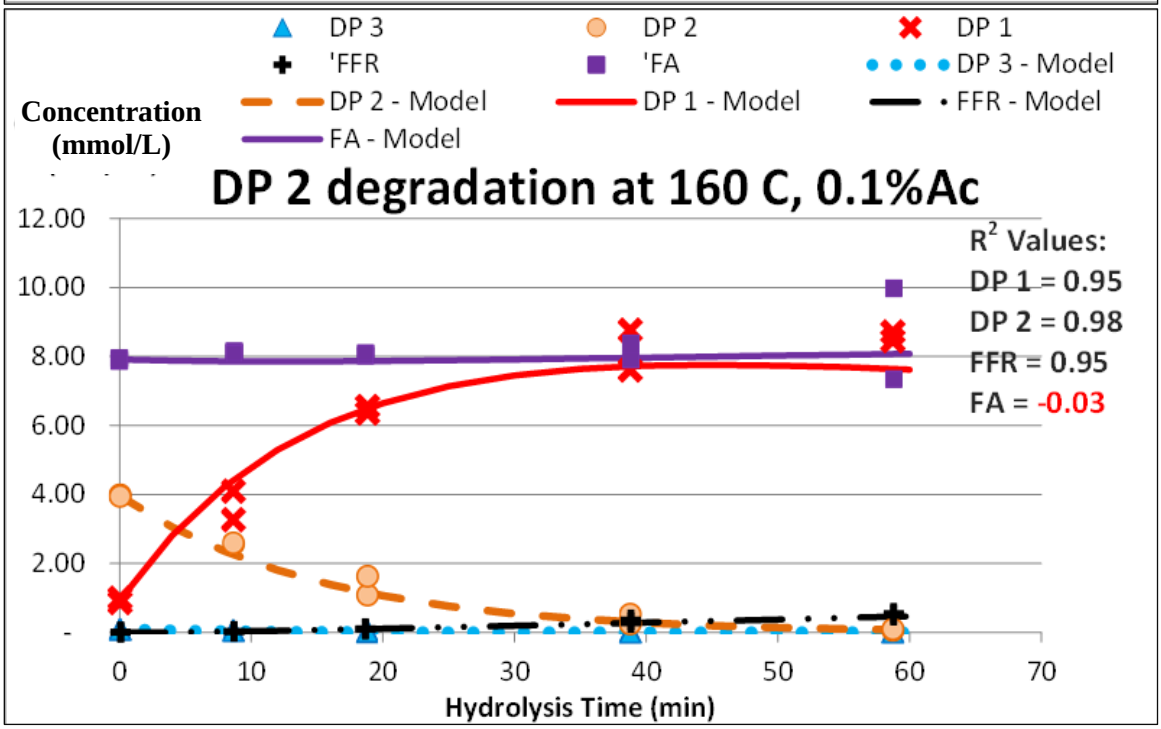

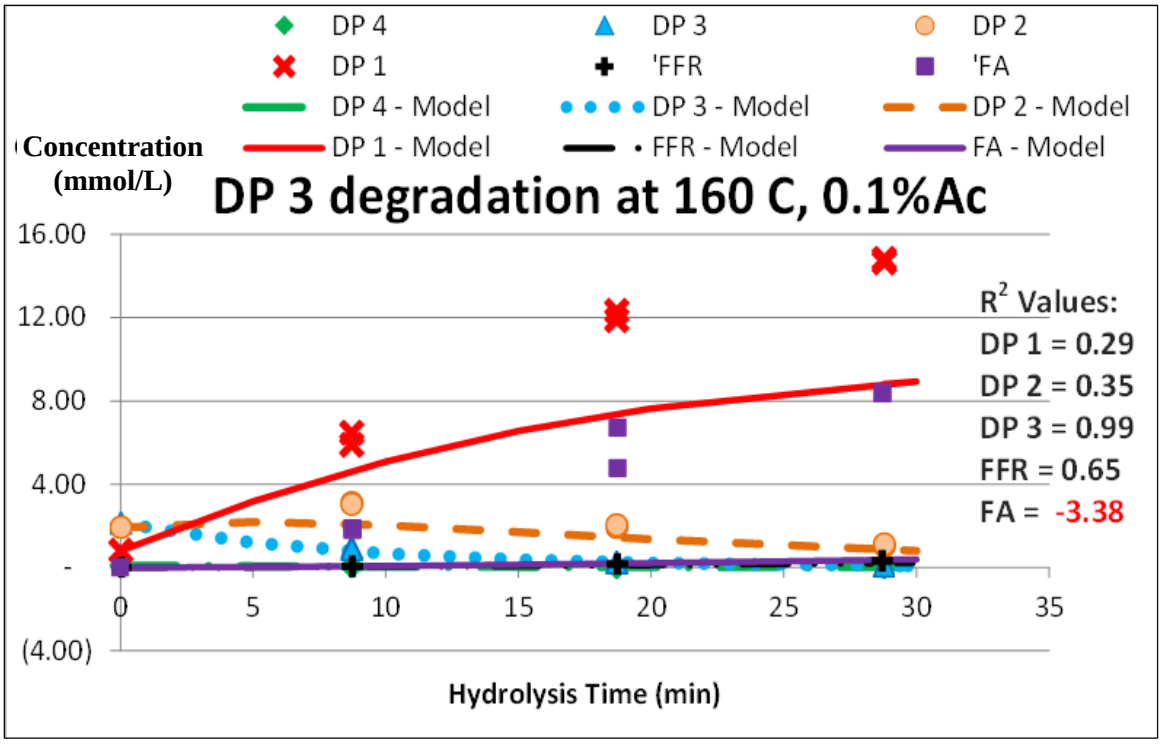
DP 4
DP 3
DP 2
DP 1
'FFR
'FA
DP 4 - Model
DP 3 - Model
DP 2 - Model
DP 1 - Model
FFR - Model
FA - Model
Concentration (mmol/L)
DP 3 degradation at 160 C, 0.1%Ac
16.00
12.00
8.00
4.00
-
(4.00)
0
5
10
15
20
25
30
35
Hydrolysis Time (min)
R2 Values:
DP 1 = 0.29
DP 2 = 0.35
DP 3 = 0.99
FFR = 0.65
FA = -3.38

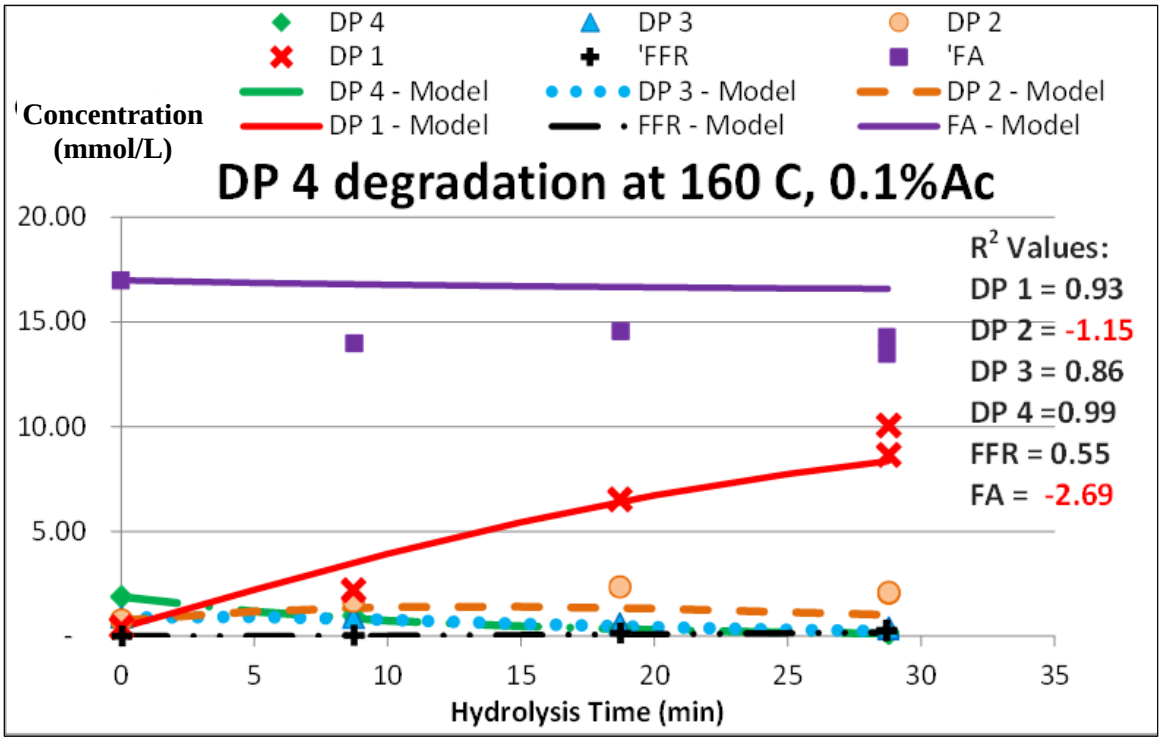
DP 4
DP 3
DP 2
DP 1
'FFR
'FA
DP 4 - Model
DP 3 - Model
DP 2 - Model
DP 1 - Model
FFR - Model
FA - Model
Concentration (mmol/L)
DP 4 degradation at 160 C, 0.1%Ac
20.00
15.00
10.00
5.00
-
0
5
10
15
20
25
30
35
Hydrolysis Time (min)
R2 Values:
DP 1 = 0.93
DP 2 = -1.15
DP 3 = 0.86
DP 4 =0.99
FFR = 0.55
FA = -2.69

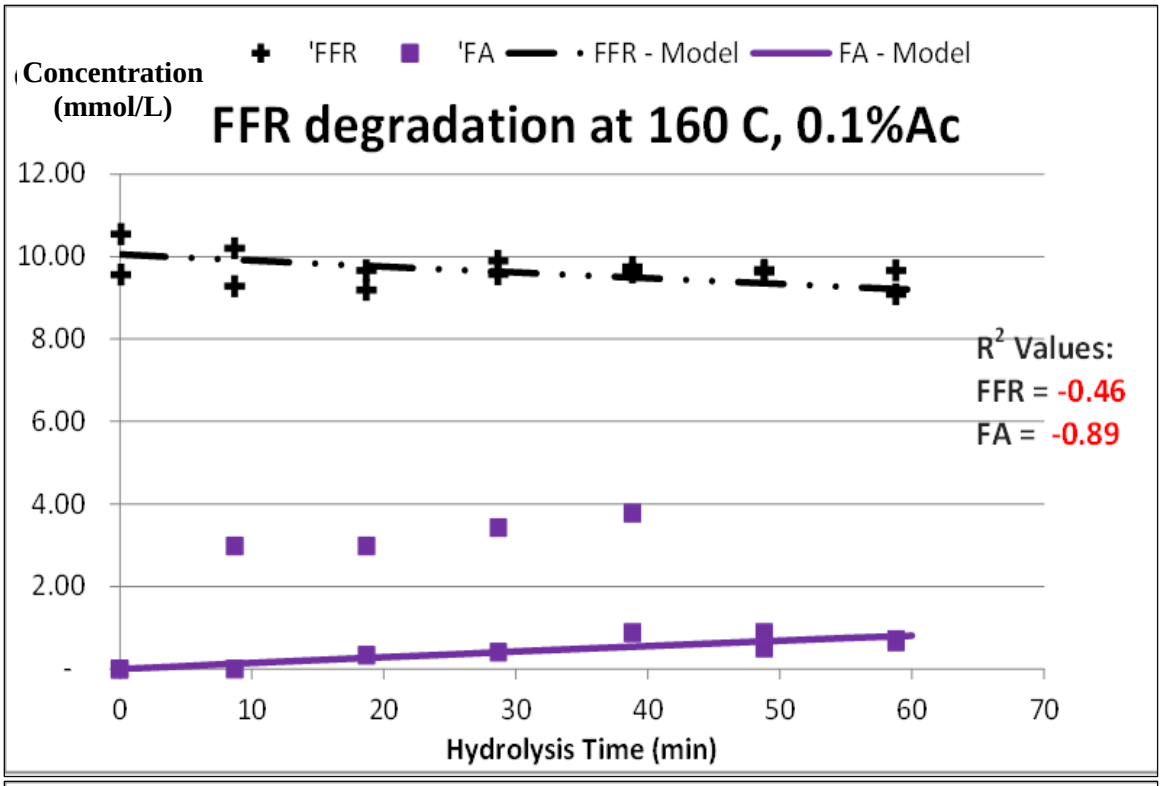
'FFR
'FA
FFR - Model
FA - Model
Concentration (mmol/L)
FFR degradation at 160 C, 0.1%Ac
12.00
10.00
8.00
6.00
4.00
2.00
-
0
10
20
30
40
50
60
70
Hydrolysis Time (min)
R² Values:
FFR = -0.46
FA = -0.89

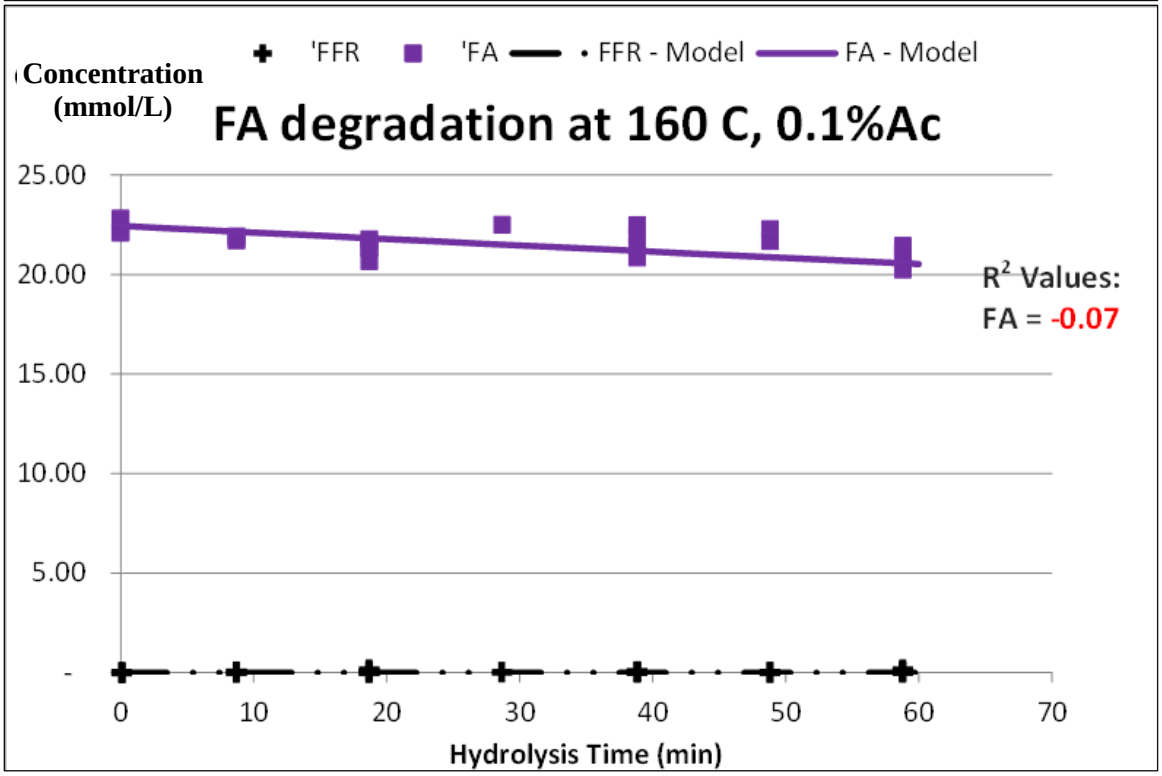
'FFR
'FA
FFR - Model
FA - Model
Concentration (mmol/L)
FA degradation at 160 C, 0.1%Ac
25.00
20.00
15.00
10.00
5.00
-
0
10
20
30
40
50
60
70
Hydrolysis Time (min)
R² Values:
FA = -0.07

6. Hydrolysis Condition at 160 ˚C, 1% Acid (Model using normalized least sum of the squares method)

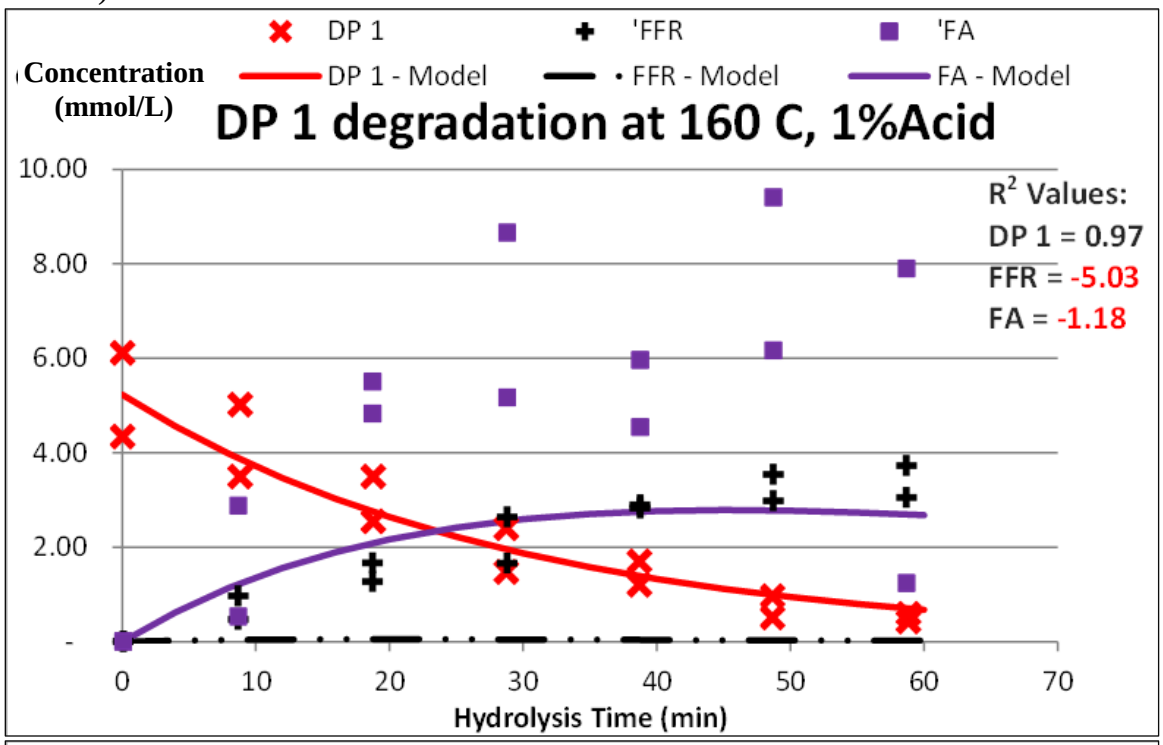

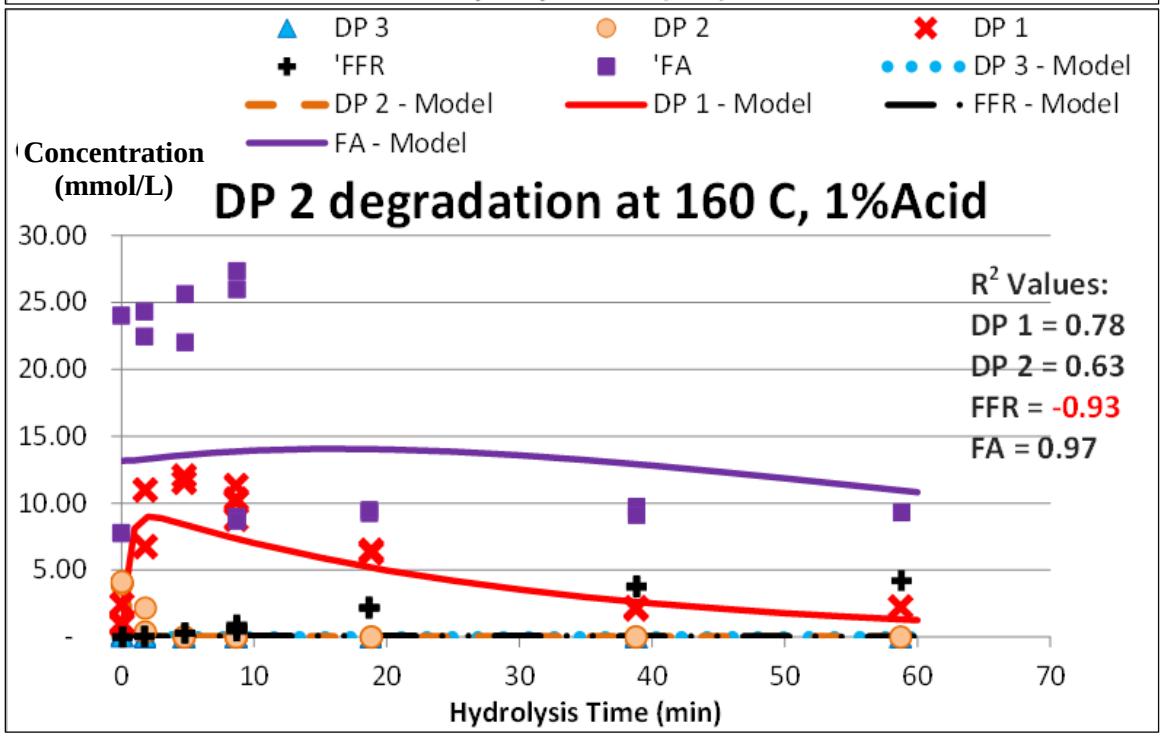

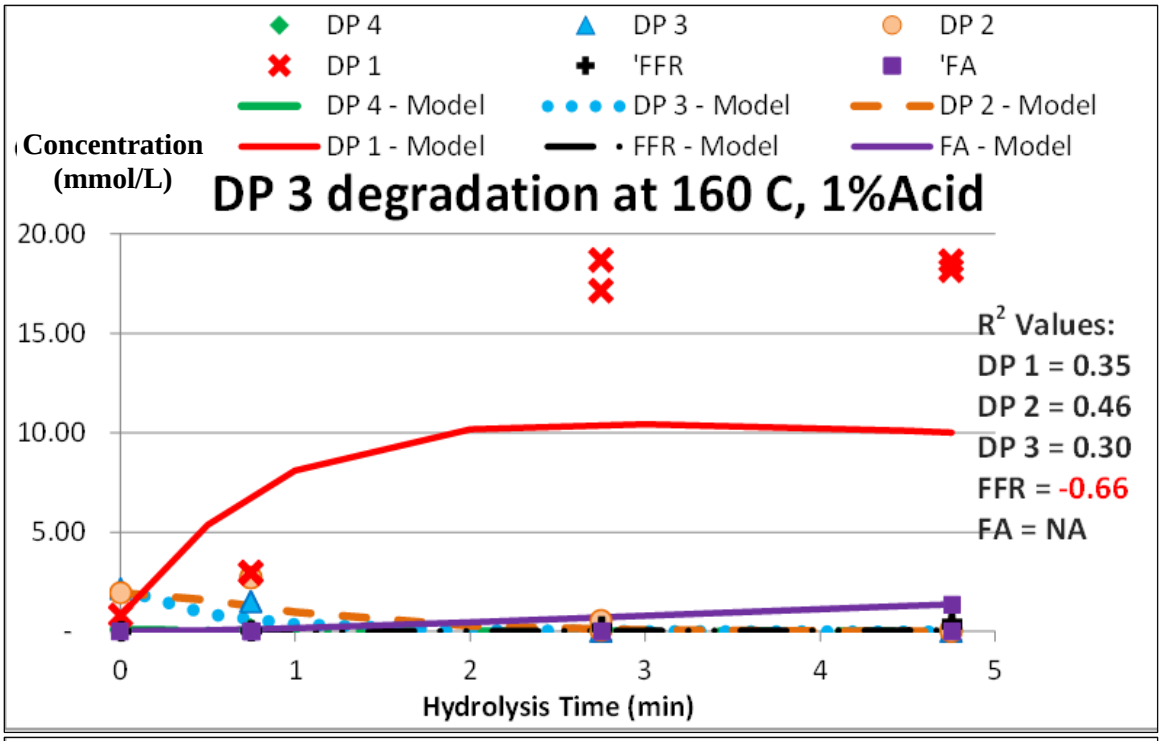
DP 4
DP 3
DP 2
DP 1
'FFR
'FA
DP 4 - Model
DP 3 - Model
DP 2 - Model
DP 1 - Model
FFR - Model
FA - Model
Concentration (mmol/L)
DP 3 degradation at 160 C, 1%Acid
20.00
15.00
10.00
5.00
-
0
1
2
3
4
5
Hydrolysis Time (min)
R² Values:
DP 1 = 0.35
DP 2 = 0.46
DP 3 = 0.30
FFR = -0.66
FA = NA

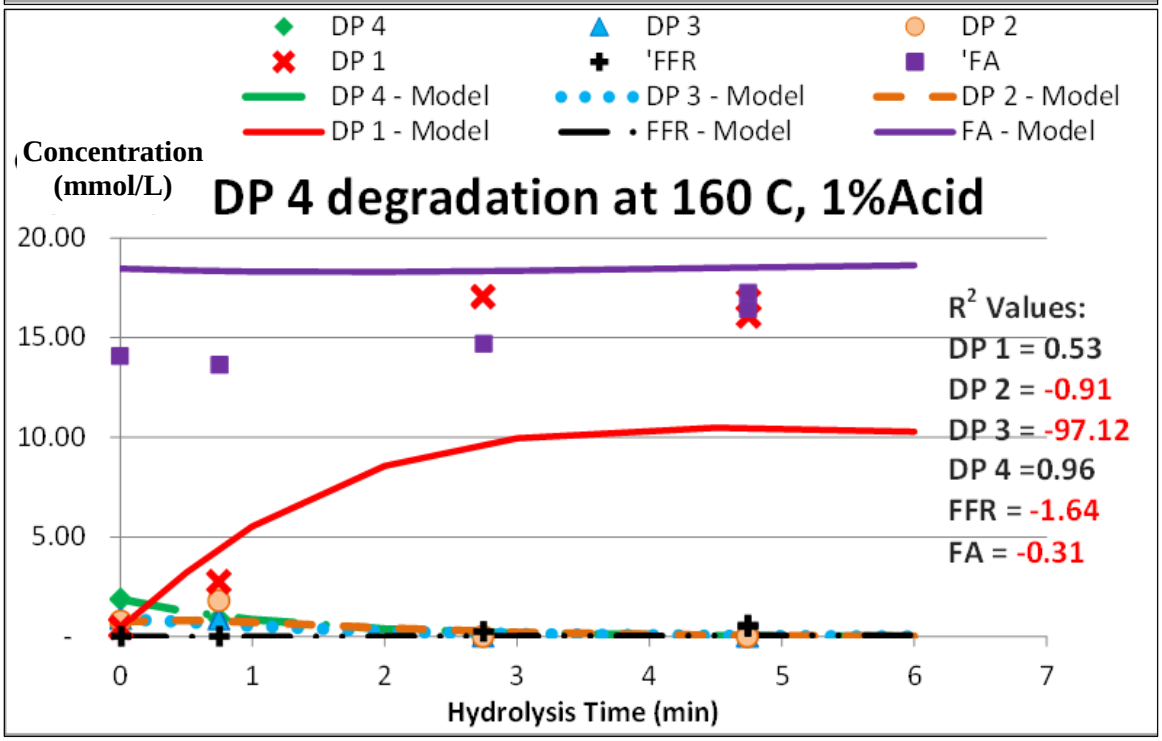
DP 4
DP 3
DP 2
DP 1
'FFR
'FA
DP 4 - Model
DP 3 - Model
DP 2 - Model
DP 1 - Model
FFR - Model
FA - Model
Concentration (mmol/L)
DP 4 degradation at 160 C, 1%Acid
20.00
15.00
10.00
5.00
-
0
1
2
3
4
5
6
7
Hydrolysis Time (min)
R² Values:
DP 1 = 0.53
DP 2 = -0.91
DP 3 = -97.12
DP 4 =0.96
FFR = -1.64
FA = -0.31

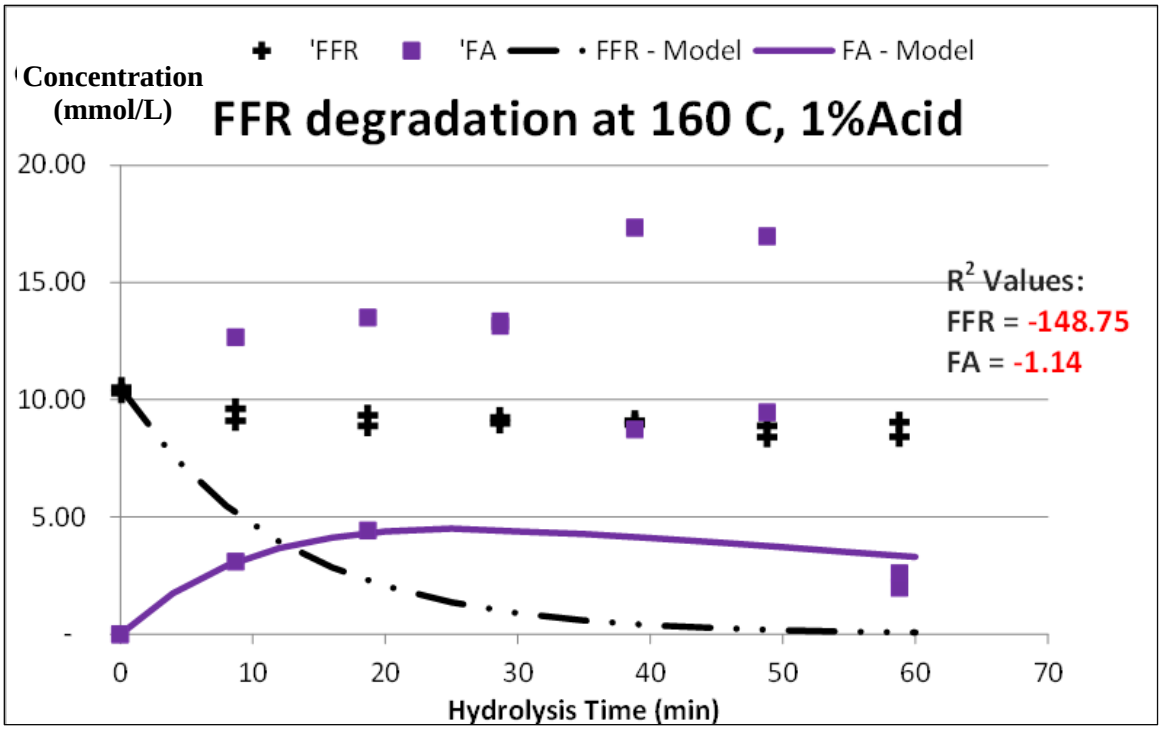
'FFR
'FA
FFR - Model
FA - Model
Concentration (mmol/L)
FFR degradation at 160 C, 1%Acid
20.00
15.00
10.00
5.00
-
0
10
20
30
40
50
60
70
Hydrolysis Time (min)
R2 Values:
FFR = -148.75
FA = -1.14

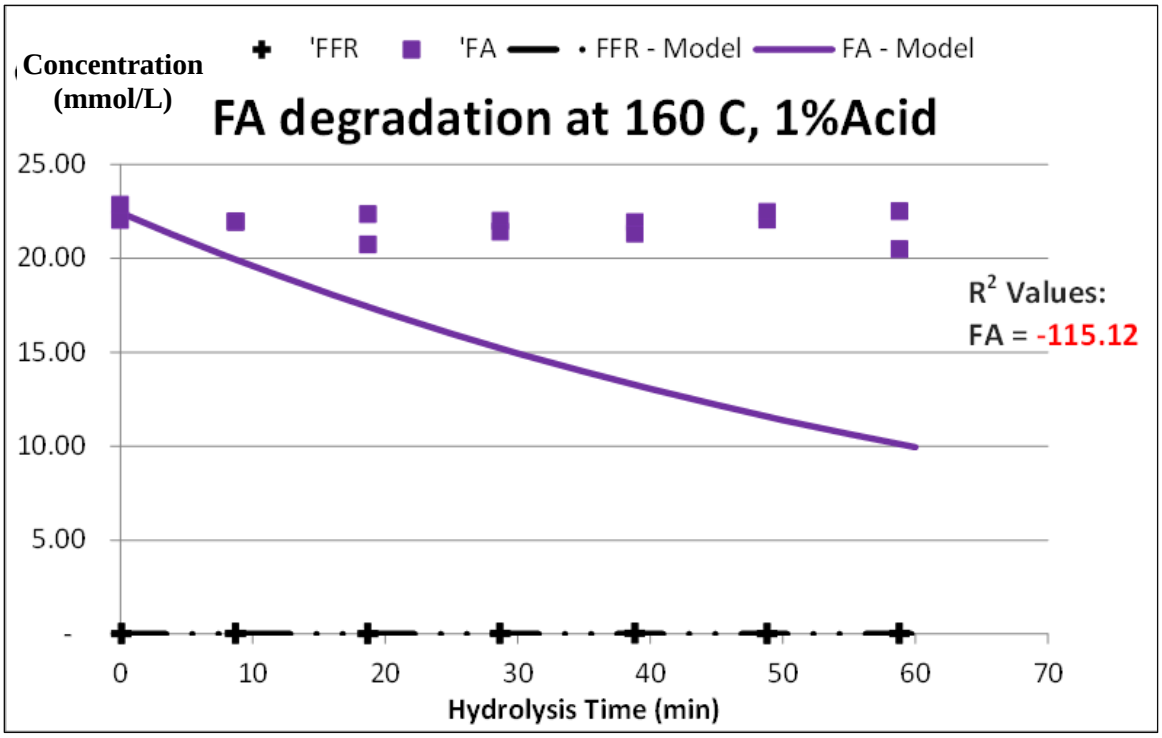
'FFR
'FA
FFR - Model
FA - Model
Concentration (mmol/L)
FA degradation at 160 C, 1%Acid
25.00
20.00
15.00
10.00
5.00
-
0
10
20
30
40
50
60
70
Hydrolysis Time (min)
R2 Values:
FA = -115.12

7. Hydrolysis Condition at 200 ˚C, Water (Model using normalized least sum of the squares method)

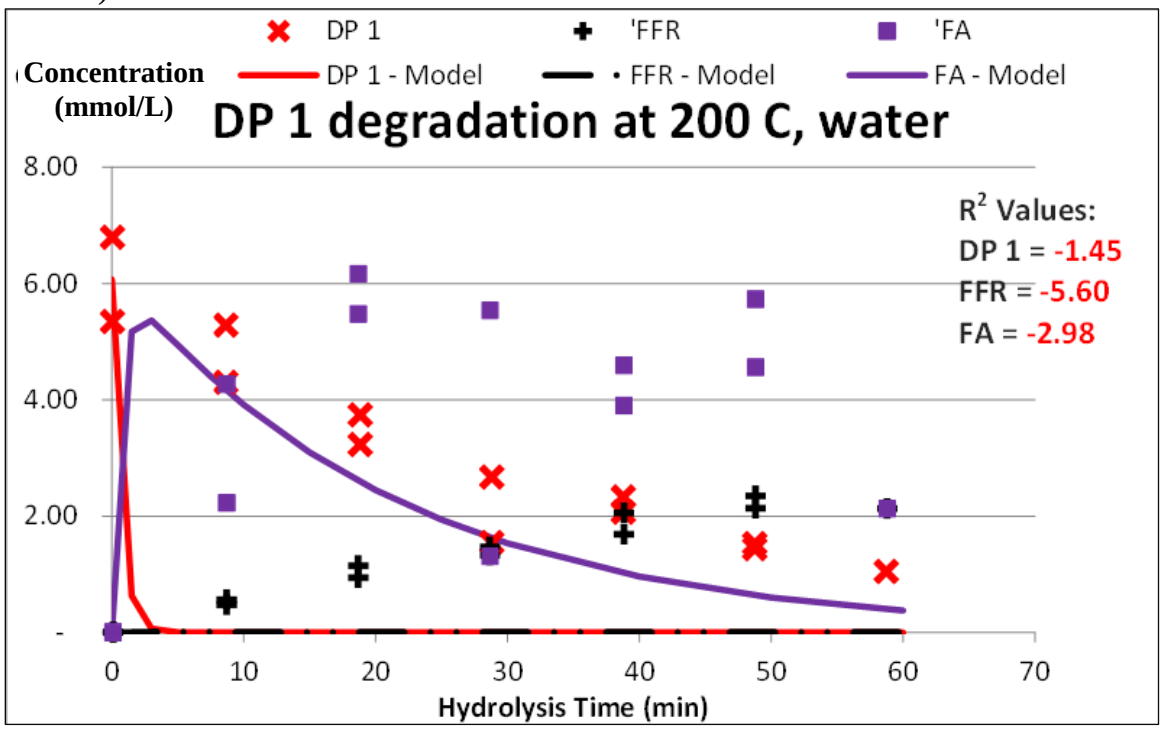

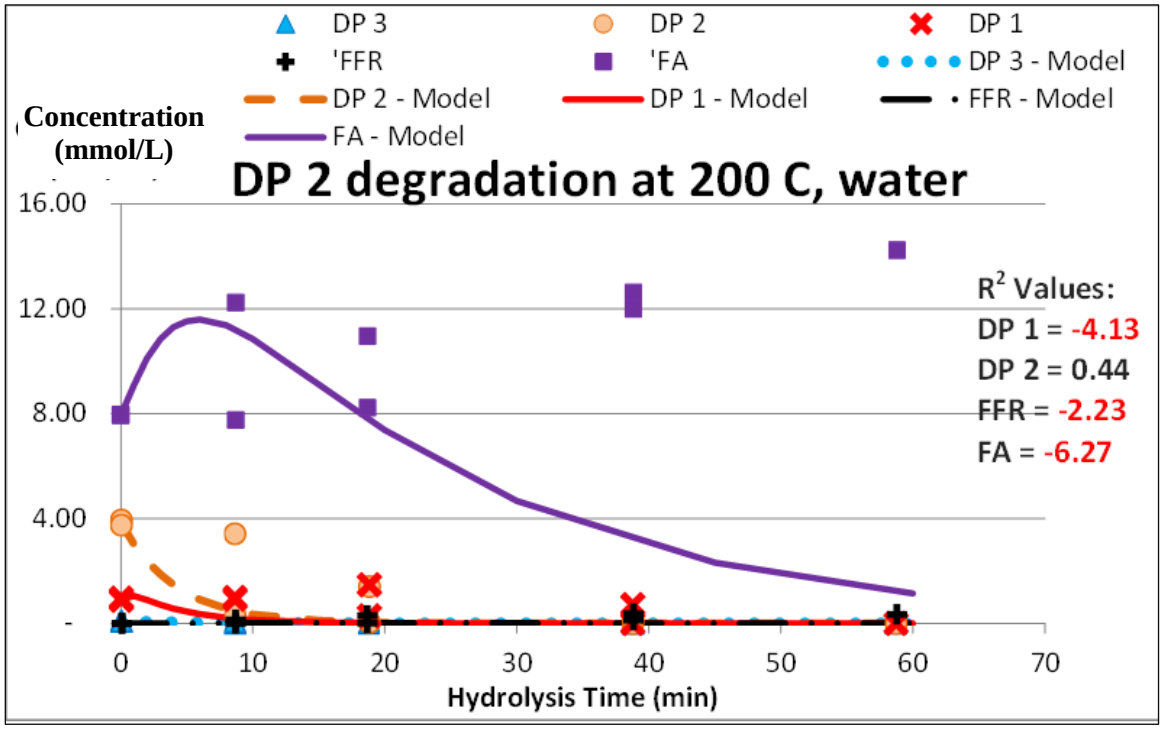

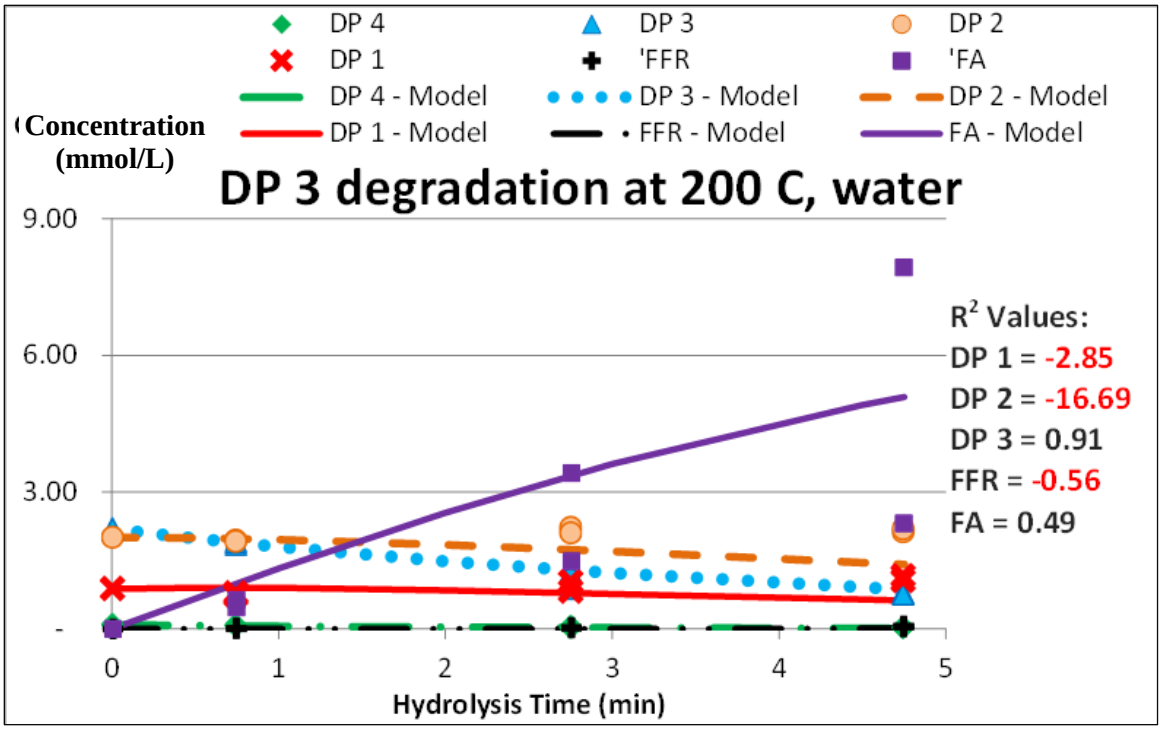
DP 4
DP 3
DP 2
DP 1
'FFR
'FA
DP 4 - Model
DP 3 - Model
DP 2 - Model
DP 1 - Model
FFR - Model
FA - Model
Concentration (mmol/L)
DP 3 degradation at 200 C, water
9.00
6.00
3.00
-
0
1
2
3
4
5
Hydrolysis Time (min)
R² Values:
DP 1 = -2.85
DP 2 = -16.69
DP 3 = 0.91
FFR = -0.56
FA = 0.49

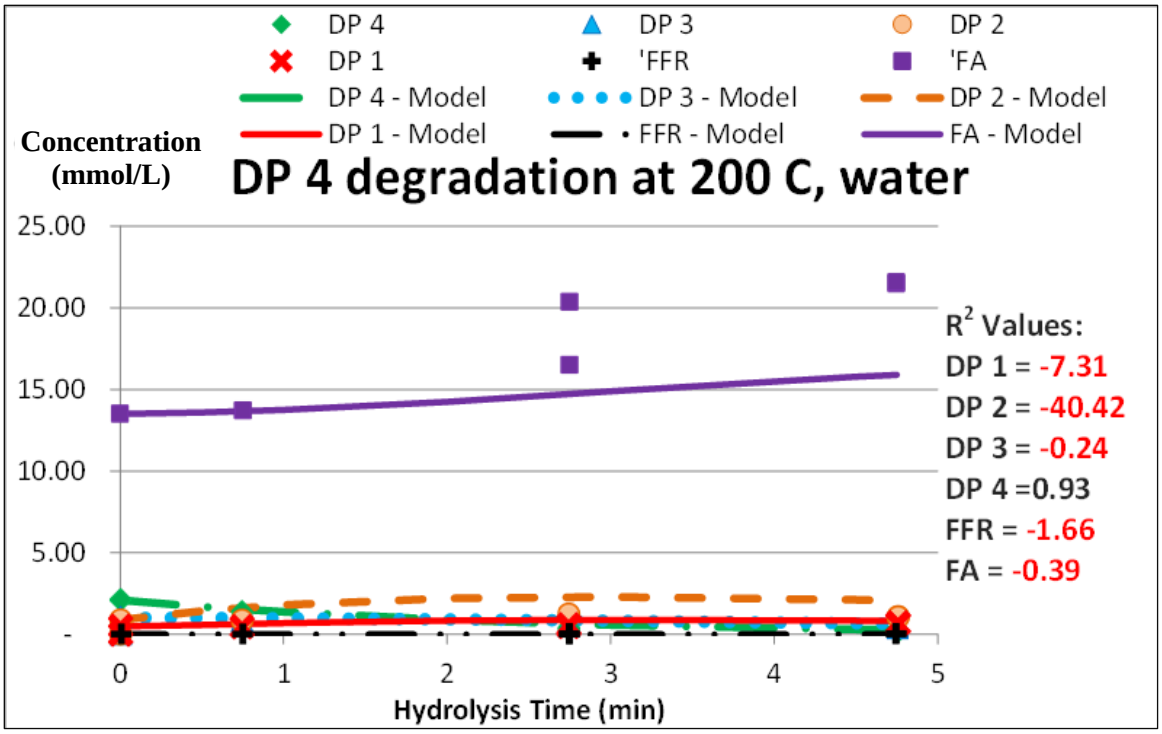
DP 4
DP 3
DP 2
DP 1
'FFR
'FA
DP 4 - Model
DP 3 - Model
DP 2 - Model
DP 1 - Model
FFR - Model
FA - Model
Concentration (mmol/L)
DP 4 degradation at 200 C, water
25.00
20.00
15.00
10.00
5.00
-
0
1
2
3
4
5
Hydrolysis Time (min)
R² Values:
DP 1 = -7.31
DP 2 = -40.42
DP 3 = -0.24
DP 4 =0.93
FFR = -1.66
FA = -0.39

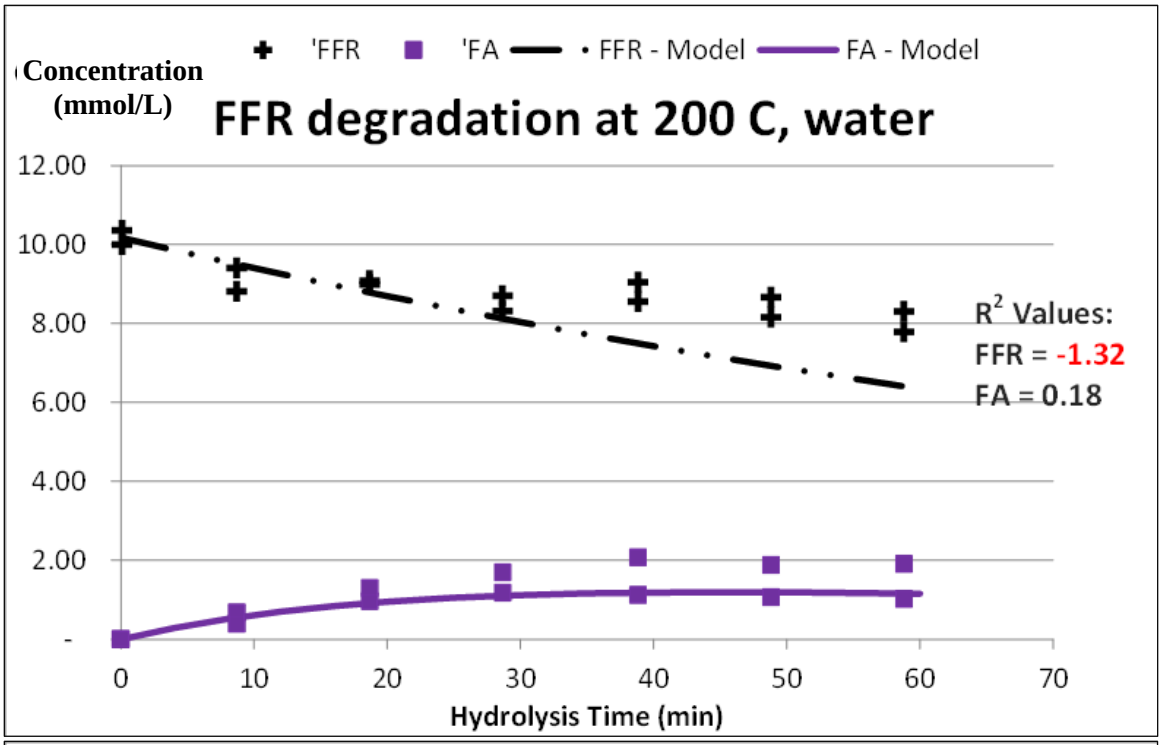
'FFR
'FA
FFR - Model
FA - Model
Concentration (mmol/L)
FFR degradation at 200 C, water
12.00
10.00
8.00
6.00
4.00
2.00
-
0
10
20
30
40
50
60
70
Hydrolysis Time (min)
R2 Values:
FFR = -1.32
FA = 0.18

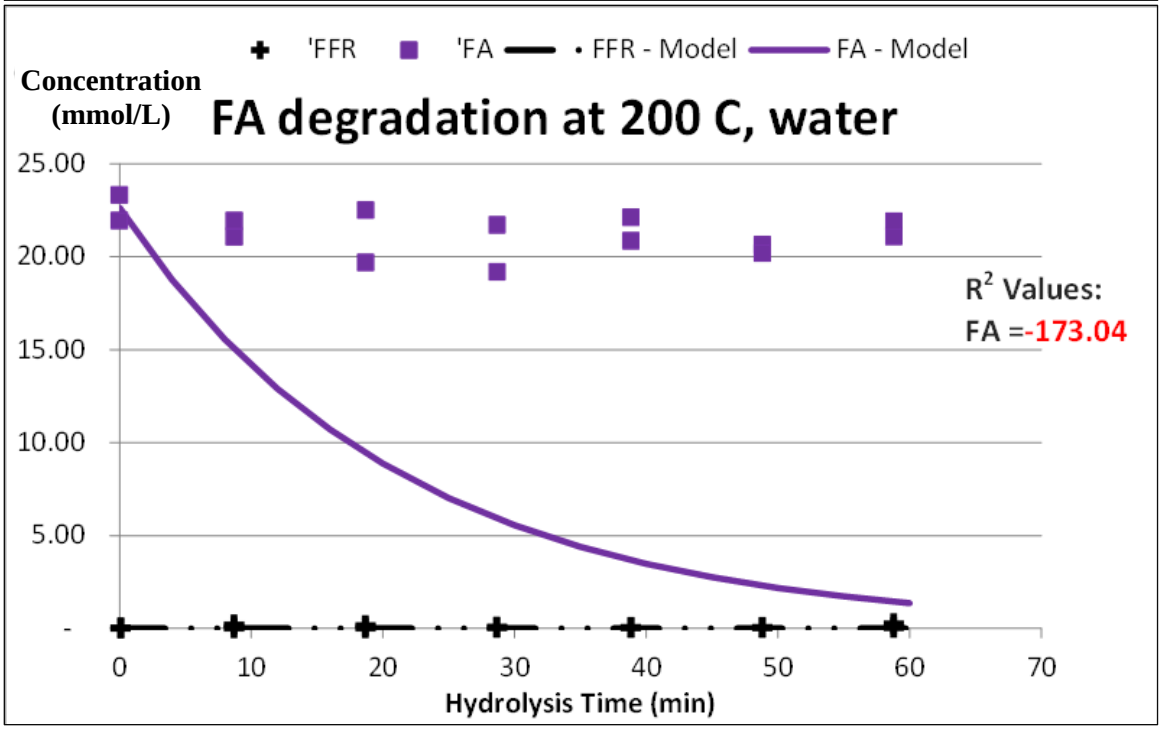
'FFR
'FA
FFR - Model
FA - Model
Concentration (mmol/L)
FA degradation at 200 C, water
25.00
20.00
15.00
10.00
5.00
-
0
10
20
30
40
50
60
70
Hydrolysis Time (min)
R2 Values:
FA =-173.04

8. Hydrolysis Condition at 200 ˚C, 0.1% Acid (Model using normalized least sum of the squares method)

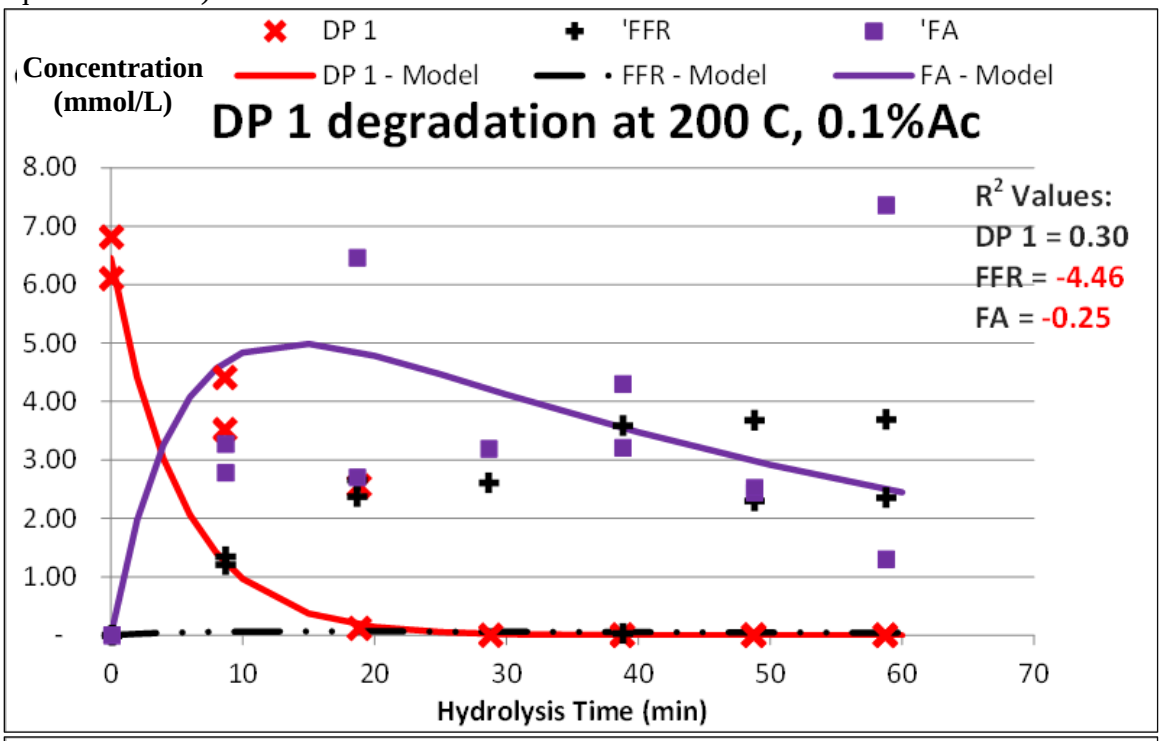

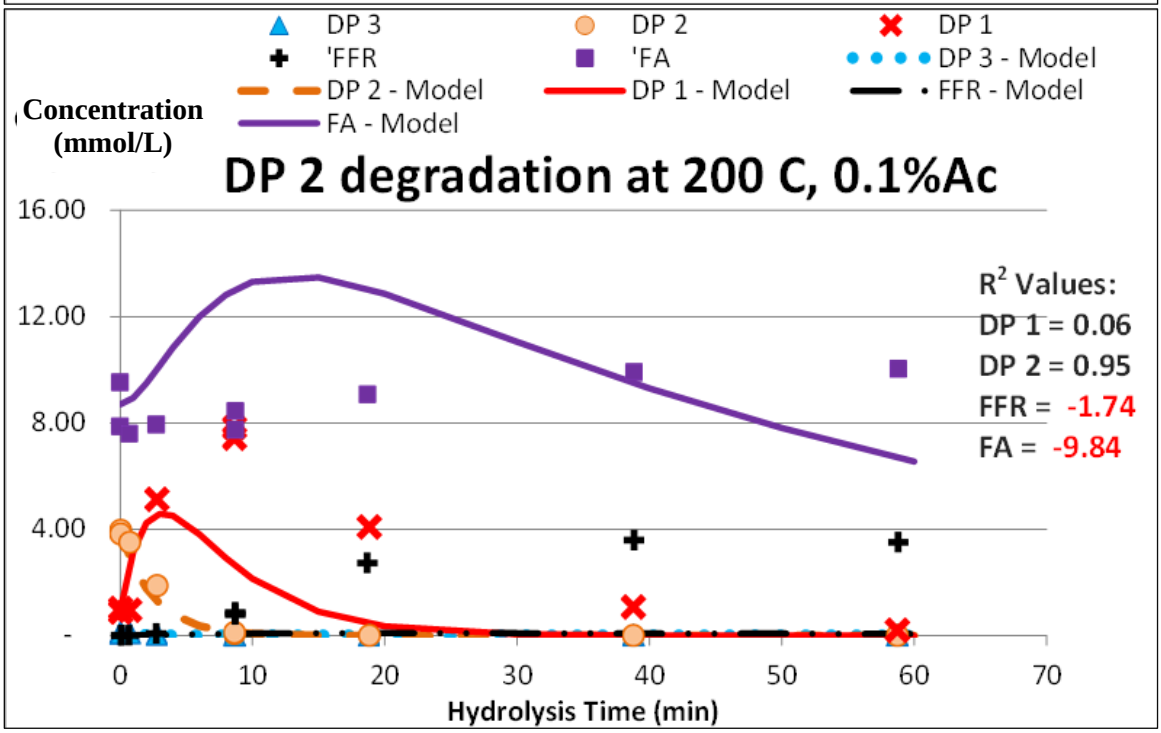

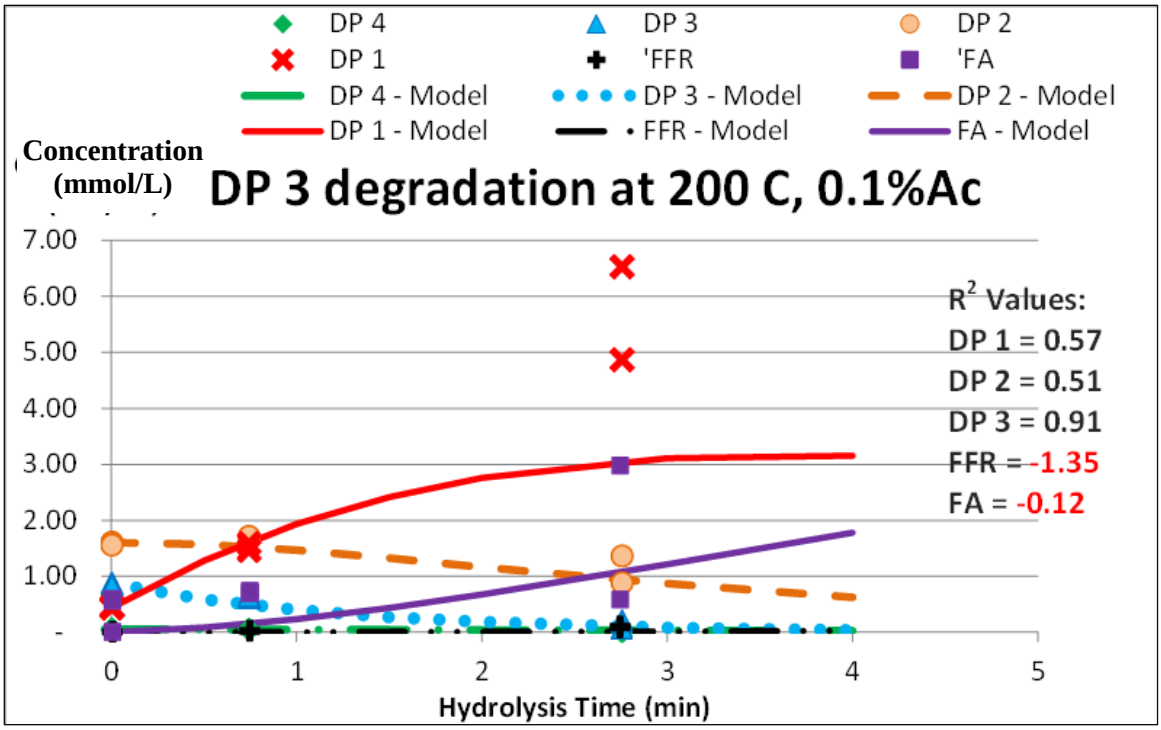
DP 4
DP 3
DP 2
DP 1
'FFR
'FA
DP 4 - Model
DP 3 - Model
DP 2 - Model
DP 1 - Model
FFR - Model
FA - Model
Concentration (mmol/L)
DP 3 degradation at 200 C, 0.1%Ac
7.00
6.00
5.00
4.00
3.00
2.00
1.00
-
0
1
2
3
4
5
Hydrolysis Time (min)
R² Values:
DP 1 = 0.57
DP 2 = 0.51
DP 3 = 0.91
FFR = -1.35
FA = -0.12

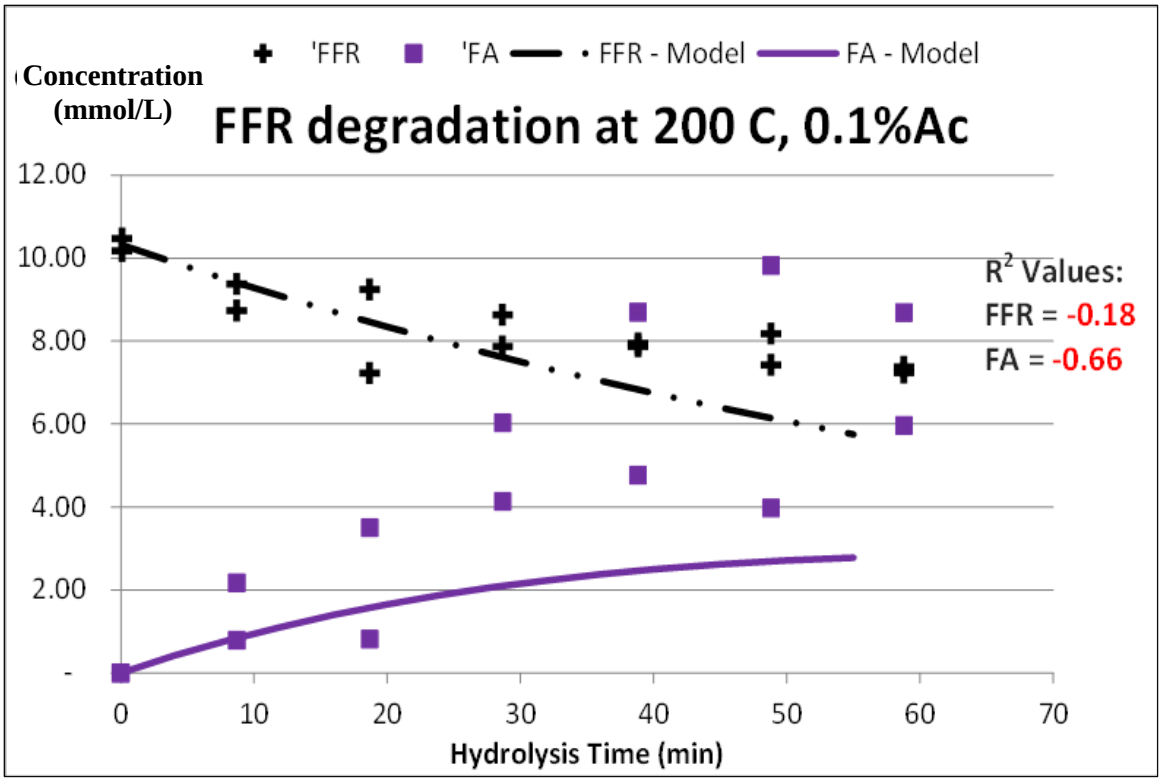
'FFR
'FA
FFR - Model
FA - Model
Concentration (mmol/L)
FFR degradation at 200 C, 0.1%Ac
12.00
10.00
8.00
6.00
4.00
2.00
-
0
10
20
30
40
50
60
70
Hydrolysis Time (min)
R² Values:
FFR = -0.18
FA = -0.66

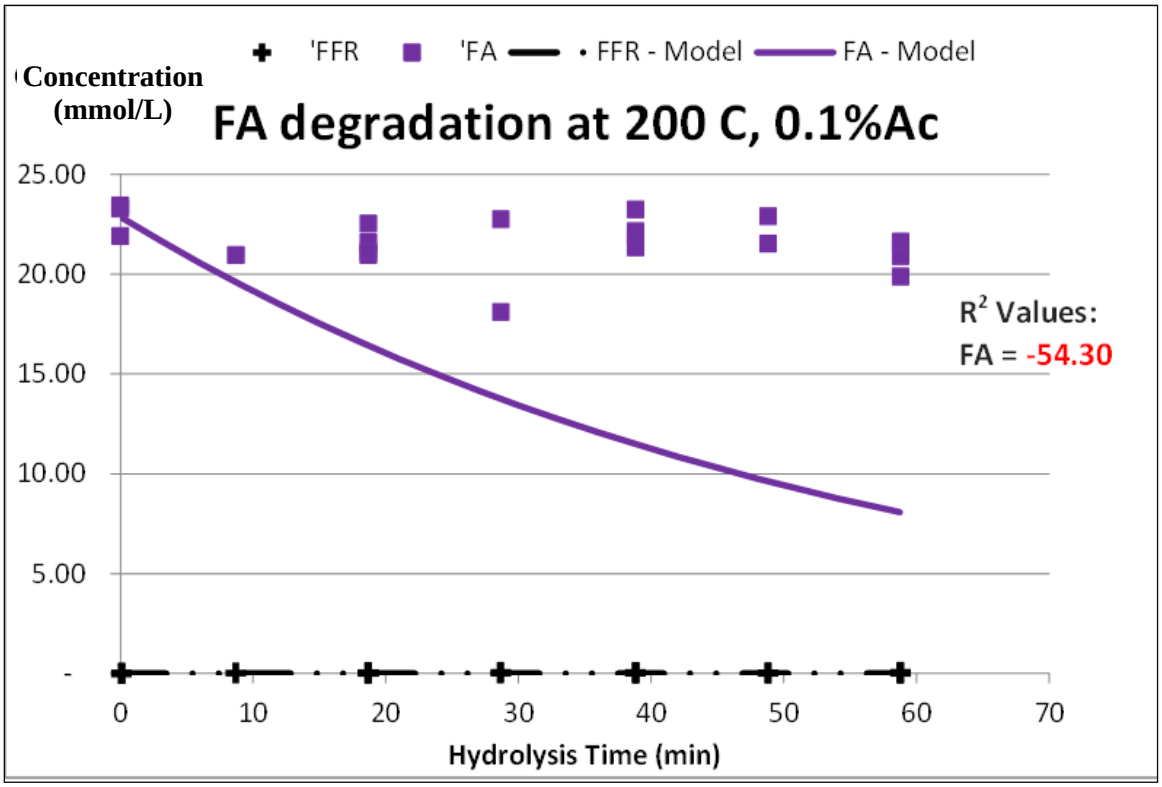
'FFR
'FA
FFR - Model
FA - Model
Concentration (mmol/L)
FA degradation at 200 C, 0.1%Ac
25.00
20.00
15.00
10.00
5.00
-
0
10
20
30
40
50
60
70
Hydrolysis Time (min)
R² Values:
FA = -54.30

9. Hydrolysis Condition at 200 ˚C, 1% Acid (Model using normalized least sum of the squares method)

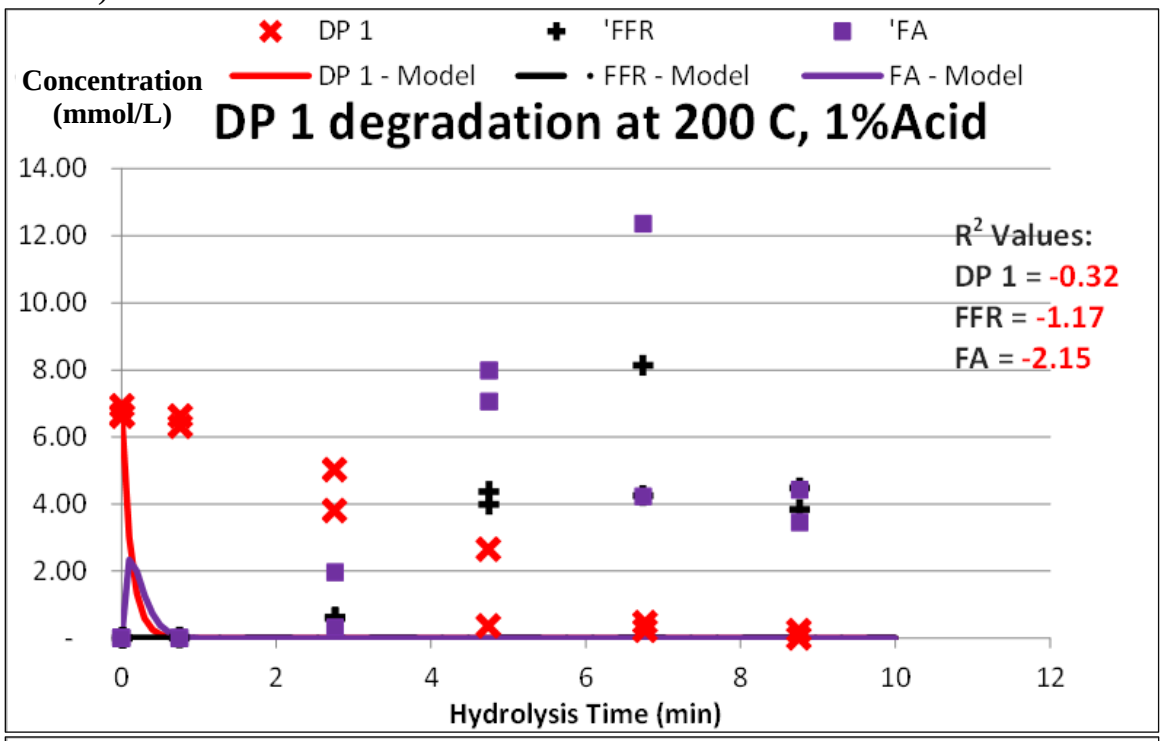

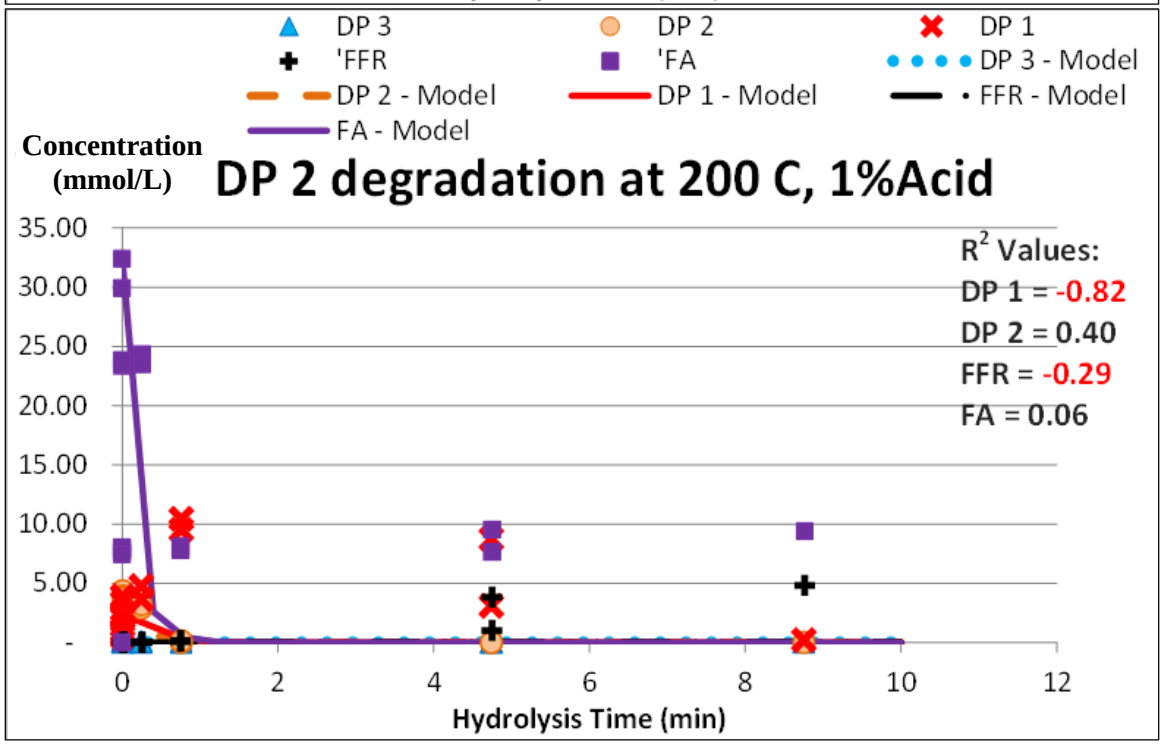

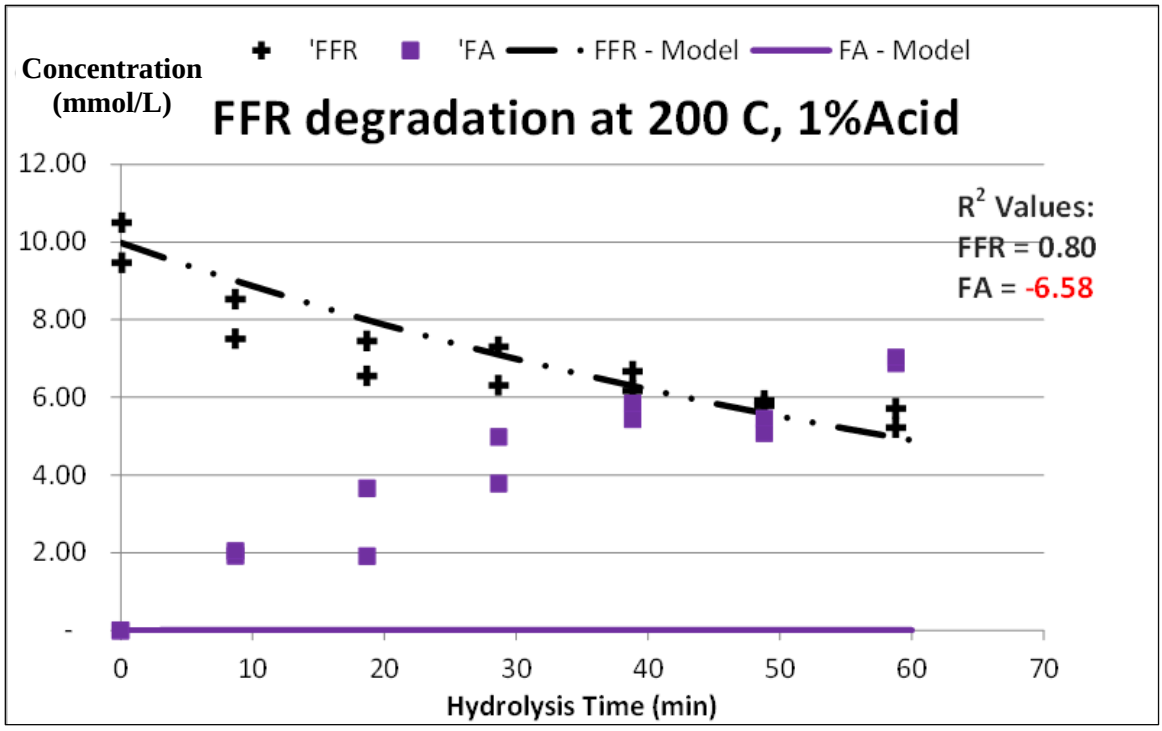
'FFR
'FA
FFR - Model
FA - Model
Concentration (mmol/L)
FFR degradation at 200 C, 1%Acid
12.00
10.00
8.00
6.00
4.00
2.00
-
0
10
20
30
40
50
60
70
Hydrolysis Time (min)
R2 Values:
FFR = 0.80
FA = -6.58

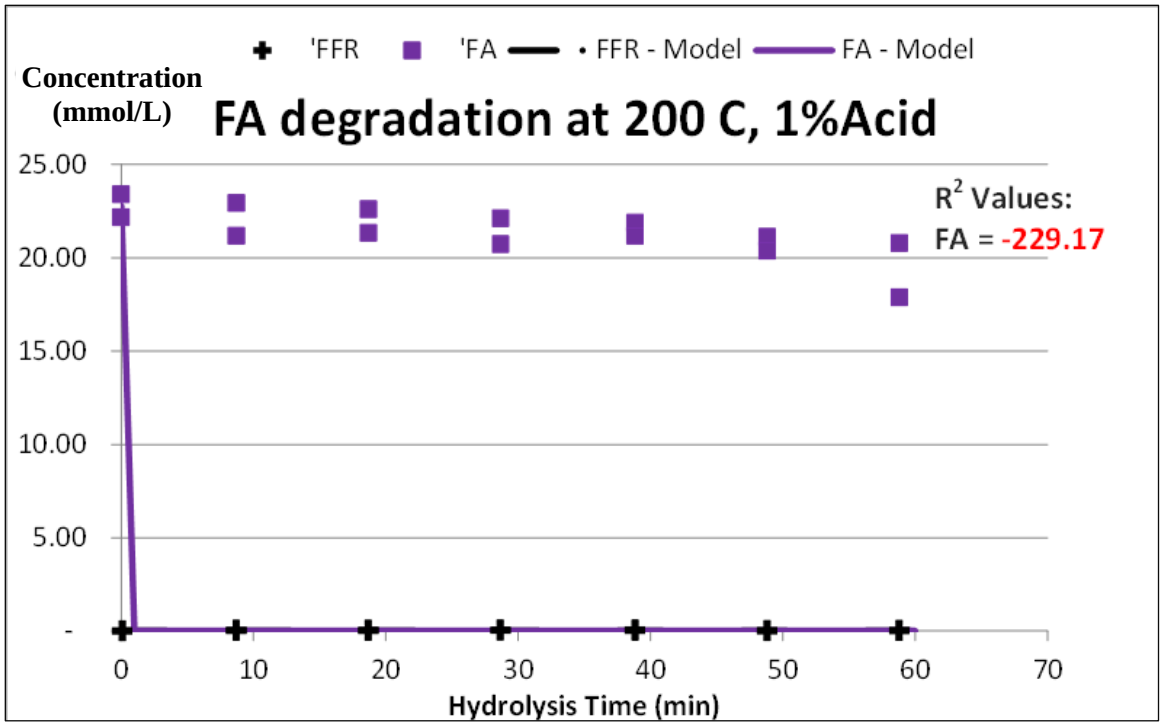
'FFR
'FA
FFR - Model
FA - Model
Concentration (mmol/L)
FA degradation at 200 C, 1%Acid
25.00
20.00
15.00
10.00
5.00
-
0
10
20
30
40
50
60
70
Hydrolysis Time (min)
R2 Values:
FA = -229.17